Modelling flexible timber diaphragms in masonry buildings subjected to seismic excitations

by

E. Liao

in partial fulfillment of the requirements for the degree of

Master of Science

in Civil Engineering

at the Delft University of Technology,
to be defended publicly on Monday March 11, 2019 at 4:00 PM.

Thesis committee:	Prof. dr. ir. J. G. Rots,	TU Delft
	Dr. ir. M. A. N. Hendriks,	TU Delft
	Dr. ir. G. J. P. Ravenshorst,	TU Delft
	Dr. F. Messali,	TU Delft

An electronic version of this thesis is available at http://repository.tudelft.nl/.

TUDelft Delft University of Technology

PREFACE

The present report is written as part of the completion of my master study in Civil Engineering at the Delft University of Technology, under the Structural Engineering department specialising in Structural Mechanics. The framework for this report is the ongoing research on the induced earthquakes in Groningen. This research focusses on the assessment and retrofitting of existing structures affected by the induced earthquakes. The TU Delft contributes to this research by conducting experimental tests and by producing numerical models. The department of Structural Engineering has numerous ongoing projects regarding the modelling of different components of masonry houses. This report concerns the numerical modelling of flexible timber diaphragms in masonry houses, such as are often found in the area of Groningen. Diaphragms may have an important effect on the failure mechanisms in houses, which is why it is of importance to broaden the current knowledge on diaphragm behaviour. The insight on diaphragm behaviour may prove to be of value in preventing degradation and failure of houses under seismic loading. This thesis report will aim to contribute to the knowledge on diaphragm behaviour and marks the end of my master study.

I would like to take this opportunity to express my gratitude to all of those who contributed to this master thesis. I would like to thank my graduation committee: Jan Rots, Geert Ravenshorst, Max Hendriks and Francesco Messali. Their knowledge, guidance and feedback have proven to be valuable in elevating the quality of my thesis. The time and critical views they offered during the whole process encouraged me and provided me with needed challenges. The process of completing my master thesis has left me many lessons, which I will take with me and which will prove to be of importance in the future.

Also, I would like to thank my family and friends for their words of encouragement and for their continuing support. Without them, finishing my thesis would have been significantly more difficult and dreadful.

E. Liao
Delft, December 2018

SUMMARY

Gas extraction in the area of Groningen has led to an increase in induced seismic activity. The seismic activity can cause considerable damage to existing structures. Generally, the houses in the area of Groningen are old and vulnerable, consisting of masonry walls and timber diaphragms. The assessment of these structures is of importance to prevent failure and to give insight in appropriate retrofitting measures. It can also provide future guidelines for the design of structures in earthquake prone areas.

In recent years, various studies have been carried out to evaluate structural behaviour under seismic loading. Especially research on the behaviour of masonry under seismic loading has been conducted extensively. However, limited studies have been carried out regarding the behaviour of flexible timber diaphragms. As diaphragms are an integral part of the houses in Groningen, they may play an important role in the failure mechanisms of the houses. Therefore, it is crucial to study diaphragm behaviour as well. This report focuses on the modelling of flexible timber diaphragms, both as-built and retrofitted. The objective of this thesis is to explore whether extensive modelling of a diaphragm is a suitable modelling approach. Additionally, this thesis seeks to produce a tool for future research on the subject of numerical diaphragm behaviour. The constructed numerical models serve as a starting point for future improvements, simplifications and modifications. To create numerical models of the diaphragms, an appropriate FEM-software must be selected which is capable of simulating the behaviour of different members within the diaphragms. Especially the nonlinear components and its numerical interpretations must be chosen carefully. Furthermore, it is of interest to determine which members can be simplified and can be modelled linearly in order to reduce computational effort.

In the framework of the ongoing research on seismic structural behaviour in Groningen, the TU Delft conducted experimental tests on as-built and retrofitted flexible timber diaphragms. The specimens of these diaphragms were constructed in the laboratory and are replicas of actual timber floors. The as-built diaphragm was constructed by placing planks perpendicular to the beams and applying two nails at each intersection between beam and plank. The retrofitted specimen was obtained by screwing plywood panels on top of the as-built specimen. Specimens were subjected to a displacement-controlled quasi-static cyclic test, with loading parallel to the joists. The hysteresis of the as-built diaphragm remained fairly linear, whereas the hysteresis of the retrofitted diaphragm was highly nonlinear and showcased a higher degree of damage. Additionally, cyclic tests were performed on the nailed and screwed connections within the diaphragms, all of which exhibited highly nonlinear behaviour. The obtained experimental results for the diaphragms and connections serve as calibration and validation points, with the numerical models aiming to reproduce experimental behaviour.

Previous numerical studies have shown similar modelling approaches for the modelling of a flexible timber diaphragm. These studies adopted the same assumptions: linear elastic material properties for the timber members and the only nonlinearity originates from the connections. These assumptions have proven to be valid in the past and are adopted for the models in this report as well. Various FEM-softwares have been used for the numerical simulation of a timber diaphragm, with each software having its own advantages. For the scope of this thesis, it is reasoned that ANSYS 18.2 is

most suitable as this software provides suitable nonlinear hysteresis models for the modelling of the nonlinear connections within the diaphragms.

First, the numerical model of the as-built diaphragm is constructed. Considering that the nailed connections are the only source of nonlinearity within the diaphragm, it is of importance to model these first. In ANSYS, the nonlinear hysteretic behaviour of a nail in 1D can be modelled by placing three COMBIN40 elements in parallel. Failure is not implemented in this model. To model a single nailed connection in the two in-plane directions of the diaphragm, a total of six COMBIN40 elements are needed. The rotational behaviour of the nails can be predicted by the behaviour in the two in-plane directions. The numerical models for the nailed connections are calibrated on the average of the experimental tests. Two calibration methods are adopted: calibration based on the experimental hysteresis and calibration based on the experimental backbone. The first calibration method is more suitable for analyses in which loading is applied gradually, which resembles the experimental tests. The second calibration approach may be more suitable for broader purposes, such as analyses in which loading is more random. With the models for the nailed connections, the model for the as-built diaphragm can be constructed. This model adopts orthotropic linear elastic material properties for its timber members and the same loading and boundary conditions as in the experimental tests. Friction and contact modelling between timber members are neglected. Four static nonlinear analyses have been carried out: adopting a coarse and a fine mesh, two calibration methods for the connections have been implemented per mesh. The four numerical results yielded an accurate overall hysteretic behaviour of the diaphragms. Numerical errors increased for higher displacements, which is caused by the increased inaccuracy in the nailed connections for higher displacements. The two calibration methods yielded similar results, with the first calibration method generating slightly better numerical results. The fine mesh yielded more accurate results for both calibration methods. For the analyses with the fine mesh, the numerical results tended to be stiffer. This is caused by the interaction between beams and planks, with a fine mesh generating more accurate deformations for the beams and causing a stiffer behaviour of the diaphragm. The most accurate result is obtained by the analysis with the fine mesh adopting the first calibration method, with the largest error being 12.6%.

With the model of the as-built diaphragm, the model of the retrofitted diaphragm can be constructed. The retrofitted diaphragm contains nonlinearities in its nails and screws. The models for these connections are the same as for the nailed connections in the as-built diaphragm (using element COMBIN40) and are calibrated on the average of experimental results. The retrofitted diaphragm contains the same elements as the as-built diaphragm, with additional contact elements formulated between timber elements to prevent them from moving into each other. Timber elements are given orthotropic linear elastic material properties. The same loading and boundary conditions are adopted as in the experimental test. Friction between timber members is neglected. Two analyses have been carried out for the retrofitted diaphragm, adopting the two calibration methods for the connections. The numerical results yielded fairly accurate results, with the overall behaviour captured correctly. The numerical results exhibited lower stiffnesses and lower peak forces, which can be attributed to the improper modelling of contact regions and to the increasing error of the connections. This also causes increasing errors for higher displacements. The two calibration methods yielded similar results.

The numerical results of this report provide several conclusions in support of the research objectives of this thesis. It can be said that modelling the separate components within a diaphragm is a suitable approach which yields accurate numerical results. Additionally, assuming that the connections are the only source of nonlinearity is justified. Furthermore, ANSYS 18.2 proves to be an

appropriate software to model flexible timber diaphragms, providing a suitable nonlinear hysteresis model for the connections. Also, it can be concluded that the first calibration method for the connections is more accurate for local behaviour for analyses with gradual loading. The lack of friction and the improper contact modelling within the diaphragms result in larger numerical errors and a lower numerical energy conservation. For future research, it is recommended to implement failure in the connections. The implementation of friction and better contact modelling between timber members may also yield better numerical results. Furthermore, it may be interesting to explore the possibility of modelling the planks through a plate to reduce computational effort. Lastly, it may be of interest to study different diaphragm geometry, by altering dimensions, changing the floor plan and changing the plank configuration.

CONTENTS

LIST OF FIGURES

LIST OF TABLES

<div align="right">

1

</div>

INTRODUCTION

In recent years, induced seismic activity has become more common in the northern part of The Netherlands. This seismic activity is induced by gas extraction from gas fields in Groningen. Due to the seismic activity, structures are subjected to earthquakes. These earthquakes can have magnitudes of up to 3 on the Richter scale and in some cases may even surpass a magnitude of 3 [1]. Figure 1-1 shows the number of earthquakes and the magnitude of these earthquakes in the Groningen gas field. The earthquakes can cause considerable damage to existing structures. Some houses in the north of The Netherlands may not be strong enough to absorb expected loads originating from earthquakes. It is therefore of importance to analyse and model the response of structures to seismic activity. The models serve to verify the capacity of houses and may be a helpful tool in providing insight in selecting appropriate retrofitting methods.

Aantal aardbevingen in het Groningen-gasveld
Van 1986 tot 2016

Bron: KNMI   Generatiedatum grafiek: 13 december 2016
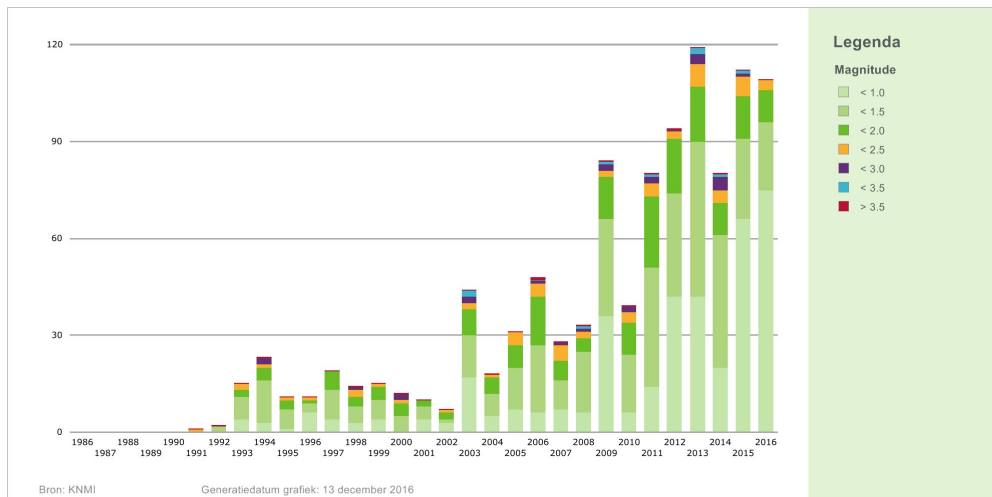
Voor vragen kunt u een e-mail sturen naar informatie@nam.nl of bellen naar 0592 - 362 100.
© 2016 NAM. Bekijk de interactieve versie van deze grafiek op namplatform.nl.

Figure 1-1: Number of earthquakes in the Groningen gas field [1]

In the light of current issues in Groningen, the Dutch government altered its policy concerning gas extraction. The amount of gas extracted from the gas fields is reduced and an extensive research programme has been set up to acquire insight in the effects of seismic loading on structures. Various universities, companies and knowledge institutes contribute to the ongoing research concerning induced earthquakes in The Netherlands. The Dutch petroleum company NAM (Nederlandse Aard-olie Maatschappij) is responsible for the extraction of gas and is greatly involved in the research.

The TU Delft also participates in the research programme regarding induced seismic activity. Multiple experimental tests have been carried out and numerical models have been constructed to illustrate the behaviour of structures under seismic loading. However, multiple aspects of the problem still remain unclear and additional research is required to create a better understanding of the problem. In the context of the research, one of the topics the TU Delft focuses on is the modelling (and testing) of flexible timber diaphragms such as commonly found in unreinforced masonry houses in the northern part of The Netherlands. About 38% of the houses in the area of the Groningen gas field are unreinforced masonry (URM) houses with flexible diaphragms, so it is of importance to assess the response of flexible diaphragms in URM buildings [27].

Flexible timber diaphragms are of importance as they transmit horizontal forces to vertical elements. The in-plane behaviour of diaphragms determine the out-of-plane behaviour of the connected shear walls, thus contributing to the overall response and resistance of a structure. Few studies and experiments have been carried out to understand the influence of various characteristics of timber diaphragms on the capacity of a structure, both nationally as internationally. Knowledge on the topic of seismic responses of structures expanded, however there is still a demand for further research.

This report will focus on constructing accurate finite element models to represent flexible timber diaphragms in masonry buildings subjected to seismic loading. To this end, parameters in different directions must be considered and nonlinear properties must be analysed. Furthermore, connecting elements and its properties must be regarded for a comprehensive understanding of diaphragm behaviour. This report will focus on all the aspects within a diaphragm, meaning that the numerical models will contain a high degree of detail. The research question of this thesis is formulated as:

Is it possible to create accurate numerical models of flexible timber diaphragms by modelling the separate components?

In support of the main research question, several subquestions can be formulated:

1. *Which FEM-software is most suitable for the modelling of a flexible timber diaphragm?*
2. *Which numerical models are suitable to simulate nonlinear components within a diaphragm?*
3. *Can certain diaphragm members be modelled linearly?*

The objective of this thesis is to explore whether extensive modelling of a diaphragm is a suitable approach to yield accurate numerical results. In support of this objective, a suitable FEM-software must be selected which is capable of modelling specific characteristics of diaphragm members. This software must have suitable models for both linear and nonlinear components within the diaphragms. To model the nonlinear components, research must be done to determine which models are available and suitable. The available nonlinear models are specific to each software and thus the most suitable software can be chosen on the basis of its nonlinear models. Furthermore, acceptable

linearisations must be explored to simplify diaphragm modelling. Certain diaphragm components may prove to be too essential to simplify and therefore cannot be omitted or linearised.

Additionally, this thesis seeks to create a tool for further development and for broader purposes. The numerical models of the diaphragms, which shall be created in this report, aim to provide a starting point for further improvements, simplifications and modifications. The research conducted in this thesis provides principal understandings regarding (numerical) diaphragm behaviour and it is desirable to expand this knowledge. Only with a full understanding of diaphragm mechanics can the structural response of houses in Groningen be assessed and suitable retrofit measures be applied.

This report is divided into two parts and consists of eight chapters:

  I Literature study
       Chapter 2: General information
       Chapter 3: Previous experimental tests on flexible timber diaphragms
       Chapter 4: Numerical theory

 II Modelling the flexible timber diaphragm
       Chapter 5: Trial tests at the TU Delft
       Chapter 6: Extensive model of as-built diaphragm
       Chapter 7: Extensive model of retrofitted diaphragm
       Chapter 8: Conclusions and recommendations

The first part comprises three chapters and will deal with the literature study. This literature study concerns general information, previous experimental tests that have been conducted on flexible timber diaphragms and numerical theory. Part II, comprising four chapters, focuses on constructing finite element models of a flexible timber diaphragm. Within part II, chapter 5 will deal with the experimental tests conducted at the TU Delft and its results. Hereafter, chapter 6 and chapter 7 will discuss extensive FEM-models for both an as-built and a retrofitted diaphragm. Lastly, conclusions and recommendations will be presented in chapter 8.

PART I

LITERATURE STUDY

The goal of the literature study is to acquire needed foreknowledge on relevant topics. The literature study is crucial for a better understanding of the problem and provides essential tools for the remainder of the report. This part consists of three chapters. First, general information will be given in chapter 2. The remainder of the needed knowledge is covered mostly in two parts: previous experimental tests on flexible timber diaphragms (chapter 3) and numerical theory (chapter 4). Previous experimental tests serve as background theory and are useful for the understanding of the behaviour of a flexible timber diaphragm. The numerical theory concerns previous modelling methods and suitable finite element programs, along with its implemented models. The numerical theory serves as a starting point for the modelling of the diaphragms in part II.

2

GENERAL INFORMATION

This chapter deals with basic information for general understanding. Section 2.1 will give a short description of common houses in Groningen. The structural components of these houses, mostly timber and masonry, will be briefly discussed in section 2.2 and section 2.3 respectively. Hereafter, section 2.4 regards diaphragm typology and specifications. Structural failure due to flexible diaphragms will be discussed in section 2.5, after which a short explanation of earthquake dynamics will be given in section section 2.6.

2.1 HOUSES IN GRONINGEN

In response to the increased seismic activity in Groningen, company ARUP investigated the different types of buildings which are present in the region of the Groningen gas field [27]. For this study, about 250.000 buildings were considered in an area that extends five kilometres beyond the boundaries of the gas field. This area also includes a region with a fifteen kilometre radius around the epicentre of the Huizinge earthquake. From the study of these buildings, it is found that the majority of the buildings are constructed out of unreinforced masonry (about 77% of the considered buildings). The remainder of the buildings are constructed out of reinforced concrete, steel, wood or other unclear materials. The unreinforced masonry buildings can be either detached, semi-detached or terraced. About 13% of these buildings were built before 1920 and in about half of the unreinforced masonry buildings the diaphragms are flexible. A flexible diaphragm is a diaphragm in which the horizontal deformation along its length is twice or more times the average storey drift. ARUP defines the storey drift as being the horizontal deflection at the top of the storey relative to the bottom of the storey [27]. Flexible diaphragms are often found as timber diaphragms and are quite common in the houses in Groningen. A timber diaphragm is displayed in figure 2-1. As there are old and vulnerable houses in Groningen, some houses are greatly affected by past earthquakes and have been temporarily strengthened (see figure 2-2). The matter has become such an issue, that about 23.000 buildings in the gas field are to be inspected for earthquake resistance on a faster rate [28]. These inspections serve to identify vulnerable buildings and to provide retrofitting measures to prevent further deterioration.

Figure 2-1: Timber floor in a house [2]

Figure 2-2: A temporarily strengthened house in Groningen [2]

2.2 STRUCTURAL TIMBER

Timber is a commonly used construction material as it is applicable for many purposes. Due to its organic nature, it is a sustainable building material. Timber is defined as processed wood and can be classified as either hardwood or softwood, depending on the type of tree from which it is obtained. As a natural product, timber has a scatter in material properties. Compared to other construction materials, timber has a relatively low density and low stiffness. Unlike most construction materials, timber is anisotropic and consists out of fibres. The fibres are of great importance when determining the material properties of timber. The highest strength in timber occurs in the direction parallel to the fibre, resulting in a higher Young's modulus parallel to the grain as compared to the Young's modulus perpendicular to the grain. Furthermore, timber has a higher compression strength as opposed to the tensile strength. In laboratory tests, it is of importance to determine the density and the (dynamic) Young's modulus of the timber specimens. The Young's modulus of timber has a fair correlation with the strength of timber and can be used as a predictor for timber strength.

2.3 MASONRY

As flexible timber diaphragms are connected to the masonry housing, the masonry and geometry of the house influence the response of a flexible timber diaphragm. Houses in Groningen are often constructed out of unreinforced masonry, which consists only of mortar and masonry units (bricks). Different types of mortar and bricks can be used in different kind of configurations, affecting the strength characteristics of masonry. As masonry consists of different materials, it is difficult to predict the overall behaviour. Properties of the bricks, the mortar and the interface between brick and mortar are of importance when assessing the masonry. Masonry can be viewed as a composite and exhibits varying behaviour in the different directions. Unreinforced masonry acts better in compression than it does in tension or shear, thus it can absorb gravity loads rather well as opposed to wind or earthquake loads. Different modes of failure can be distinguished in both in-plane and out-of-plane directions. The failure mode of masonry does not solely depend on its properties and the loading, but it is also depending on the overall structure and the connections within the structure. Thus, it is hard to determine which failure mode will occur beforehand.

2.4 CHARACTERISTICS OF DIAPHRAGMS

Diaphragms are horizontal or inclined members used as roofs and floors, which serve to transmit lateral forces to resisting structural elements. In houses, the diaphragms often transmit forces to shear walls. Diaphragms can be rigid or flexible and can be classified as being either one-way or two-way. One-way diaphragms are usually supported at two parallel edges, thus the loads will be transmitted in one direction. Between the supports, parallel beams are placed to transmit forces. Two-way diaphragms are supported at all edges, thus loads can be transmitted in two directions. Diaphragms roughly consist of three elements:

- Joists
- Sheathing
- Connections (nails and/or screws)

The joists are beam members which serve to support loads and transmit loads to the shear walls. On top of the joists, sheathing is placed. Sheathing consists of panels or boards which are typically interlocked through a tongue and groove connection. Wooden boards can be positioned into three different configurations (see figure 2-3). The sheathing elements are connected to the joists through connectors, such as nails and screws. Typically, the sheathing boards are connected with two nails at each joist.

(a) Configuration 1

(b) Configuration 2
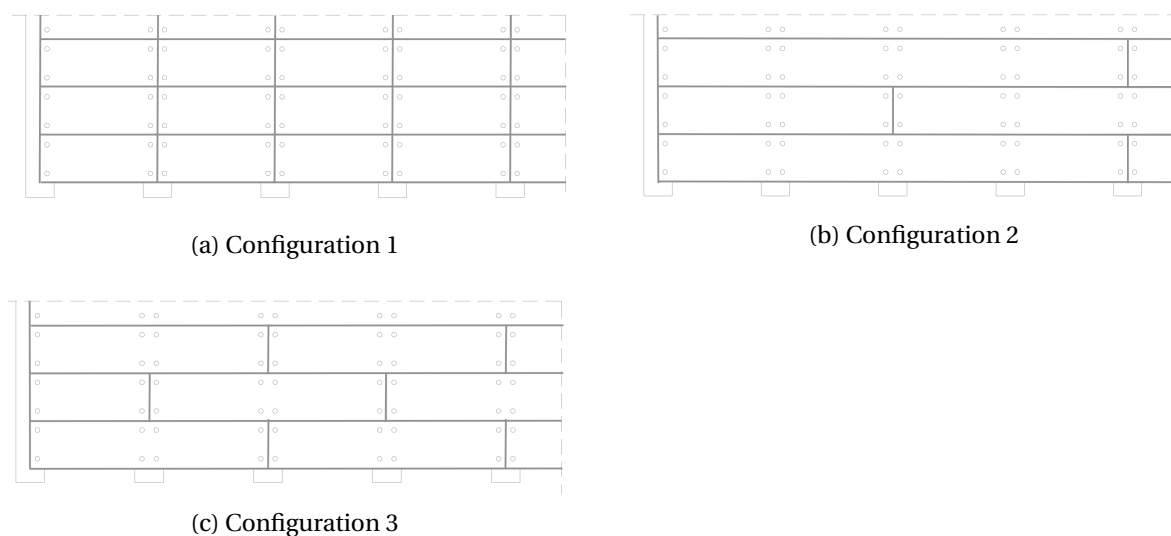
(c) Configuration 3

Figure 2-3: Different configurations of wooden boards [3]

According to ASCE/SEI 41-06 and NZSEE 2006, different types of diaphragms can be distinguished: [29] [30]:

- Single straight sheathing: In this diaphragm type, a single layer of sheathing is placed perpendicular to the joists.

- Double straight sheathing: For this diaphragm, a layer of sheathing is placed perpendicular to the joists and another layer of sheathing is placed on top of the first layer of sheathing. The second layer of sheathing can be placed either perpendicular or parallel to the first layer of sheathing.

- Single diagonal sheathing: In this diaphragm, a single layer of sheathing is placed at an angle of 45 degrees to the joists.

- Double diagonal sheathing: For this diaphragm, a layer of sheathing is placed at an angle of 45 degrees to the joists. A second layer of sheathing is then placed perpendicular to the first layer of sheathing.

- Diagonal and straight sheathing: In this diaphragm, diagonal and straight sheathing are combined. The first layer of sheathing is placed at angle of 45 degrees to the joists and the second layer of sheathing is installed perpendicular to the joists.

- Panel sheathing: For this diaphragm, the sheathing consists of wooden structural panels.

In addition, diaphragms can be blocked or unblocked [31]. In blocked diaphragms, sheathing panel edges which are not supported by framing members or joists are supported by wood blocking. This ensures that all panel edges are supported, which is not the case with unblocked diaphragms.

2.5 FAILURE DUE TO FLEXIBLE DIAPHRAGMS

As a result of earthquake excitations, diaphragms deform and excite forces onto the surrounding structure. Mostly in-plane deformations are of importance when regarding floor units, as these deformations can cause failure of the overall structure. The in-plane deformation of a floor unit largely depends on the in-plane stiffness. The stiffness of timber floor units consists of two components: the in-plane stiffness of the diaphragm and the stiffness of the connections between floor and wall (see figure 2-4). The system of diaphragm and connectors are in series, meaning that the total displacement is the sum of the displacements of individual elements. For this model, the relation for the equivalent stiffness of the floor system is given as follows: [3]

$$\frac{1}{k_{eq,c+d}} = \frac{1}{k_{eq,d}} + \frac{1}{k_c} \tag{2.1}$$

In the above equation, $k_{eq,c+d}$ is the equivalent stiffness of the floor system, $k_{eq,d}$ is the equivalent stiffness of the diaphragm only and k_c is the stiffness of the connectors between the floor and the wall. Previous studies have shown that the in-plane stiffness of diaphragms are of great importance when assessing the response of a structure, as the in-plane stiffness has a great influence on the out-of-plane displacement of the walls [3] [9]. Some norms offer reference values or analytical relations for the evaluation of the in-plane stiffness of diaphragms, however it is worth noting that experimental tests are crucial to support these values.
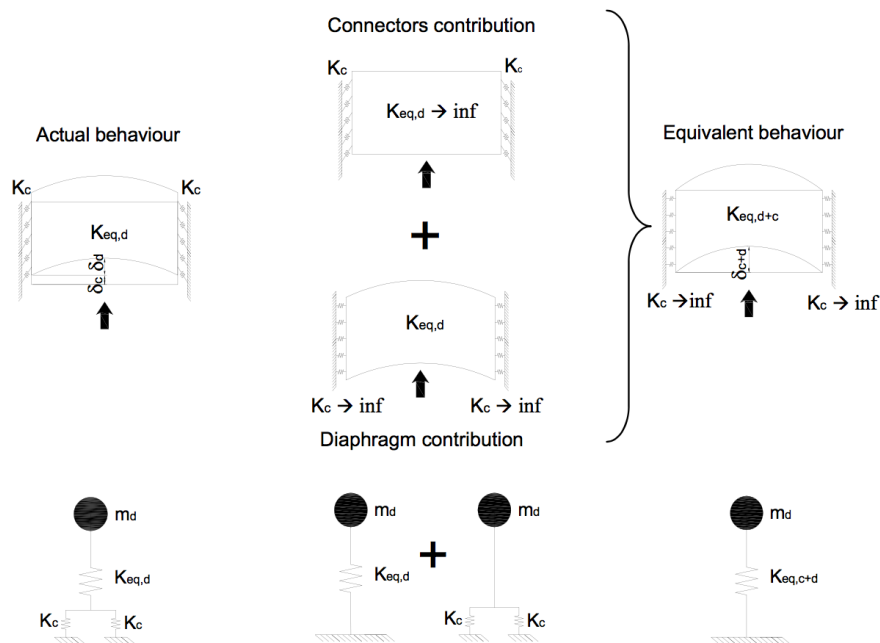
Figure 2-4: Floor stiffness components [3]
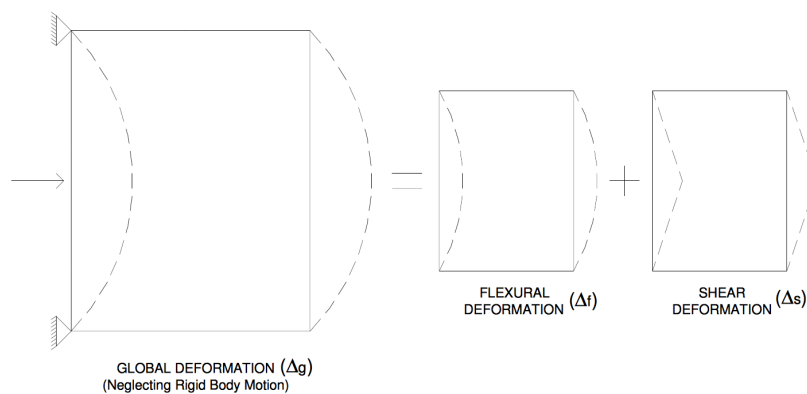
Figure 2-5: Deformation of a diaphragm [4]

The global in-plane deformation of a diaphragm can be attributed to both flexural deformation and shear deformation (see figure 2-5). The more flexible a diaphragm is, the larger the deformation will be. This can lead to first modes of failures. So-called first modes of failures are brittle modes of failures in which out-of-plane overturning of walls perpendicular to seismic loading occur due to high flexibility of the diaphragm (see figure 2-6). Examples of out-of-plane wall mechanisms can be seen in figure 2-8. Poor connection between the floors and the walls can also contribute to a first mode failure. First mode failures are typically the least desirable as they result in an excessive amount of damage and possible dangers to humans. First mode failures can be prevented by implementing diaphragms with sufficient stiffness, such that the lateral forces can be transmitted to the shear walls which are parallel to the seismic loading (see figure 2-6 and figure 2-7). This load transmission prevents out-of-plane failure of masonry walls and leads to a better shear distribution in the lateral walls, thus it is more favourable [3].
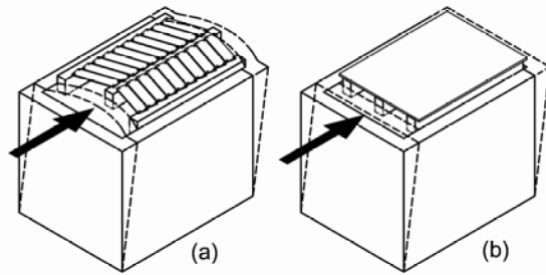
Figure 2-6: (a) Flexible diaphragms cause overturning of walls perpendicular to seismic action; (b) Stiffer diaphragms transmit forces to walls parallel to seismic action [5]
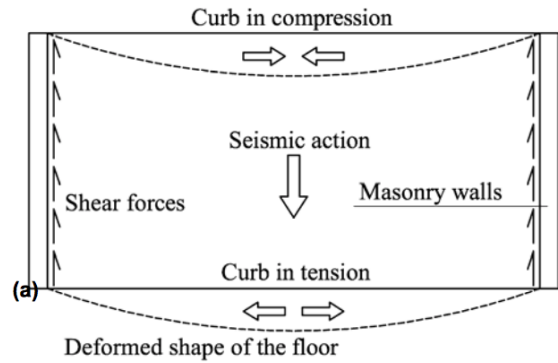
Figure 2-7: Behaviour of a diaphragm in masonry housing [5]

Figure 2-8: Out-of-plane failure mechanisms of outer walls [6]

To prevent first mode failures, flexible diaphragms can be retrofitted to obtain stiffer properties. However, retrofitting a diaphragm to obtain stiffer properties does not always prove to be beneficial. Many factors, such as the connection between the wall and floor, are of importance when considering the probability of local and global failure mechanisms. Retrofitting should lead to an efficient redistribution of forces, such that the least desirable failure mechanism is avoided during an earthquake and an advantageous hierarchy of collapse mechanisms is obtained. An important note here is that for proper functioning of the diaphragm, the connections between diaphragm and walls are crucial. Connections between wall and floor have a great influence on the ability of a structure to act as a box (in 3D) and this box-action is desirable. Proper connections activate the box behaviour of a structure and decreases the probability of undesirable collapse mechanisms. One can consider to retrofit the wall-to-floor connections if retrofitting the diaphragm only is not sufficient. Needless to say, the interaction between diaphragm and connectors contribute to the response of a structure and are important aspects to consider when evaluating a structure under seismic loading.

2.6 EARTHQUAKES

Earthquakes are random vibrations of the earth's surface of either tectonic or induced nature. Induced earthquakes are usually shorter and milder than tectonic earthquakes. Earthquakes can be characterised by its magnitude and intensity, the magnitude of an earthquake is usually measured on the Richter scale. The source of an earthquake is called the hypocentre and the point on the earth's surface directly above the hypocentre is called the epicentre. If the distance between the hypocentre and the epicentre (the focal depth) is small for an earthquake of big magnitude, the ground acceleration is significant and the damage to structures becomes bigger. If for the same magnitude the focal depth increases, the ground accelerations decrease and the damage to structures will become less (thus decreasing the risk of casualties). The signal of an earthquake can be represented in an accelerogram, in which the ground acceleration is measured over time (see figure 2-9). In the accelerogram, the ground acceleration is often normalised to the gravitational acceleration.
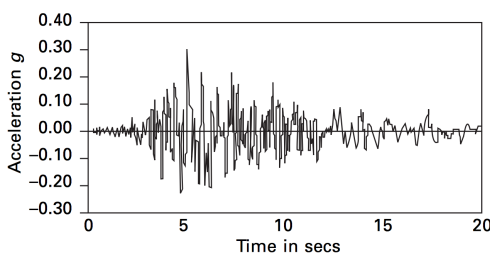
Figure 2-9: Signal of an earthquake [7]
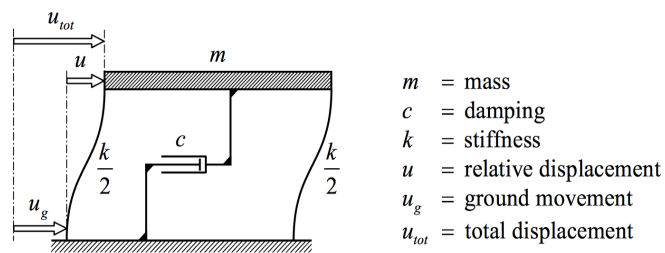
Figure 2-10: Simple 1DOF spring-dashpot system [8]

Earthquakes excite forces on structures through the base of the structure. The base movements cause inertial forces in structures, these inertial forces are dependent on the acceleration of the ground movements and the mass of the structure. The inertial forces that occur due to earthquakes are of great significance, as they determine the effect of an earthquake on a structure. The ground motion of an earthquake consists of three spatial components: two horizontal components and a vertical component. The two horizontal components are of approximately equal magnitude and the vertical component is smaller [8]. To simplify the problem, structures subjected to earthquake loading can often be represented by a single degree of freedom system (figure 2-10). The equation of motion for this system can be obtained by simply using Newton's second law of motion (equation 2.2). The general solution for the displacement in this equation of motion can be represented through a Duhamel integral (equation 2.3).

$$m\ddot{u} + c\dot{u} + ku = -m\ddot{u}_g \tag{2.2}$$

$$u(t) = \frac{1}{\omega_e \sqrt{1-\zeta^2}} \int_0^t \ddot{u}_g exp(-\zeta\omega_e(t-\tau)) sin(\omega_e \sqrt{1-\zeta^2}(t-\tau)) d\tau \tag{2.3}$$

An important parameter of a structure is the eigenfrequency, the eigenfrequency (or natural frequency) is the frequency at which a system tends to oscillate under free vibration. If the frequency of the earthquake is equal to the eigenfrequency of a structure, the displacement of the structure reaches a maximum (and thus leads to the most dangerous situation).

<div align="right">

3

</div>

PREVIOUS EXPERIMENTAL TESTS ON FLEXIBLE TIMBER DIAPHRAGMS

In this chapter, previous experimental tests will be studied in order to create a better understanding of current knowledge on flexible timber diaphragms. Both tests on as-built and retrofitted specimens will be regarded. Two experimental studies shall be discussed in this chapter, one from New Zealand from 2012 (section 3.1) and one from New Zealand from 2013 (section 3.2). From these studies, general conclusions will be drawn in section 3.3.

3.1 NEW ZEALAND, 2012

In 2012, two researchers from Italy and a researcher from New Zealand carried out experimental tests in which ten timber diaphragms were tested [9]. Three types of boundary conditions were used to test as-built and retrofitted diaphragms, with one type of boundary condition representing a non-retrofitted connection between diaphragm and walls (figure 3-1). Two as-built diaphragms and two retrofitted diaphragms were tested with this set of boundary conditions, which will be discussed in this section.
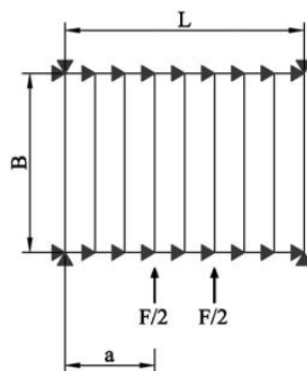
Figure 3-1: Boundary conditions [9]

3.1.1 TEST SETUP
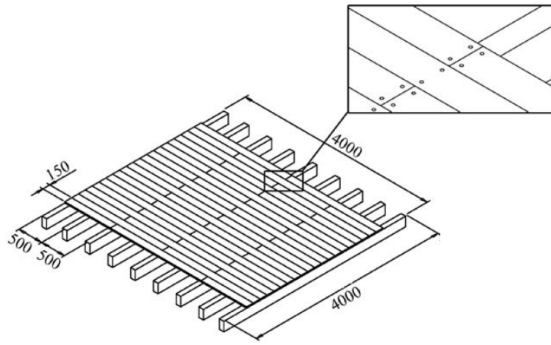
Figure 3-2: As-built specimen [9]
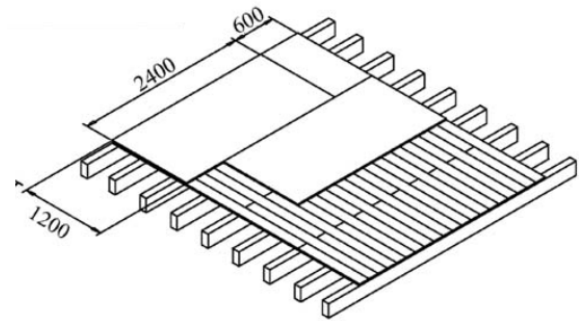
Figure 3-3: Retrofitted specimen [9]
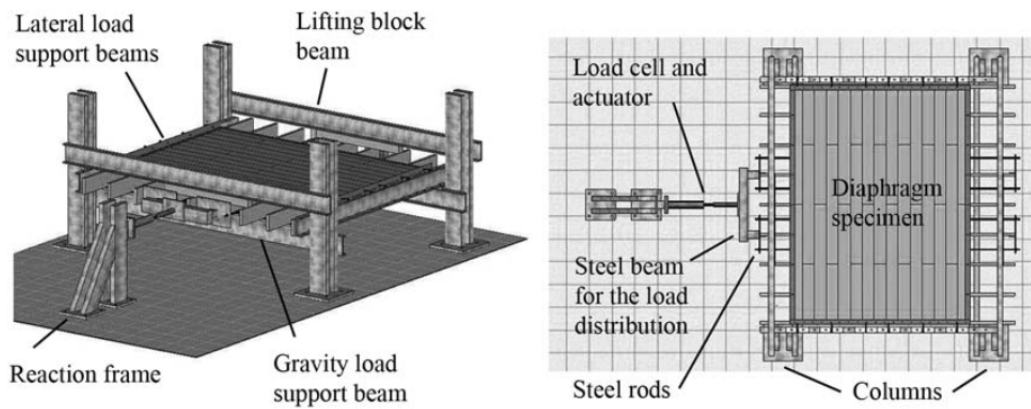
Figure 3-4: Test setup [9]

Table 3-1: Specimen specifications

Joists	Cross section (mm x mm)	50x250
	Free span (m)	3
	Centre-to-centre distance (m)	0.5
Flooring boards	Cross section (mm x mm)	25x150
	Length (m)	1 or 2
Nails	Diameter (mm)	3.15
	Number of nails at each board-joist intersection	2 or 4
Panels	Length (m)	2.4
	Width (mm)	1.2
	Thickness (mm)	19
Screws (panel to boards)	Diameter (mm)	≥4.17
	Length (mm)	50
	Spacing (mm)	150
Screws (panel to joists)	Diameter (mm)	≥4.17
	Length (mm)	120
	Spacing (mm)	150
Specimen	Width (m)	4
	Length (m)	4

Schematisations of the as-built and retrofitted floor specimens are shown in figure 3-2 and figure 3-3. Specimens were constructed with pinewood and consisted of nine joists. The flooring boards were configured in a staggered manner, thus boards of one and two meters were used. No tongue and groove connection was used to interlock the flooring boards. For the retrofitted specimens, plywood panels were screwed onto the boards and joists. The screws were placed around the perimeter of each panel. An overview of the specifications of the floor specimens is given in table 3-1.

The test setup as used in the experiments can be seen in figure 3-4. The joists of the specimens were simply supported on two steel beams. The contact surface between steel beam and timber joist was made such that sliding was permitted and that the friction forces were minimised. The end of each joist was laterally constrained to restrict in-plane rotation. The specimens were loaded cyclically parallel to the joists and the load was applied symmetrically through two joists. The amplitudes of the loading cycles were determined as a percentage of the maximum expected displacement, with loading rates between 0.1 mm/s (smallest amplitude) and 0.2 mm/s (largest amplitude). The amplitudes for the loading cycles are given as 3, 6, 12, 30, 40, 60, 80 and 100 mm. For each amplitude, one or two loading cycles were applied to the specimen. The loading pattern can be seen in figure 3-5. The experiments can be classified as cyclic quasi-static displacement-controlled tests.
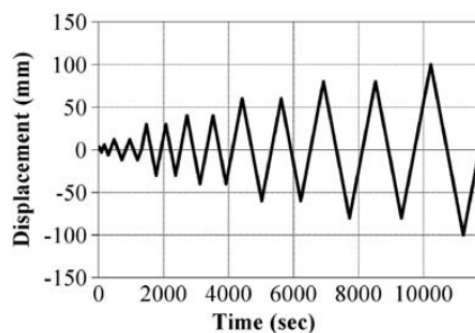
Figure 3-5: Loading pattern for the displacement-controlled experiments [9]

The response of the displacement-controlled experiments was measured using linear variable displacement transducers (LVDTs) and rotary potentiometers. A series of these sensors was placed at the end of the joists on the side of the diaphragm opposite to the forcing. The measurements on this side of the diaphragm (measured in the direction of the loading) characterise the global deformation of the diaphragm. Additionally, four rotary potentiometers were placed diagonally between the loaded joists and the outer joists to measure the shear deformation. Lastly, 42 LVDTs were placed diagonally in the middle of the diaphragm to measure the local shear deformation. The positioning of the sensors can be seen in figure 3-6.
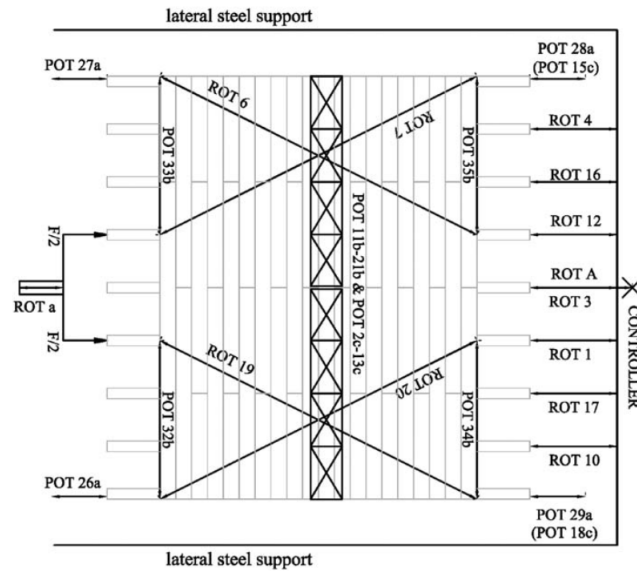
Figure 3-6: Configuration of instrumentation [9]

3.1.2 TEST RESULTS

AS-BUILT SPECIMENS

For the first as-built specimen (AB-1), failure occurred at a displacement of 100 mm and a corresponding force of 55 kN. For the second as-built specimen (AB-4), failure occurred at a displacement of 80 mm and a force of 45 kN respectively. The failure of the two as-built diaphragms in the as-built test setup can be attributed to the flexural resistance of the flooring boards. The global displacement as obtained by the sensors at the end of the joists of specimen AB-1 is given in figure 3-7 for each load cycle. It can be noted that the overall deformed shape of the diaphragm is similar to the flexural deformed shape of flooring boards only. Thus, it can be said that the diaphragm acts comparable to a beam subjected to bending.
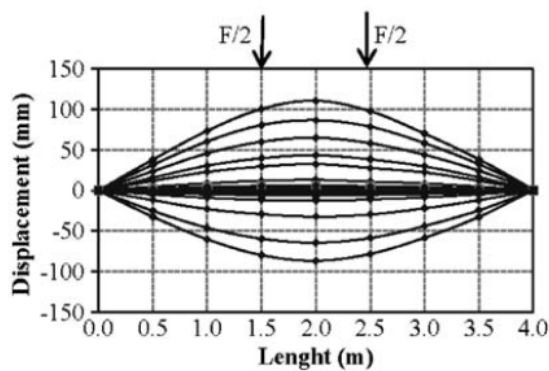
Figure 3-7: Global deformed shape of as-built specimen per cycle [9]
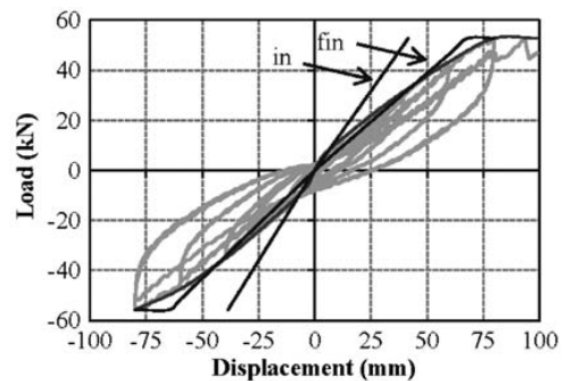
Figure 3-8: Hysteresis diagram for the midspan deflection [9]

In figure 3-8, the midspan displacement for as-built specimen AB-1 is shown. One can see that the load-displacement diagram consists of fairly linear branches and only exhibits slight pinching behaviour. For cycles with a displacement up to 3 mm, the initial stiffness was recorded to be 1.7 kN/mm. Upon increasing the displacement amplitude for successive cycles, the stiffness reduced to 0.7 kN/mm and remained so until failure. When repeating load cycles, the residual displacement

(when the force reaches zero) grows. Residual displacements can be attributed to the fact that nailed connections loosen when loaded cyclically. The nails are then no longer fully embedded in timber, resulting in a residual displacement. This behaviour also causes pinching in the hysteresis curve: the stiffness upon reloading is initially lower until the nails come in contact with the timber again.

The local angular deformations of the top layer of the diaphragms were measured using the sensors at the midspan of the specimen, these sensors were placed diagonally. The load-displacement diagrams for this set of sensors is displayed in figure 3-10 for as-built specimen AB-1. The diagonal displacements are larger near the edges of the diaphragm than in the middle of the diaphragm, which is comparable to a simple beam in bending. For all sensors at the midspan of the diaphragm, the load-displacement curves exhibit slight pinching behaviour and the curves appear to be bilinear (consisting of two near linear branches). Using the measured diagonal displacements, one can calculate an average equivalent shear stiffness. The shear deformation can be determined using the formula $\gamma = \frac{\sqrt{h_1^2 + h_2^2}}{h_1 * h_2} * \frac{d_1 - d_2}{2}$, with the parameters as in figure 3-9. The shear stiffness can then be calculated using equation 3.1. In this formula, B is the width of the diaphragm and F_{shear} is half of the total force. The shear stiffness is independent of diaphragm geometry.

$$G_d = \frac{F_{shear}}{B * \gamma} \tag{3.1}$$

Two shear stiffnesses can be calculated, related to the displacements corresponding to the two branches in the load-displacement diagram. Using the sensors (LVDTs) at midspan, shear stiffnesses of 0.36 kN/mm (for the initial displacement) and 0.22 kN/mm (for the final displacement) are found. These can be regarded as 'local' shear stiffnesses. One could also use the rotary potentiometers located between the loaded joists and outer joists to calculate equivalent shear stiffnesses. The values for the shear stiffnesses are then calculated as 0.36 kN/mm and 0.22 kN/mm and can be seen as 'global' shear stiffnesses. One can see that the values for the shear stiffnesses are the same using both measurements from the LVDTs at midspan and the rotary potentiometers near the edges of the diaphragm for specimen AB-1. A third method to determine equivalent shear stiffnesses is to use the curve of figure 3-8. This curve gives the overall displacement and corresponding load of the diaphragm, resulting in overall global shear stiffnesses. The shear stiffnesses based on this curve are 0.34 kN/mm and 0.20 kN/mm, which are very close to the values as calculated using the two previous methods.
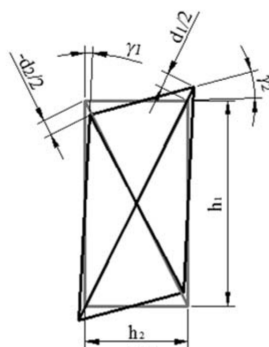
Figure 3-9: Determination of shear deformation [9]
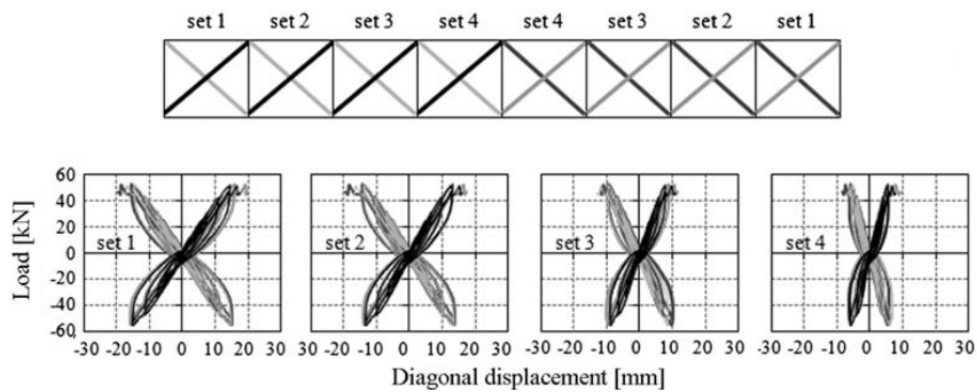
Figure 3-10: Load versus diagonal displacement diagrams for the midspan sensors of specimen AB-1 [9]

Table 3-2: Shear stiffnesses of as-built specimens

	Overall global shear stiffness G_1 (kN/mm)		Global shear stiffness G_2 (kN/mm)		Average local shear stiffness G_3 (kN/mm)	
Specimen	Initial	Final	Initial	Final	Initial	Final
AB-1	0.34	0.20	0.36	0.22	0.36	0.22
AB-4	0.33	0.20	0.33	0.20	0.32	0.20

For specimen AB-4 (the second as-built specimen tested with as-built boundary conditions), similar values for shear stiffnesses are found as for specimen AB-1. The shear stiffnesses calculated using three different methods are summarised in table 3-2. The local and global shear stiffnesses are related to the deformation of the top layer of the diaphragm, whereas the overall global shear stiffnesses are related to the overall behaviour of the diaphragm. From the table, it can be seen that the shear stiffnesses are very close using the three calculation methods for both specimens. Thus, it can be concluded that the global and mean local shear stiffnesses are congruent for an as-built diaphragm.

RETROFITTED SPECIMENS

For the first retrofitted specimen (R-1), failure occurred at a displacement of 80 mm and a corresponding force of 150 kN. For the second retrofitted specimen (R-4), failure occurred at a displacement of 100 mm and a force of 175 kN respectively. The failure of the two retrofitted diaphragms can be attributed to the failure of the screws connecting the panels to the boards and joists. The global displacement as obtained by the sensors at the end of the joists of specimen R-1 is given in figure 3-11 for each load cycle. The overall deformed shape is less smooth than for the as-built diaphragm, which can be attributed to shear deformation being more dominant than flexural deformation.
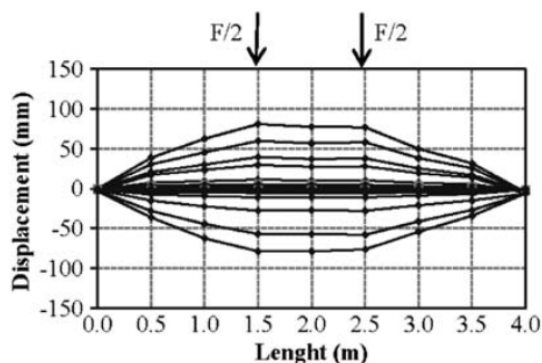
Figure 3-11: Global deformed shape of retrofitted speci-men per cycle [9]
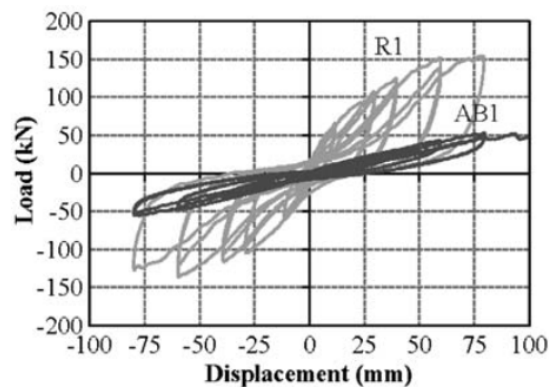
Figure 3-12: Hysteresis diagram for the midspan deflec-tion of specimen R-1 and AB-1 [9]

In figure 3-12, the midspan displacement for retrofitted specimen R-1 is shown. The hysteresis of the retrofitted diaphragm is highly nonlinear and exhibits pinching behaviour. One can see that the strength and the stiffness of the retrofitted diaphragm is far greater than for the as-built specimen. Initially, the stiffness of the retrofitted diaphragm is high, before decreasing after a certain displace-ment. The strength of the retrofitted specimen degrades before ultimately failing.

The local angular deformations at the midspan of retrofitted specimen R-1 can be seen in figure 3-13. These diagrams are less consistent and show more variability than the diagrams of the as-built specimen. For the retrofitted specimen, the top layer deformation is lumped into the joints between panels. The sensors which are placed on the same panel exhibit close to zero deformations. The cal-culated shear stiffnesses for specimens R-1 and R-4 can be seen in table 3-3. As expected, the overall global shear stiffness differs very much from the local shear stiffness for the retrofitted specimens. This is due to the concentrated displacements between the panels. The global and local shear stiff-ness related to the top layer of the diaphragms are quite similar to each other. For both retrofitted specimens, the overall global shear stiffnesses are similar.
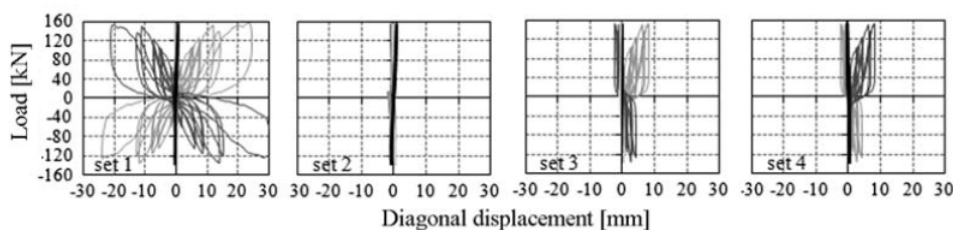
Figure 3-13: Load versus diagonal displacement diagrams for the midspan sensors of specimen R-1 [9]

Table 3-3: Shear stiffnesses of retrofitted specimens

	Overall global shear stiffness G_1 (kN/mm)		Global shear stiffness G_2 (kN/mm)		Average local shear stiffness G_3 (kN/mm)	
Specimen	Initial	Final	Initial	Final	Initial	Final
R-1	1.66	0.90	5.57	2.21	5.62	2.51
R-4	1.60	0.87	-	-	2.91	2.29

3.1.3 Side notes

The experimental study as discussed in this section also considers varying boundary conditions, which are not considered in this report. A short summary of the experimental results implementing these boundary conditions will be given in this subsection. If one wishes to elaborate this matter further in a later stage, one can refer back to this experimental study for an extension of knowledge.

The varying boundary conditions as adopted in the experiments are meant to represent the different connections that exist between floor and wall in reality. One of the boundary conditions involved applying a steel chord around the perimeter of the floor, increasing the strength and stiffness of the floor. An other boundary condition implemented flexible supports to the joists instead of rigid supports. This type of boundary condition reduced the ductility and strength of the floor unit, as failure can then also occur in the connectors instead of the diaphragm. As a last boundary condition, steel strips were added to the test setup to reduce the slip between boards or panels. These strips increase the initial stiffness, but the ultimate strength remains roughly the same.

The study showed that the in-plane stiffness of a floor unit is indeed dependent on the stiffness of the diaphragm and the stiffness of the floor-to-wall connectors. The system of diaphragm and connectors are in series. It is worth noting that the resistance of a floor unit is dependent on various parameters, such as the diaphragm configuration, the nails and screws which are used and the type of wall-to-floor connection. Due to this dependence, it is hard to predict the ultimate strength of a floor unit beforehand. Laboratory tests are necessary to verify the actual behaviour of a floor unit.

3.2 New Zealand, 2013

In 2013, three researchers from New Zealand performed experimental tests on as-built and retrofitted diaphragms [10]. The diaphragms were tested perpendicular to the joists as well as parallel to the joists. In addition, the researchers also tested diaphragms with discontinuous joists and diaphragms with a non-rectangular floor plan. Discontinuous joists are often found in diaphragms with larger spans, such that a single joist cannot cover the whole span. Diaphragms with non-rectangular floor plans represent the opening in a floor for a stairwell as found in higher storeys. Two as-built regular diaphragms and two retrofitted regular diaphragms (that is, diaphragms with rectangular floor plans) were tested parallel and perpendicular to the joists. These diaphragms shall be regarded in this section.

3.2.1 Test setup

One as-built rectangular diaphragm was tested parallel to the joists and one as-built rectangular diaphragm was tested perpendicular to the joists. These specimens were labelled 1a-PARA and 1a-PERP respectively. The same tests were carried out for two retrofitted rectangular diaphragms, labelled 1b-PARA and 1b-PERP respectively. Each specimen measured 10.4 m x 5.5 m and was constructed using 27 joists. Joists were oriented parallel to the edge of 5.5 m and sheathing boards were oriented parallel to the edge of 10.4 m. For the retrofitted specimens, plywood panels and stapled sheet metal blocking were fastened onto the boards and joists. The plywood panels were fastened through field nailing (at the location of the joists) and additional nailing along the perimeter of the diaphragm was applied. Sheet metal straps were placed on the plywood panel edges through staples. Furthermore, retrofitted diaphragms were fitted with chords to absorb tensile and compressive forces. Specimen 1b-PARA implemented compression and tension chords. Compression chords were introduced by nailing full-depth blocking between the joists, whereas tension chords comprised 40x6 mm steel flats fastened to the timber blocking with 7x3.57 mm screws at a centre-to-centre distance of 100 mm. For specimen 1b-PERP, only full-depth blocking was fastened between

the joists along the edges of the diaphragm. Detailed specifications of the specimens are given in
table 3-4. Schematisations of the as-built and retrofitted specimens can be seen in figure 3-14 and
figure 3-15. Note that in these figures, the upper right corner of the diaphragm is absent to illustrate
a diaphragm with irregular floor plan. For the experimental tests which are regarded in this section,
the upper right corner is still present and thus the diaphragm remains rectangular.

Table 3-4: Specimen specifications

Joists	Cross section (mm x mm)	45x290
	Centre-to-centre distance (mm)	400
Flooring boards	Cross section (mm x mm)	135x18
Nails	Number of nails at each board-joist intersection	2
	Diameter (mm)	3.15
	Length (mm)	75
	Spacing (mm)	95
Plywood panels	Length (mm)	2400
	Width (mm)	1200
	Thickness (mm)	15
Nails for the panels	Diameter (mm)	3.15
	Length (mm)	75
	Field nailing spacing (mm)	300
	Diaphragm edge nail spacing (mm)	100
Sheet metal straps	Length and diameter (mm x mm)	75x0.635
Staples	Centre-to-centre distance (mm)	100
	Wire cross section (mm x mm)	1.24x1.00
	Wire leg length (mm)	15
Specimen	Measurements (m x m)	10.4x5.5
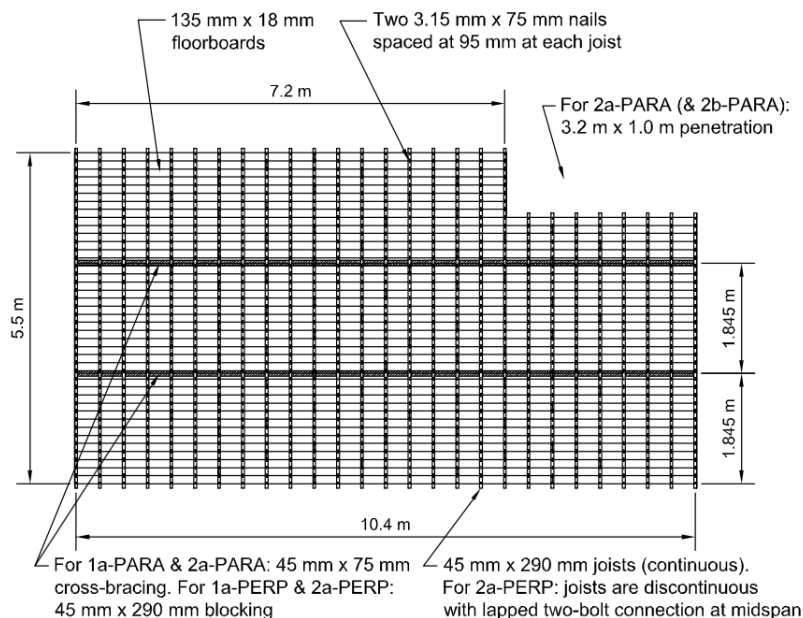
Figure 3-14: Schematisation of as-built specimen [10]
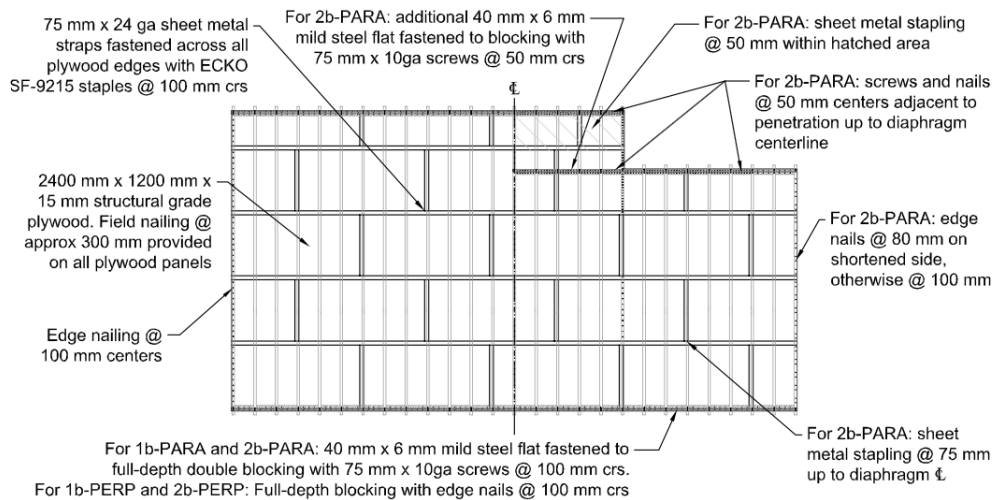
Figure 3-15: Schematisation of retrofitted specimen [10]

Two test setups have been adopted in order to load the diaphragms in the two in-plane directions (see figure 3-16). For the test setup for loading parallel to the joists, loading was applied through a truss and beam structure. Two beams were attached to the truss and the truss was attached to the actuator. The two beams distributed four equal forces onto the specimen through the joists. The loaded joists were selected such that a parabolic load distribution was realised. The beams were enabled to rotate with the deforming diaphragm, preventing the setup from applying bending moments onto the specimen. Post-tensioned loaders were placed at both ends of the loaded joists to impose cyclic loads. This type of loading also represents the inertial forces which are excited on diaphragms from shear walls. Lateral constraint was provided by bolting the outer joists onto steel sections, which were fastened to the laboratory floor. The bolted connection between steel and timber were constructed such that almost no slip occurred. By fastening the steel sections to the floor, movements of the outer joists were constrained. To provide vertical support, the ends of the joists were supported on steel sections which were bolted to the floor. The friction between these steel sections and the joists were minimised such that the diaphragm could deform freely. Additionally, specimens to be loaded parallel to the joists were fitted with timber cross bracings (45x75 mm) at one third of the joist length to prevent lateral joist buckling.

For the test setup to load specimens perpendicular to the joists, loading was applied through a truss structure. The truss distributed two equal loads onto the diaphragm through its joists using joist loaders. The positioning of these loads were selected again such that a parabolic load distribution was realised. Post-tensioned loaders were used again to achieve cyclic loading. Lateral support was provided by inserting the ends of the joists into pockets in unreinforced masonry (URM) walls. Two URM walls were placed along the two longitudinal edges of the specimen to represent realistic boundary conditions. However, the pockets were not filled with mortar, thus the diaphragm to wall connection was relatively weak. The constructed URM walls were six bricks high, two bricks wide and 11.5 metres in length. The cross section of the walls measured 600x230 mm. The pockets for the joists were one brick deep and 49 mm wide. The centre-to-centre distance between the pockets was 400 mm. The URM walls were fixed to the laboratory floor and sliding between the walls and floor was prevented. The URM walls were not tested on their strength, as it was not the purpose of the experimental campaign.

The instrumentation used to measure the deformation of the specimens can be seen in figure 3-16. For both test setups, three string potentiometers were placed at the edge opposite of the loading. Quasi-static cyclic loading was applied to the specimens, with each midspan displacement amplitude repeated for three cycles. The amplitudes of the displacements were 2.5, 5, 15, 25, 50, 75, 100 and 150 mm. The average rate of load application was 20 mm/min.

(a) Loading parallel to the joists [10]

(b) Loading perpendicular to the joists [10]
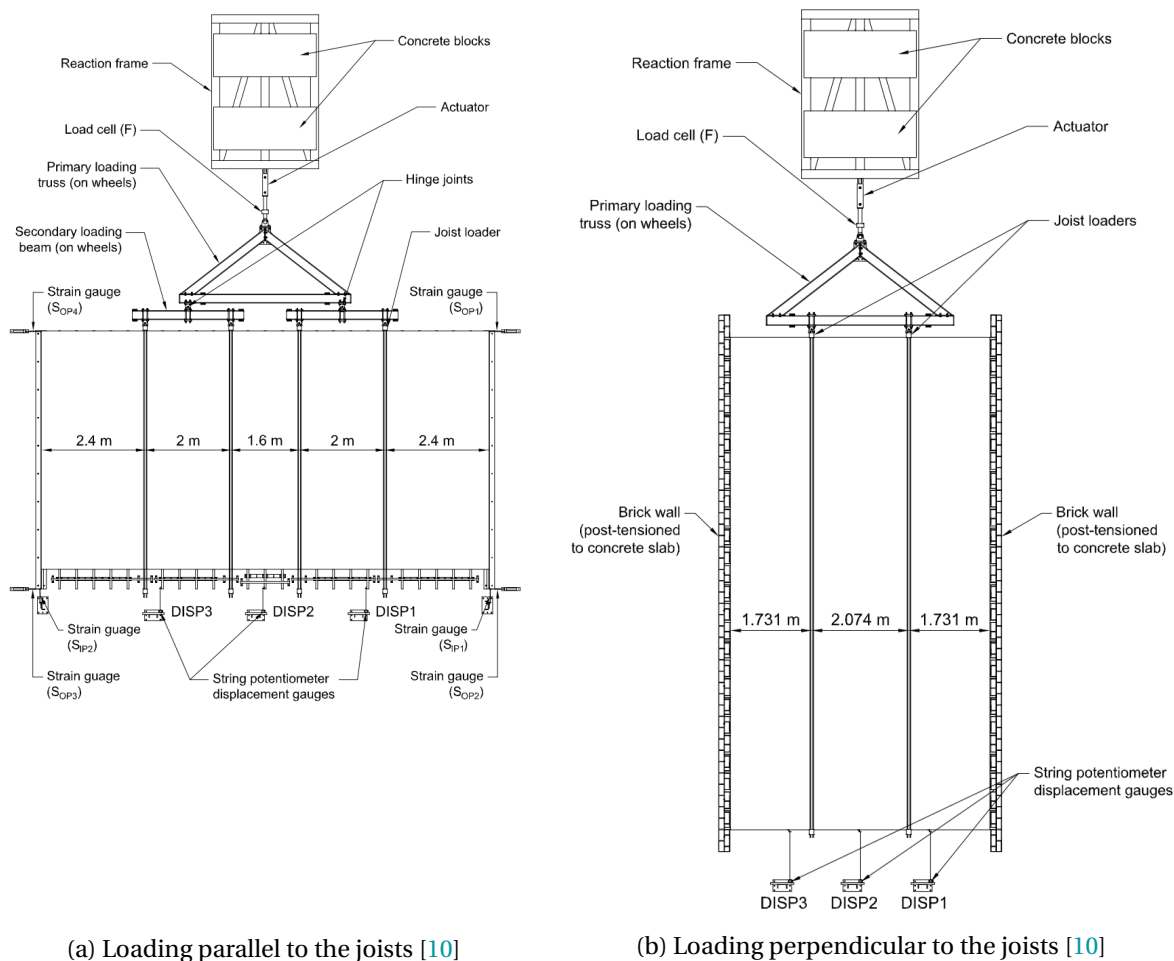
Figure 3-16: Test setups and instrumentation [10]

3.2.2 Test results

As-built specimens

The force-displacement relationship for the two as-built diaphragms (specimens 1a-PARA and 1a-PERP) can be seen in figure 3-17. These specimens were not tested until failure, thus an ultimate strength cannot be concluded. The maximum displacement and maximum load that were reached for specimen 1a-PARA measured 193 mm and 36.8 kN respectively. For specimen 1a-PERP, a maximum displacement of 148.7 mm and a maximum load of 102.9 kN were reached. As the diaphragms barely degraded (due to high flexibility), little strength losses were found between successive cycles of the same amplitude. The joists could rotate freely in the pockets in the URM walls up to a midspan displacement of 50 mm. For loading parallel to the joists, the deformation was governed by the flexural bending of the boards, whereas for loading perpendicular to the joists, the deformation was determined by the joists. For both loading directions, shear deformation occurred in the nailed connections between boards and joists, which contributed to the overall resistance of the

specimens.
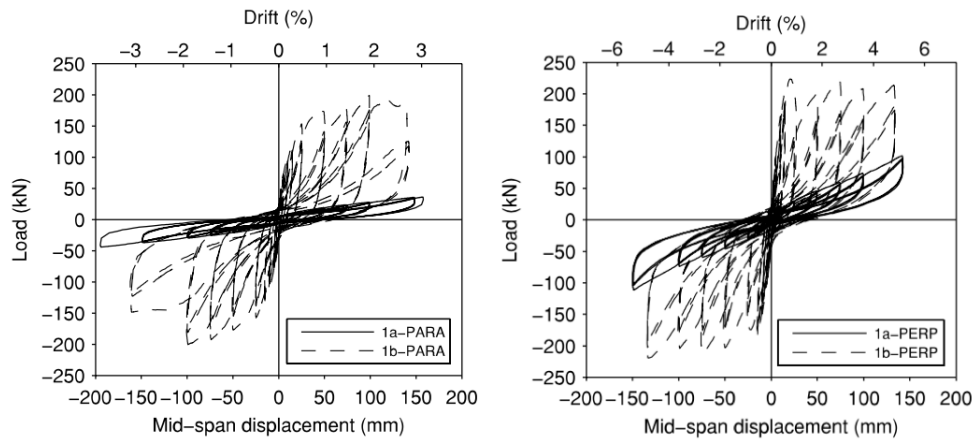
Figure 3-17: Force-displacement curves for specimen 1a-PARA and 1a-PERP [10]

From figure 3-17, it can be seen that the in-plane stiffness of an as-built diaphragm is higher when loaded perpendicular to the joists as opposed to loading parallel to the joists. At first, the hysteresis curves of the as-built diaphragms seem fairly linear, but they exhibit nonlinear behaviour if one takes a closer look. Slight pinching behaviour can be seen as the nailed connections do degrade to a certain extent. The backbone of the hysteresis curves exhibit roughly two branches, with the first branch being highly nonlinear (due to the nailed connections) and the second branch being near linear. The backbone curve for as-built specimens can be represented through a bilinear model which conserves the same energy as the original curve (see figure 3-18). The first linear segment is valid up until the so-called yield displacement, even though there is no distinct yield point in the backbone curve. The second linear segment has a lower slope than the first segment and is valid up until the maximum or ultimate displacement. The slope of the second linear segment is taken as the average gradient of the backbone curve for displacements above 50 mm. The backbone curve for specimen 1a-PARA can be seen in figure 3-19, along with its bilinear representation. For this specimen, the yield displacement is 26.8 mm and the initial stiffness and final stiffness are calculated as 0.644 kN/mm and 0.159 kN/mm respectively. For specimen 1a-PERP, the yield displacement is found as 16.9 mm with an initial stiffness of 1.605 kN/mm and a final stiffness of 0.569 kN/mm. From these results, it can be seen that the yield point for loading perpendicular to the joists occurs at a lower displacement than for loading parallel to the joists. From the initial stiffnesses, the shear stiffnesses can be determined for the two specimens. The shear stiffness is calculated using:

$$G_d = \frac{K_d(a + \frac{b}{2})}{2B} \tag{3.2}$$

In which K_d is the initial stiffness of the bilinearisation of the backbone, a is the distance between the side of the diaphragm and the first point load, b is the distance between the first and second point load and B is the width of the diaphragm. With above formula, the shear stiffness is independent of diaphragm geometry and thus can be compared between various diaphragm configurations. The shear stiffnesses are calculated as 0.198 kN/mm and 0.134 kN/mm for specimens 1a-PARA and 1a-PERP respectively. One can see that the shear stiffness is lower for a specimen loaded perpendicular to the joists as opposed to a specimen loaded parallel to the joists, even though the in-plane initial and final stiffnesses are higher. The results for both specimens are summarised in table 3-5. However, the results as presented in this subsection do not give solid conclusions as only one specimen was tested parallel to the joists and only one specimen was tested perpendicular to the

joists.
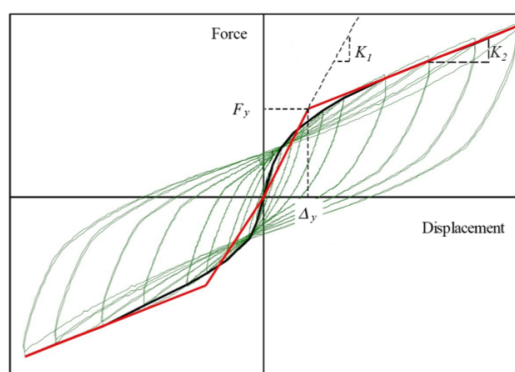
Figure 3-18: Bilinear representation of backbone curve [10]
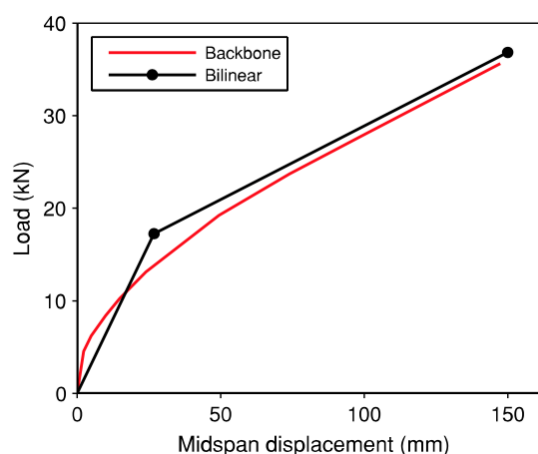
Figure 3-19: Backbone curve and bilinear representation for specimen 1a-PARA [10]

Table 3-5: Values for bilinear representation of specimens 1a-PARA and 1a-PERP

			Initial stiffness			Final stiffness	Shear stiffness
	F_y	Δ_y	K_1	F_{max}	Δ_{max}	K_2	G
Diaphragm	*(kN)*	*(mm)*	*(kN/mm)*	*(kN)*	*(mm)*	*(kN/mm)*	*(kN/mm)*
1a-PARA	17.2	26.8	0.644	36.8	193.0	0.159	0.198
1a-PERP	27.0	16.9	1.605	102.9	148.7	0.569	0.134

RETROFITTED SPECIMENS

The force-displacement relationship for the two retrofitted diaphragms (specimens 1b-PARA and 1b-PERP) can be seen in figure 3-17. For specimen 1b-PARA, failure occurred at a displacement of 149.9 mm and a force of 175.8 kN. Specimen 1b-PERP failed after reaching a displacement of 132.6 mm and a load of 204.7 kN. The hysteresis of the retrofitted diaphragms exhibit a high degree of pinching behaviour and strength losses can be seen between cycles of the same amplitude. The high initial stiffness can be attributed to the sheet metal blocking which transfers forces between the panels. A more defined yield point can be seen for the retrofitted diaphragms, as the secondary stiffness is significantly lower than the initial stiffness.

For the retrofitted diaphragms, the in-plane stiffness is higher when loading is applied perpendicular to the joists as opposed to loading parallel to the joists. This is similar to the as-built specimens. The nonlinear behaviour is more evident when regarding retrofitted diaphragms, with the backbone curve strongly degrading as the amplitude increases. The backbone curve of retrofitted diaphragms can be represented through a bilinear curve which conserves the same energy as the original curve. For retrofitted diaphragms, the bilinear curve for the backbone is an elastic-plastic curve, meaning that the secondary stiffness is equal to zero. The principle for obtaining the bilinear curve is shown in figure 3-20. For specimen 1b-PARA, the initial stiffness is calculated as 14.518 kN/mm with a yield displacement of 12.1 mm. For specimen 1b-PERP, the initial stiffness is 22.409 kN/mm with a yield displacement of 9.1 mm. Similar to the as-built specimens, the yield point occurs at a lower displacement for loading perpendicular to the joists than for loading parallel to the joists for the retrofitted diaphragms. From the initial stiffnesses, the shear stiffnesses can be determined

for the two specimens. The shear stiffnesses are calculated as 4.459 kN/mm and 1.864 kN/mm for specimens 1b-PARA and 1b-PERP respectively. One can see that the shear stiffness is lower for a specimen loaded perpendicular to the joists as opposed to a specimen loaded parallel to the joists, even though the in-plane initial stiffness is higher. The results for both specimens are summarised in table 3-6. However, the results as presented in this subsection do not give solid conclusions as only one specimen was tested parallel to the joists and only one specimen was tested perpendicular to the joists.
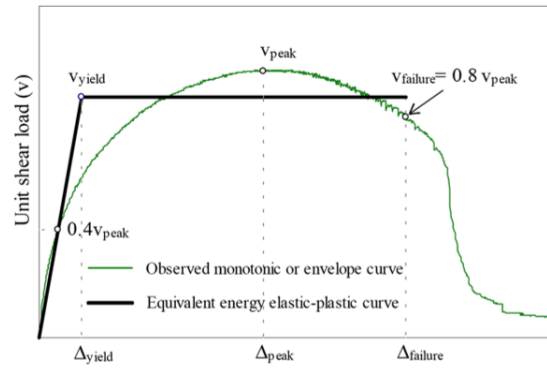
Figure 3-20: Bilinear representation of backbone for retrofitted diaphragms [10]

Table 3-6: Values for bilinear representation of specimens 1b-PARA and 1b-PERP

			Initial stiffness			Final stiffness	Shear stiffness
Diaphragm	F_y (kN)	Δ_y (mm)	K_1 (kN/mm)	F_{max} (kN)	Δ_{max} (mm)	K_2 (kN/mm)	**G** (kN/mm)
1b-PARA	175.8	12.1	14.518	175.8	149.9	0	4.459
1b-PERP	204.7	9.1	22.409	204.7	132.6	0	1.864

Comparing the results from the retrofitted specimens to the results from the as-built specimens, one can see that the in-plane (shear) stiffnesses are much higher if the diaphragm is strengthened. For loading parallel to the joists, the shear stiffness of the retrofitted specimen is more than 20 times higher than for the as-built specimen. For loading perpendicular to the joists, the shear stiffness of the retrofitted specimen is more than 10 times higher than the as-built specimen. One can see that the improvement resulting from added plywood panels seems to be greater in the direction parallel to the joists as opposed to the direction perpendicular to the joists. This may be due to the orientation of the plywood panels relative to the flooring boards, causing localised shear flow weaknesses. Overall, the plywood panels and sheet metal blocking system performed well, but this retrofit method is prone to serviceability issues.

3.2.3 SIDE NOTES

The experimental campaign as discussed in this section also considered diaphragms with discontinuous joists and diaphragms with non-rectangular floor plans. The results of these tests shall be discussed concisely in this subsection, though it is not the primary focus of this report. These results may however be useful if additional subquestions are regarded in a later stage.

As-built and retrofitted diaphragms with non-rectangular floor plans were tested parallel to the joists. Non-rectangular floor plans were obtained by removing a segment of 3.2x1.0 m from the

corner of a diaphragm (6% of total area) in order to represent stairwell openings. For both as-built and retrofitted diaphragms it was found that a stairwell opening does reduce the shear stiffness slightly, however it does not have severe consequences for its performance. It is worth noting that for retrofitted diaphragms, the retrofit should be performed well around the stairwell opening to prevent unnecessary strength loss.

Additionally, as-built and retrofitted diaphragms with discontinuous joists were tested perpendicular to the joists. The discontinuous joists had a two-bolt lapped connection at midspan, thus creating a discontinuous beam. Such beams are often found for larger spans as a single beam cannot cover the whole length. During testing, the two-bolt lapped connection exhibited no damage. Surprisingly, specimens with discontinuous joists exhibited an increase in shear stiffness, with this increase being more substantial for retrofitted specimens. Loading perpendicular to the joists imposes a large bending moment on the joists, thus it is expected that a discontinuity would have a negative effect on the resistance. The tests from this campaign show no detrimental effect of discontinuous joists on diaphragm performance, however this may be due to favourable circumstances. Further tests are desirable to accurately investigate the effect of discontinuous joists.

3.3 CONCLUSIONS

Experimental studies on flexible timber diaphragms have been carried out in the past, however these studies are scarce and comprehensive data is lacking. Due to the scarceness of previous studies, it is difficult to give conclusive statements regarding diaphragm behaviour. More studies are needed to accurately capture the behaviour of flexible timber diaphragms and to determine characteristic parameters. These studies will also aid in improving existing standards, as these standards often over- or underestimate diaphragm parameters. The conditions of previous experiments vary for different experimental campaigns, making it complicated to compare test results. Different campaigns may develop different boundary conditions to which a specimen is subjected. Additionally, the loading may differ between campaigns, resulting in varying load distributions (uniform, parabolic). Furthermore, the used materials and specimen geometry may be different between experiments.

For the studies as discussed in this chapter, the test setups and specimen geometry differed. A summary of the differences between the study in New Zealand from 2012 and the study in New Zealand from 2013 is given in table 3-7. Only experiments in which loading was applied parallel to the joists are considered in this section for comparison purposes. Both studies implemented comparable boundary conditions, with the outer joists being restrained from movement and the rest of the diaphragm being able to deform nearly frictionless on its supports. The global shear stiffnesses are very similar for the as-built specimens in both studies, having a value of approximately 0.20 kN/mm. This may be attributed to the fact that the nails used in specimens from both studies have the same diameter and that the cross section of the joists and boards do not differ too much. For cyclically loaded as-built diaphragms, the hysteresis curve is often largely near linear and shows little pinching behaviour. The nonlinearities within a diaphragm can mostly be attributed to the behaviour of nailed connections between joists and sheathing. For retrofitted diaphragms, the in-plane stiffnesses were higher than for as-built diaphragms in both studies. The shear stiffnesses for the retrofitted diaphragms differ very much in both studies, with the study from 2013 obtaining a much larger shear stiffness than the study from 2012. Furthermore, the increase in shear stiffness when retrofitting the specimens is much higher for the study of 2013. For the study of 2012, the increase in shear stiffness is about 300 to 400 percent, whereas the increase is about 2200 to 2300 percent for the study of 2013. This difference in increase can be attributed to the fact that the study

of 2013 implemented a sheet metal blocking system, benefitting the shear flow between panels and thus increasing the stiffness of the diaphragm. The hysteresis for retrofitted diaphragms exhibits a higher degree of pinching behaviour and evident strength losses can be seen between successive cycles of the same amplitude. The behavioural nonlinearity is much more visible for retrofitted diaphragms, as more nailed or screwed connections are present.

Table 3-7: Comparison between experimental tests

	New Zealand, 2012	New Zealand, 2013
Specimen dimensions (m x m)	4.0x4.0	10.4x5.5
Cross section of joists (mm x mm)	50x250	45x290
Cross section of boards (mm x mm)	25x150	18x135
Diameter of nails (mm)	3.15	3.15
Number of loaded joists	2	4
Number of cycles per load amplitude	2	3
Load amplitudes (mm)	3, 6, 12, 30, 40, 60, 80, 100	2.5, 5, 15, 25, 50, 75, 100, 150
Rate of load application	0.1-0.2 mm/s	20 mm/min
Number of as-built specimens tested parallel to the joists	2	1
Failure of as-built specimens	Yes	No
Global shear stiffness of as-built specimens (kN/mm)	0.20	0.198
Number of retrofitted specimens tested parallel to the joists	2	1
Failure of retrofitted specimens	Yes	Yes
Global shear stiffness of retrofitted specimens (kN/mm)	0.90, 0.87	4.459

From the studies in this chapter, it can be concluded that an as-built diaphragm loaded parallel to the joists often behaves comparable to a bending beam, provided that the sheathing boards are sufficiently interlocked. The deformation of such a diaphragm is mostly dependent on the flexural deformation of the sheathing boards and the deformation of the nailed connections. Additionally, it can be said that retrofitted diaphragms have increased in-plane stiffnesses, though the increase depends on the retrofit method. Furthermore, the backbone of the hysteresis curve of a cyclically loaded as-built and retrofitted diaphragm can be represented through a bilinear curve. The gradients of the segments of this curve can be determined through experimental tests. The shear stiffness is a favourable parameter to compare different diaphragms, as this parameter is independent from diaphragm geometry and characterises the in-plane behaviour of a diaphragm. In both studies from this chapter, the shear stiffness is calculated such that it is independent from diaphragm geometry, enabling comparisons between the studies. However, both studies used different formulas for the calculation of the shear stiffness and therefore they may not be entirely comparable.

4

NUMERICAL THEORY

This chapter will deal with the numerical theory that is needed to construct models of flexible timber diaphragms. In the first section (section 4.1), general knowledge regarding the idealisation of a flexible timber diaphragm will be provided. Section 4.2 will give an overview of previous numerical modelling of flexible diaphragms. Hereafter, section 4.3 and section 4.4 will discuss the roles of the sheathing boards and joists in the models of diaphragms. Section 4.5 to 4.7 will deal with the nonlinear aspects within a diaphragm, with section 4.5 focussing on the nailed connections between sheathing and joists. Section 4.6 will regard friction between sheathing boards. Closing off the sections regarding nonlinearities, section 4.7 deals with the connection between masonry wall and diaphragm. Different approaches to implement earthquake loading in numerical models will be discussed in section 4.8. Lastly, section 4.9 regards different FEM-softwares which may be suitable for modelling flexible timber diaphragms.

4.1 MODELLING A FLEXIBLE TIMBER DIAPHRAGM

A flexible diaphragm can be regarded as a plate and thus two in-plane directions and one out-of-plane direction can be distinguished. However, the out-of-plane behaviour of the diaphragm is of lesser importance for the purpose of this report and will be neglected hereafter. The two in-plane directions have different properties due to the orientation of the joists and sheathing, hence the diaphragm will exhibit different behaviours in these two directions. As mentioned previously, the in-plane behaviour of a diaphragm is governed mostly by its in-plane stiffness. For the direction parallel to the joists, the in-plane stiffness is dependent on the in-plane bending of the sheathing boards and the slip in nailed connections. For the direction perpendicular to the joists, the in-plane stiffness is dependent on the bending of the joists around the weakest axis and the slip in nailed connections. Generally, the following three properties play a significant part in the in-plane behaviour of a timber diaphragm:

- E_x Young's modulus in x-direction
- E_y Young's modulus in y-direction
- G Shear modulus

31

In a finite element model of a timber diaphragm, one can identify two main parts, namely the joists and the sheathing. However, one must also consider the interfaces, such as the nailed connections between joists and sheathing and possible friction surfaces. Furthermore, the boundary conditions and the loading must be implemented correctly.

4.1.1 NONLINEAR COMPONENTS

Nonlinear components can have a great effect on the overall response of a structure and may even be the decisive factor for structural failure. Thus, these nonlinear components are of importance when modelling the behaviour of a structure and must be distinguished beforehand. Nonlinear components also restrict the number of computation methods that can be used in finite element analyses. When considering a flexible timber diaphragm, nonlinearities often arise from friction surfaces and from joints (interfaces), but can also arise if yielding of the materials is reached. Components of a diaphragm that can cause nonlinear behaviour are:

- Connection between sheathing and joist
- Connection between sheathing/joists and panels (in case of retrofitted diaphragm)
- Friction between sheathing boards
- Connection between floor and wall

These nonlinear components will be elaborated later in this chapter. Only the connections between sheathing, joists and panels are regarded for the numerical models in this thesis.

4.1.2 CONNECTING THE DIAPHRAGM TO THE HOUSING

The response of a diaphragm cannot be isolated completely, as it also depends on the housing and the overall structure in which the diaphragm is located. Thus when considering a diaphragm only, the boundary conditions follow from the surrounding structure and one must resolve how to model this appropriately. The forces on the diaphragm resulting from base excitation at structure level must be well represented in this model. For this report, the response of a diaphragm in an unreinforced masonry building is considered. The effect of the masonry housing on diaphragm behaviour can be expressed through boundary conditions or by designing a (simple) auxiliary system to support the diaphragm.

4.2 PREVIOUS MODELLING

In the past, few numerical models have been constructed to represent the behaviour of a timber diaphragm. These models were constructed using different FEM-softwares and yielded varying results. In the following subsections, previous numerical representations of diaphragms will be discussed. In conclusion, a short summary will be given.

4.2.1 TEXAS, 2003

In 2003, researchers D.F. Peralta, J.M. Bracci and M.B. Hueste in Texas constructed FEM-models of as-built and retrofitted diaphragms in correspondence with their experimental results [11]. As-built specimens consisted of joists, sheathing boards, nailed connections between joists and boards, and bridging between joists. The bridging elements will not be regarded in this section, as they are irrelevant for the purpose of this report. Retrofitted specimens were obtained by nailing plywood panels onto as-built specimens. The constructed numerical models assumed linear elastic material models for the sheathing, boards and bridging. The only nonlinearities were the ones arising from nailed connections. Friction and mechanical interaction within the diaphragm were neglected.

FEM-software ABAQUS was used for the numerical models, in which the sheathing boards and plywood panels were modelled through 8-noded rectangular plane stress elements. These quadratic elements have two degrees of freedom per node: u_x and u_y. The joists were modelled as Timoshenko beam elements with three degrees of freedom per node (u_x, u_y and ϕ_z). The required input parameters for the sheathing boards and joists are the Young's modulus, the density and the Poisson's ratio. For the plywood panels, no density input is required. The material properties were taken from wood databases and were not measured during the experiments, so each board and joist were given the same properties. Both the joists and sheathing boards were given isotropic properties. The nailed connections between sheathing and joist were modelled differently for the monotonic and cyclic analysis. For the monotonic analysis, joint elements were used, whereas a user-defined element was used for the cyclic analysis. The backbone of the nailed connections was dependent on the member in which the head of the nail was positioned. If this member was a sheathing board with straight or tongue and groove edges, the backbone was based on an empirical logarithmic equation as proposed by McLain. The parameters in this equation are dependent on the specific gravities of the timber members. McLain has proposed values for these parameters for different species of wood with standard nails. These values are supported by experimental tests. If the member in which the head of the nail is located was a plywood panel, the backbone curve was based on a polynomial equation as proposed by the Engineered Wood Association (APA). For the hysteresis of the nailed connections, a three-parameter model was adopted. This model implements a trilinear backbone curve which conserves the same energy as the original backbone curve. Three characteristics were of importance for the modelling of the hysteresis, namely the stiffness degradation, strength deterioration and pinching behaviour. Upon unloading, the hysteresis path moves to a defined point until it reaches zero force (figure 4-1a). When reloaded (force changes sign), the target point is lowered along the previous unloading line such that pinching behaviour is simulated. After the wood comes in contact with the nail again, the stiffness increases in the reloading branch and moves towards the initial target point (see figure 4-1b). Strength deterioration is defined through a parameter related to the hysteretic energy (see figure 4-1c). Cycles with the same amplitude then show strength loss as the maximum force decreases for each cycle. The parameters which were needed to define the hysteresis model were obtained through iteration, fitting the numerical result to experimental data. To simplify the FEM-modelling, nails were modelled at the edges of the boards, meaning that the spacing is larger in the numerical model.
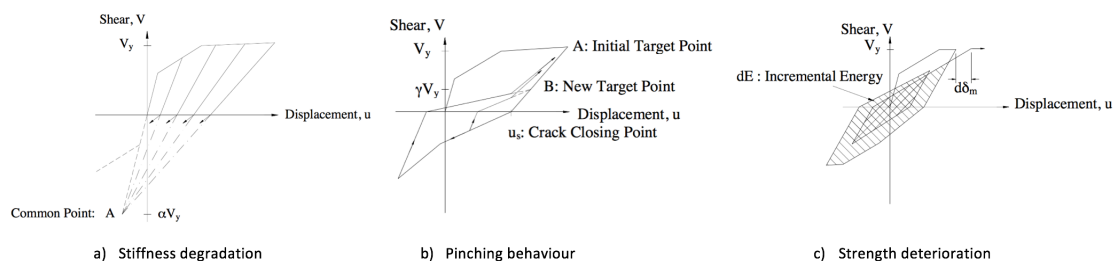
Figure 4-1: Hysteresis model adopted in ABAQUS [11]

The constructed FEM-models were subjected to displacement controlled quasi-static monotonic and cyclic analyses. Numerical results were shown to underestimate diaphragm stiffness and strength for both as-built and retrofitted configurations. Furthermore, energy dissipation was lower as compared to experimental results. This may be attributed to the lack of implementation of frictional forces between sheathing boards (and joists). It is worth noting that the adopted hysteresis model for the nails has a great impact on numerical results, thus this model may be altered to obtain better results. The study showed that the model for the nailed connections performed better for the as-built diaphragms. It is recommended that further research be performed in order to calibrate the

FEM-models as the results were not accurate.

4.2.2 NEW ZEALAND, 2012

The researchers who performed experimental tests in New Zealand as published in 2013 (see chapter 3) also constructed corresponding numerical models of as-built timber diaphragms in FEM-software SAP2000 [12]. The diaphragms consisted of joists, sheathing, cross-bracing and nailed connections between sheathing and joists. For the scope of this report, the cross-bracing will be disregarded. The numerical models assumed linear elastic material properties for the timber and the only nonlinearity is assumed to be lumped into the nailed connections. Mechanical interaction and friction within the diaphragm were neglected.

In SAP2000, the sheathing boards and joists were modelled as frame elements which take into account biaxial bending, torsion, axial deformation and biaxial shear deformations. These frame elements were modelled with only centreline geometry. Each node of a frame element exhibits six degrees of freedom: $u_x, u_y, u_z, \phi_x, \phi_y$ and ϕ_z [32]. Only Young's modulus and density were assigned and no anisotropic properties were given to the wood. The material properties were the same for all boards and joists. The nailed connections in the diaphragm were modelled using couplers and link elements. The link elements were given nonlinear properties to represent the nailed connections, whereas the couplers served to connect the link elements to the timber boards. The couplers were frame elements which were needed to represent nail spacing, as the board frame elements were not modelled with a width. Assuming that the shear deformation in the nailed connection is negligible as opposed to the nail slip, the coupler frame elements were given isotropic material properties, with a very high Young's modulus as compared to that of the timber boards. No weight was assigned to the coupler elements. The link elements were placed vertically between joist elements and couplers. In SAP2000, link elements have six controllable degrees of freedom represented through springs (three translational springs and three rotational springs) which can be assigned the desired nonlinear behaviour. The link element can be seen in figure 4-2. Nonlinear behaviour was implemented through in-plane springs U2 and U3, which account for the shear behaviour of the nailed connection. Spring U1 was set to be fixed, considering that compression of the nailed connection is negligible and that nail pull out is accounted for in the shear springs. Bending springs R2 and R3 were also fixed to prevent rotations between joists and boards, as these rotations are negligible if the diaphragm is loaded laterally. Torsional spring R1 was assigned a stiffness of zero. For translational springs U2 and U3, different properties were assigned for both monotonic and cyclic analyses. For monotonic analyses, a multi-linear Takeda plasticity property was used for the backbone of the springs. This backbone can be determined using experimental data or theoretical load-slip characteristics. As a previous study found that connection behaviour does not depend on grain orientation, springs U2 and U3 were given the same properties. Furthermore, these springs were completely uncoupled. For cyclic analyses, a multi-linear plastic link element was used, which followed hysteretic rules according to the pivot model. In this model, unloading and reloading moves into the direction of defined pivot points. These pivot points are dependent on the yield force and empirical parameters $\alpha_1, \alpha_2, \beta_1$ and β_2 (see figure 4-3). Upon unloading, the force-displacement path moves to point P1 or P2, defined as the intersection between the elastic segment of the backbone and $\alpha_2 F_{y2}$ or $\alpha_1 F_{y1}$. For reloading (when the force changes sign), the curve moves to point PP1 or PP2, which is the intersection between the elastic segment of the backbone and $\beta_2 F_{y2}$ or $\beta_1 F_{y1}$. The numerical hysteresis (and thus its parameters) can be calibrated using experimental data. The pivot model was deemed suitable to represent nail connection behaviour, as it captures pinching behaviour. However, the model does not account for strength losses between successive cycles of the same amplitude.
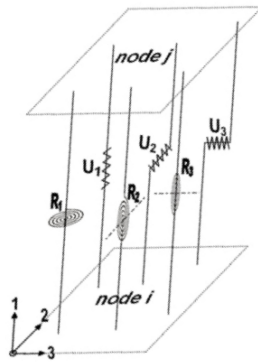
Figure 4-2: Link element in SAP2000 [12]
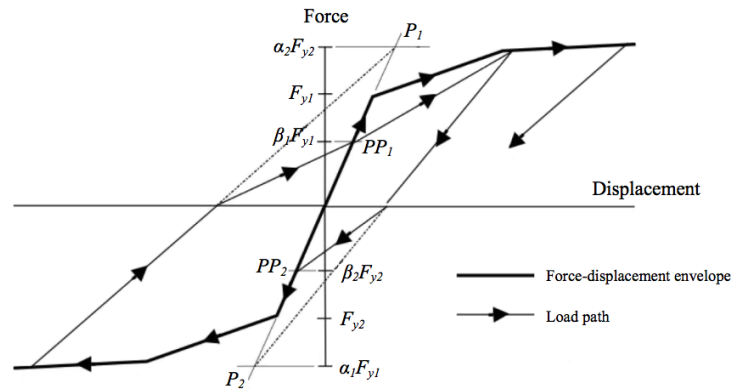
Figure 4-3: Pivot hysteretic model in SAP2000 [12]

The constructed numerical model as discussed in this section is shown to be able to accurately capture the behaviour of a simple diaphragm. Monotonic and cyclic comparison to experimental tests yielded fairly accurate results. Both the monotonic and cyclic FEM-analyses produced realistic backbone curves and displacement profiles along the length of the diaphragm. For the cyclic analysis, the hysteresis curve exhibited pinching behaviour and was similar to experimental data, albeit the numerical result was far more linear than the data. Moreover, strength losses between successive cycles of the same amplitude could not be captured. Furthermore, the model cannot account for timber cracking as well as glued connections between sheathing boards. These aspects however are assumed to have a relatively small effect on diaphragm behaviour and thus it is concluded that the FEM-model is sufficient to simulate a simple diaphragm.

4.2.3 NEW YORK, 2015
In 2015, researchers from New York constructed FEM-models of as-built diaphragms in both OpenSees and SAP2000 [33]. The models were calibrated with the experimental results from the study in 2003 in Texas as discussed in subsection 4.2.1. First, the model in OpenSees will be discussed. Secondly, the model in SAP2000 will be discussed. In both models, the joists and boards were assumed to be linear elastic and the only source of nonlinearity were the nailed connections. Mechanical interaction and friction within the diaphragm were neglected.

In OpenSees, the boards were modelled using 4-noded isotropic elements in a state of plane stress. Each node has two degrees of freedom: u_x and u_y. The sheathing boards required Young's modulus, Poisson's ratio and density as input for the material. No anisotropic properties were assigned to the sheathing and no connectivity existed between sheathing boards. The joists were modelled as Bernoulli beam elements and exhibited three degrees of freedom at each node: u_x, u_y and ϕ_z. The beams were isotropic and required Young's modulus and Poisson's ratio as input. The material properties were the same for all boards and joists and were taken from a database. Nailed connections between beam and joist elements were modelled through zero-length springs in two perpendicular in-plane directions. Uniaxial material model SAWS was used, which specifies hysteretic rules in one dimension (see figure 4-4). For the SAWS model, the first loading path follows the backbone curve (path OA). After unloading, the hysteresis follows a path with preset stiffnesses. These stiffnesses are required in order to simulate pinching behaviour of the connection. The first branch after unloading (path AB) represents the elastic deformation of the connection. Subsequently, the unloading stiffness decreases, representing the contact loss between the connector and wood (path BC). This branch of the unloading path passes through a preset zero-displacement point. Upon reloading for the first time, the path follows the backbone curve again (path CD). Unloading then follows the

same rules as mentioned before. If reloading does not happen for the first time, the path does not follow the backbone curve but instead follows a multi-linear path of preset stiffnesses (which represent contact loss and elastic deformation within the connection). Reloading initially starts with the specified reduced pinching stiffness (the same as after unloading), after which the stiffness increases as the wood comes in contact with the connector again. This stiffness increase is calculated based on the loading history, thus the SAWS model is capable of implementing strength losses between cycles of the same amplitude. If the connection is loaded cyclically at the same displacement amplitude, the energy dissipation will eventually stabilise. The SAWS hysteretic model implements model parameters which can be calibrated on experimental data [13].
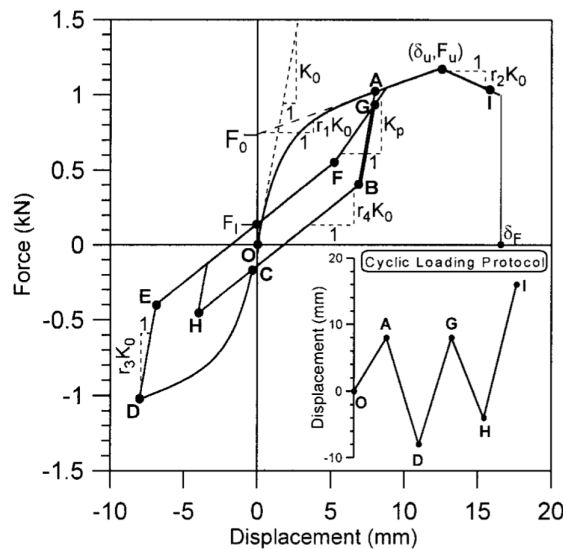
Figure 4-4: SAWS hysteretic model [13]

The numerical model in OpenSees yielded very accurate results when compared to the experimental tests in Texas in 2003. Cyclic comparison showed that pinching behaviour was well represented in the numerical results and that diaphragm nonlinearity was well accounted for. The model however did overestimate the maximum strength and the degraded reloading stiffness. It was observed that for larger displacements, the model error increased. This may be attributed to the defined hysteresis of the nailed connections, thus it may be desirable to update the given properties to the SAWS model based on numerical results. Nonetheless, the numerical model is a very neat simulation and can be used for future applications. It is recommended that the discussed model only be used for representation of simple timber diaphragms.

The second model in this study was constructed in SAP2000 and shows similarity with the model as constructed by researchers in New Zealand. Sheathing boards were modelled through plane elements in a state of plane stress. Nodes of a plane element have three translational degrees of freedom (u_x, u_y and u_z) [34]. The joists were modelled as frame elements with three degrees of freedom per node: u_x, u_y and ϕ_z. These frame elements take into account biaxial bending, torsion, axial deformation and biaxial shear deformations. For both board and joist elements, isotropic material properties were assumed which required Young's modulus, Poisson's ratio, density, shear modulus and coefficient of thermal expansion as input. All boards and joists were given the same material properties. The nailed connections were modelled using link elements, specifically as two zero-length springs in the two in-plane directions. The pivot hysteretic model was applied to the springs, the hysteretic rules of this model have already been discussed in subsection 4.2.2. Comparing the

numerical results to the experimental results from the study in Texas in 2003, it was found that the model in SAP2000 resembles experimental behaviour and that it is a good representation of reality. Pinching behaviour could be seen in the numerical results. However, the model overestimated the ultimate strength and did not account for strength losses for cycles of the same amplitude [33]. If one compares the numerical model in OpenSees and the model in SAP2000, the model in OpenSees yields more accurate results. The error is smaller and diaphragm nonlinearity is better represented through the model in OpenSees. Furthermore, this model is capable of capturing strength losses between cycles of the same amplitude.

4.2.4 UNITED STATES OF AMERICA, 2008

For the modelling of the nailed connections between sheathing and joists, researchers in America have proposed a model using software ANSYS. ANSYS already has several pre-programmed connector elements, which is convenient as no user-supplied element needs to be generated. To model typical hysteretic behaviour as found in nailed connections in timber floors, element COMBIN40 is used (see figure 4-5). This nonlinear element consists of two springs, a slider, a damper and a gap element and is positioned between two nodes. All of these sub-elements can be removed individually from the element. The input parameters for COMBIN40 are two spring constants (K1 and K2), a sliding force (F), a damping coefficient (C), a mass (M) and an initial gap size (length). The mass can be assigned such that it is equally divided over the two nodes or such that one node carries all the mass. If the initial gap size is zero, the element has both tension and compression capability. For a positive or negative initial gap size, the gap remains closed in compression and opens in tension. If the gap is open, no force is transmitted. The gap can also be made such that it remains closed after initial contact. The slider represents the force in the first spring (which is in series with the slider) which must be exceeded before sliding occurs. If sliding occurs, the force remains constant. If the sliding force is inserted with a negative value, the stiffness of the first spring (K1) drops to zero once the sliding force is reached. The element has one degree of freedom at each node (but the same for both nodes), which can be either a translation or a rotation [14].
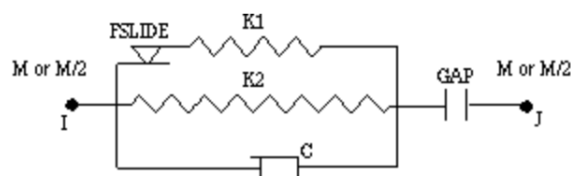
Figure 4-5: Element COMBIN40 in ANSYS [14]

From the study in 2008, researchers found that a single nail connection can be modelled by two COMBIN40 elements in each in-plane direction, thus a total of four COMBIN40 elements are needed per nail. These elements are placed between two nodes, with one node belonging to the joist and the other belonging to the sheathing. The degree of freedom is the translation along the length of the element. For each direction, two COMBIN40 elements are placed in parallel. The first element models the pinched region of the hysteresis curve, whereas the second element models the peaks. The first element only implements a slider in parallel with a spring. The sliding force represents half of the width of the pinched region and the spring constant represents the slope of the pinched region. The second element implements a slider and spring in parallel with another spring, which are all in series with a gap element. This element divides the reloading peaks of the hysteresis into two linear segments. The sliding force represents the transition point of the two linear segments. The gap element is needed such that the transition point between the two linear segments occurs at higher displacements for subsequent cycles. The gap is initially very small. The spring constants are representative for the slopes of the two linear segments [15]. The unidirectional configuration of the

elements for one in-plane direction can be seen in figure 4-6. It was determined that the proposed model for the connections was a representative and fairly accurate simulation.
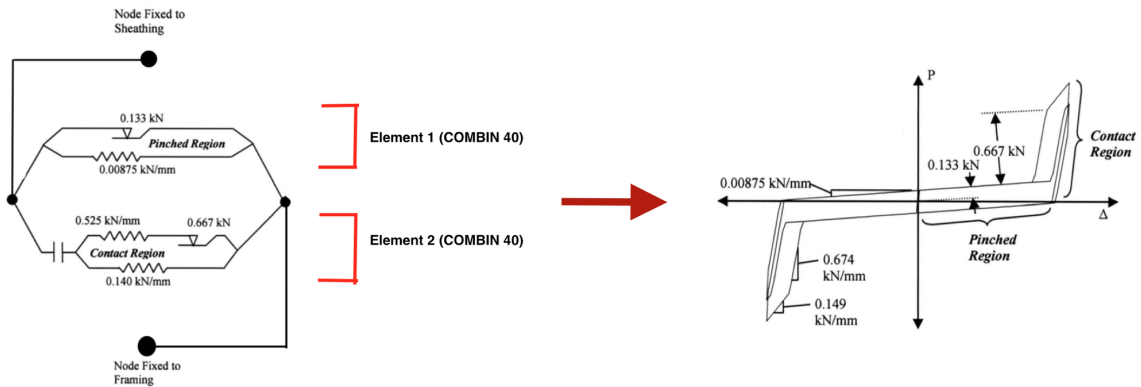
Figure 4-6: Unidirectional model for one nail in one direction using two COMBIN40 elements [15]

4.2.5 SUMMARY

The numerical studies as discussed in this chapter propose different models, with varying results. The study in Texas yielded inaccurate numerical results, whereas the other studies yielded fairly accurate results. The study in Texas was the only study to include retrofitted diaphragms, so comparison between retrofitted numerical models cannot be made. A summary of the numerical approaches to model an as-built diaphragm is given in the tables below. Characteristics of joists, sheathing boards and nailed connections are given in these tables.

Table 4-2: Previous modelling of sheathing boards

Study	Software	Element	Material model	DOF	Input parameters
Texas, 2003	ABAQUS	Plane stress element (8-noded)	Linear elastic isotropic	u_x, u_y	E (N/mm^2), $\rho(kg/m^3)$, ν
New Zealand, 2012	SAP2000	Frame element	Linear elastic isotropic	$u_x, u_y, u_z,$ ϕ_x, ϕ_y, ϕ_z	E (N/mm^2), $\rho(kg/m^3)$
New York, 2015	OpenSees	Plane stress element (4-noded)	Linear elastic isotropic	u_x, u_y	E (N/mm^2), $\rho(kg/m^3)$, ν
	SAP2000	Plane stress element	Linear elastic isotropic	u_x, u_y, u_z	E (N/mm^2), G (N/mm^2), $\rho(kg/m^3)$ $\nu,$ α

Table 4-3: Previous modelling of joists

Study	Software	Element	Material model	DOF	Input parameters
Texas, 2003	ABAQUS	Timoshenko beam element (2-noded)	Linear elastic isotropic	u_x, u_y, ϕ_z	E (N/mm^2), $\rho (kg/m^3)$, ν
New Zealand, 2012	SAP2000	Frame element	Linear elastic isotropic	$u_x, u_y, u_z,$ ϕ_x, ϕ_y, ϕ_z	E (N/mm^2), $\rho (kg/m^3)$
New York, 2015	OpenSees	Bernoulli beam element (2-noded)	Linear elastic isotropic	u_x, u_y, ϕ_z	E (N/mm^2), ν
	SAP2000	Frame element	Linear elastic isotropic	u_x, u_y, ϕ_z	E (N/mm^2), G (N/mm^2), $\rho (kg/m^3)$ ν, α

Table 4-4: Previous modelling of nailed connections

Study	Software	Element	Hysteresis model	Pinching	Strength loss (energy dissipation)
Texas, 2003	ABAQUS	Joint/ user-defined element	Three-parameter model with trilinear backbone	Yes	Yes
New Zealand, 2012	SAP2000	Couplers + link elements	Pivot model	Yes	No
New York, 2015	OpenSees	Zero-length springs	SAWS model	Yes	Yes
	SAP2000	Link element	Pivot model	Yes	No
United States of America, 2008	ANSYS	COMBIN40	Multilinear	Yes	Yes

The numerical studies showed several similarities:
- Beams and joists are modelled with isotropic linear elastic material properties.
- The only nonlinearity in the diaphragm originates from nailed connections.
- Friction and mechanical interaction between diaphragm members are neglected.
- Pinching behaviour is accounted for in the hysteresis model for nailed connections.

Though the boards and joists were given the same material models, the deformation mechanics however did differ for the different studies. The degrees of freedom and material input parameters also differed for the numerical models. As different FEM-softwares were used, these characteristics depended on the chosen element type.

The numerical studies were calibrated on laboratory tests with different circumstances for each study, thus it is worth noting that the boundary conditions, loads and analysis method affect the accuracy of the model.

4.3 SHEATHING BOARDS

When loading occurs parallel to the joists, sheathing boards are mostly subjected to in-plane bending moments and shear forces. In this case, the nails in the connections between boards and joists move primarily perpendicular to the wood fibres in the sheathing boards. For loading perpendicular to the joists, the boards are mainly subjected to normal forces. The nails will then move parallel to the woods fibres in the sheathing boards. The largest deformations in the flooring boards occur when the diaphragm is loaded parallel to the joists (see figure 4-7). As the sheathing boards are constructed from timber, the boards have different properties in different directions. Assuming that the sheathing does not yield and that the lumped nonlinearity originating from the connections is decisive for diaphragm behaviour, linear material properties can be assigned to the sheathing elements. As timber is orthotropic, different linear properties have to be assigned in different directions.

Currently, the TU Delft modelling strategy assumes that the Young's modulus in the direction of the length of the board is the full value as determined from laboratory tests. For directions perpendicular to the board direction, either the full value or a reduced value of the Young's modulus can be assumed. The Poisson's ratios are assumed to be zero. The in-plane shear modulus G_{xy} is assumed to be 1% of the full timber value, values of other shear moduli are taken as the full timber value.

(a) Relative joist displacement and floorboard bending   (b) Nail couple rotation
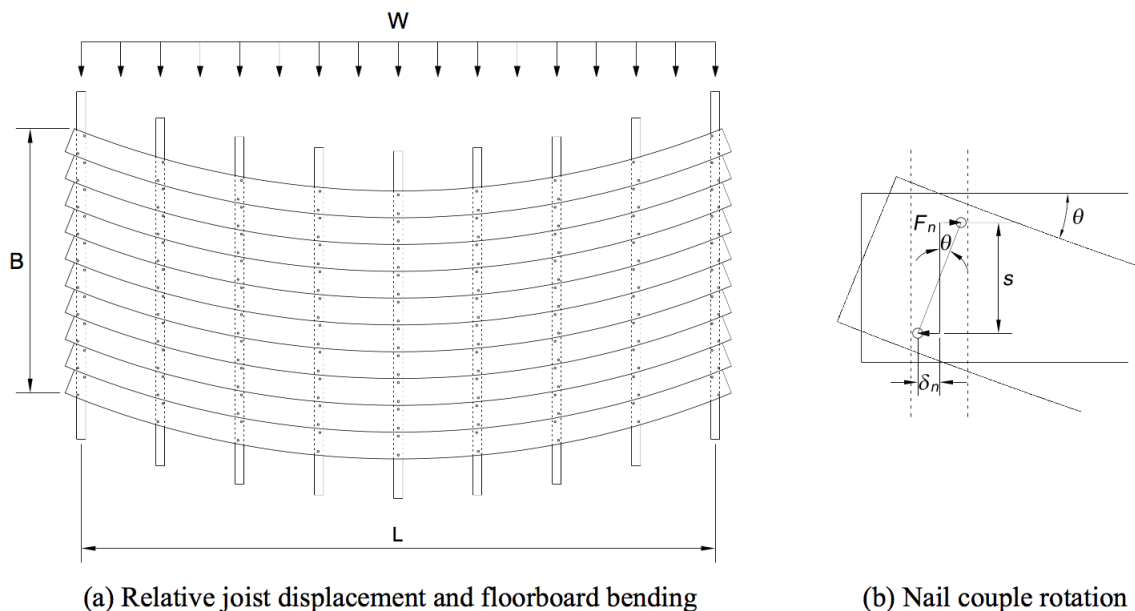
Figure 4-7: Diaphragm deformation for loading parallel to joists [12]

4.4 JOISTS

Joists are mostly subjected to normal forces when loading is applied parallel to the joists. In this case, the nails will move parallel to the wood fibres in the joists. For loading perpendicular to the joists, the joists are subjected to bending moments and shear forces. The nails will then move perpendicular to the wood fibres in the joists. The largest deformation in the joists occur when loading is applied perpendicular to the joists (see figure 4-8). Assuming that the joists do not yield and that the lumped nonlinearity originating from the connections is decisive for diaphragm behaviour, orthotropic linear elastic material properties can be assigned to the joist elements.

(a) Flexural bending of joists and relative floorboard displacement　　(b) Nail couple rotation
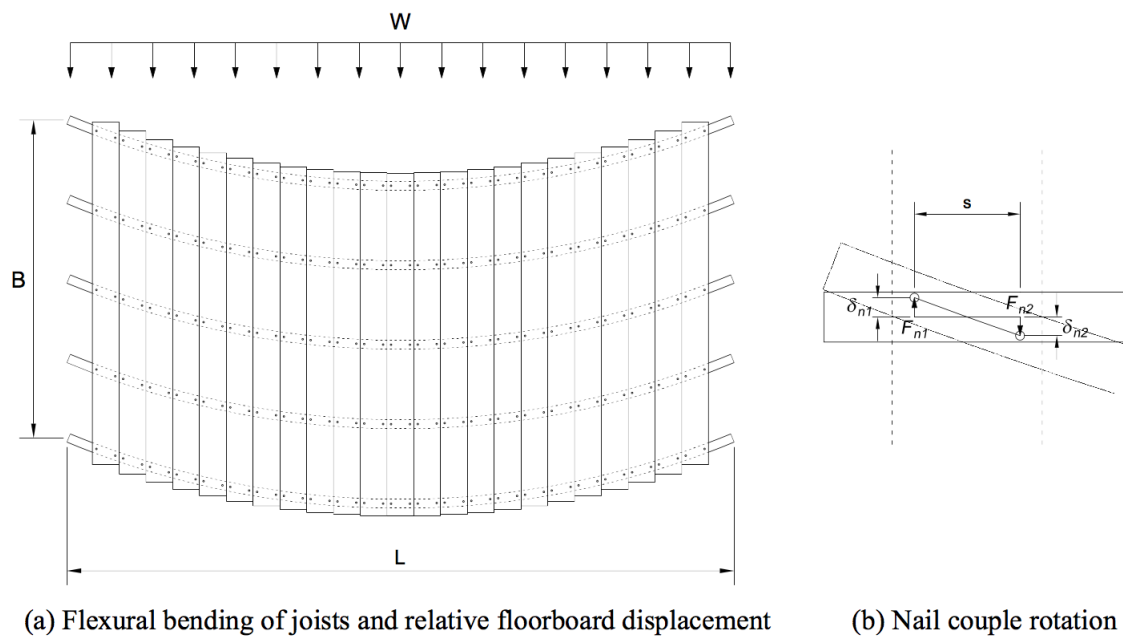
Figure 4-8: Diaphragm deformation for loading perpendicular to joists [12]

4.5 Nailed connections between sheathing and joists

Nailed connections occur between joists and sheathing. The sheathing boards are typically connected to each joist with two nails, with one board usually spanning several joists. The nailed connections contribute largely to the nonlinear response of a diaphragm and are thus an important aspect to consider. Under seismic loading, nailed connections exhibit three degrees of freedom: two in-plane translations and one in-plane rotation.

For nails, the maximum tensile strength and the plastic bending moment are important properties. The maximum tensile strength indicates the highest load the nail can withstand before it breaks, whereas the plastic bending moment indicates the amount of nail deformation it can withstand. The relevant characteristics of nails can be determined through monotonic and cyclic tests. When performing laboratory tests on nailed connections, the three in-plane motions should be considered (the two in-plane translations and one in-plane rotation). The behaviour of the nails can largely be described using the results of these tests.

4.5.1 Nail behaviour
Cyclic loading of nails results in a hysteretic response in the force-displacement diagram, which means that, if put simply, the response of the element is dependent on its loading history. The hysteretic response in the force-displacement diagram is illustrated in figure 4-10, along with an illustration of how a nailed connection deforms in figure 4-9. The hysteretic response occurs in both in-plane directions of the connection.

For the first cycles, the response of the connection remains in the elastic zone and the force-displacement relationship remains linear if small displacements are imposed on the connection (figure 4-11a). If the displacement is increased and more cycles pass, the behaviour of the nailed connection becomes more and more nonlinear (figure 4-11b and figure 4-11c). This nonlinearity is caused by crushing of wood and yielding of nails. Due to the crushing of wood, the nail is not entirely embedded in timber any more. This leads to a reduced stiffness of the connection (as there

is no resistance from the timber) if the loading is reversed in later cycles (figure 4-11b and figure 4-11c). Repeated loading results in pinching behaviour of the connector as the stiffness is reduced due to the crushed wood (see figure 4-11c). As more cycles pass, the stiffness becomes more and more reduced for small displacements and the pinching behaviour becomes more distinct. For each loading cycle, a maximum load is reached. The curve which connects the maximum load that is reached in each cycle is called the envelope (or backbone) curve. This envelope curve can be approximated by performing monotonic tests on the connections. The dashed line in the force-displacement diagrams in figure 4-11 represents the envelope curve.
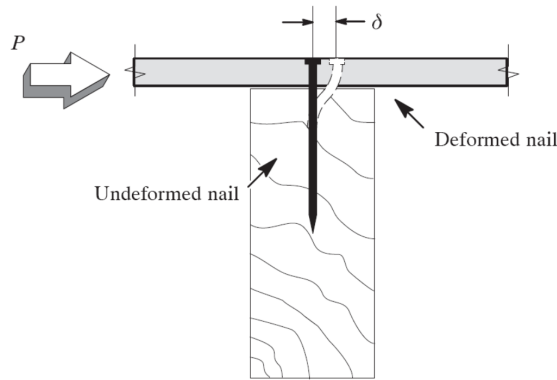
Figure 4-9: Nailed connection between sheathing and joists [16]
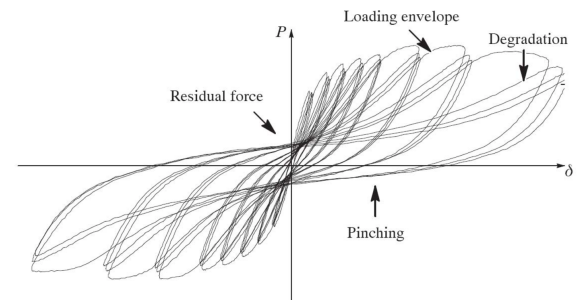
Figure 4-10: Hysteretic behaviour of nailed connections [16]
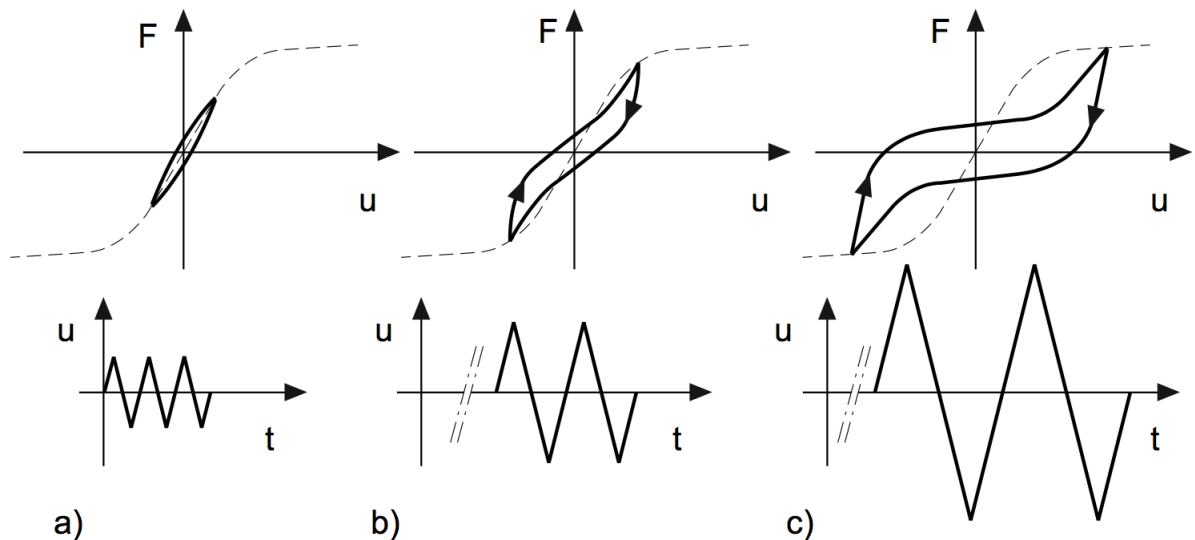
Figure 4-11: Hysteresis curves for different load cycles [17]

4.5.2 IDEALISED MODELS FOR THE CYCLIC BEHAVIOUR OF NAILED CONNECTIONS

Two important characteristics that need to be considered when modelling nailed connections are the envelope curve and the hysteresis. An important property of nailed connections is that the resistance deteriorates if the connection is subjected to cyclic loading, which contributes to the nonlinear behaviour. Implementing the nonlinear behaviour of nails in a numerical environment can prove to be quite difficult, which is why the behaviour has to be idealised. The idealisation can be done in different manners. The idealisations presented in this subsection serve to create a better understanding on how the behaviour of a nailed connection can be modelled. These idealisations

will not be used for the numerical modelling in chapters hereafter.

ENVELOPE CURVE
The envelope curve for deteriorating nailed connections is point symmetric and roughly four segments can be distinguished if idealised (see figure 4-12). The first segment is dominated by the linear-elastic behaviour of the connection, for which the elastic stiffness K_e is the decisive parameter. After the yield strength F_y is reached, the second segment can be identified in the envelope curve. The second segment is characterised by a reduced stiffness K_s, which is often called the strain-hardening stiffness. The second segment ends at the peak strength F_c, whereafter deterioration sets in (the third segment). Deterioration of the connection is characterised by a negative stiffness K_c and is often called softening. At the end of the softening, a residual strength F_r can be implemented in the envelope curve (fourth segment). The stiffnesses can be determined by laboratory tests. If a non-deteriorating model is considered, the last two segments of the envelope curve are not relevant. The envelope curve may differ depending on the type of connection, thus the amount of linear segments may be altered based on the connection and based on experimental results.
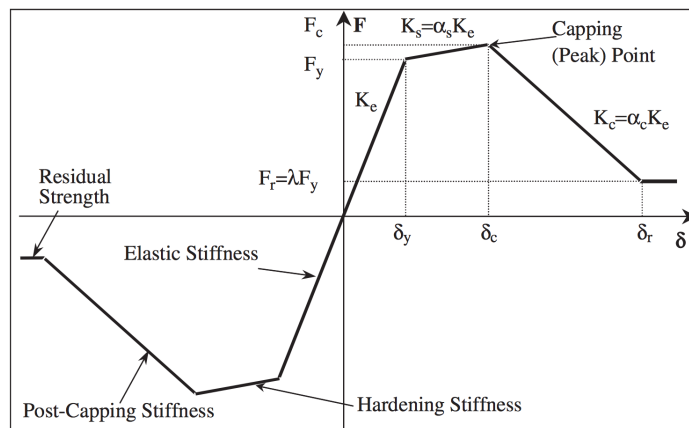
Figure 4-12: Envelope curve for deteriorating hysteretic models [18]

HYSTERESIS
For the hysteresis, various models have been constructed and different studies have been carried out on how to implement hysteretic behaviour in numerical models. Both cyclically deteriorating and non-deteriorating models have been developed, of which few will be elaborated hereafter.

Bilinear hysteresis model
The bilinear hysteresis model is non-deteriorating as the stiffnesses in each segment of the hysteresis curve remain the same for each load cycle (see figure 4-13). The force-displacement curve for this model is bilinear and is parameterised by the elastic stiffness K_e, the strain-hardening stiffness K_s and the yield force F_y. Upon unloading and reloading, the hysteresis follows the same loop for each load cycle. The bilinear model can be made deteriorating by imposing a strength limit corresponding to the smallest strength in the segment with a negative stiffness in the envelope curve (see figure 4-14). The strength limit implies that in later load cycles, the strength will not surpass this limit and that the strain-hardening stiffness is equal to zero.
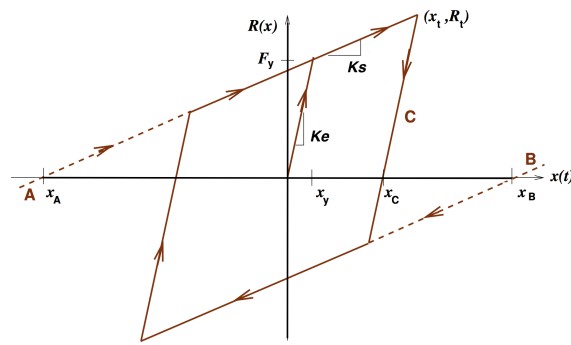
Figure 4-13: Bilinear hysteresis model [19]
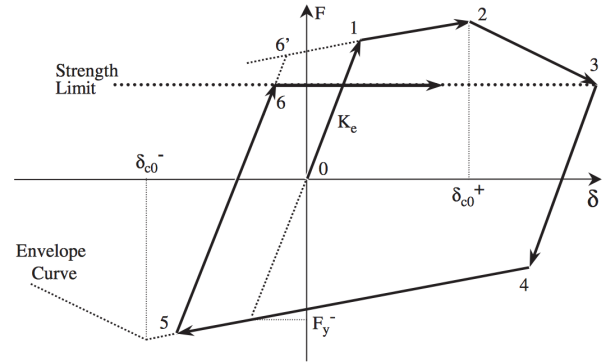
Figure 4-14: Bilinear hysteresis model with deterioration [18]

Peak-oriented hysteresis model

The peak-oriented hysteresis model (similar to a Clough hysteresis model) implements the deteriorating nature of a connection as the reloading stiffness reduces in cyclic loading. Upon unloading, the force-displacement curve is parallel to the unloading curve from the previous loading cycle. Once the unloading curve switches to the reloading curve (when the force changes sign), the stiffness decreases and the reloading path then moves to the previous maximum displacement (in the same load direction). In figure 4-15, this unloading and reloading path can be seen through the numbers 1 to 11. The maximum displacement of each loading cycle follows the defined envelope curve.
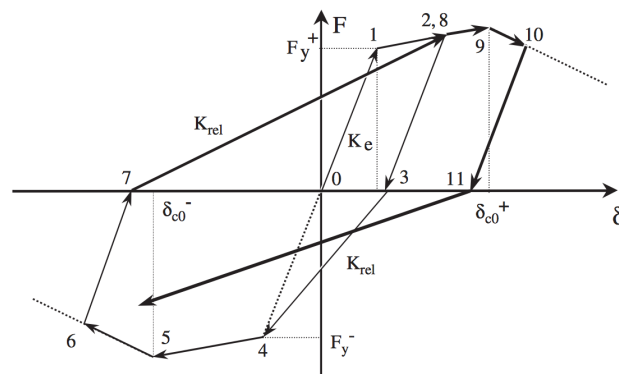
Figure 4-15: Peak-oriented hysteresis model [18]

Pinching hysteresis model

The pinching hysteresis model is the most suitable deteriorating model for the nailed connections between sheathing and joists as considered in this report. The model is similar to the peak-oriented hysteresis model, but the reloading path differs as it implements two parts to ensure pinching behaviour. Upon reloading, the hysteresis path moves to a defined 'break point'. This part of the hysteresis path has a very low stiffness and represents the pinching behaviour. Once the reloading path passes the break point, the stiffness increases again and the curve moves to the maximum displacement of earlier cycles. The behaviour of the pinching hysteresis model is demonstrated in figure 4-16, where the numbers 1 to 8 represent the unloading and reloading path. However, if the reloading path is cut off before the break point is reached, the subsequent reloading curve consists of just one part which is directed towards the previous maximum displacement (see figure 4-17).
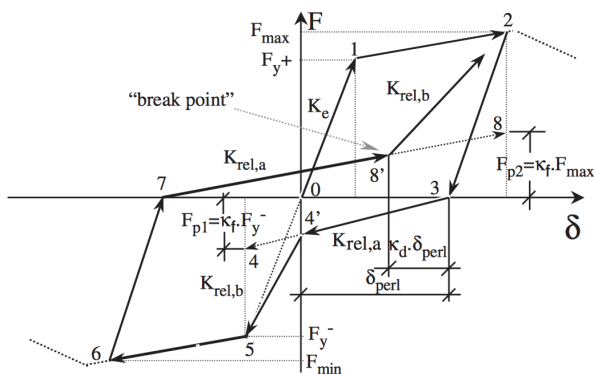
Figure 4-16: Pinching hysteresis model [18]
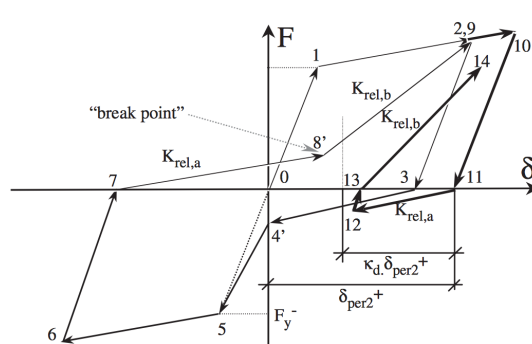
Figure 4-17: Pinching hysteresis model if reloading did not pass break point [18]

4.6 FRICTION BETWEEN SHEATHING BOARDS

The sheathing boards in a timber diaphragm are usually (slightly) connected to each other through a tongue and groove interlocking. This connection is often moderate as no glue or pins are present to provide a full connection. The boards can move relative to each other due to the lack of a full connection, resulting in a friction surface. The friction between sheathing boards can be another source of nonlinearity, albeit less significant than the nonlinearity due to the nailed connections.

Frictional behaviour between two surfaces can be divided into two regimes, namely the pre-sliding regime and the gross sliding regime (see figure 4-18). The pre-sliding regime is valid for very small displacements and shows linear behaviour. This regime is dominated by adhesive forces due to asperity contacts and can be seen as a threshold before actual sliding occurs. Gross sliding occurs when asperity contacts break and become less, enabling the surfaces to slide along each other. During gross sliding, the asperity contacts have less time to reform, resulting in a lower friction force than at the transition between pre-sliding and gross sliding [20].
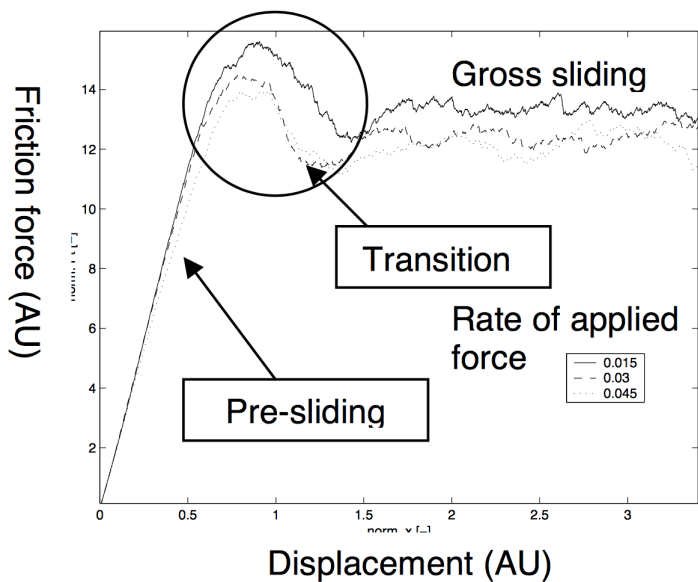
Figure 4-18: General friction behaviour [20]

In pre-sliding, cyclic loading of the contact surfaces results in a hysteretic response and the friction force depends mainly on the displacement. As the relative displacements between timber boards are very small, the friction surface is assumed to be non-deteriorating. This means that the force-displacement relationship is conservative and that the hysteresis loop for cyclic loading will remain the same for each cycle. The force-displacement curve can be seen in figure 4-19. The unloading and reloading path follows the same curve for each cycle, unless unloading occurs at a displacement which is smaller than the specified maximum displacement. In that case, the curve follows an internal hysteresis loop.

The idealised model for the hysteretic behaviour in pre-sliding is shown in figure 4-20. The model implements a simple bilinear force-displacement relationship for cyclic loading and can be represented numerically through (a set of) springs. For the gross sliding regime, the friction force depends mostly on the sliding velocity. The friction force initially decreases with increasing velocity, however it starts increasing again after it passes its minimum. The increase in friction force is attributed to the built up shear forces on the sliding surface. The friction surface exhibits a hysteresis in the velocity domain for the gross sliding regime, due to normal creep. Normal creep causes an increase in adherence on contact surfaces by pushing them against each other. This means that in time, the friction force changes with changing velocity. The hysteresis in velocity domain is shown in figure 4-21.
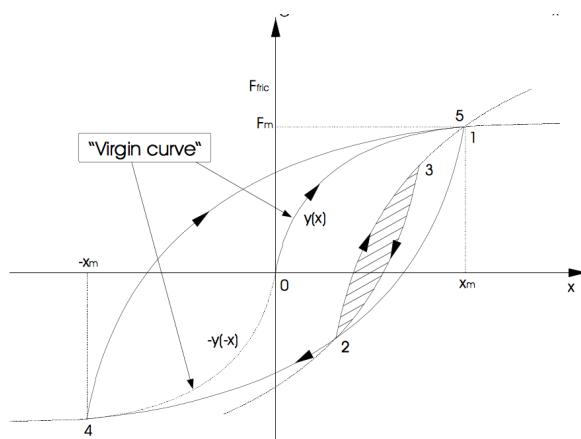
Figure 4-19: Hysteresis for pre-sliding [20]
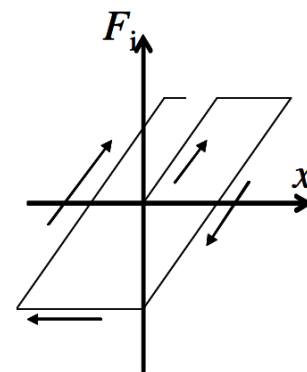
Figure 4-20: Idealised hysteresis for pre-sliding [20]
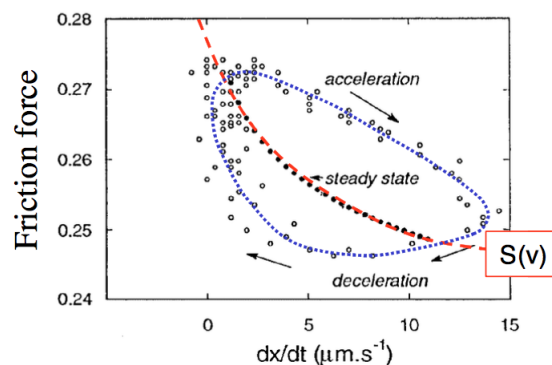
Figure 4-21: Hysteresis in velocity domain for gross sliding [20]

Combining the pre-sliding and gross sliding regime, one can construct a model for the friction surface between timber boards. This model can be seen in figure 4-22, where the friction surface is represented through a set of hysteretic springs and point mass pendulums. The point masses move against a surface, constantly attaching and detaching from asperities. Once detached from an asperity, all energy is dissipated. The relationship between friction force and sliding velocity for this model is shown in figure 4-23.

In previous (numerical) studies, the nonlinearity arising from friction between timber boards has been neglected, as it proves to be significantly small in comparison to the nonlinearity in the connections. The workload of implementing friction surfaces between each timber board in a numerical model is expected to be non proportional to the accuracy and efficiency obtained by doing so. Thus, it is assumed that the nonlinear behaviour of a diaphragm can be predominantly attributed to the connections between sheathing and joists. Furthermore, experimental tests to support the characteristics of friction surfaces between timber boards are lacking, complicating the process of constructing a proper model for nonlinear friction between boards. Based on previous observations, it is chosen to neglect the (nonlinear) friction between boards for the remainder of this thesis.
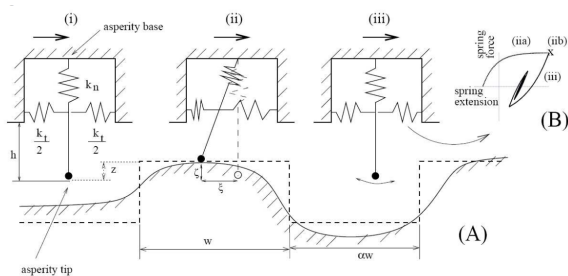
Figure 4-22: Model for friction surface between sheathing boards [20]
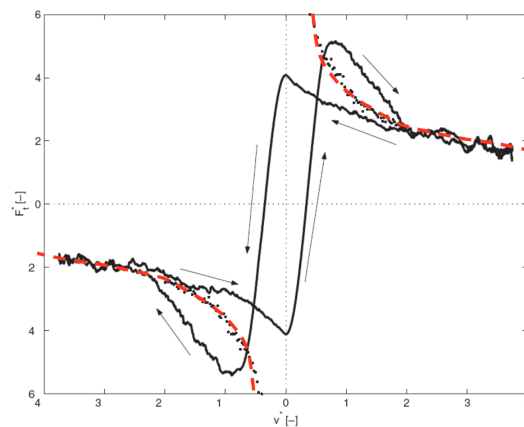
Figure 4-23: Relationship between friction force and sliding velocity for model in figure 4-22 [20]

4.7 CONNECTION BETWEEN MASONRY WALL AND DIAPHRAGM

The connection between masonry wall and timber diaphragm is very important as this connection contributes to the box behaviour and failure mode of a structure. An inadequate connection between floor and walls can lead to out-of-plane collapse mechanisms of the walls, which is highly undesirable. The connection between floor and walls also provides information about the boundary conditions when considering a sole timber diaphragm. In an unreinforced masonry building, a timber diaphragm is connected to the walls through its joists. Generally, two types of non-retrofitted connections between timber joists and masonry walls can be distinguished. The connection is either provided by simply inserting the timber beams in the masonry walls (so called joist-pocket connections), or by anchoring the timber beams to the walls by means of steel. These connections shall be elaborated in this section. For the scope of this report, the connection between wall and diaphragm is not of importance and therefore shall be neglected hereafter.

Joist-pocket connections

The behaviour of a joist-pocket connection is based on friction and impact [35]. Friction occurs between horizontal surfaces where the joist slides along the pocket in the masonry wall. Impact occurs when the end of the joist collides with the end of the pocket connection. Vertical earthquake motion can cause a looser embedment of the joist in the masonry, which lowers the friction forces and can even result in complete loss of connection if the joist detaches from the pocket. The hysteresis curve for the cyclic behaviour of a joist-pocket connection as obtained through experimental tests can be seen in figure 4-24 [21]. The dotted graph exhibits high forces in the compressive regime, this is due to the joist hitting the end of the masonry pocket. If no impact occurs, the connection relies solely on friction and the stiffness is relatively low.
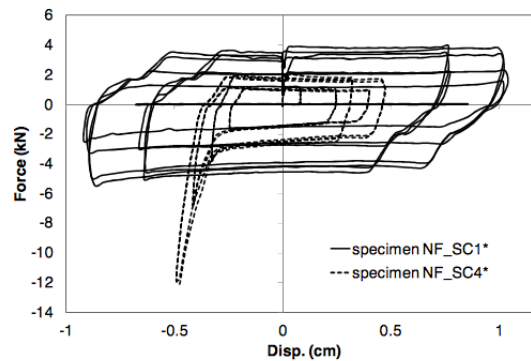
Figure 4-24: Hysteresis curve for joist-pocket connections [21]

For the friction in a joist-pocket connection, a Coulomb-friction model can be used which implements a static friction force and a kinetic friction force. The kinetic friction force is proportional to the velocity at which the contact surfaces slide along each other. A finite element model to represent Coulomb-friction was proposed by Cross and Jones in 1993, in which the joist and the masonry pocket are modelled through beam elements. The joist and masonry wall are connected through a pocket element which deforms if the joist hits the end of the pocket connection [35]. For the impact in a joist-pocket connection, a restitution coefficient can be determined for the collision between two bodies. The restitution coefficient sets a relation between the kinetic energy before impact and after impact. If the collision is perfectly elastic, no kinetic energy is lost and the restitution coefficient is one. If the collision is completely plastic, all kinetic energy is lost and the restitution coefficient is zero. In reality, the collision will never be completely elastic or plastic, resulting in a restitution coefficient between zero and one. The impact in a joist-pocket connection can be modelled numerically through a spring-dashpot system [35].

Anchored wall-floor connections

For anchored wall-floor connections, the joist is inserted into the masonry wall (like a joist-pocket connection) and steel straps are nailed to the joist and anchored into the wall. Anchored wall-floor connections rely on friction and the mechanical connection of the nails in the joist. Experimental tests have shown that the hysteretic behaviour of these connections depend on the failure mode of the nails, as the nails can either shear off or be pulled out. The hysteresis curve also depends on the type of loading, which can be either static cyclic or dynamic cyclic. However, the hysteresis curves for the two types of cyclic loading are comparable (see figure 4-25 and figure 4-26). The hysteresis curve is asymmetric as the behaviour of the connection is different in tension and in compression. If the connection is subjected to compressive loading, the joist will hit the end of the masonry pocket at a certain displacement. This impact generates large forces in the compressive branch of the hysteresis curve. If the connection is subjected to tensile loading, the connection relies on friction and

nail behaviour only. Thus, the tensile branch of the hysteresis curve generates relatively lower forces than the compressive branch [21].

The hysteresis curve for anchored wall-floor connections can be idealised for numerical purposes (see figure 4-27 and figure 4-28). The envelope curve for the compressive and tensile branch differs, as the compressive branch takes into account the impact forces resulting from collision between joist and masonry. A simple numerical model can be proposed to represent an anchored wall-floor connection (figure 4-29). The model implements two parallel springs to simulate the two nails in the steel straps. The springs are given different ductilities, ensuring that the nails do not shear off simultaneously. The numerical model also accounts for friction and impact. The friction and impact models can be seen in figure 4-30. As the friction force depends on whether the nails have failed, an average friction force model is proposed. Three impact models have been introduced, depending on the maximum collision force (see figure 4-30) [21].
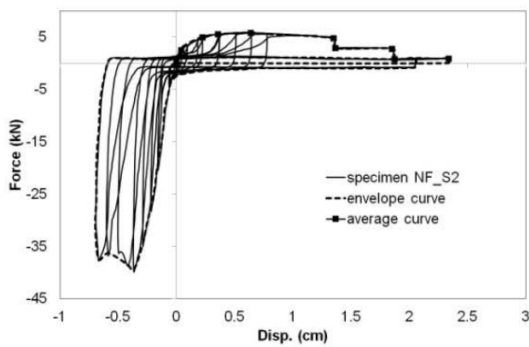
Figure 4-25: Hysteresis curve for static cyclic loading [21]
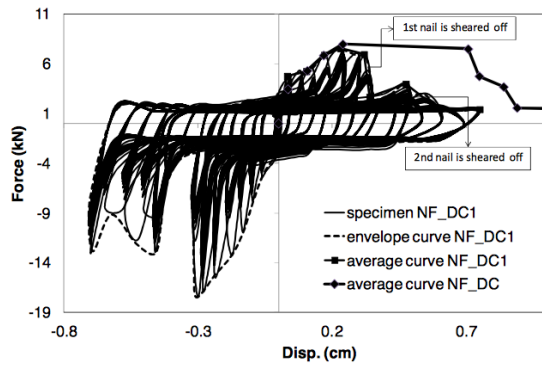
Figure 4-26: Hysteresis curve for dynamic cyclic loading [21]
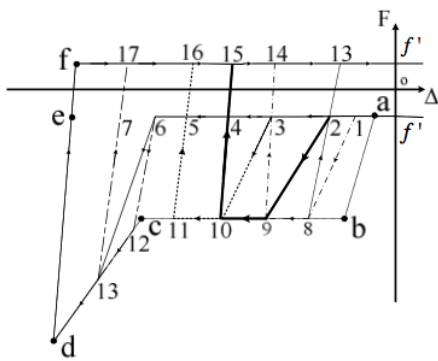
Figure 4-27: Idealisation of compressive branch of hysteresis curve [21]
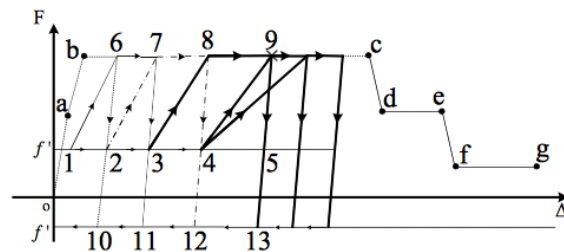
Figure 4-28: Idealisation of tensile branch of hysteresis curve [21]
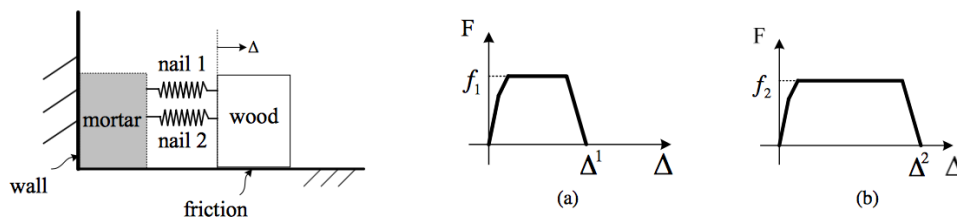
Figure 4-29: Numerical model and spring characteristics [21]
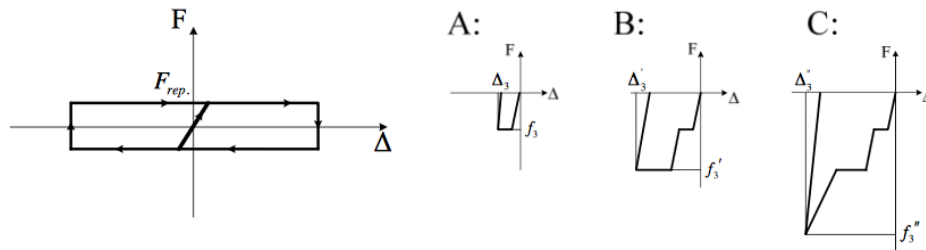
Figure 4-30: Average friction and impact model [21]

4.8 MODELLING EARTHQUAKE LOADING

To assess the resistance of a structure against earthquakes, a nonlinear analysis needs to be carried out as nonlinear material properties are present within structures. Nonlinear properties implies that the relation $F = ku$ no longer holds and thus linear analyses are not compatible. Nonlinear analyses are relevant for earthquake engineering, as these analyses reveal the stress redistribution and the capacity of a structure beyond elasticity. Two types of nonlinear analyses are suitable for earthquake engineering: a static pushover analysis and a dynamic time history analysis. These analysis methods shall be elaborated in this section.

4.8.1 NONLINEAR STATIC PUSHOVER ANALYSIS

In a nonlinear pushover analysis, the structure is subjected to monotonically increasing lateral loads until a specified maximum displacement is reached or until the structure fails. The specified maximum displacement must be chosen such that it represents the maximum displacement as can be expected for the chosen design earthquake. The lateral loads represent the inertial forces which are subjected to the structure due to earthquake loading, these lateral loads should be applied at the location of the masses in the model. As the lateral inertial loads vary over the height of a structure, different equivalent lateral force distributions have been proposed in the past (see figure 4-31). Generally, two equivalent lateral force distributions can be distinguished, namely the uniform and modal distribution. The uniform load distribution is proportional to the mass of each floor in a system and is constant over the height of a structure. For the modal force distribution, different codes offer different relations. For instance, EN 1998-1 states that the modal force distribution should be based on the lateral forces as determined in elastic analysis. Many regulations and guidelines (e.g. FEMA 356, EN 1998-1) have been developed over the past years in order to propose a standardised procedure for a pushover analysis. These guidelines often offer certain relations to determine needed parameters, such as the specified maximum displacement and characteristics of the lateral force distribution.
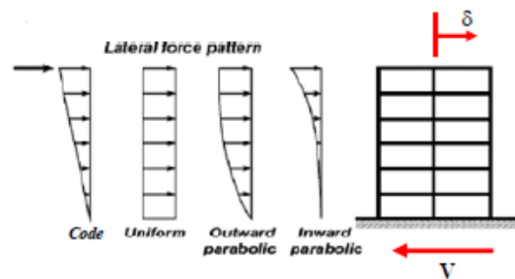
Figure 4-31: Lateral force distributions for pushover analysis [22]

The pushover method simplifies the system into (a) single-degree-of-freedom system(s), meaning that the vibrations of the structure are governed by the first mode [36]. One can account for multiple modes of vibration by performing a modal pushover analysis. In a modal pushover analysis, a pushover analysis is performed for each (significant) mode [37]. For simple symmetric structures, the dominant mode is often the first one. For cases in which the dominant mode is not evident, one can perform an eigenvalue analysis prior to the pushover analysis to determine the dominant mode. For a pushover analysis, the nonlinearities are implemented in the numerical model. The stiffness matrices are calculated after each load step, resulting in an iterative process. At the target displacement, internal forces and stresses are calculated, which are considered reasonable approximations of the actual forces and stresses during such an earthquake. A pushover analysis does not represent cyclic behaviour, but the analysis can be made cyclic by performing several pushover analyses one after another in opposite directions.

In the light of the current research in Groningen, a pushover analysis may prove to be of value as it can be used to assess existing structures. A pushover analysis is less accurate than a time history analysis, however a pushover analysis requires less computation effort and may be preferred over a time history analysis in some cases. Nowadays, pushover analyses are often used to predict and assess the behaviour of a structure. Pushover analyses are suitable for capturing the overall behaviour of a non-complex structure and are often sufficient enough for assessing most structures.

4.8.2 Nonlinear dynamic time history analysis

In a time history analysis, the model is subjected to forcing from an accelerogram. An accelerogram represents the ground acceleration during an earthquake. This accelerogram may differ in different loading directions and can either be artificial or recorded. An artificial accelerogram must be constructed such that it represents an earthquake which can occur on the site of the to-be-assessed structure. An example of an accelerogram can be seen in figure 4-32, this accelerogram was measured during the 2012 Huizinge earthquake in Groningen. Figure 4-32 shows three accelerograms for the three spatial directions.
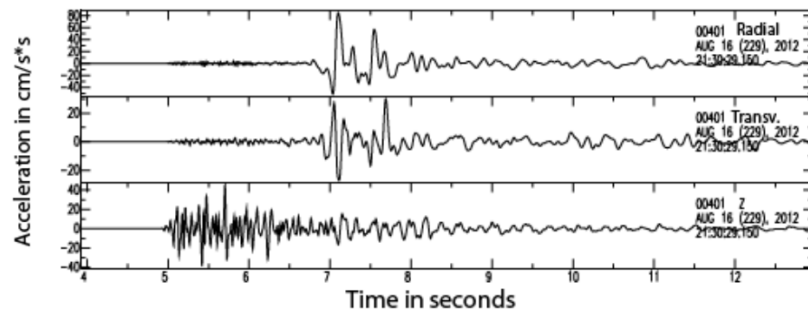
Figure 4-32: Accelerograms for the 2012 Huizinge earthquake in Groningen [23]

A nonlinear dynamic analysis can be used to assess existing structures in Groningen. For this analysis method, the nonlinear components are implemented in the numerical model. The initial conditions at each time step are updated, creating an iterative scheme.

A nonlinear dynamic time history analysis is the most exact analysis method for earthquake engineering as it directly implements ground movements. However, due to the high level of accuracy, this method also requires more computation time and computation effort. Sometimes, the accuracy of a nonlinear dynamic analysis is not required or may be non proportional to the workload and a pushover analysis is preferred. A pushover analysis may almost be as accurate as a time history analysis in some cases and a great advantage is that the computational effort is reduced significantly. For complex structures, a pushover analysis is no longer suitable and one must perform a time history analysis.

Another drawback of a time history analysis is that the generated response only holds for the specified accelerogram. If the loading changes, the response will change too. This leads to an uncertainty in structural behaviour. Often, it is required that a number of accelerograms are taken into account instead of only one. This assures that the response of the model remains representative for the actual structure and validates the numerical model more thoroughly.

4.8.3 CONNECTING CYCLIC LOADING TO NUMERICAL COMPUTATIONAL METHODS

For experimental research on the effects of earthquakes on structures, specimens are usually subjected to cyclic loading to represent earthquake behaviour. The loading pattern as used in these experiments is often prescribed in (national) standards. This loading pattern differs from the loading patterns as used in numerical nonlinear analysis methods (elaborated in the previous subsections). To relate a numerical model to experimental tests, the loading must be comparable and it is therefore of importance to accurately represent the cyclic loading in a numerical model.

A pushover analysis is a non-cyclic numerical analysis method, therefore it is often difficult to directly relate a pushover analysis to cyclic laboratory tests. As a pushover analysis is static and monotonic, it will only yield an envelope curve. This envelope curve can be compared to the envelope curve obtained from laboratory tests.

A time history analysis has loading of cyclic nature, albeit this loading is more random (depending on the chosen accelerogram). A time history analysis implements a correct representation of an actual earthquake, but may be difficult to directly relate to laboratory tests which are often less random. The gap between a time history analysis and laboratory tests can be reduced by constructing an accelerogram that creates the same time-displacement behaviour as in the laboratory.

The method as used in the laboratory at the TU Delft to test timber diaphragms can be categorised as a displacement-controlled cyclic pushover experiment. The loading scheme is not completely random as an actual earthquake, but is conform the guidelines of ISO 21581. For the numerical representation of these laboratory tests, the most suitable analysis method can be chosen based on the desired level of accuracy.

4.9 FEM-SOFTWARES

For the modelling of a flexible timber diaphragm, a compatible finite element method software needs to be chosen. As it is avoided to use user-supplied routines, the software should be chosen such that all needed material models have been implemented in the software. Furthermore, suitable analysis methods must be present in the software package. Several finite element method softwares have been developed for various purposes within civil engineering, such as DIANA FEA, ABAQUS, LS-DYNA and many more. For the scope of this report, it is of importance that the software has a material model to represent the hysteretic behaviour of nailed and screwed connections. As these connections are the only source of nonlinearity, they are a decisive factor when choosing a software to work with. In this section, various FEM-softwares will be reviewed for their abilities to model the hysteretic behaviour of nailed/screwed connections. Ideally, the hysteretic model within the software should implement pinching behaviour and strength loss for cycles of the same amplitude. These characteristics ensure an accurate representation of the behaviour of the nailed/screwed connections. The two mentioned characteristics serve as criteria on which the software shall be assessed. In table 4-5, various softwares are compared on their implemented hysteretic models.

Table 4-5 disregards user-supplied routines and only regards softwares for cyclic analyses. Five different softwares have been compared, namely DIANA FEA, ABAQUS, SAP2000, OpenSees and ANSYS. One can see that DIANA FEA provides no suitable hysteresis model for the purpose of this report. DIANA FEA does implement hysteretic models, however these models are destined for other purposes. ABAQUS has a hysteretic material model, however this model is very simple and not suitable to model nailed connections. The hysteretic model in ABAQUS does not implement strength loss and energy dissipation, which makes it an inaccurate model for the purpose of this report. Software SAP2000 has a hysteretic model which takes into account the pinching behaviour, but does not account for the strength loss between cycles of the same amplitude. SAP2000 is often only used to construct simple models. OpenSees has a very suitable hysteresis model, however this software has no user interface and is often only used for macro-modelling. Constructing a detailed model in OpenSees requires a lot of effort due to the lack of a user interface. FEM-software ANSYS provides several connector elements which can be combined to construct the desired hysteresis model. These elements can be combined such that pinching behaviour and strength loss can be accounted for. The advantages and disadvantages for each software are given in table 4-6. Considering the pros and cons of each software, it is chosen to work with ANSYS. This software is available for students and has been used at the TU Delft previously. ANSYS provides suitable hysteretic models to simulate nonlinear connections and can be used for the construction of larger models. Furthermore, the GUI makes the software easier to work with.

Table 4-5: Hysteretic models for various FEM-softwares
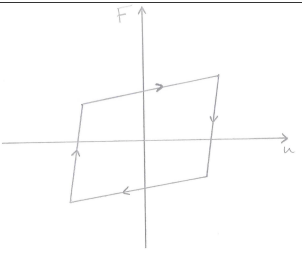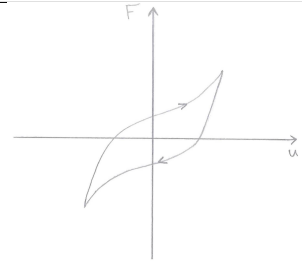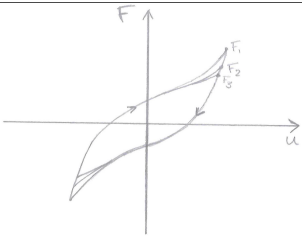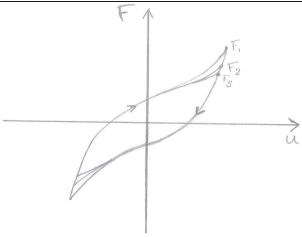
Software	Hysteresis model	Pinching behaviour	Strength loss for cycles of same amplitude	Material model
DIANA FEA	No	No	No	-
ABAQUS	Yes	No	No	
SAP2000	Yes	Yes	No	
OpenSees	Yes	Yes	Yes	
ANSYS	Yes	Yes	Yes	

Table 4-6: Pros and cons of various softwares

	Advantages	Disadvantages
ABAQUS	• Available for students • User interface available	• No suitable hysteresis model implemented
SAP2000	• Hysteresis models available	• Not available for students • Often only used for macro-modelling
OpenSees	• Very suitable implemented hysteresis model • Available for everyone	• No user interface • Often only used for macro-modelling • Great workload for detailed models
ANSYS	• Hysteresis models available • Available for students • User interface available	• Specific hysteresis model still needs to be constructed

PART II

MODELLING THE FLEXIBLE TIMBER DIAPHRAGM

In this part, finite element models will be constructed in ANSYS 18.2 to represent flexible timber diaphragms. The models will aim to represent the diaphragms as tested in the laboratory at the TU Delft. The results of the experimental tests at the TU Delft shall be discussed in chapter 5. The literature studies and experimental tests provide the starting point for the numerical models. First, an extensive model of a replicated as-built diaphragm will be constructed in chapter 6. From the model of the as-built diaphragm, a model for a retrofitted diaphragm can be constructed. This is done so in chapter 7. Lastly, chapter 8 will provide conclusions and recommendations regarding the numerical modelling of both diaphragms.

<div align="right">

5

</div>

TRIAL TESTS AT THE TU DELFT

Two diaphragm specimens have been trial tested in June 2017 at the Stevin laboratory at Delft University of Technology. One replicated as-built diaphragm and one replicated retrofitted diaphragm were subjected to quasi-static tests in the direction parallel to the joists. The tests were displacement controlled. The two specimens will serve as a validation for the numerical models that shall be constructed in this report. The trial tests serve as preliminary experiments in preparation for further tests which shall be performed at the TU Delft. In this testing campaign, more as-built and retrofitted diaphragms will be tested and in-situ specimens will also be subjected to testing.

In this chapter, the experimental results of the trial tests will be discussed. Section 5.1 elaborates the experimental result of the replicated as-built diaphragm. Hereafter, experimental results of the tests on nailed connections will be discussed in section 5.2. Nailed connections occur between joist and plank and can be found in both the as-built and the retrofitted diaphragm. The specimens of the nailed connections are tested in three loading cases: loading parallel to the joist, loading perpendicular to the joist and rotational loading. Section 5.3 will focus on the experimental result of the retrofitted diaphragm. Subsequently, section 5.4 will discuss the experimental results of the tests on screwed connections. Screwed connections can be found in the retrofitted diaphragm, connecting the panels onto the planks and beams. Two types of screwed connections were tested: a screwed connection between panel and plank, and a screwed connection between panel, plank and beam. The specimens of the screwed connections were tested in the two in-plane directions. Lastly, section 5.5 will provide comparisons between the experimental results of the as-built and the retrofitted diaphragm.

5.1 AS-BUILT DIAPHRAGM

5.1.1 TEST SETUP

The tested as-built timber floor specimen was constructed of pinewood and measured 3870x2650 mm. Initially, the floor specimen measured 4900x2650 mm. However, a segment was sawn off to produce specimens for the testing of the nailed connections. The floor specimen consisted of 4 joists and 23 flooring boards. The dimensions of the flooring boards measured 18x165x2650 mm. The timber beams used for the joists measured 130x60x3870 mm. The joist at the edge of the diaphragm consisted of two timber beams glued together, thus measuring 130x120x3870 mm. The flooring boards were continuous, with each flooring board spanning all joists and all boards interlocked through a tongue and groove connection. The centre-to-centre distance between the joists was 650 mm. The boards were connected to the joists with two nails at each board-joist intersec-

tion. The diameter of the nails was 3.5 mm and the spacing between the nails was 100 mm. A schematic representation of the timber specimen can be seen in figure 5-1 and a summary of geometric properties is given in table 5-1. Before the specimen was produced, the measurements, weight and dynamic Young's modulus were determined for each board and beam. These specifications are included in appendix A.

The produced specimen represents half a floor, with one edge representing the edge which is connected to the masonry wall and one edge representing the midspan of a floor. It is chosen to test only half a floor (instead of a whole floor) due to symmetry considerations. The diaphragm specimen was placed with its joists parallel to the laboratory floor into the loading frame, such that the midspan of the diaphragm is at the bottom of the loading frame. The upper edge represents the edge which is connected to a shear wall. The joist at the upper edge consists of two timber beams glued together. As the midspan rotation of a diaphragm is zero (flexural behaviour), the midspan specimen edge at the bottom of the loading frame is clamped to the loading frame, thus preventing translational and rotational degrees of freedom. This clamping was achieved by glueing plywood strips on both sides of the boards and mounting this edge to the steel loading frame. The joist at the upper edge (composed of two timber beams) was connected to an LVL I-beam through screws. These screws had a diameter of 10 mm and were spaced at a distance of 150 mm. The LVL beam was connected to the actuator which applied loading. The test setup and the mechanical scheme for the testing of the diaphragms is shown in figure 5-2 and figure 5-3.

Table 5-1: Specimen specifications

Joists	Cross section (mm x mm)	60x130
	Centre-to-centre distance (mm)	650
Flooring boards	Cross section (mm x mm)	165x18
Nails	Number of nails at each board-joist intersection	2
	Diameter (mm)	3.5
	Length (mm)	65
	Spacing (mm)	100
Specimen	Measurements (m x m)	3.870x2.650
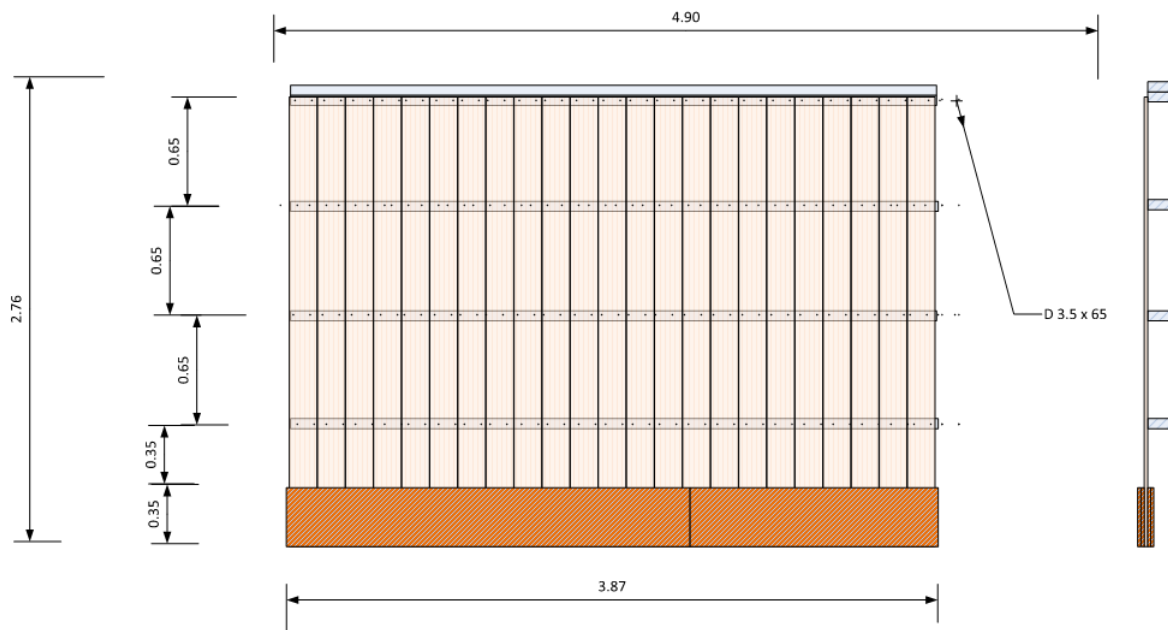
Figure 5-1: Schematisation of tested as-built timber floor specimen
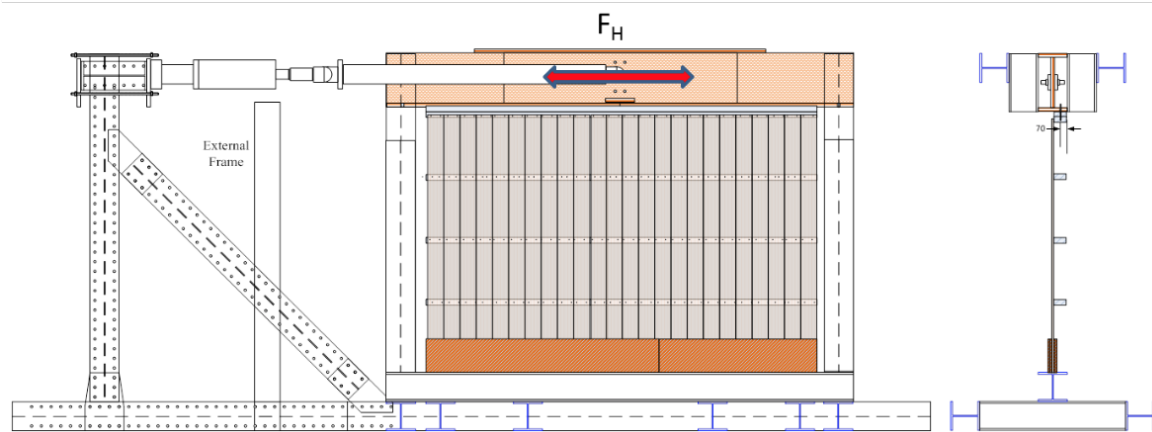
Figure 5-2: Test setup
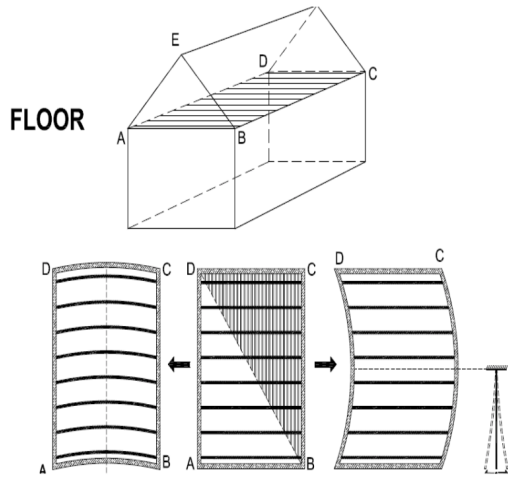
Figure 5-3: Mechanical scheme for testing   Figure 5-4: Loading scheme
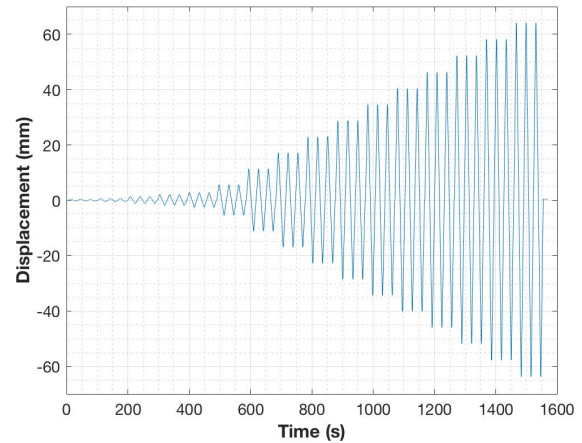
The test can be regarded as quasi-static cyclic, with the loading protocol for the test conform ISO 21581. This standard states that up to an amplitude of 20 percent of the ultimate displacement, only one cycle needs to be carried out for each amplitude. These cycles need to be performed at an amplitude of 1.25, 2.5, 5, 7.5 and 10 percent of the ultimate displacement. If the amplitude exceeds the value of 20 percent of the ultimate displacement, three cycles need to be carried out for each amplitude. These repeated cycles need to be performed at an amplitude of 20, 40, 60, 80 and 100 percent of the ultimate displacement. If the ultimate displacement is exceeded, increments of 20 percent of the ultimate displacement can be added to the loading scheme, with three cycles for each amplitude again. The ultimate displacement for the as-built diaphragm is taken as 30 mm. It is favourable to obtain the ultimate displacement from monotonic tests. However, this would require twice as much specimens and therefore it is chosen not to perform monotonic tests. The loading scheme as applied to the as-built diaphragm can be seen in figure 5-4. This scheme started with an amplitude of 0.3 mm and ended with an amplitude of 64.2 mm. Various sensors were placed on the specimen and loading frame to measure displacements. The instrumentation as adopted for the tests can be seen in figure 5-5. A list of the utilised sensors is annexed in appendix B. A picture of the setup in the laboratory is shown in figure 5-6.
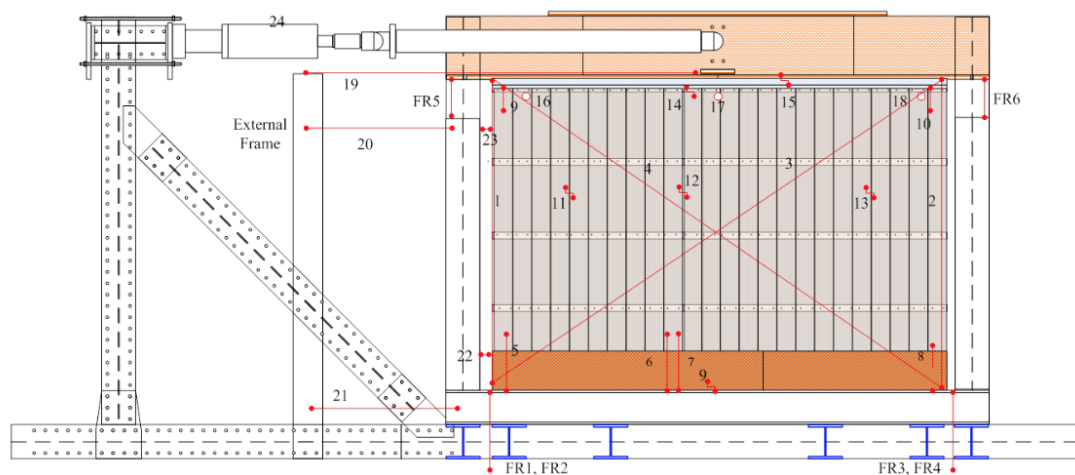
Figure 5-5: Instrumentation of the test
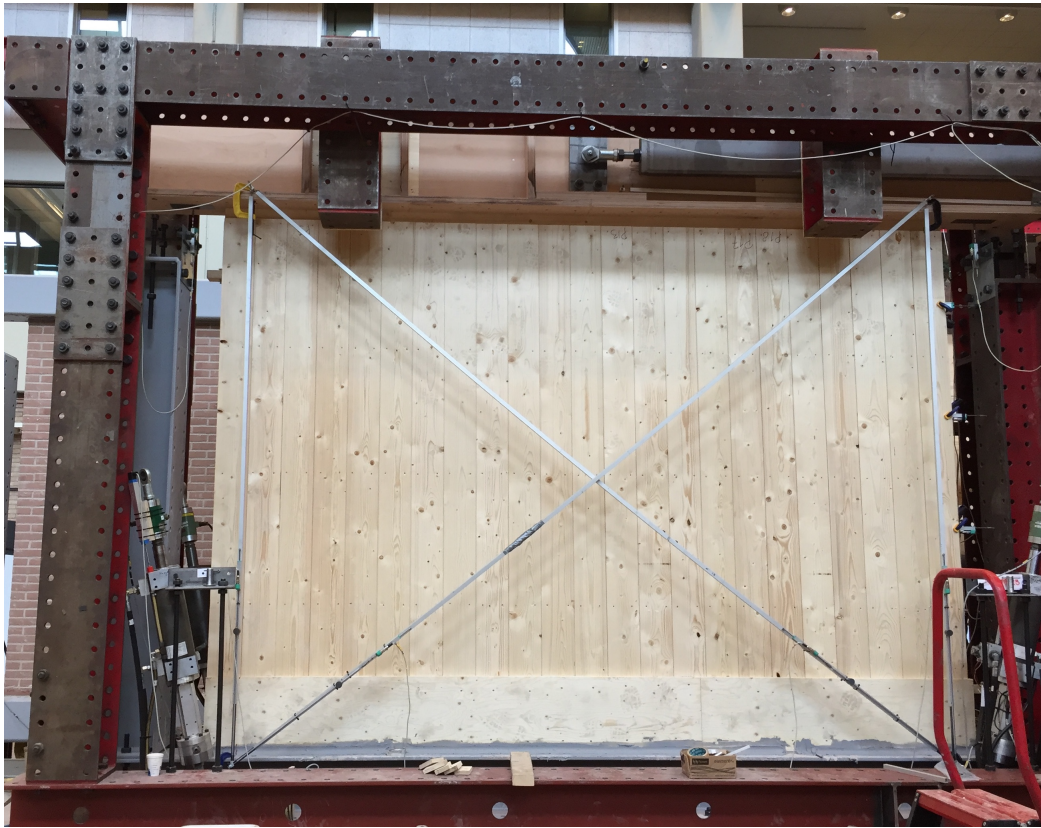
Figure 5-6: Photo of test setup

5.1.2 Test results

The as-built diaphragm was not tested until failure, thus an ultimate failure load and an ultimate failure displacement cannot be concluded. There was no visible damage to the diaphragm after testing. The load-displacement diagram of the tested as-built diaphragm can be seen in figure 5-7. This diagram is point-symmetric and shows (almost) no pinching behaviour. The maximum load during cyclic loading was approximately 22.3 kN with a corresponding displacement of 63.3 mm. Strength losses between cycles of the same amplitude were quite small, especially for the smaller amplitudes. This is consistent with the observation of little to no degradation of the diaphragm. The envelope curve of the hysteresis of the diaphragm is shown in figure 5-8, along with its linear idealisation. The envelope is fairly linear, thus it can be represented through a linear curve. The slope of the linear idealisation is 0.372 kN/mm.
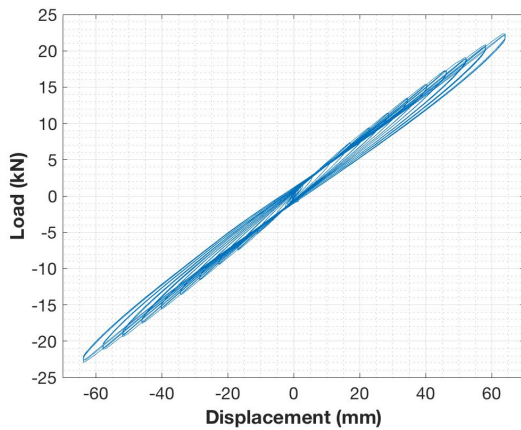
Figure 5-7: Load-displacement diagram for the as-built specimen
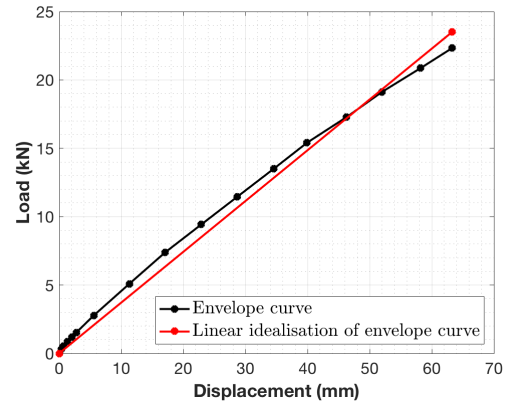
Figure 5-8: Envelope curve and linear representation for the positive part of the hysteresis of the as-built specimen

5.2 CONNECTIONS WITHIN AS-BUILT DIAPHRAGMS

To obtain data for the nailed connections between sheathing and joists, monotonic and cyclic experimental tests have been carried out on these connections. Within the testing campaign, two types of connections can be distinguished: connections which were extracted from floor specimens from houses in Groningen and connections which were replicated at the TU Delft laboratory. Some of the replicated specimens were extracted from the replicated diaphragms that were tested in the laboratory in June 2017. As these diaphragms are considered for the scope of this report, only the results of the replicated connection specimens extracted from these diaphragms will be discussed in this section. Three types of tests were conducted: loading parallel to the joists, loading perpendicular to the joists and rotational loading (see figure 5-9). For the three types of tests, the connection specimens consisted of a segment of a joist and a segment of a plank, connected by two nails.
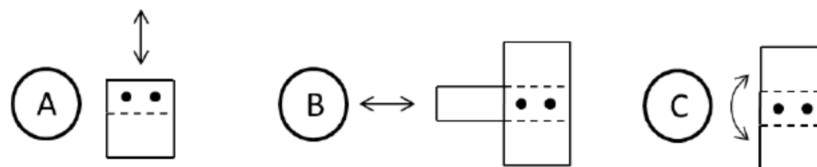
Figure 5-9: A-Loading perpendicular to joists, B-Loading parallel to joists, C-Rotational loading [24]

The loading protocol for the connections is according to ISO 16670. Prior to the cyclic tests, monotonic tests have to be carried out to determine the ultimate displacement. This ultimate displacement is taken either as the displacement at failure or the displacement at 80% of the maximum force in the descending part of the load-displacement curve (see figure 5-10). One monotonic test was carried out for loading perpendicular to the joists and one for rotational loading. The result of the monotonic test for loading perpendicular to the joists was also used to determine the ultimate displacement for tests in which loading was parallel to the joists. For the rotational tests, the displacement is converted to radians. With the ultimate displacement as found from monotonic tests, the cyclic loading scheme is determined. For the cyclic loading scheme, only one cycle is carried out for each amplitude up to 10 percent of the ultimate displacement. These cycles are performed at an amplitude of 1.25, 2.5, 5, 7.5 and 10 percent of the ultimate displacement. For each amplitude that exceeds 10 percent of the ultimate displacement, three cycles need to be carried out. These cycles

are performed at an amplitude of 20, 40, 60, 80 and 100 percent of the ultimate displacement. If the ultimate displacement is exceeded, increments of 20 percent of the ultimate displacement can be added to the loading scheme, with three cycles for each amplitude again. The loading scheme can be seen in figure 5-11. Loading is applied at a rate between 0.1 and 10 mm/s. Prior to testing, the measurements and the density of the boards and joists were measured. For the nails, the measurements and distances were measured. The measurements of the nailed connection specimens can be found in appendix C.
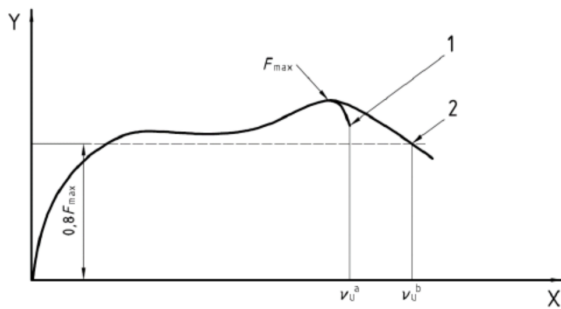
Figure 5-10: Load-displacement curve for monotonic testing of nailed joint [25]
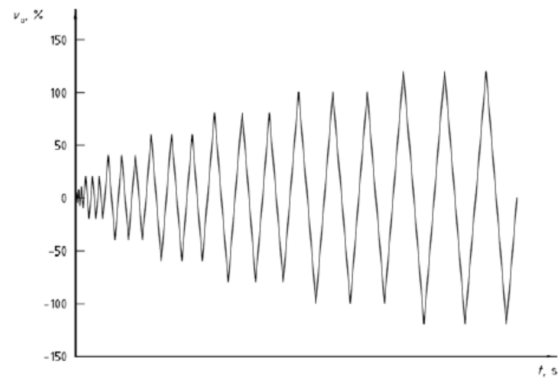
Figure 5-11: Cyclic loading scheme according to ISO 16670 [25]

5.2.1 LOADING PERPENDICULAR TO JOISTS
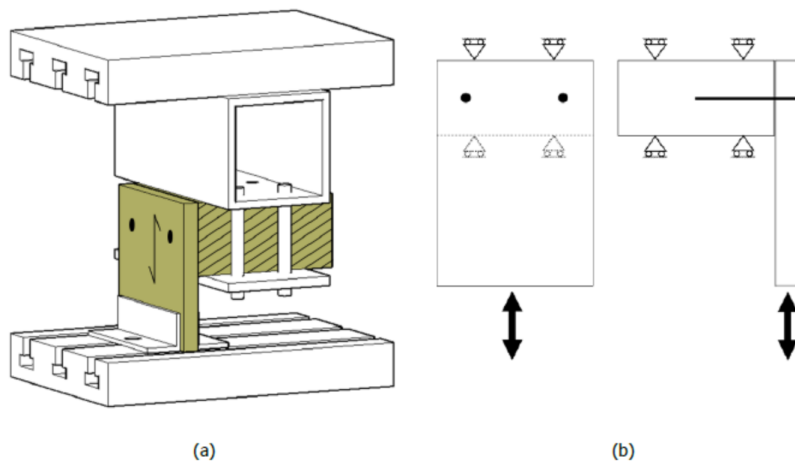
Figure 5-12: (a) Test setup for connections (b) Forces on specimen [24]

The test setup for loading perpendicular to the joists can be seen in figure 5-12. The joist and the board were clamped to the test apparatus and the displacement between joist and board was measured. One replicated specimen was tested monotonically and six replicated specimens were tested cyclically. Of those tested cyclically, five specimens yielded reliable results. Only these five specimens will be taken into consideration. The monotonic test served to determine the ultimate displacement on which the cyclic loading scheme will be based. The result of the monotonic test can be seen in figure 5-13. The maximum force was 2.07 kN at a displacement of 33.3 mm. Failure occurred due to both nails pulling out through the plank. According to ISO 16670, the ultimate displacement would be 52 mm based on the experimental result. However, this ultimate displacement may cause plastic deformation during the first loading cycle of the cyclic scheme. This is undesirable, as the

elastic stiffness cannot be determined. Therefore, the ultimate displacement is taken as 22 mm to ensure that only elastic deformation occurs during the first cycle of the cyclic loading scheme. With this ultimate displacement, the cyclic loading scheme is set and cyclic tests can be carried out.
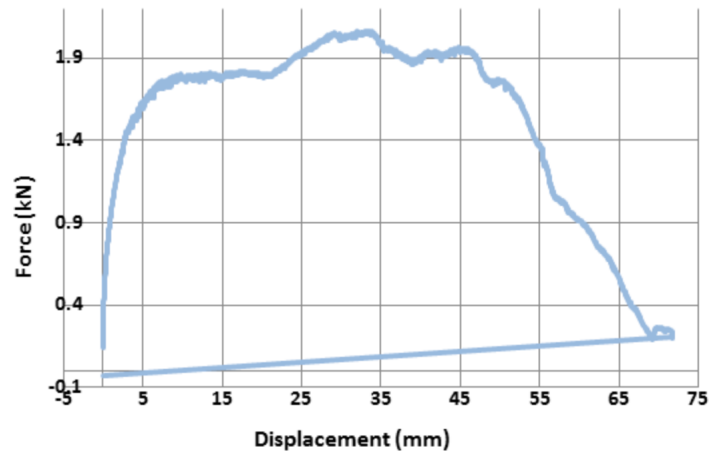
Figure 5-13: Result of monotonic test on replicated connection specimen

The hysteresis diagrams of the cyclically tested specimens can be seen in figure 5-14, along with the corresponding backbone curves. All the hysteresis diagrams show a nonlinear backbone curve with a high initial stiffness. After a certain "yield" point, the stiffness of the backbone decreases. The stiffness of the backbone curve even becomes negative as the specimen degrades. The hysteresis of the specimens also show high nonlinear behaviour, as evident from the unloading and reloading paths. High pinching behaviour can be seen and a reduced strength for cycles of the same amplitude is visible. This strength reduction is greater for cycles of bigger amplitudes. All cyclically loaded specimens failed due to the bending of both nails. The test results are summarised in table 5-2. The average maximum load for the five specimens is 2.13 kN. For the comparison of the tested specimens, the backbone curves have been plotted in one graph in figure 5-15 and the hystereses in figure 5-16. The average backbone curve of the cyclically loaded specimens and the average hysteresis can be seen in figure 5-17 and figure 5-18 respectively.
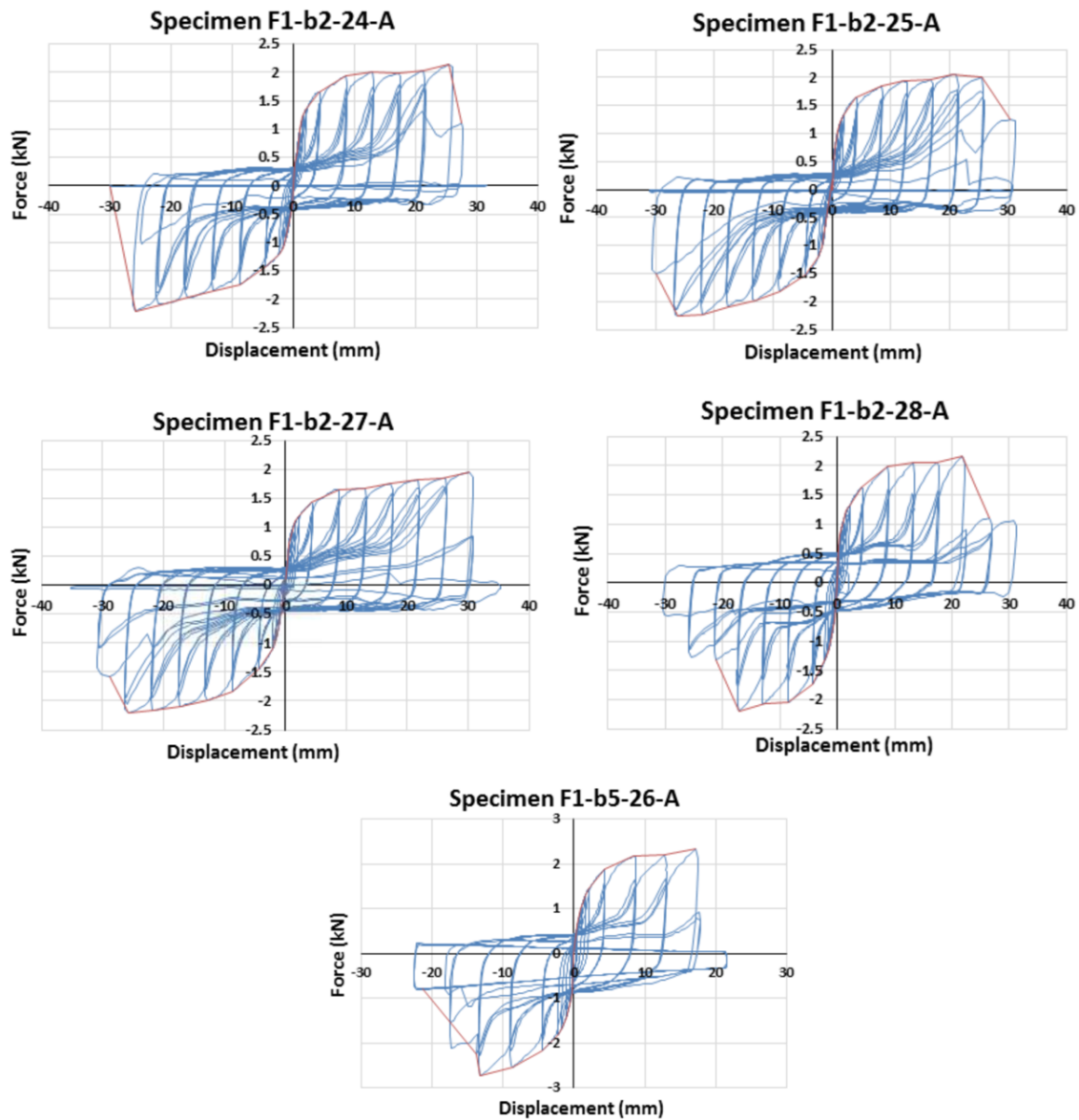
Figure 5-14: Results of cyclic tests on replicated connection specimens

Table 5-2: Test results

Specimen	Test	Maximum load (kN)	Corresponding displacement (mm)	Failure mode
F1-b2-26-A	Monotonic	2.07	33.30	Pulling out of both nails
F1-b2-24-A	Cyclic	2.14	25.44	Bending failure of both nails
F1-b2-25-A	Cyclic	2.05	20.53	Bending failure of both nails
F1-b2-27-A	Cyclic	1.96	30.15	Bending failure of both nails
F1-b2-28-A	Cyclic	2.16	21.79	Bending failure of both nails
F1-b5-26-A	Cyclic	2.34	17.23	Bending failure of both nails

Figure 5-15: Backbone curves of specimens loaded perpendicular to the joists
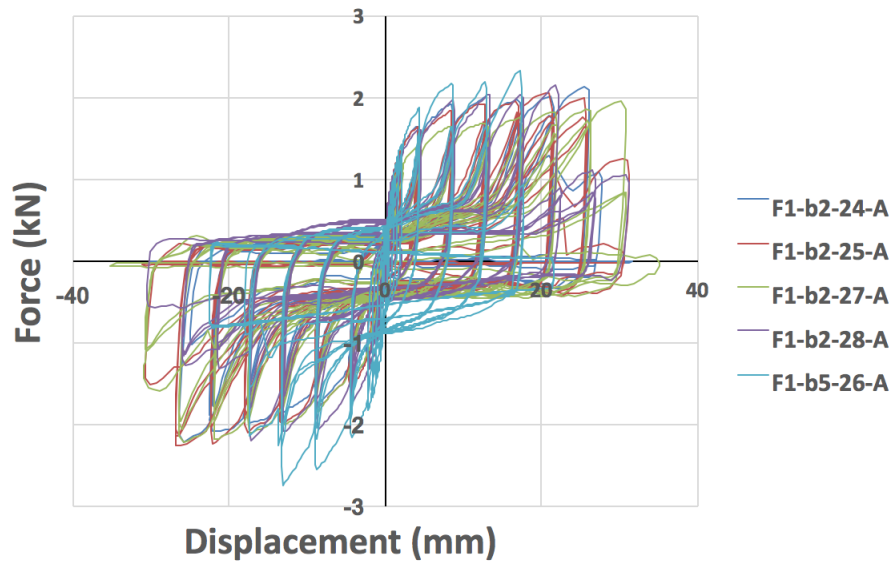
Figure 5-16: Hysteresis diagrams of specimens loaded perpendicular to the joists
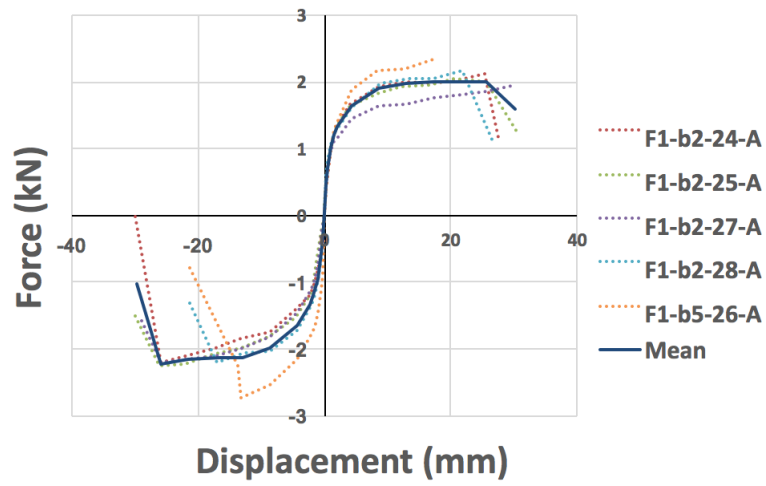
Figure 5-17: Average backbone curve of specimens loaded perpendicular to the joists
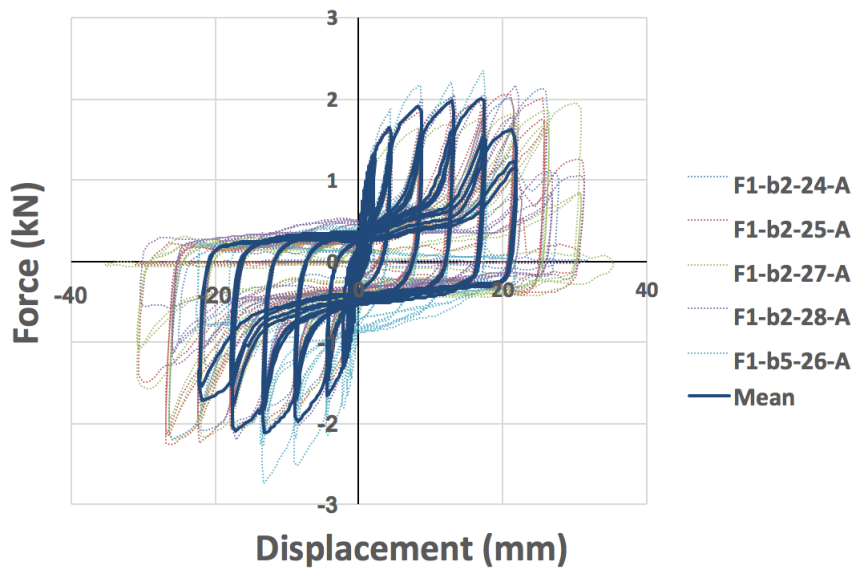
Figure 5-18: Average hysteresis diagram of specimens loaded perpendicular to the joists

5.2.2 LOADING PARALLEL TO JOISTS
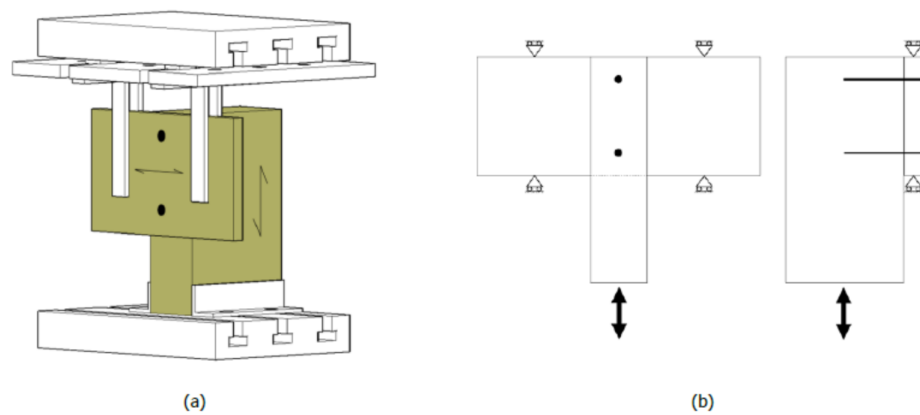
Figure 5-19: (a) Test setup for connections (b) Forces on specimen [24]

The test setup for loading parallel to the joists can be seen in figure 5-19. The joist and the board were clamped to the test apparatus and the displacement between joist and board was measured. Four replicated specimens were tested cyclically, of which three yielded reliable results. Only these three specimens will be taken into consideration for cyclic purposes. For the cyclic loading scheme, an ultimate displacement of 14 mm was taken. The hysteresis diagrams of the cyclically tested specimens can be seen in figure 5-20, along with the corresponding backbone curves. The hysteresis diagrams all show a nonlinear backbone curve with a high initial stiffness. After a certain "yield" point, the stiffness of the backbone decreases. The stiffness of the backbone curve even becomes negative as the specimen degrades. The hysteresis of the specimens also show high nonlinear behaviour, as evident from the unloading and reloading paths. High pinching behaviour can be seen and a reduced strength for cycles of the same amplitude is visible. This strength reduction is greater for cycles of bigger amplitudes. The specimens failed due to different mechanisms, two specimens failed due to pulling out of one nail and bending failure of the other nail. The other specimen failed due to the bending of both nails. The test results are summarised in table 5-3. The average maximum load for the three specimens is 2.38 kN. For the comparison of the tested specimens, the backbone curves have been plotted in one graph in figure 5-21 and the hystereses in figure 5-22. The average backbone curve of the cyclically loaded specimens and the average hysteresis can be seen in figure 5-23 and figure 5-24.
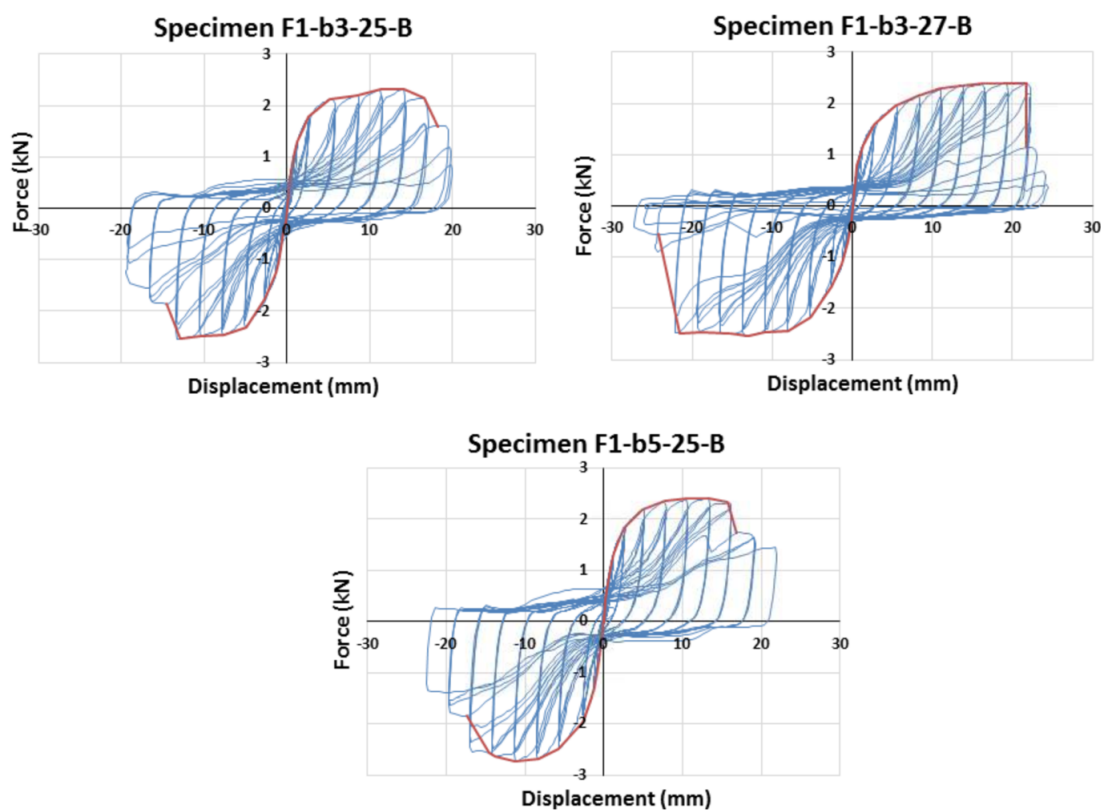
Figure 5-20: Results of cyclic tests on replicated connection specimens

Table 5-3: Test results

Specimen	Test	Maximum load (kN)	Corresponding displacement (mm)	Failure mode
F1-b3-25-B	Cyclic	2.32	14.11	Pulling out of one nail, bending failure of one nail
F1-b3-27-B	Cyclic	2.39	21.78	Bending failure of both nails
F1-b5-25-B	Cyclic	2.42	13.33	Pulling out of one nail, bending failure of one nail
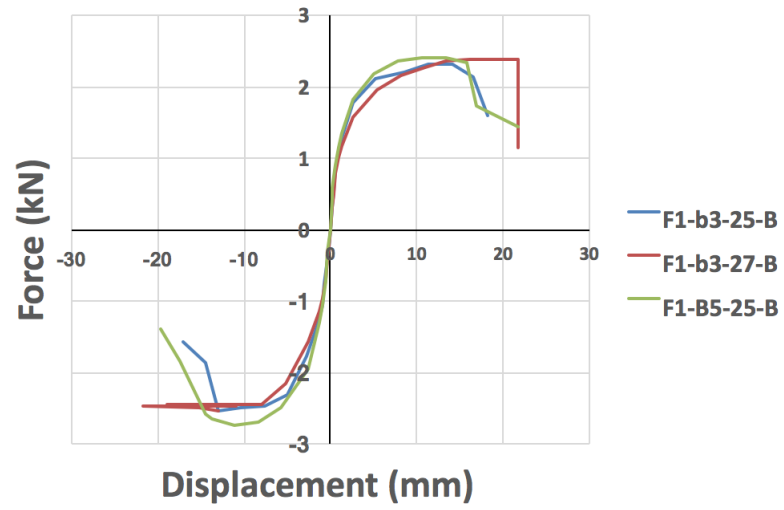
Figure 5-21: Backbone curves of specimens loaded parallel to the joists
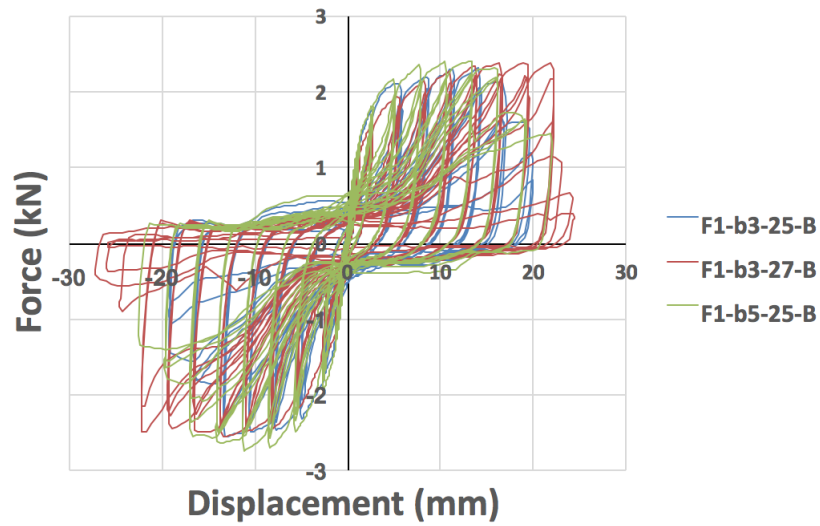
Figure 5-22: Hysteresis diagrams of specimens loaded parallel to the joists
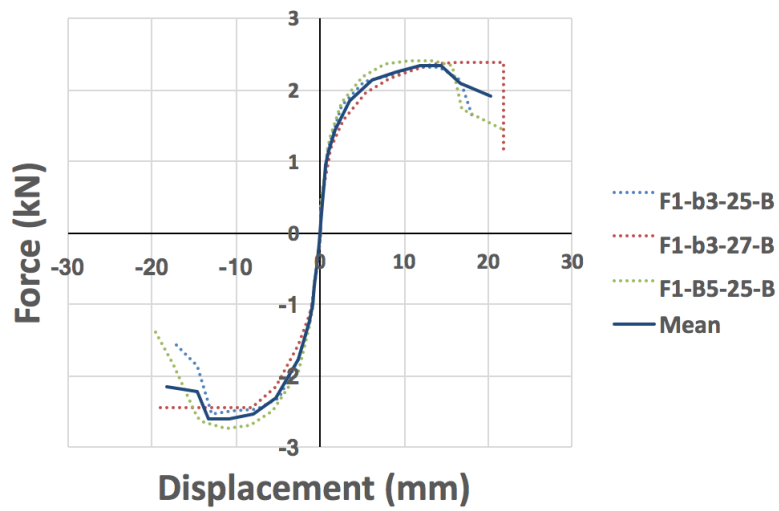
Figure 5-23: Average backbone curve of specimens loaded parallel to the joists
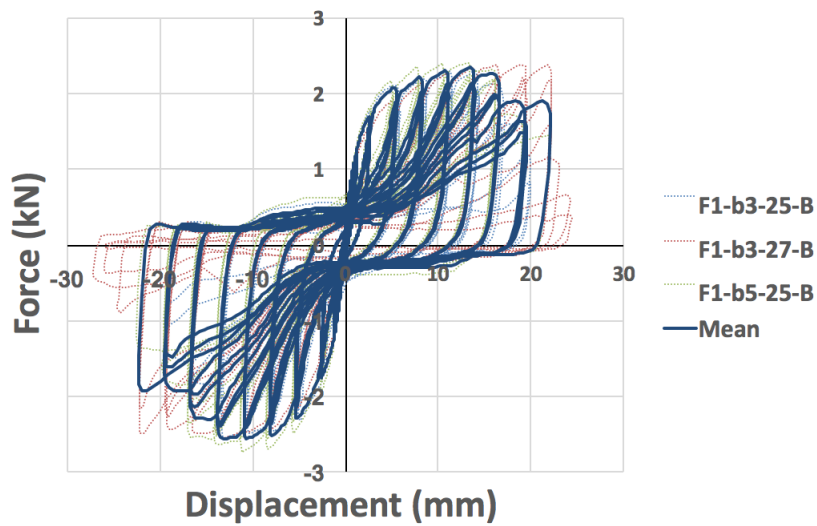
Figure 5-24: Average hysteresis diagram of specimens loaded parallel to the joists

5.2.3 Rotational loading
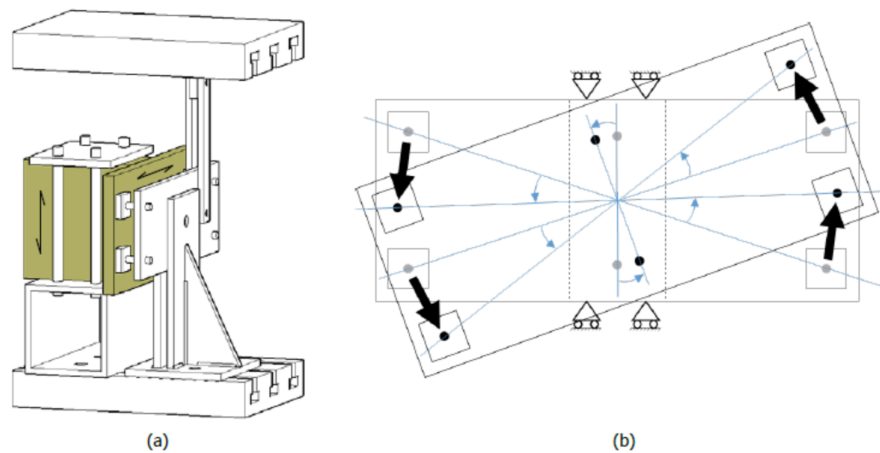
Figure 5-25: (a) Test setup for connections (b) Forces on specimen [24]

The test setup for rotational loading can be seen in figure 5-25. Two replicated specimens were tested monotonically to determine the ultimate displacement. The results of these tests can be seen in figure 5-26. However, these tests did not result in failure of the specimens, thus the ultimate displacement could not be determined based on these tests. The ultimate displacement was assumed to be 15 mm, as this was also used for previous tests. Five replicated specimens were tested cyclically, of which three yielded reliable results. Only these three specimens will be taken into consideration for cyclic purposes. The hysteresis diagrams of the cyclically tested specimens can be seen in figure 5-27, along with the corresponding backbone curves. The hysteresis diagrams all show a nonlinear backbone curve with a high initial stiffness. After a certain "yield" point, the stiffness of the backbone decreases. The stiffness of the backbone curve even becomes negative as the specimen degrades. The hysteresis of the specimens also show high nonlinear behaviour, as evident from the unloading and reloading paths. High pinching behaviour can be seen and a reduced strength for cycles of the same amplitude is visible. This strength reduction is greater for cycles of bigger amplitudes. All specimens failed due to the bending of the nails. The test results are summarised in table 5-4. The average maximum moment for the three specimens is 93.51 kNmm. For the comparison of the tested specimens, the backbone curves have been plotted in one graph in figure 5-28 and the hystereses in figure 5-29. The average backbone curve of the cyclically loaded specimens can be seen in figure 5-30.
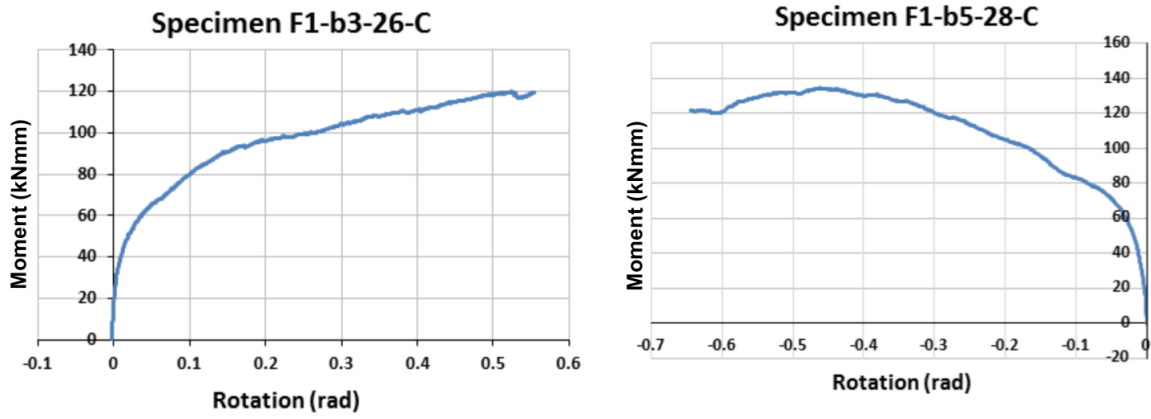
Figure 5-26: Results of monotonic tests on replicated connection specimens
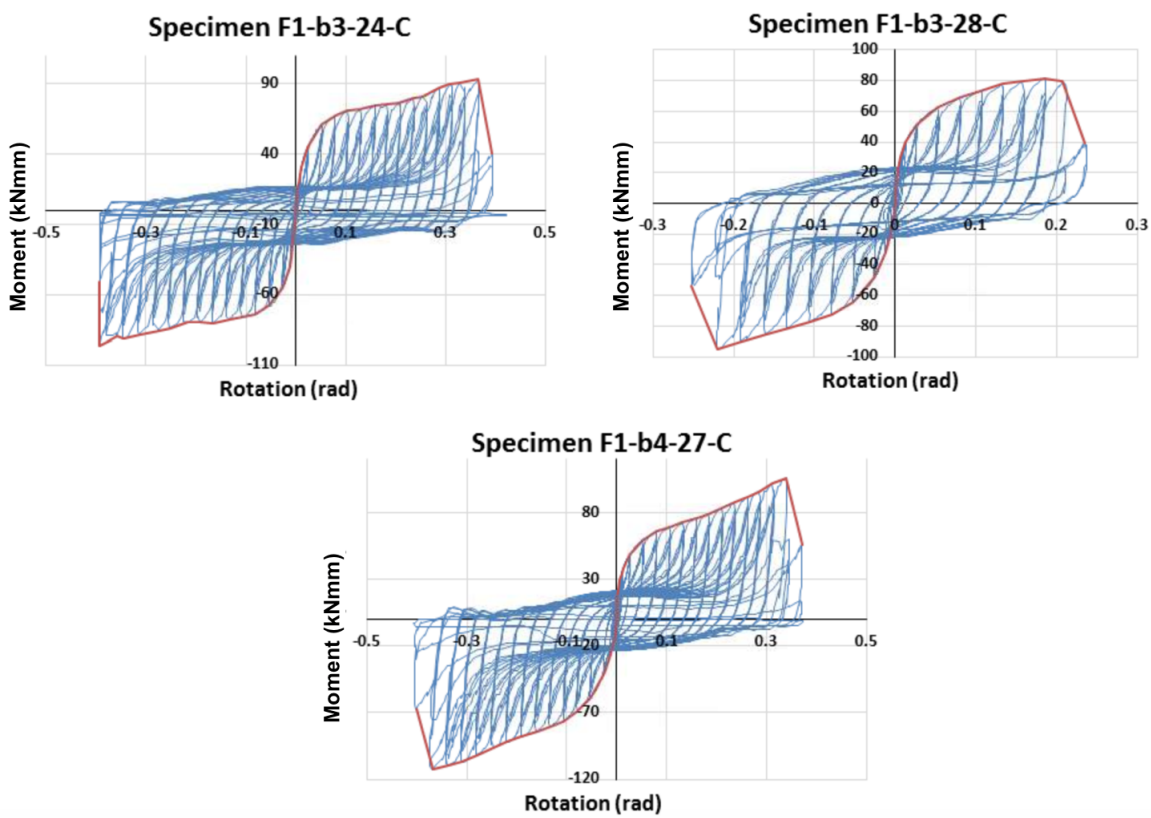
Figure 5-27: Test results

Table 5-4: Test results

Specimen	Test	Maximum moment (kNmm)	Corresponding rotation (rad)	Failure mode
F1-b3-26-C	Monotonic	119.77	0.52	-
F1-b5-28-C	Monotonic	134.58	0.46	-
F1-b3-24-C	Cyclic	92.72	0.37	Bending failure of both nails
F1-b3-28-C	Cyclic	81.64	0.19	Bending failure of both nails
F1-b4-27-C	Cyclic	106.17	0.34	Bending failure of both nails

Figure 5-28: Backbone curves of rotational loaded specimens
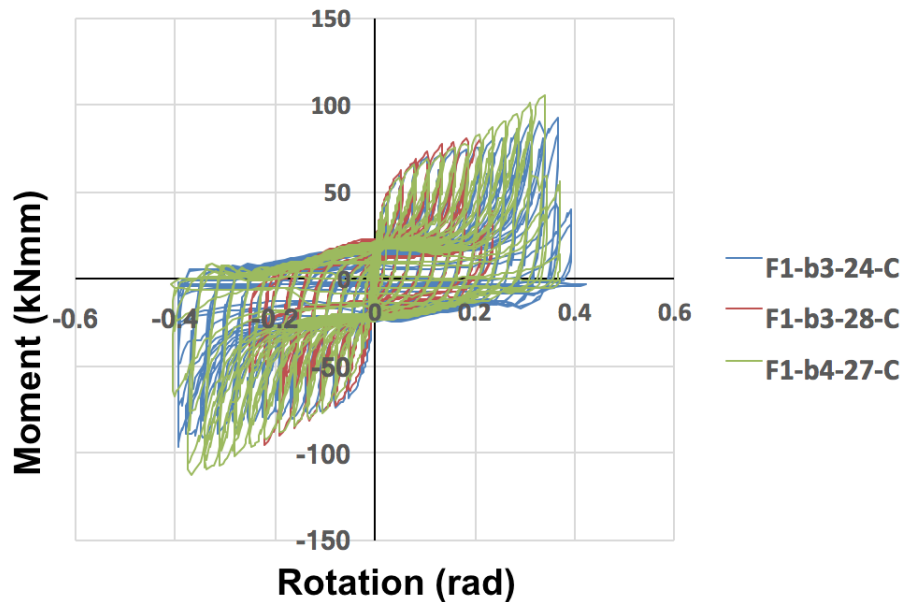
Figure 5-29: Hysteresis diagrams of rotational loaded specimens
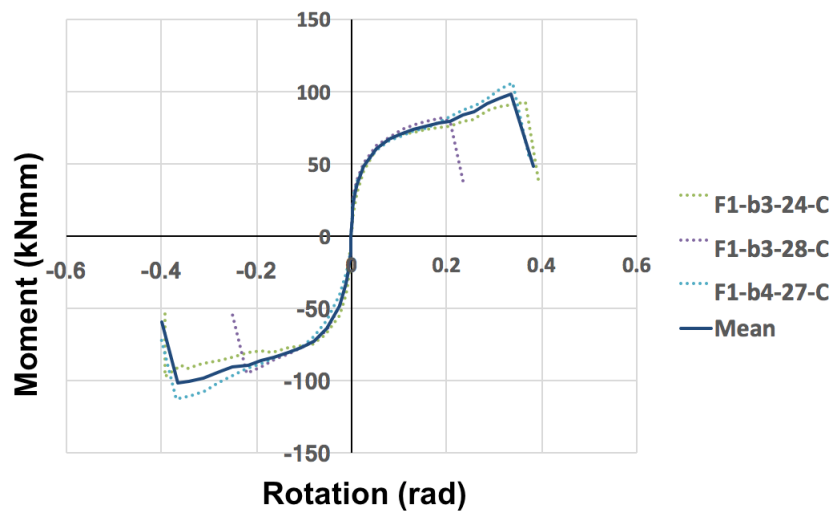
Figure 5-30: Average backbone curve of rotational loaded specimens

5.3 Retrofitted diaphragm

5.3.1 Test setup

For the testing of the retrofitted diaphragm, the same test setup as for the as-built diaphragm was adopted. The as-built specimen was not tested until failure, so this specimen was strengthened to obtain the retrofitted diaphragm. Strengthening was achieved by screwing spruce plywood panels onto the sheathing boards. These screws had a diameter of 4.5 mm and a length of 40 mm. For the top joist (at which loading was applied), the panels were screwed through the planks and into the joist. These screws had a diameter of 5.0 mm and a length of 70 mm. The measurements of the panels varied as the configuration was made to fit the dimensions of the diaphragm. A schematisation of the retrofitted specimen can be seen in figure 5-31. A photo of the test setup is shown in figure 5-32.

The same testing protocol as used for the as-built diaphragm was adopted for the retrofitted diaphragm. The loading scheme started with an amplitude of 0.3 mm and ended with an amplitude of approximately 63 mm (see figure 5-33). After the loading cycles with amplitudes 38 mm and 44 mm, the loading was paused for a while. The instrumentation of the retrofitted diaphragm was largely the same as for the as-built diaphragm, except for a few added sensors. Notably, two sensors were placed at the bottom right of the specimen to measure the relative horizontal and vertical displacements between adjacent plywood panels. These sensors can be seen in figure 5-32. An overview of the instrumentation is annexed in appendix B.
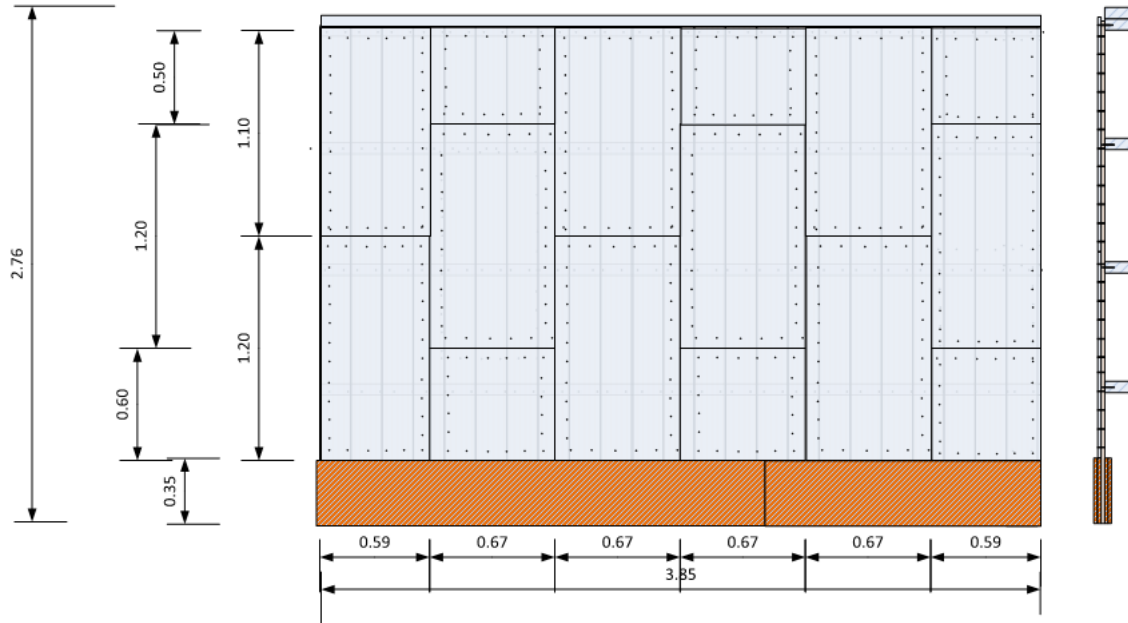
Figure 5-31: Schematisation of tested retrofitted specimen
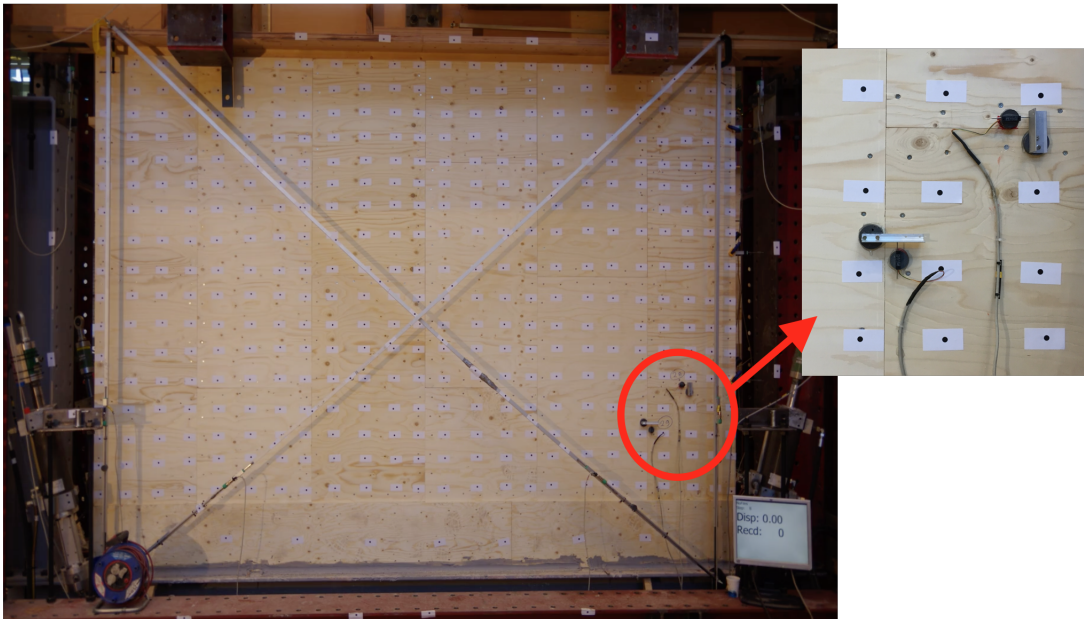
Figure 5-32: Test setup
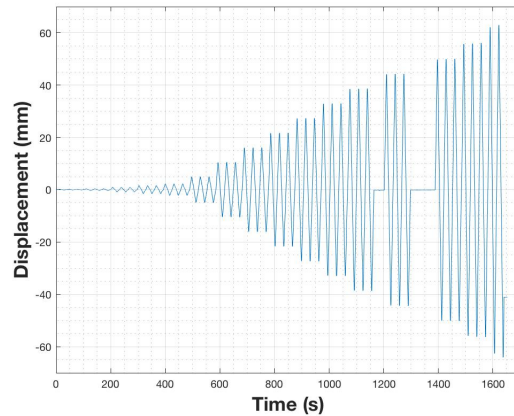
Figure 5-33: Loading scheme

5.3.2 Test results

The retrofitted diaphragm was tested until failure, which occurred at a displacement of approximately 63 mm and a load of approximately 55 kN. Failure occurred due to the top row of screws breaking off, these screws connected the plywood panels to the boards and loaded joist. At this location, the nails (which connected the boards to the joist) were also pulled out. The failure of the screws and nails can be seen in figure 5-34, in which the red circles indicate the broken screws and the blue circle indicates the pulled out nail. The load-displacement curve of the retrofitted diaphragm can be seen in figure 5-35, along with its backbone curve in figure 5-36. The hysteresis of the retrofitted diaphragm exhibits a high degree of pinching, with the stiffness significantly decreasing after multiple load cycles. Between successive cycles of the same displacement amplitude, a strength drop can be seen as the maximum load decreases each cycle. This strength loss can be up to 20%. From the backbone curve, it can be seen that the initial stiffness up to a displacement of 2 mm is quite high. After a displacement of about 2 mm, the stiffness decreases and is near linear up to a displacement of approximately 55 mm. When the displacement exceeds a value of 55 mm, the stiffness becomes negative as the diaphragm begins to deteriorate and eventually fails.

Figure 5-34: Failure of nails and screws at top joist
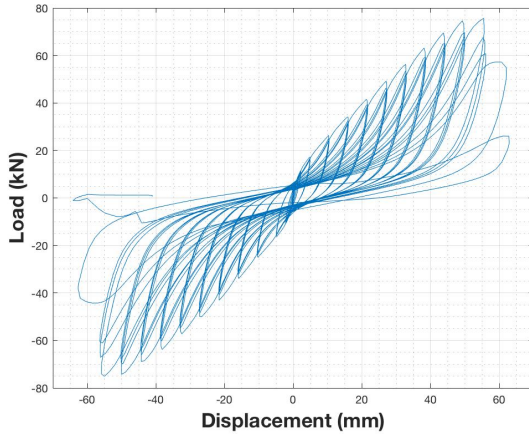
Figure 5-35: Load-displacement diagram for the retrofitted specimen
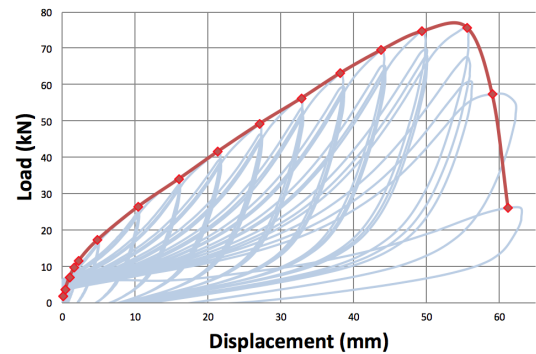
Figure 5-36: Envelope curve for the positive part of the hysteresis of the retrofitted specimen
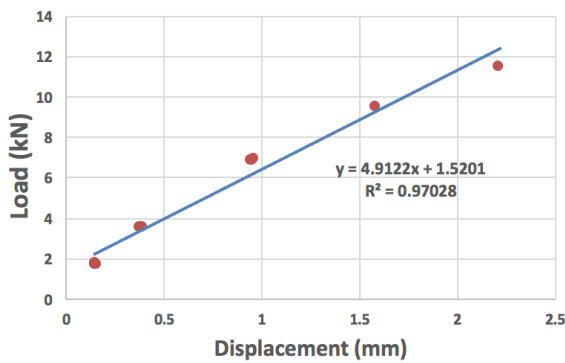
Figure 5-37: Backbone and linearisation up to a displacement of 2 mm
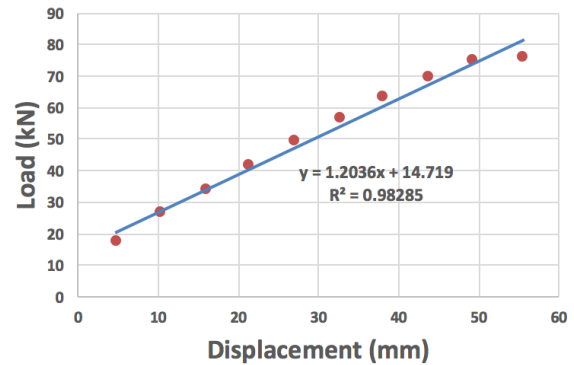
Figure 5-38: Backbone and linearisation from a displacement of 2 mm up to 55 mm

Taking a closer look at the backbone curve up to a displacement of 55 mm (before the diaphragm deteriorates and fails), one can see that this part of the curve is near bilinear. The two linear segments can be distinguished between a displacement of 0 up to 2 mm and a displacement of 2 up to 55 mm. The initial stiffness up to a displacement of 2 mm is calculated as 4.9 kN/mm (see figure 5-37). The correlation coefficient of the linearisation of this part of the backbone is very close to 1.0, meaning that the linearisation is accurate and that the data can be well represented linearly. This also holds for the second segment of the backbone (displacement 2 mm to 55 mm), the stiffness for this part is calculated as 1.2 kN/mm (see figure 5-38). It can be seen that the second stiffness is almost five times lower than the initial stiffness.

The envelope curve can be idealised by a bilinear curve, in which the conserved energy (thus the area under the curve) is the same as the original curve. To construct the bilinear idealisation, the procedure as adopted in the paper written by A. Wilson, P.J. Quenneville and J.M. Ingham is modified [10]. The procedure as used in this section implies that the following requirements must be met by the bilinear curve:

1. The energy conserved in the original curve and the bilinear curve must be approximately the same.
2. The bilinear curve must pass through zero displacement and zero load.

3. The so-called yield point of the bilinear curve must be chosen at the point after which the original curve is near linear.
4. The final displacement of the bilinear curve is taken as the maximum displacement from the original curve.
5. The slopes of the segments of the bilinear curve must be similar to the slopes as exhibited in the original curve.

The bilinear representation only holds up to a displacement of approximately 55 mm, as the specimen begins to fail hereafter. The bilinear curve starts at a displacement and force of zero. The yield point is taken at a displacement of 2.2 mm and a force of 14.8 kN. The yield point on the original curve is at a displacement of 2.2 mm and load of 11.45 kN. The final point on the bilinear curve is at a displacement of 55.5 mm and a force of 84.5 kN, as opposed to the original displacement of 55.5 mm and force of 75.69 kN. The initial stiffness of the bilinear curve is calculated as 6.7 kN/mm, which is significantly higher than the actual initial stiffness of 4.9 kN/mm. The secondary stiffness of the bilinear curve is valued at 1.3 kN/mm, which is close to the actual secondary stiffness of 1.2 kN/mm. The envelope curve and its bilinear idealisation can be seen in figure 5-39. In order to conserve the same energy, the stiffnesses of the idealisation deviate from the original stiffnesses. These deviations are not desirable. Furthermore, the bilinear backbone overestimates the ultimate strength. Nevertheless, the constructed idealisation still captures the overall behaviour of the envelope curve quite well and may be sufficient for numerical purposes. Do note that this idealisation is only valid for the pre-failure regime.
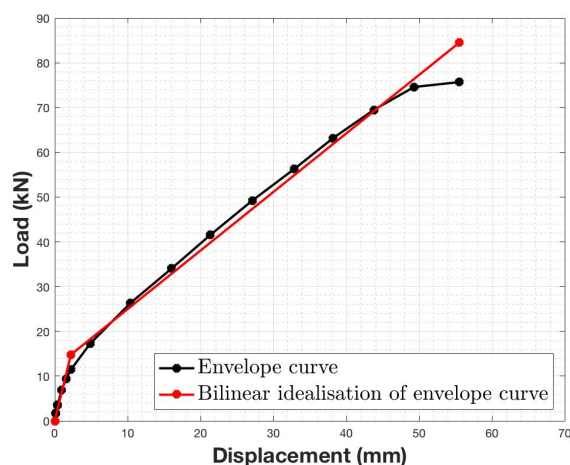
Figure 5-39: Envelope curve and bilinear idealisation up to a displacement of 55 mm

5.4 CONNECTIONS WITHIN RETROFITTED DIAPHRAGMS

For the connections within the retrofitted diaphragm, the same test setup and testing protocol as for the connections within the as-built diaphragm is adopted (see section 5.2). Two new types of connections were tested for the retrofitted diaphragm: screwed connections between panel and plank, and screwed connections between panel, plank and beam. The latter connection occurs at the top of the tested retrofitted diaphragm where loading was applied. For each type of connection, two types of tests were carried out in which loading was applied perpendicular and parallel to the main timber element. Each type of test was carried out on seven specimens, of which one was loaded monotonically to determine the yield displacement for the cyclic loading scheme. The remaining

six specimens were tested cyclically. The specifications of the tested specimens are annexed in appendix D.

5.4.1 Screwed connection between panel and plank

The retrofitted diaphragm was produced from the as-built diaphragm by screwing timber panels on top of the planks. The screws only connected the panels to the planks and do not penetrate the joists. The screws were placed around the perimeter of each panel with a spacing of approximately 100 mm. Screws with a length of 40 mm and a diameter of 4.5 mm were used. For the testing of the screwed connection between panel and plank, the specimens consisted of a segment of a panel screwed on top of a segment of a plank. Each specimen contained two screws.

Loading perpendicular to the plank

For loading perpendicular to the plank, the result of the monotonic test can be seen in figure 5-40. The maximum reached force for the monotonic test was 3.73 kN at a displacement of 15.37 mm. Failure occurred due to both screws pulling out. From the monotonic test, a yield slip of 24 mm is determined. With this yield slip, the cyclic loading scheme is set and the cyclic tests can be carried out.
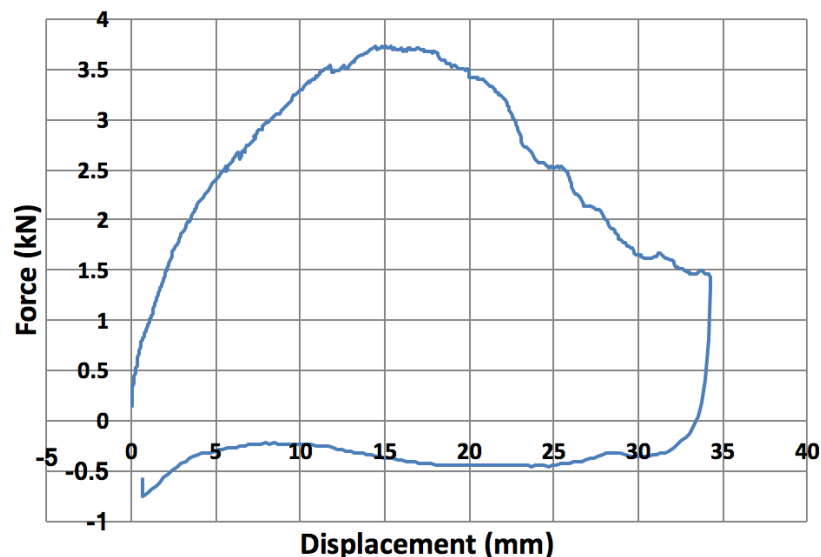
Figure 5-40: Monotonic response of connection between panel and plank

The hysteresis diagrams of the cyclically tested specimens can be seen in figure 5-41, along with the corresponding backbone curves. After the first three cyclic tests, it was decided to reduce the yield slip from 24 to 16 mm to better capture the elastic and plastic behaviour of the connection. Thus, the cyclic loading scheme was changed. All specimens show a similar hysteresis with a narrow pinching region and similar maximum forces. Test results are summarised in table 5-5. The average maximum load for the seven specimens is 3.38 kN. Failure occurred mostly due to pulling out of the two screws. For the comparison of the tested specimens, the backbone curves and hysteresis curves have been plotted in figure 5-42 and figure 5-43. Comparing the backbone curves, the specimens exhibit a very similar behaviour with a high initial stiffness. After reaching a certain yield point, the backbone curve assumes a negative stiffness and thus a decrease in strength can be seen. Both the backbone curves and hystereses are highly nonlinear. The average backbone curve is plotted in figure 5-44.
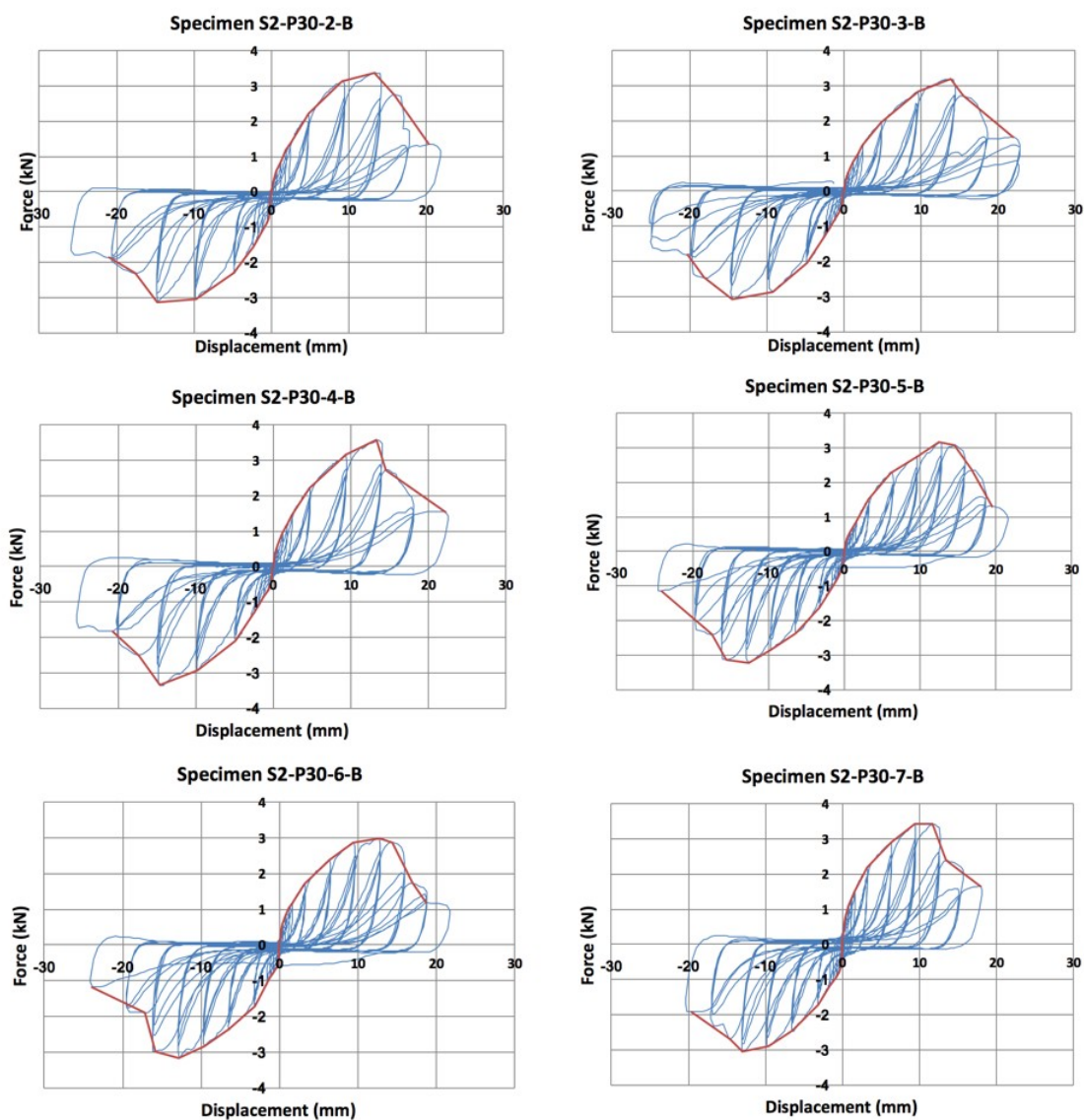
Figure 5-41: Hysteresis diagrams for loading perpendicular to the plank

Table 5-5: Test results

Specimen	Test	Maximum load (kN)	Corresponding displacement (mm)	Failure mode
S2-P29-1-B	Monotonic	3.73	15.37	Pulling out of both screws
S2-P30-2-B	Cyclic	3.38	13.31	Pulling out of both screws
S2-P30-3-B	Cyclic	3.19	13.80	Pulling out of both screws
S2-P30-4-B	Cyclic	3.58	13.33	Pulling out of both screws
S2-P30-5-B	Cyclic	3.22	12.66	Pulling out of both screws
S2-P30-6-B	Cyclic	3.10	12.86	Pulling out of one screw, bending failure of one screw
S2-P30-7-B	Cyclic	3.43	9.43	Pulling out of both screws

Figure 5-42: Backbone curves of specimens loaded perpendicular to the plank
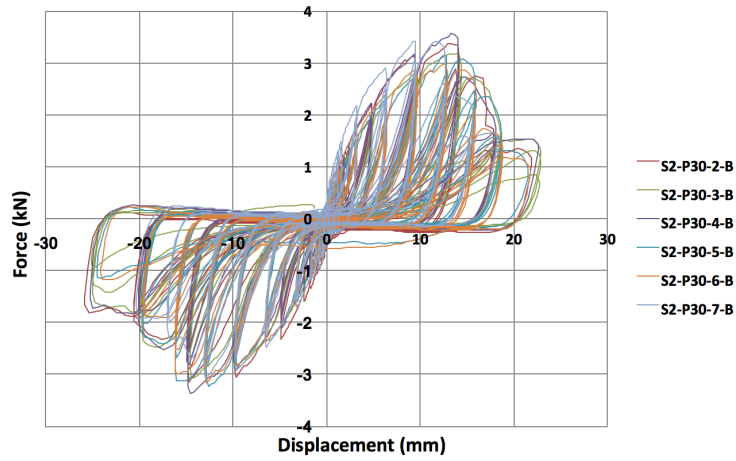
Figure 5-43: Hysteresis curves of specimens loaded perpendicular to the plank
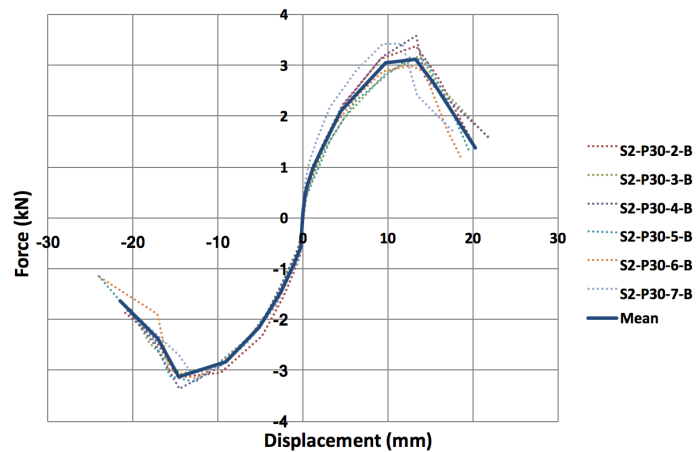
Figure 5-44: Average backbone curve of specimens loaded perpendicular to the plank

LOADING PARALLEL TO THE PLANK

For loading parallel to the plank, the result of the monotonic test can be seen in figure 5-45. The maximum reached force for the monotonic test was 3.93 kN at a displacement of 18.30 mm. Failure occurred due to cracking of the plank and one screw pulling out. From the monotonic test, a yield slip of 20 mm is determined. With this yield slip, the cyclic loading scheme is set and the cyclic tests can be carried out. The hysteresis diagrams of the cyclically tested specimens can be seen in figure 5-46, along with the corresponding backbone curves. The hystereses all show a narrow pinching part. The backbone curves are nonlinear and show a high initial stiffness. Test results are summarised in table 5-6. The average maximum force for the seven tested specimens is 3.81 kN. For the comparison of the tested specimens, the backbone curves and hysteresis curves have been plotted in figure 5-47 and figure 5-48. The average backbone curve is plotted in figure 5-49. For the first two specimens, the backbone curve seems to have a residual strength after reaching a certain yield point. This may be attributed to the fact that both screws did not fail at the same time. The hystereses and backbone curves of the first two specimens differ from the other specimens, which may be attributed to the fact that failure did not occur due to pulling out of both screws. For the last four specimens, failure does occur due to pulling out of both screws and thus the hystereses and backbone curves show more similarities.
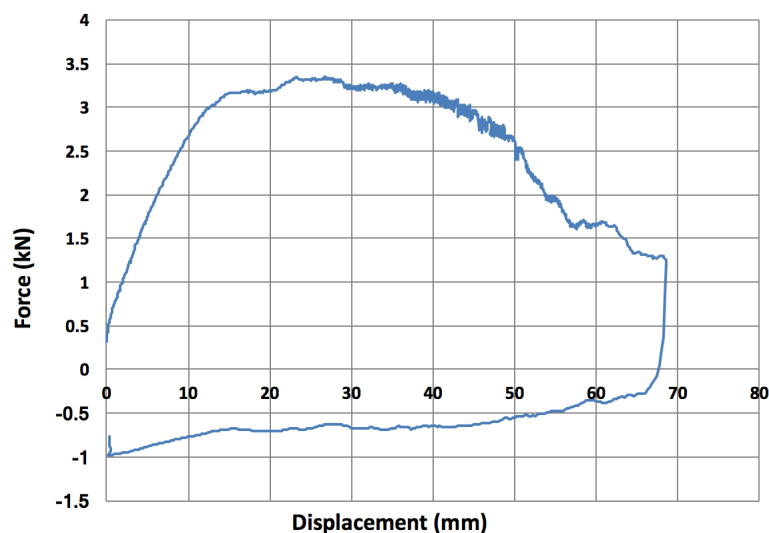
Figure 5-45: Monotonic response of connection between panel and plank
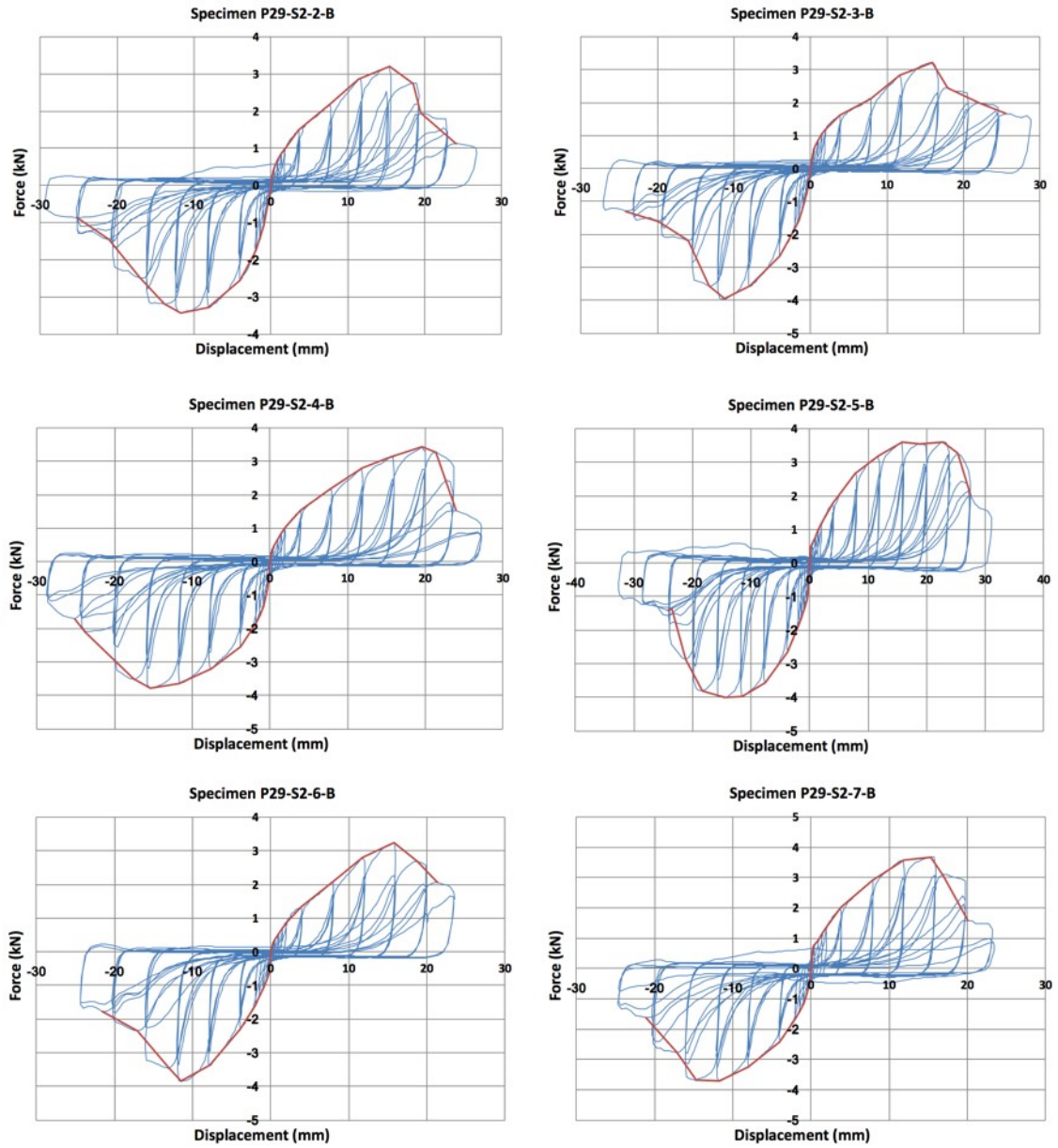
Figure 5-46: Hysteresis diagrams for loading parallel to the plank

Table 5-6: Test results

Specimen	Test	Maximum load (kN)	Corresponding displacement (mm)	Failure mode
P29-S2-1-B	Monotonic	3.93	18.30	Crack in plank, pulling out of one screw
P29-S2-2-B	Cyclic	3.43	11.73	Pulling out of one screw, bending failure of one screw
P29-S2-3-B	Cyclic	3.96	11.31	Crack in plank
P29-S2-4-B	Cyclic	3.79	15.42	Pulling out of both screws
P29-S2-5-B	Cyclic	3.99	14.47	Pulling out of both screws
P29-S2-6-B	Cyclic	3.85	11.44	Pulling out of both screws
P29-S2-7-B	Cyclic	3.73	11.75	Pulling out of both screws

Figure 5-47: Backbone curves of specimens loaded parallel to the plank
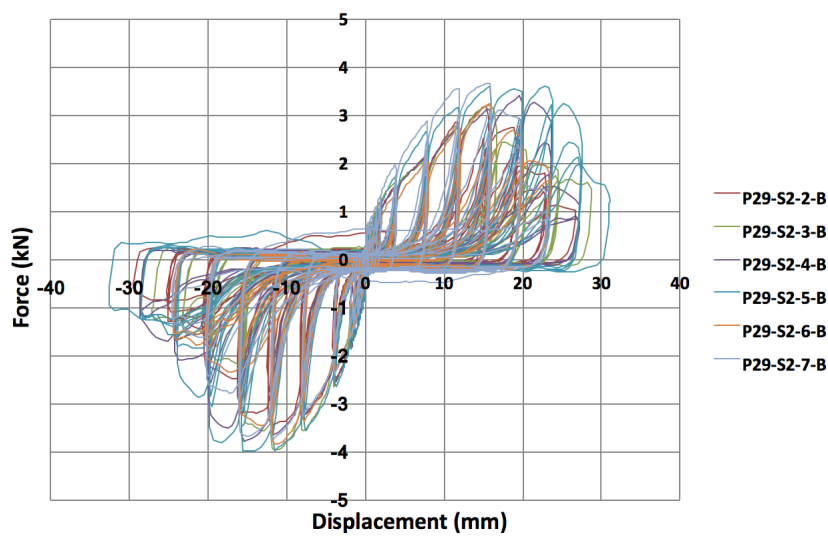
Figure 5-48: Hysteresis curves of specimens loaded parallel to the plank
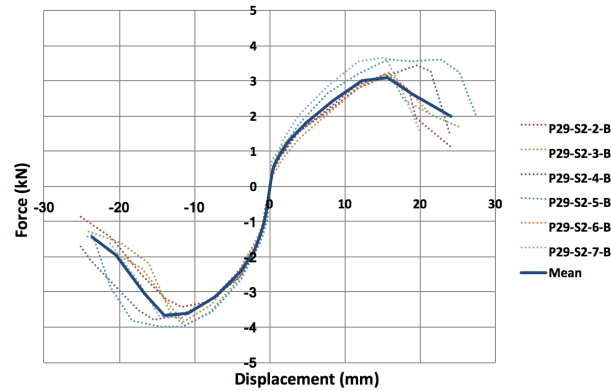
Figure 5-49: Average backbone curve of specimens loaded parallel to the plank

5.4.2 SCREWED CONNECTION BETWEEN PANEL, PLANK AND JOIST

At the top of the retrofitted diaphragm (at the joist where loading was applied), the panels were connected to the planks and the top joist. The screws that were used to attach the panels went through the planks into the top joist. Screws with a length of 75 mm and a diameter of 5 mm were used at a spacing of approximately 165 mm. For the testing of the screwed connection between panel, plank and joist, the specimens consisted of a segment of a panel screwed on top of a segment of a plank and beam. Each specimen contained two nails and one screw, with the two nails connecting only the plank and the beam. The screw connected all timber members.

LOADING PARALLEL TO THE JOIST

For loading parallel to the joist, the result of the monotonic test can be seen in figure 5-50. The maximum force for the monotonic test was 3.35 kN at a displacement of 26.70 mm. Failure occurred due to pulling out of the nails and screw. From the monotonic test, a yield slip of 24 mm is determined. With this yield slip, the cyclic loading scheme is set and the cyclic tests can be carried out. The hysteresis diagrams of the cyclically tested specimens can be seen in figure 5-51, along with the corresponding backbone curves. The pinching part is less narrow as opposed to the connections between panel and plank. Furthermore, the backbone curves show a high initial stiffness for the first few millimeters. Additionally, the backbone curves still exhibit residual strength after the ultimate strength is reached. This may be attributed to the fact that only the screws failed, thus the nails are still able to absorb some forces. Test results are summarised in table 5-7. The average maximum force for the seven tested specimens is 3.17 kN. For the comparison of the tested specimens, the backbone curves and hysteresis curves have been plotted in figure 5-52 and figure 5-53. The average backbone curve is plotted in figure 5-54.
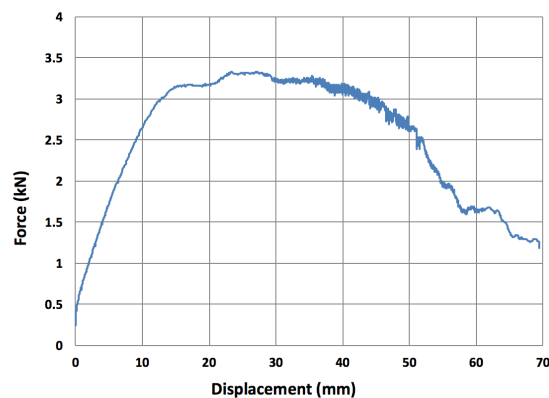
Figure 5-50: Monotonic response of connection between panel, plank and joist
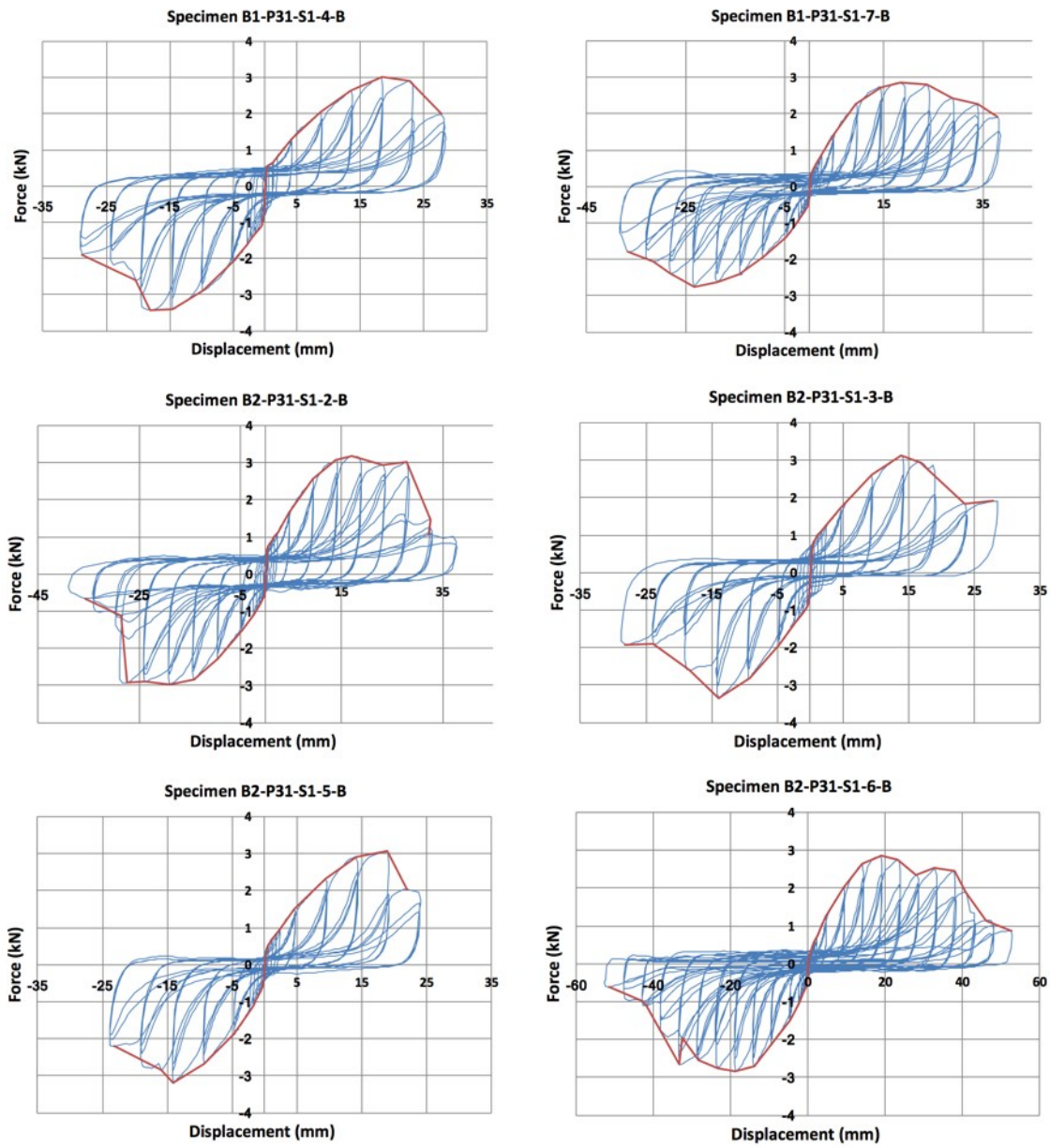
Figure 5-51: Hysteresis diagrams for loading parallel to the joist

Table 5-7: Test results

Specimen	Test	Maximum load (kN)	Corresponding displacement (mm)	Failure mode
B1-P31-S1-1-B	Monotonic	3.35	26.70	Pulling out of nails and screw
B1-P31-S1-4-B	Cyclic	3.43	18.06	Pulling out/bending failure of screw
B1-P31-S1-7-B	Cyclic	2.80	23.78	Pulling out of screw
B2-P31-S1-2-B	Cyclic	3.18	17.06	Pulling out of screw
B2-P31-S1-3-B	Cyclic	3.36	13.93	Pulling out of screw
B2-P31-S1-5-B	Cyclic	3.20	14.05	Pulling out of screw
B2-P31-S1-6-B	Cyclic	2.87	18.88	Pulling out of screw

Figure 5-52: Backbone curves of specimens loaded parallel to the joist
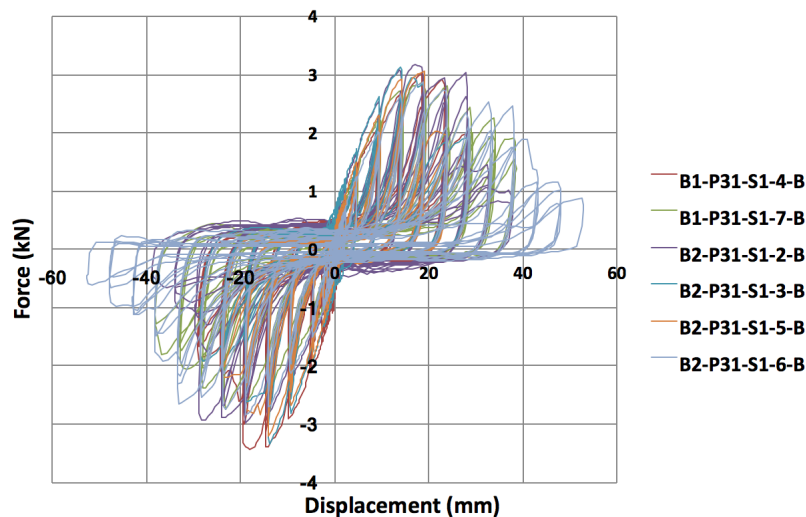
Figure 5-53: Hysteresis curves of specimens loaded parallel to the joist
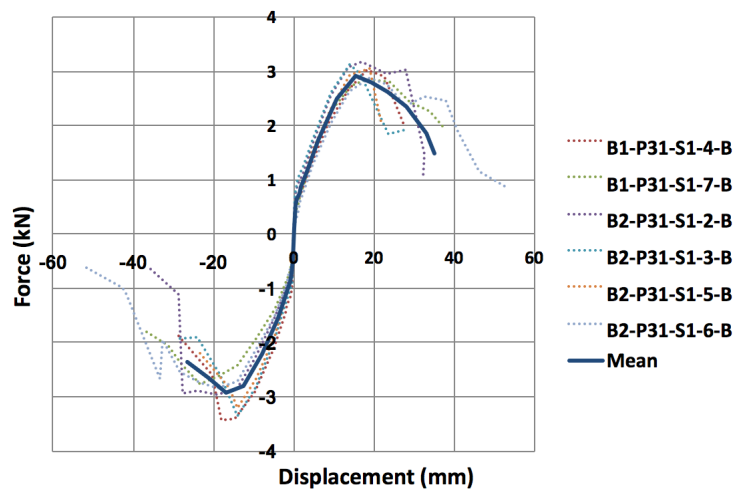
Figure 5-54: Average backbone curve of specimens loaded parallel to the joist

LOADING PERPENDICULAR TO THE JOIST

For loading perpendicular to the joist, the result of the monotonic test can be seen in figure 5-55. The maximum force for the monotonic test was 2.86 kN at a displacement of 33.30 mm. Failure occurred due to pulling out of the nails and screw. It was decided to assume a yield slip of 7.2 mm to fully capture the elastic and plastic behaviour of the connection. With this yield slip, the cyclic loading scheme is set and the cyclic tests can be carried out. The hysteresis diagrams of the cyclically tested specimens can be seen in figure 5-56, along with the corresponding backbone curves. For the last four specimens, it can be seen that the hysteresis is not symmetric. For negative displacements, the connection behaves weaker as the maximum strength is lower. There was no immediate evidence for this asymmetric behaviour during the testing of the connections. A possible explanation could be that some timber members were cracked at certain positions, hindering the interaction between nails and/or screw in certain directions. The backbone curves show a residual of strength after the ultimate strength is reached, which may be attributed to the fact that often only the screws fail. Test results are summarised in table 5-8. The average maximum force for the seven tested specimens is 3.09 kN. For the comparison of the tested specimens, the backbone curves and hysteresis curves have been plotted in figure 5-57 and figure 5-58. The average backbone curve is plotted in figure 5-59.
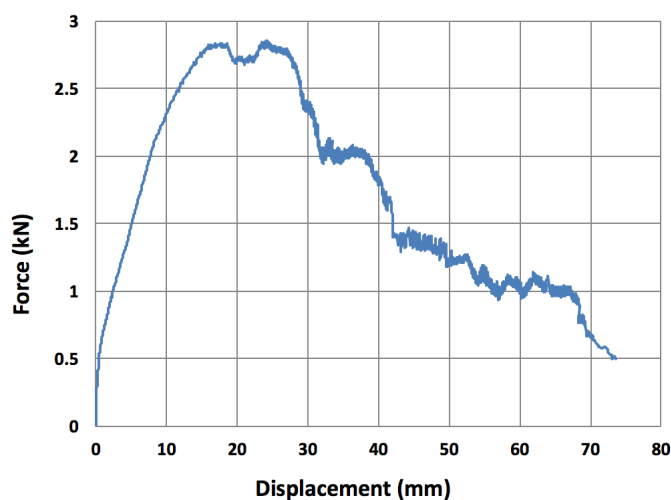
Figure 5-55: Monotonic response of connection between panel, plank and joist
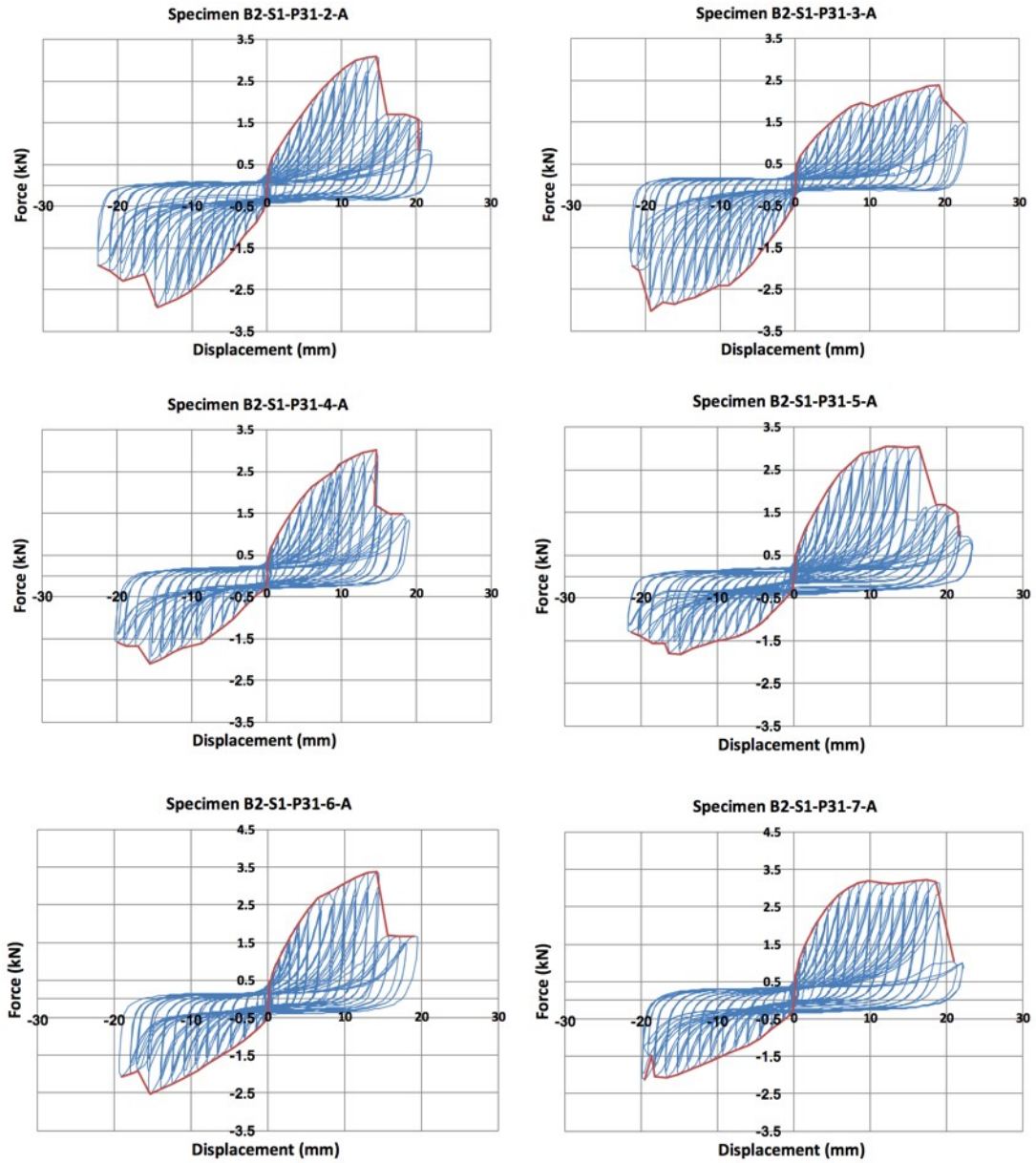
Figure 5-56: Hysteresis diagrams for loading perpendicular to the joist

Table 5-8: Test results

Specimen	Test	Maximum load (kN)	Corresponding displacement (mm)	Failure mode
B2-S1-P31-1-A	Monotonic	2.86	33.30	Pulling out of nails and screw
B2-S1-P31-2-A	Cyclic	3.08	14.62	Failure of nail and screw
B2-S1-P31-3-A	Cyclic	3.02	19.37	Failure of screw
B2-S1-P31-4-A	Cyclic	3.02	14.60	Failure of screw
B2-S1-P31-5-A	Cyclic	3.04	11.92	Pulling out of nails and screw
B2-S1-P31-6-A	Cyclic	3.39	14.15	Bending failure of screw
B2-S1-P31-7-A	Cyclic	3.23	17.41	Bending failure of screw

Figure 5-57: Backbone curves of specimens loaded perpendicular to the joist
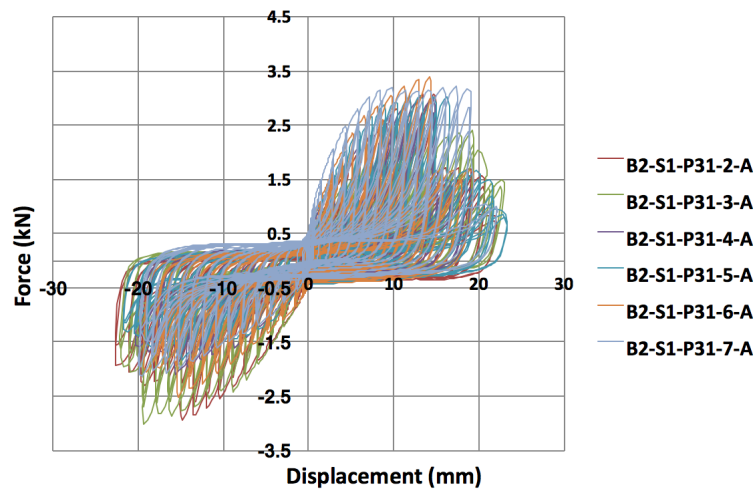
Figure 5-58: Hysteresis curves of specimens loaded perpendicular to the joist
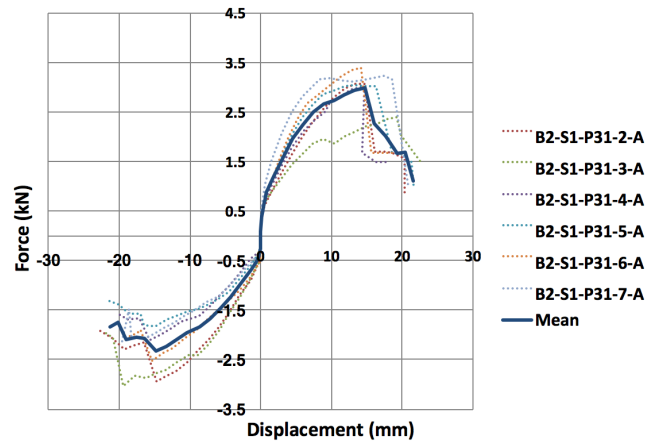
Figure 5-59: Average backbone curve of specimens loaded perpendicular to the joist

5.5 Comparison between as-built and retrofitted diaphragm

A crucial difference between the tested as-built and retrofitted diaphragm is that the as-built diaphragm was not tested until failure, whereas the retrofitted diaphragm was tested until failure. This gives an ultimate strength for the retrofitted diaphragm, but not for the as-built diaphragm. The hysteresis of both specimens can be seen in figure 5-60, and the backbone curves are shown in figure 5-61. The hysteresis of the specimens differs very much, as the stiffness of the retrofitted diaphragm is much higher. The initial stiffness of the as-built diaphragm is about 0.47 kN/mm, which is ten times lower than the initial stiffness for the retrofitted diaphragm (4.9 kN/mm). The secondary stiffness for the as-built specimen is 0.31 kN/mm and 1.2 kN/mm for the retrofitted diaphragm. Overall, the as-built specimen is much more flexible, but 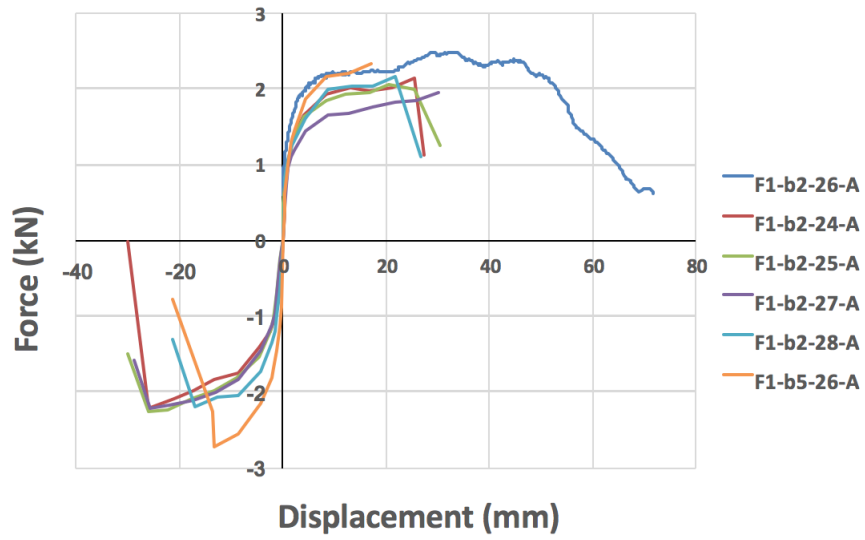the relative difference between initial and secondary stiffness is lower. Additionally, the retrofitted diaphragm exhibits high pinching behaviour as opposed to the as-built diaphragm. This may be due to the higher amount of nailed and screwed connections in the retrofitted diaphragm. Furthermore, the strength loss between successive cycles of the same amplitude is relatively higher for the retrofitted specimen. Behaviour of both diaphragms were nonlinear, however the nonlinearity is best seen in the retrofitted diaphragm. Comparing the backbone curves, the as-built specimen behaves fairly linear, whereas the retrofitted specimen behaves highly nonlinear with a visible degradation. For both backbone curves, the part before degradation and failure can be idealised by a bilinear curve.
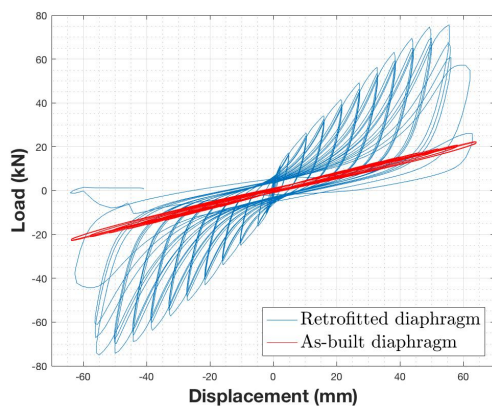
Figure 5-60: Hysteresis of as-built and retrofitted specimens
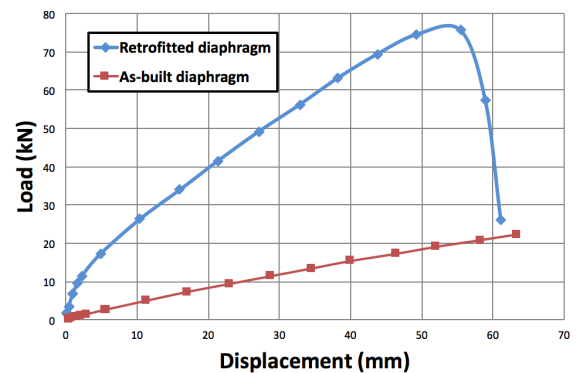
Figure 5-61: Envelope curve for as-built and retrofitted specimens

<div align="right">

6

</div>

EXTENSIVE MODEL OF AS-BUILT DIAPHRAGM

In this chapter, an extensive finite element model for the as-built diaphragm will be presented. This model is constructed in ANSYS 18.2. For the modelling of the nailed connections, ANSYS Workbench 18.2 is used for the convenience of the graphical user interface. For the modelling of the whole diaphragm, ANSYS Mechanical APDL 18.2 is used. ANSYS Mechanical APDL requires the scripting of a finite element model, which may be quite cumbersome as opposed to the user interface. However, the scripting of a model gives more control to the user regarding certain aspects of the analysis. Thus, it is chosen to model the diaphragm through the ANSYS Mechanical APDL scripting language. The diaphragm as regarded for numerical interpretation is a simple single sheathed diaphragm as tested in June 2017 at the TU Delft as discussed in chapter 5. This chapter will first deal with the numerical modelling of the nailed connections, taking into consideration both uniaxial (section 6.1) and rotational (section 6.2) behaviour. With the numerical models of the nails, the timber diaphragm can be modelled cyclically in its entirety (section 6.3).
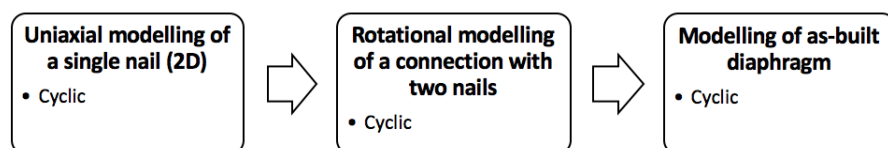
Figure 6-1: Workflow for the modelling of the as-built diaphragm

6.1 UNIAXIAL MODELLING OF A CONNECTION WITH A SINGLE NAIL

For the modelling of a connection with a single nail, the results of the laboratory tests as presented in chapter 5 are used to calibrate the numerical model. As the laboratory tests were conducted on specimens containing two nails, it is assumed that one nail absorbs half the force in the connection for the modelling of a single nail. Half of the average hysteresis and backbone curve of a connection with two nails is deemed to be representative for a single nail. As software ANSYS is used, previous modelling of nailed connections as discussed in subsection 4.2.4 provides an excellent starting point. This literature will be used extensively for the modelling of the connections. The laboratory tests which were carried out at the TU Delft have been classified as quasi-static, thus it is chosen to work with a static structural analysis within ANSYS Workbench 18.2. This analysis type is deemed suitable, as inertia effects are negligible for quasi-static experiments. ANSYS Workbench

automatically selects the Newton-Raphson solver for nonlinear analyses. The same loading scheme is applied to the numerical models as in the experimental tests.

For the uniaxial modelling of a single nail, four numerical models are constructed. For both loading perpendicular and parallel to the joist, two numerical models are constructed. This gives a total of four models. A summary of the numerical models for the modelling of a single nail can be seen in figure 6-2. It is chosen to use two approaches to calibrate the numerical model with the experimental results in both loading directions. The first approach is to calibrate the numerical hysteresis on the experimental hysteresis such that the unloading and reloading branches match (the stiffnesses are similar). This gives an accurate local representation of the behaviour of the nails. The first calibration approach is suitable for the modelling of nailed connections for experiments in which loading is applied gradually. However, it cannot be used for more extensive purposes with random loading schemes such as a time history analysis. By calibrating based on the hysteresis curve, the numerical backbone curve deviates from the experimental backbone. This means that the numerical preserved energy does not match the experimental preserved energy, causing errors if the model would be used for other purposes. The numerical backbone keeps increasing when using the first calibration method, resulting in a high energy conservation and an overestimation of strength if loading is not applied gradually. If loading is applied gradually, the damage from the previous cycle affects the subsequent cycle and thus results in lower forces. If loading is not applied gradually, damage of the previous cycle does not affect the subsequent cycle, resulting in higher forces. As the backbone curve keeps increasing (the error becomes bigger) with the first calibration method, these forces can become very high and unrealistic (see figure 6-3). The second calibration approach is to calibrate the numerical backbone such that it preserves the same energy as the experimental backbone. This means that the area under these graphs are the same. By calibrating on the preserved energy, the numerical hysteresis differs from the experimental hysteresis. Thus, the local behaviour cannot be predicted accurately. However, this calibration approach can be used to model nailed connections for broader purposes with random loading schemes such as time history analyses. With the second calibration method, the numerical backbone does not keep increasing and thus the error does not increase (see figure 6-3). For random loading schemes, this is desirable as the forces in the nails do not become unrealistically large (even though damage of the previous cycle does not affect the subsequent cycle). Instead, it tends to yield an underestimation of the forces, thus providing a conservative model.
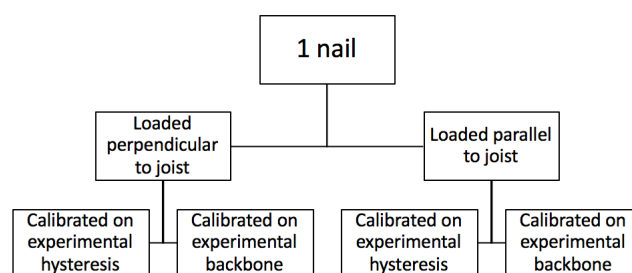
Figure 6-2: Numerical models for a single nail
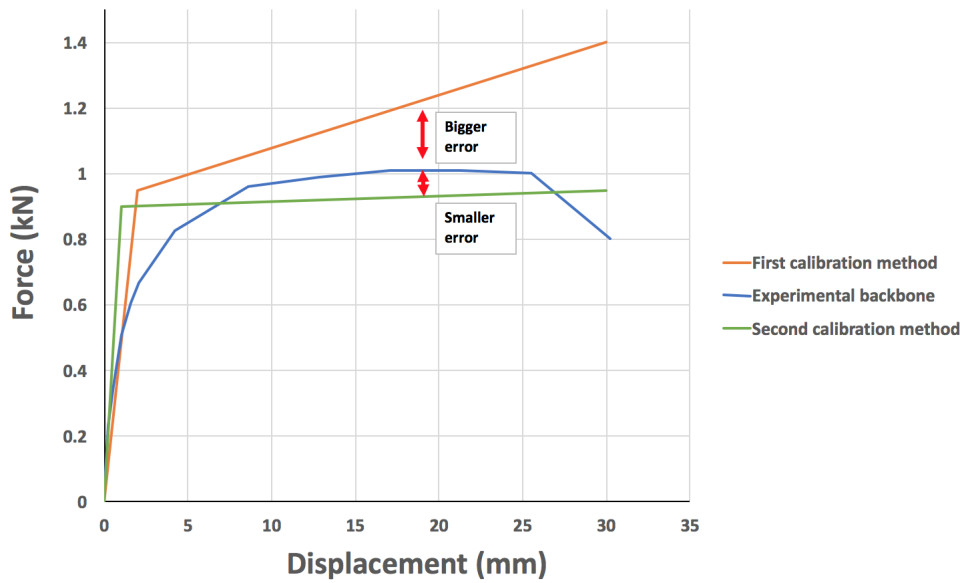
Figure 6-3: Error for calibration methods of nailed connection

6.1.1 LOADING PERPENDICULAR TO THE JOIST
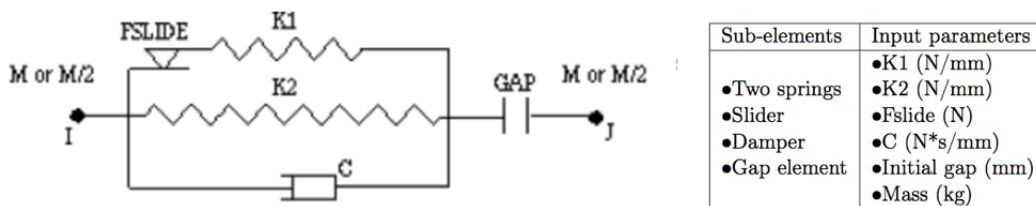
Figure 6-4: Element COMBIN40

For a single nail which is loaded perpendicular to the direction of the joist, three COMBIN40 elements are needed. As discussed in chapter 4.2.4, element COMBIN40 is a combination of two springs, a slider, a damper and a gap element (see figure 6-4). COMBIN40 is a nonlinear element, which acts between two nodes and has one degree of freedom. A total of three elements are needed to simulate different parts of the hysteresis curve.

The three COMBIN40 elements are placed in parallel (see figure 6-5). Each element has one translational degree of freedom along the length of the element (same degree of freedom for all elements). The ends of each element are attached to a node from the joist and a node from the board. With this model, the reloading part of the peaks in the hysteresis curve is modelled as a bilinear curve. The first COMBIN40 element serves to model the pinching part of the hysteresis curve. This element implements a slider in parallel with a spring. The sliding force of the slider represents half the width of the pinched region, whereas the spring constant represents the slope of the pinched region. The second COMBIN40 element models the hysteresis peaks for negative displacements. This element contains a slider and spring in parallel with another spring, all of which are in series with a gap element. The sliding force for the slider determines the transition point of the two linear segments of the reloading branch of the peaks in the hysteresis curve. The sliding force is the force which is added to the pinched region after which the transition must take place. The slider also ensures that the gap size increases for successive loading cycles, causing the peaks in the hysteresis to appear

at greater displacements for successive cycles. For each cycle, the amount of sliding is added to the gap. The gap size determines the point at which the pinching part transitions into a peak. The spring constant of the first spring correlates with the slope of the first linear segment of the peaks. The second spring constant correlates with the slope of the second linear segment of the peaks. The third COMBIN40 element has the same purpose as the second COMBIN40 element, but instead it models the hysteresis peaks for positive displacements. This element is reversed, meaning that the nodes at the ends of the elements are interchanged. The sub-elements of the third COMBIN40 element have the same parameters and purpose as the second COMBIN40 element. The contribution of each COMBIN40 element to the hysteresis curve can be seen in figure 6-6. The correlation between input parameters and hysteresis curve is summarised in figure 6-7 and table 6-1.
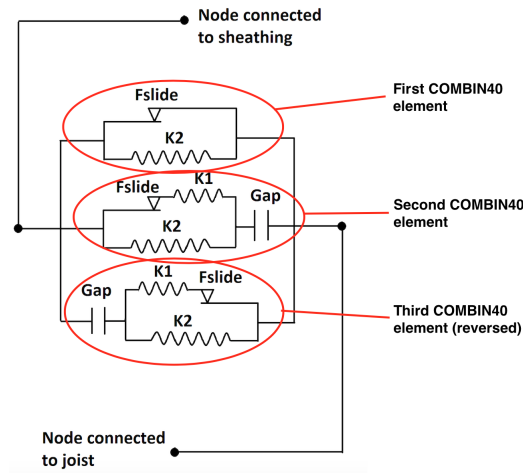
Figure 6-5: Three COMBIN40 elements in parallel
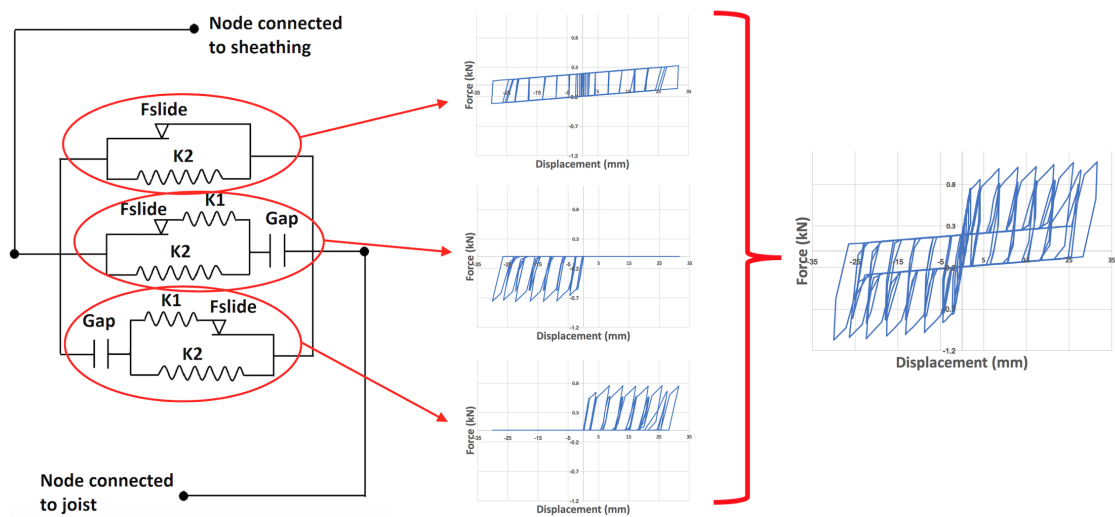
Figure 6-6: Contribution of COMBIN40 elements to hysteresis curve
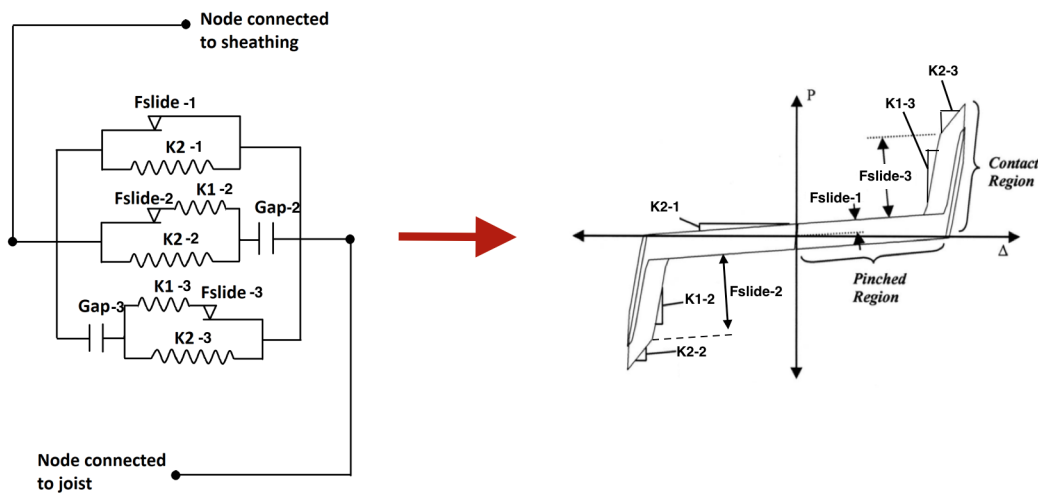
Figure 6-7: Correlation between input parameters and hysteresis curve

Table 6-1: Correlation between input parameters and hysteresis curve

	Parameter	Purpose
COMBIN40 - 1	K2	Slope of pinched region
	Fslide	Width of pinched region
COMBIN40 - 2	K1	Slope of first linear segment of reloading part of hysteresis peaks for negative displacements
	K2	Slope of second linear segment of reloading part of hysteresis peaks for negative displacements
	Fslide	Transition point between the two linear segments of reloading path
	Initital gap	Needed to model peaks at higher displacements for successive cycles
COMBIN40 - 3	K1	Slope of first linear segment of reloading part of hysteresis peaks for positive displacements
	K2	Slope of second linear segment of reloading part of hysteresis peaks for positive displacements
	Fslide	Transition point between the two linear segments of reloading path
	Initial gap	Needed to model peaks at higher displacements for successive cycles

The proposed numerical model as elaborated above can simulate the nonlinear hysteretic behaviour of a nailed connection in a timber diaphragm quite accurately, implementing pinching behaviour and strength degradation for successive cycles of the same amplitude. However, the model does not implement failure of the nails. This is a major drawback, as the nailed connections are an important cause of failure in a timber diaphragm. It is not possible to directly implement failure in the numerical model, so it is chosen to continue with the model as it is.

For the first calibration approach, in which the numerical hysteresis curve is calibrated on the average experimental hysteresis, the parameters for each of the COMBIN40 elements are given in table 6-2. The numerical model is subjected to the same cyclic loading scheme as applied in the experimental tests. The numerical result can be seen in figure 6-8. From this figure, it can be seen

that the reloading branch is modelled as a bilinear curve once the elastic phase is passed. Also, no failure occurs. As no failure mechanism is implemented, the highest force occurs at the load cycle with the highest displacement (the force keeps increasing with increasing displacement). Comparing the numerical result to the experimental result (figure 6-9), one can see that the hysteresis curves are similar. The numerical stiffnesses of the reloading branches give an accurate representation of experimental data and the hysteresis peaks are predicted accurately. However, after a displacement of about 15 mm, the numerical result is not accurate as the failure mechanism is initiated. The comparison between numerical and experimental backbone can be seen in figure 6-10. It is evident that the numerical model does not implement failure, as the envelope curve keeps increasing (thus the conserved energy is high). The experimental backbone curve conserves less energy and is far more nonlinear as compared to the numerical backbone.

Taking a closer look at the initial stages of the response, the behaviour of the numerical model can be better understood. For small displacements, the model remains elastic and thus no energy is lost (see figure 6-11). For its elastic phase, no pinching behaviour is exhibited. Once the elastic phase is surpassed and plasticity is reached, the reloading branch moves onto the secondary stiffness. The secondary stiffness is accompanied with sliding within the connection. The amount of sliding is equal to the displacement over which the secondary stiffness runs. After each cycle, the sliding is added to the total sliding. The total amount of sliding determines when the reloading branch moves from the pinching part onto the peaks. This mechanism ensures that the peaks start at higher displacements for successive cycles, thus extending the length of the pinched region for higher displacements. The sliding mechanism also ensures that the peak forces are lower for successive cycles, thus implementing damage. Regarding the backbone curve, the initial stages can be seen in figure 6-12. For lower displacements, the connection remains elastic and its stiffness is higher. Once elasticity is reached, the stiffness decreases. The behaviour of the connection is similar for each model which is constructed in this report, therefore a zoom-in on the initial stages (for the first calibration method) will be omitted for the remainder of the report.

Table 6-2: Parameters for the COMBIN40 elements calibrated on the experimental hysteresis

	K1 (N/mm)	K2 (N/mm)	Fslide (N)	Initial gap (mm)	C (N*s/mm)	M (kg)
COMBIN40 - 1	100.000	4.22	192	0	0	0
COMBIN40 - 2	250	50	450	0.001	0	0
COMBIN40 - 3	250	50	450	0.001	0	0
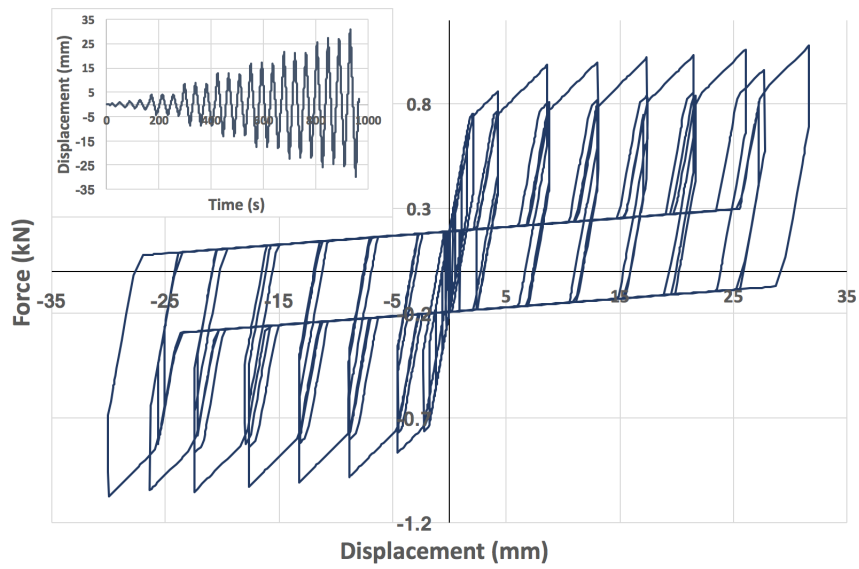
Figure 6-8: Numerical result for loading perpendicular to joist
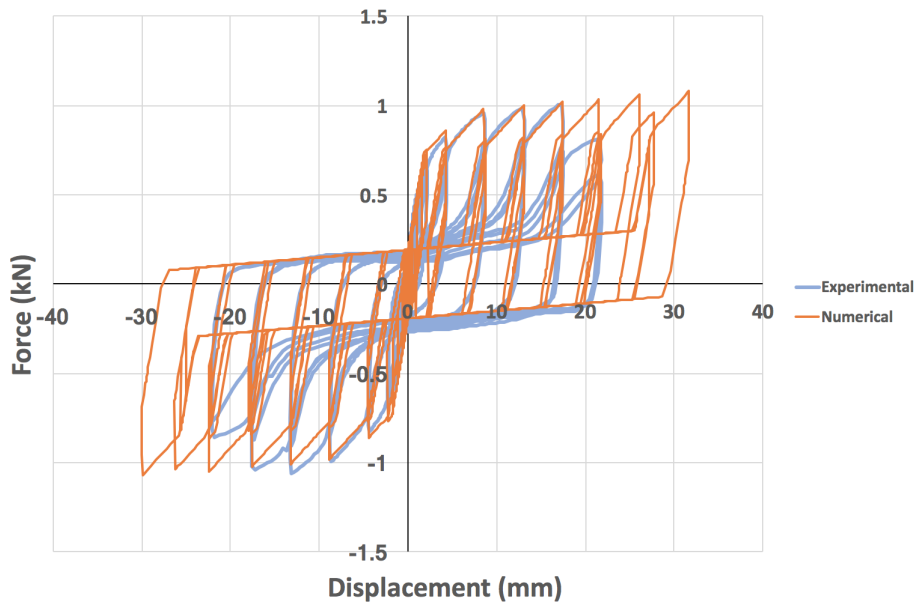
Figure 6-9: Comparison between numerical and experimental result
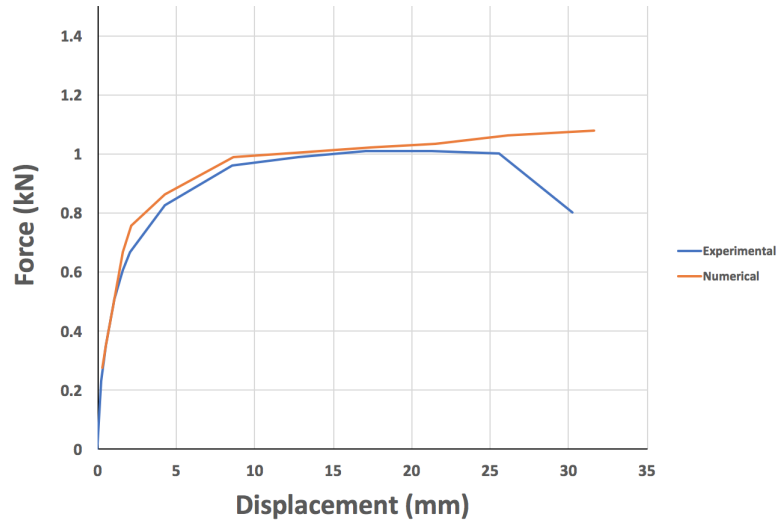
Figure 6-10: Comparison between numerical and experimental backbone
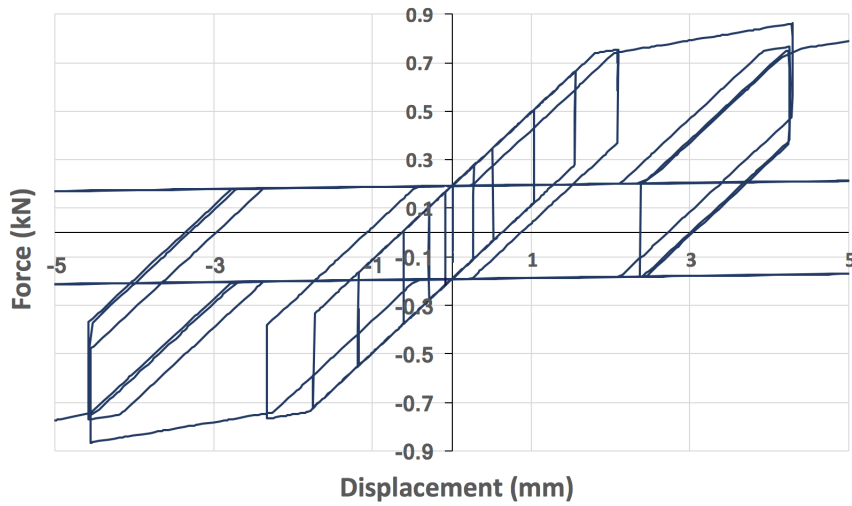
Figure 6-11: Zoom-in on initial stages of hysteresis
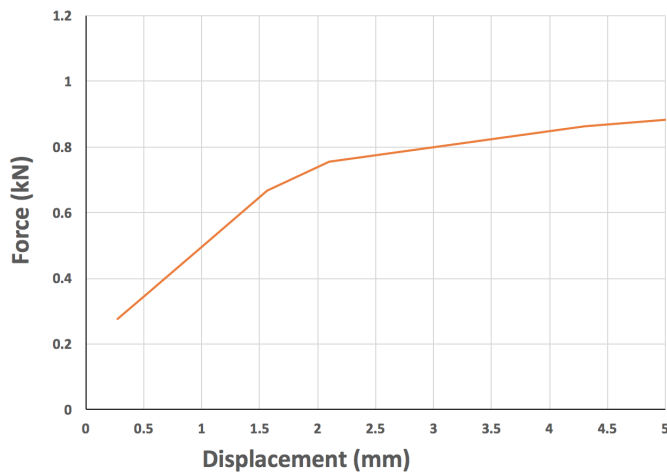
Figure 6-12: Zoom-in on initial stages of backbone

For the second calibration approach, in which the numerical backbone curve is calibrated on the average experimental backbone, the parameters for each of the COMBIN40 elements are given in table 6-3. Only the parameters for the second and third COMBIN40 elements are changed. The area under the numerical backbone matches the area under the experimental backbone up to a displacement of 30 mm. The numerical model is subjected to the same cyclic loading scheme as applied in the experimental tests. The numerical result can be seen in figure 6-13. Comparing this approach to the previous approach in which the numerical hysteresis was matched to the experimental hysteresis, one can see that the bilinear reloading path exhibits lower stiffnesses. Due to the newly calibrated parameters of the COMBIN40 elements, strength degradation for successive cycles of the same amplitude does not occur. The pinching part is the same as for the previous approach. Comparing the numerical result to the experimental result (figure 6-14), one can see that the hysteresis is not captured accurately. The hysteresis peaks are flattened and the initial load cycles give a greater error. The comparison between numerical and experimental backbone can be seen in figure 6-15. The numerical backbone curve is bilinear and exhibits lower stiffnesses. This backbone curve shows greater similarity to the experimental backbone curve as opposed to the previous calibration approach.

For small displacements, the model remains elastic and thus no energy is lost (see figure 6-16). For its elastic phase, no pinching behaviour is exhibited. Once the elastic phase is surpassed and plasticity is reached, the reloading branch moves onto the secondary stiffness. For the second calibration method, the secondary stiffness is near zero. The secondary stiffness is accompanied with sliding within the connection. The amount of sliding is equal to the displacement over which the secondary stiffness runs. After each cycle, the sliding is added to the total sliding. The total amount of sliding determines when the reloading branch moves from the pinching part onto the peaks. This mechanism ensures that the peaks start at higher displacements for successive cycles, thus extending the length of the pinched region for higher displacements. The sliding mechanism also ensures that the peak forces are lower for successive cycles, thus implementing damage. However, due to the near zero secondary stiffness for the second calibration method, the peak forces for successive cycles are similar. Furthermore, successive cycles of the same amplitude are barely visible due to the low secondary stiffness. Regarding the backbone curve, the initial stages can be seen in figure 6-17. For lower displacements, the connection remains elastic and its stiffness is higher. Once plasticity is reached, the stiffness decreases to nearly zero. The behaviour of the connection is similar for each model which is constructed in this report, therefore a zoom-in on the initial stages (for the second calibration method) will be omitted for the remainder of the report.

Table 6-3: Parameters for the COMBIN40 elements calibrated on the preserved energy

	K1 (N/mm)	K2 (N/mm)	Fslide (N)	Initial gap (mm)	C (N*s/mm)	M (kg)
COMBIN40 - 1	100.000	4.22	192	0	0	0
COMBIN40 - 2	150	0.0001	700	0.001	0	0
COMBIN40 - 3	150	0.0001	700	0.001	0	0
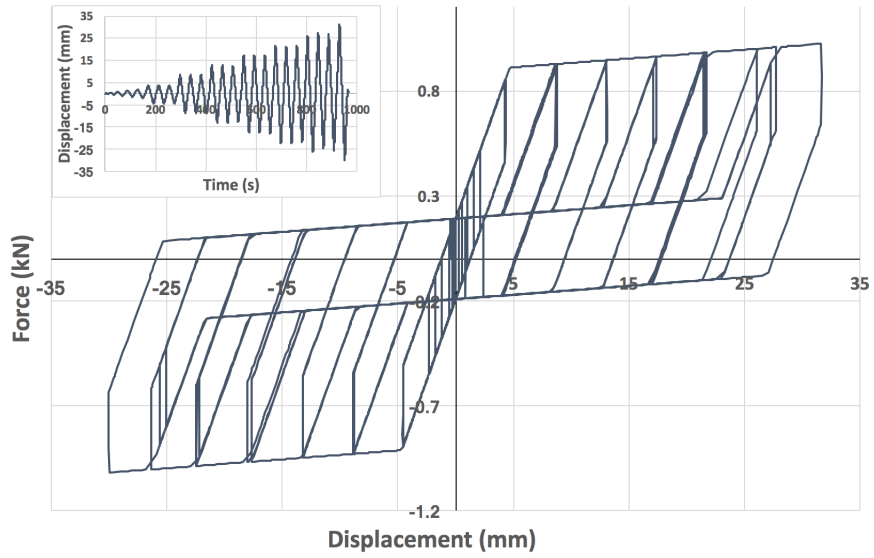
Figure 6-13: Numerical result for loading perpendicular to joist
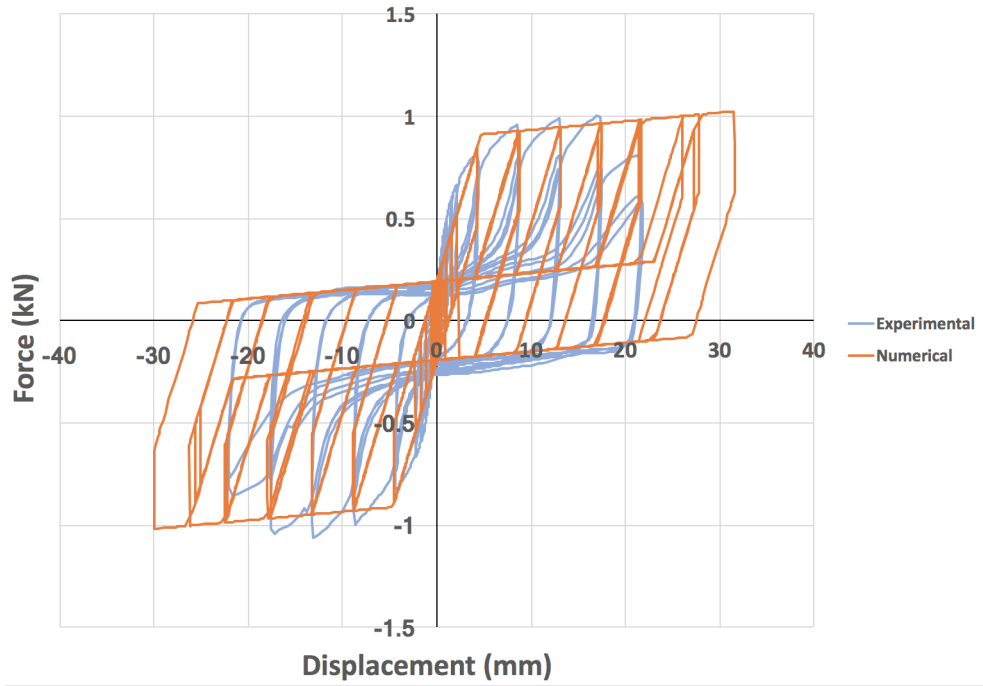
Figure 6-14: Comparison between numerical and experimental result
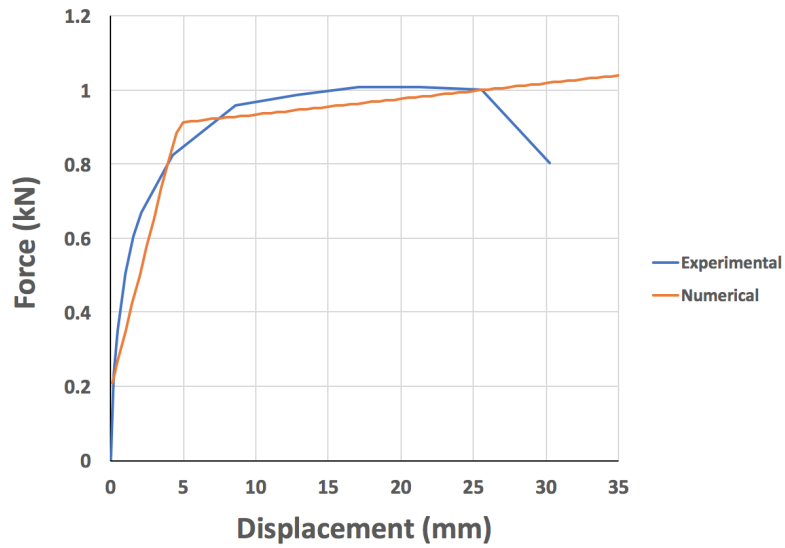
Figure 6-15: Comparison between numerical and experimental backbone
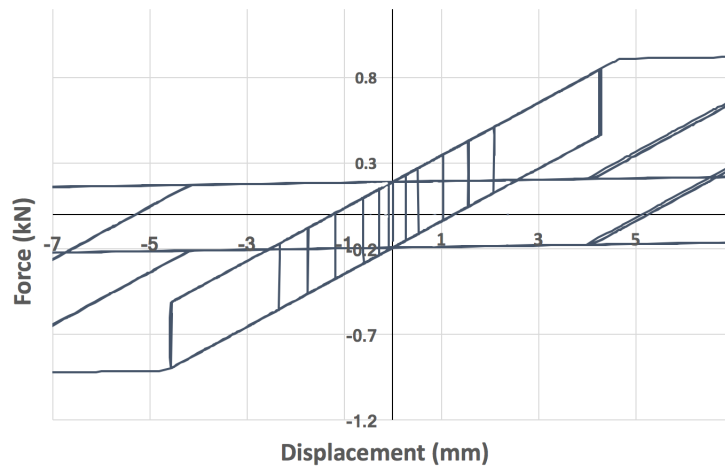
Figure 6-16: Zoom-in on initial stages of hysteresis
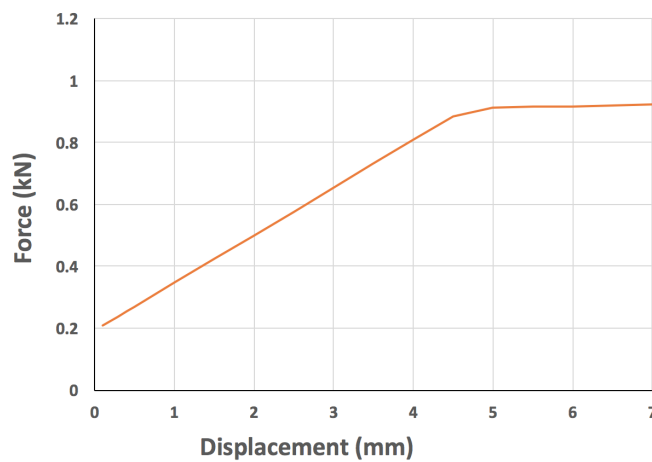
Figure 6-17: Zoom-in on initial stages of backbone

6.1.2 Loading parallel to the joist

For loading parallel to the joists, the same model is used as for loading perpendicular to the joist. However, the parameters of the nonlinear springs are modified such that the generated hysteresis matches the one found experimentally. For the approach in which the numerical hysteresis curve is calibrated on the experimental hysteresis curve, the parameters for the COMBIN40 elements can be seen in table 6-4. The numerical model is subjected to the same cyclic loading scheme as applied in the experimental tests. The numerical result can be seen in figure 6-18. Comparing the numerical result to the experimental result (figure 6-19), one can see that the hysteresis curves show more dissimilarities than for loading perpendicular to the joist. This is is caused by the fact that the experimental hysteresis shows more nonlinearities for loading parallel to the joist. Especially the reloading branches show high nonlinearity. The numerical reloading stiffnesses are higher than the experimental reloading stiffnesses. However, if the numerical reloading stiffnesses would be reduced, the pinching part and the peaks of the hysteresis would not be captured accurate enough. Thus, it is chosen to move forward with this generated numerical hysteresis. These parameters give quite a good estimation of the maximum loads per cycle and capture the pinching behaviour sufficiently accurate. The comparison between numerical and experimental backbone can be seen in figure 6-20. The numerical backbone keeps increasing as it does not implement failure, thus the numerical backbone differs quite a bit from the experimental backbone. The experimental backbone curve conserves less energy and is far more nonlinear as compared to the numerical backbone.

Table 6-4: Parameters for the COMBIN40 elements calibrated on the experimental hysteresis

	K1 (N/mm)	K2 (N/mm)	Fslide (N)	Initial gap (mm)	C (N*s/mm)	M (kg)
COMBIN40 - 1	100.000	2.5	145	0	0	0
COMBIN40 - 2	210	45	700	0.001	0	0
COMBIN40 - 3	210	45	700	0.001	0	0
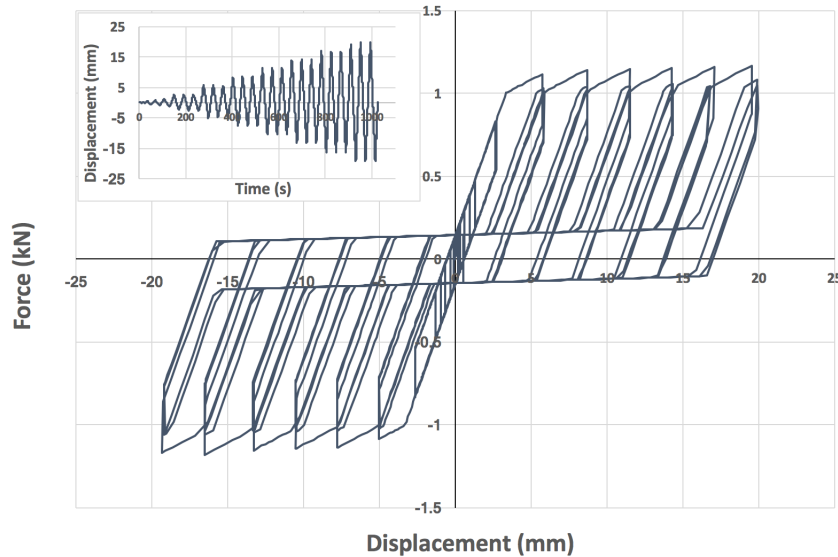
Figure 6-18: Numerical result for loading parallel to joist
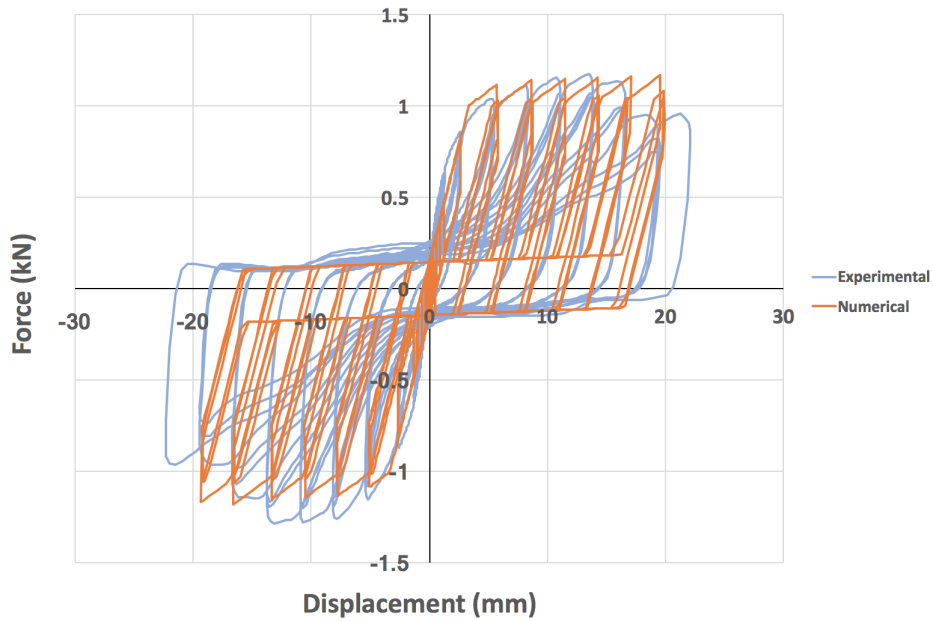
Figure 6-19: Comparison between numerical and experimental result
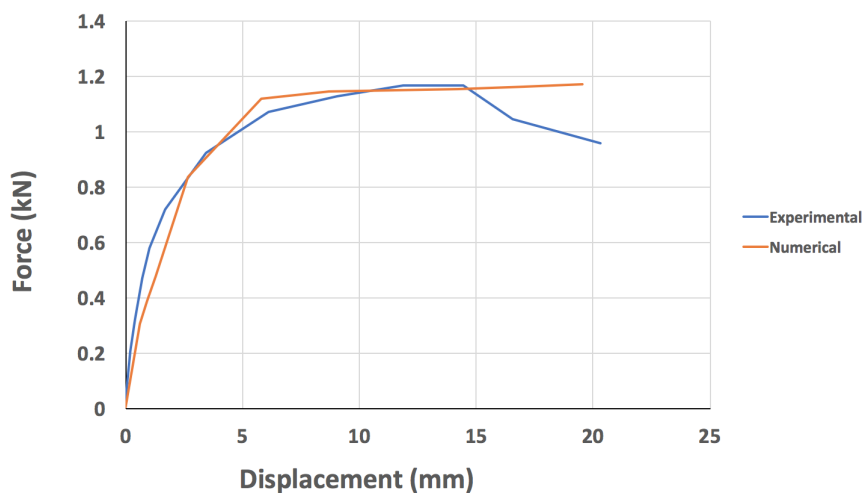
Figure 6-20: Comparison between numerical and experimental backbone

For the second approach, in which the numerical backbone curve is calibrated on the experimental backbone, the parameters for each of the COMBIN40 elements are given in table 6-5. Only the parameters for the second and third COMBIN40 elements are changed. The area under the numerical backbone matches the area under the experimental backbone up to a displacement of 20 mm. The numerical model is subjected to the same cyclic loading scheme as applied in the experimental tests. The numerical result can be seen in figure 6-21. Comparing this approach to the previous approach in which the numerical hysteresis was matched to the experimental hysteresis, one can see that the second stiffness of the peaks is very much lower. The pinching part is the same as for the previous approach. Comparing the numerical result to the experimental result (figure 6-22), one can see that the hysteresis is not captured accurately. The maximum loads per cycle show greater errors and the reloading stiffnesses are far more higher for the numerical results. The comparison between numerical and experimental backbone can be seen in figure 6-23. The initial stiffness of the numerical backbone curve is very similar to the initial stiffness of the experimental backbone

curve. Thus it can be said that initially, the model captures the real behaviour more accurately. This backbone curve shows greater similarity to the experimental backbone curve as opposed to the first calibration approach.

Table 6-5: Parameters for the COMBIN40 elements calibrated on the preserved energy

	K1 (N/mm)	K2 (N/mm)	Fslide (N)	Initial gap (mm)	C (N*s/mm)	M (kg)
COMBIN40 - 1	100.000	2.5	145	0	0	0
COMBIN40 - 2	500	0.001	840	0.001	0	0
COMBIN40 - 3	500	0.001	840	0.001	0	0
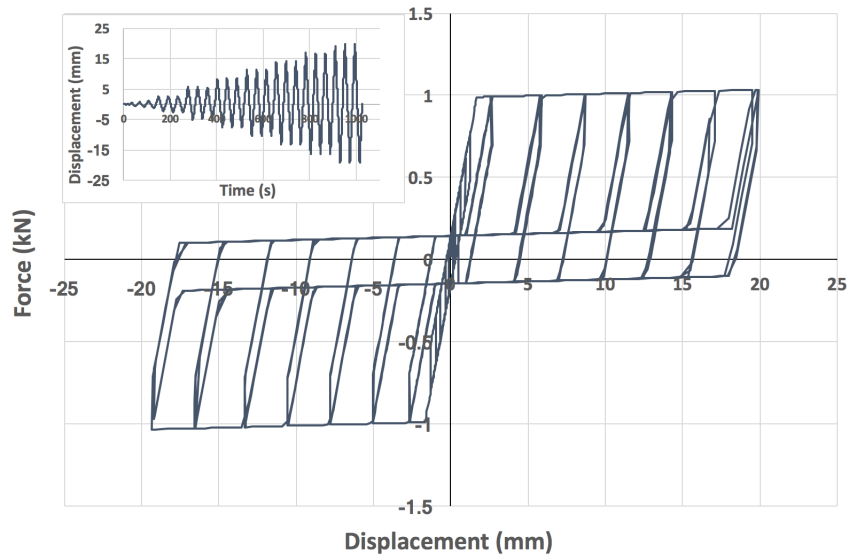
Figure 6-21: Numerical result for loading parallel to joist
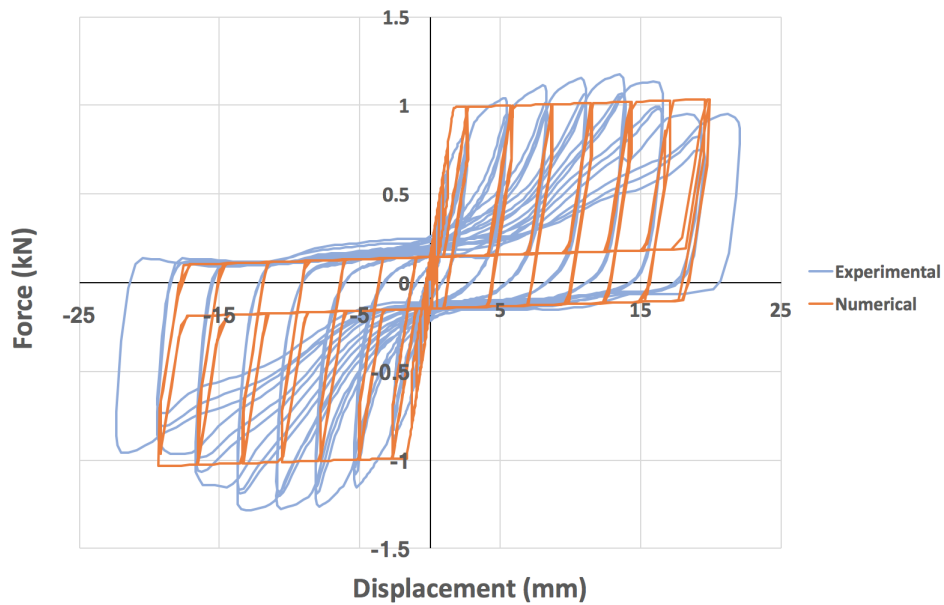
Figure 6-22: Comparison between numerical and experimental result
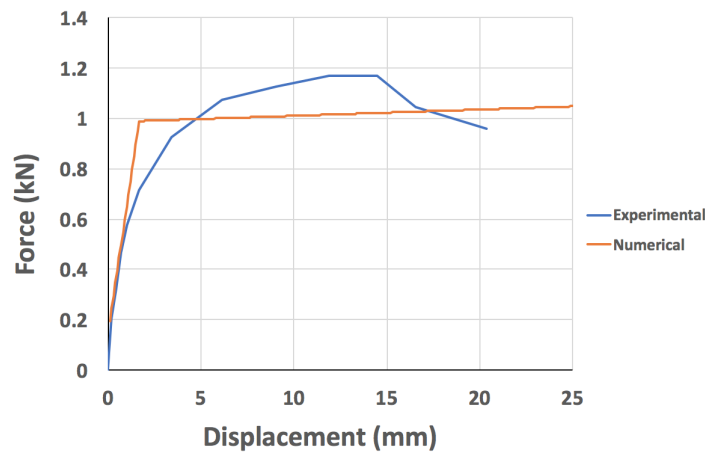
Figure 6-23: Comparison between numerical and experimental backbone

6.2 ROTATIONAL MODELLING OF A CONNECTION WITH TWO NAILS

Using the models for a single nail loaded perpendicular to the joist and parallel to the joist, the rotational behaviour of a connection with two nails can be predicted. Each nail is then modelled separately. As one nail is modelled with three COMBIN40 elements in each in-plane direction, a total of six COMBIN40 elements is needed to model one nail in 2D. The spacing between the two nails is 100 mm. The model is subjected to the same loading scheme as in the experiments. For the first approach, in which the numerical translational behaviour of the nails is calibrated on the experimental hysteresis, the numerical result can be seen in figure 6-24. Comparing this result to experimental data (see figure 6-25), one can see that the rotational behaviour is predicted quite accurately. There are a few overestimations, but the overall hysteresis behaviour is similar to the experimental result. Thus it can be concluded that the rotational behaviour can be accurately predicted by the behaviour in the two in-plane directions of a connection.
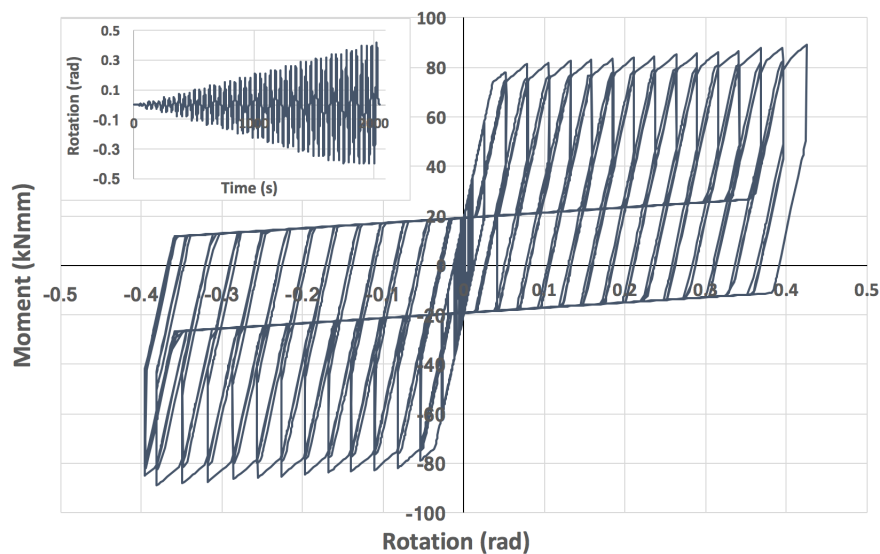
Figure 6-24: Numerical result for rotational loading
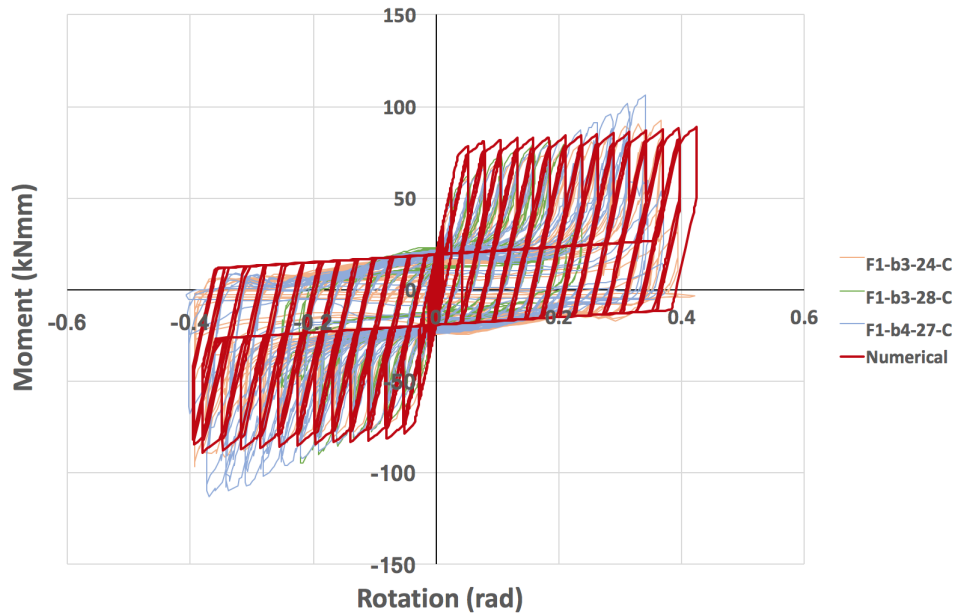
Figure 6-25: Comparison between numerical and experimental result

For the second approach, in which the translational behaviour of the nails is calibrated on the experimental backbone curves, the numerical result is shown in figure 6-26. A comparison between experimental and numerical result can be seen in figure 6-27. For this approach, the numerical result overestimates the real moments for each load cycle and the initial stiffness of the hysteresis is lower than found experimentally. The second approach produces more errors if used to predict the rotational behaviour of a connection with two nails.
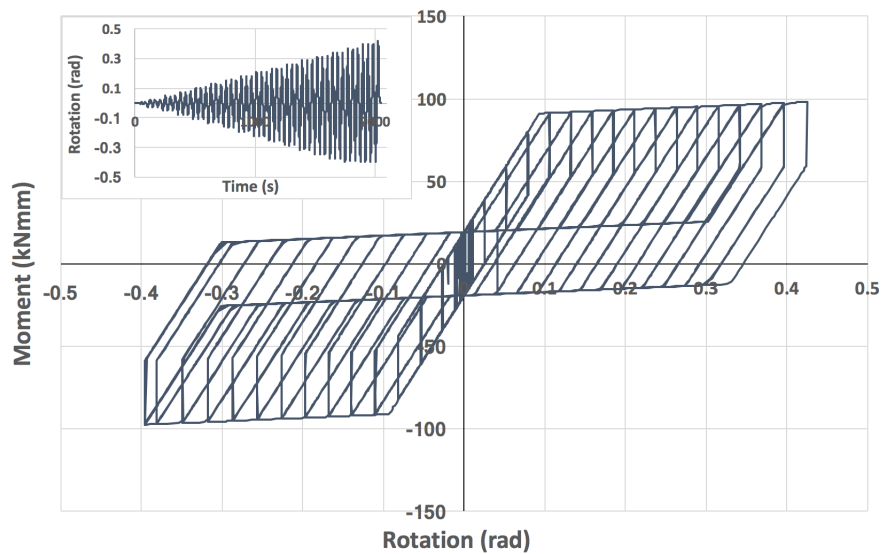
Figure 6-26: Numerical result for rotational loading
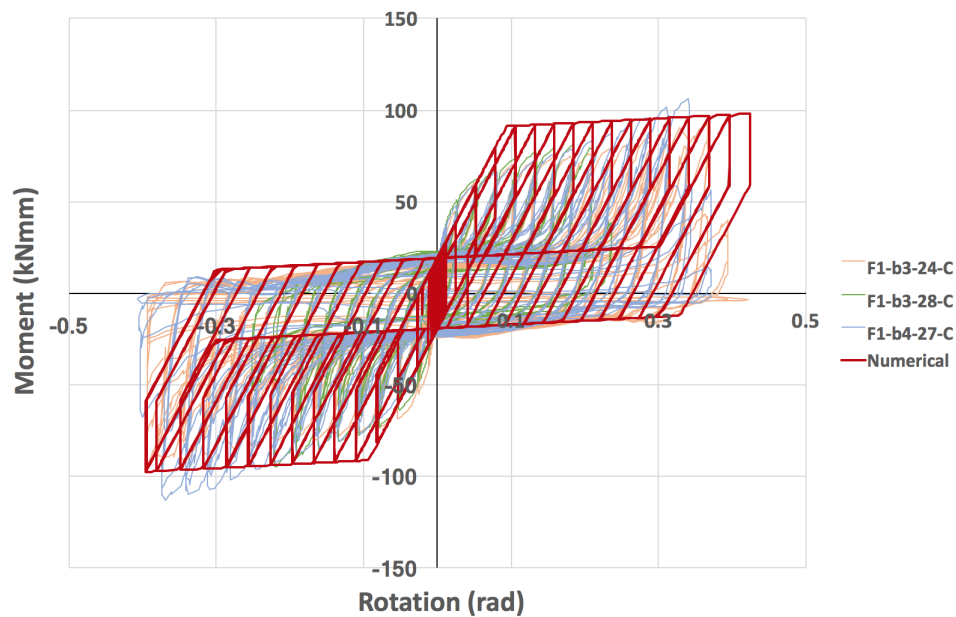
Figure 6-27: Comparison between numerical and experimental result

6.3 CYCLIC MODELLING OF THE AS-BUILT DIAPHRAGM

With the numerical models for the nailed connections, the model of the as-built diaphragm can be constructed. The model of the as-built diaphragm is scripted in ANSYS Mechanical APDL 18.2. For the numerical modelling of the as-built diaphragm it is chosen to divert from the graphical user interface and instead use the ANSYS APDL scripting language. This is due to the fact that the graphical user interface does not give the user control over certain aspects. As the nailed connections have specific locations that should be assigned to a node, the scripting language offers greater possibilities and is a better choice than the graphical user interface. The scripting language for ANSYS is program specific, meaning that ANSYS wields its own commands (which can be found online). The script is written in a simple text file, which is then imported into the ANSYS Mechanical application. The application reads the script and runs the model. The workflow for writing the script can be seen in figure 6-28. The geometry is defined in the preprocessor, which requires element types, element parameters, material properties, node locations, element locations, boundary conditions and loading as input. After the preprocessor, the solver is initiated in which the user can call the solver type and define the solver settings. ANSYS 18.2 often chooses the most optimal solver settings based on the solver type and used elements, so it is common to let ANSYS determine the solver settings. Lastly, the postprocessor is initiated in which the user can call for the needed results and plots.
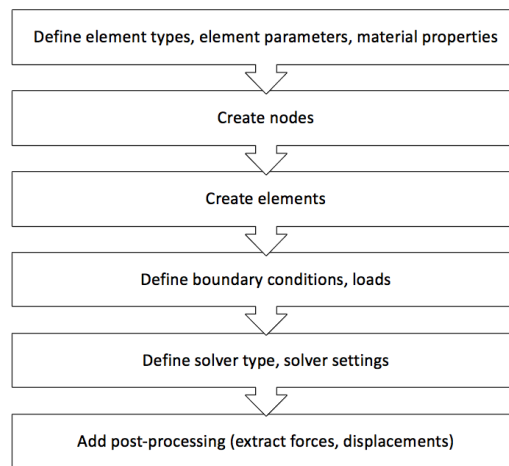
Figure 6-28: Structure of the ANSYS APDL script

Geometry

The numerical model of the as-built diaphragm is modelled such that it closely resembles the experimentally tested diaphragm. The model can be divided into three components: the beams, the planks and the nails. The diaphragm consists of 23 timber planks and 4 timber beams, which are connected with a pair of nails at each beam-plank intersection. The spacing between each nail in a pair is 100 mm. A total of 184 nails is implemented in the diaphragm. The 23 timber planks have a thickness of 18 mm, a width of 165 mm and a length of 2680 mm. The spacing between each plank is 2 mm, meaning that the centre-to-centre distance of each plank is 167 mm. Perpendicular to the direction of the planks, 4 timber beams are placed with a width of 60 mm, a height of 130 mm and a length of 1870 mm. The centre-to-centre distance of each beam is 650 mm. For a summary of the dimensions of the as-built diaphragm, refer to table 6-6. The coordinate system for the diaphragm is defined as follows: the x-axis runs along the length of the planks, the y-axis is placed along the length of the beams and the z-axis is the out-of-plane axis perpendicular to the beams and planks.

Material properties

For the modelling of the as-built diaphragm, it is assumed that the nails are the only source of non-linearity. Furthermore, the effects of friction between planks and the closing and opening of the gap between planks are neglected. The timber members are given orthotropic linear elastic material properties ($E_x, E_y, E_z, G_{xy}, G_{yz}, G_{xz}, \nu_{xy}, \nu_{yz}, \nu_{xz}$). The Young's modulus along the grain of the timber members was measured in the laboratory of the TU Delft and is adopted for the numerical model. The Young's moduli in other directions and the shear moduli can be determined from the measured Young's modulus using empirical relations from the Wood Handbook [38]. The Poisson's ratios are also taken from the Wood Handbook. The material properties as used for the numerical model are annexed in appendix E.

Elements

A total of three elements are used to model the three different members within the as-built diaphragm. For the beams, it is chosen to use linear beam element BEAM188. This element seems suitable, as one dimension of the beam is far greater than the other two dimensions. BEAM188 is a two-noded element with six degrees of freedom at each node. For the planks, linear shell element SHELL181 is used. Shell elements are used for the planks considering one dimension is very small as opposed to the other two main dimensions. SHELL181 has four nodes with six degrees of freedom per node. For the nailed connections, nonlinear element COMBIN40 is used. This element is a combination of two springs, a slider, a gap element and a damper. The workings of this element

is detailed in section 6.1. COMBIN40 is a two-noded element with one degree of freedom per node. The parameters for the COMBIN40 elements are the same as presented in the previous sections. However, to prevent divergence, the stiffness of the first spring of the first COMBIN40 element is reduced from 100.000 to 10.000 N/mm^2. A summary of the elements can be seen in table 6-7, along with a schematisation of the elements in figure 6-29.

Table 6-6: Dimensions of as-built diaphragm

	Width (mm)	Height (mm)	Length (mm)	Thickness (mm)	Centre-to-centre distance (mm)
Joists	60	130	3870	-	650
Planks	165	18	2680	-	167
Nails	-	-	64.2	3.0	100
Specimen	-	2680	3870	-	-

Table 6-7: Elements for the members

Member	Element	Number of nodes	Element behaviour	Degrees of freedom per node	Material input parameters
Joists	BEAM188 (Line element)	2	Linear	6	E_x, E_y, E_z G_{xy}, G_{yz}, G_{xz} ν_{xy}, ν_{yz}, ν_{xz}
Planks	SHELL181 (Shell element)	4	Linear	6	E_x, E_y, E_z G_{xy}, G_{yz}, G_{xz} ν_{xy}, ν_{yz}, ν_{xz}
Nails	COMBIN40 (Line element)	2	Nonlinear	1	K_1, K_2, F_{slide}, initial gap, C, M

a) Element BEAM188

b) Element SHELL181

c) Element COMBIN40

Figure 6-29: Schematisations of used elements [26]

BOUNDARY CONDITIONS

The boundary conditions are chosen such that the numerical model represents the laboratory test. The upper edge of the diaphragm is constraint against rotations about the x-axis and against translations in z-direction. These constraints are applied at the top nodes of the planks (near the loaded beam). The lower edge of the diaphragm is clamped, meaning that the bottom nodes of the planks are constrained against all degrees of freedom. All nodes of the beams are constraint against translations in z-direction and rotations about the y-axis. This is to prevent rigid body motions of the beams. The boundary conditions can be seen in figure 6-30.

LOADING

The same cyclic loading scheme as used in the laboratory test is applied to the numerical model. This loading scheme imposes three cycles for each displacement amplitude. The loading is displacement controlled and is applied at the nodes along the length of the top beam. Gravitational loads are neglected as these are assumed to have little effects on the response of the diaphragm.

ANALYSIS SETTINGS

As the laboratory test was quasi-static, it is chosen to use a static structural analysis in ANSYS 18.2. This analysis type is deemed suitable, as inertial effects can be neglected for a quasi-static test. Due to the nailed connections, the static analysis is nonlinear. For this analysis type, the default analysis method in ANSYS 18.2 is full Newton-Raphson. To properly solve the implemented nonlinearities, an iterative solver is used. For a better convergence of a nonlinear analysis, it is of importance that the loading is applied gradually. This can be done by ramping the loads and by increasing the number of substeps. The analysis settings are summarised in table 6-8.

Figure 6-30: Boundary conditions

Table 6-8: Analysis settings

Analysis type	Static nonlinear
Analysis method	Full Newton-Raphson
Solver type	Iterative
Loading	Displacement controlled
Load step size	0.5 s
Load stepping method	Ramped loads
Maximum number of substeps	30 000
Maximum number of iterations	2 000

ANALYSES

A total of four analyses are carried out for the as-built diaphragm. The first two analyses implement a coarse mesh, in which the largest element size can be up to 130 mm. The difference between the two analyses with a coarse mesh is the calibration method of the nailed connections. In the first analysis, the numerical hysteresis of the nails is calibrated to match the experimental hysteresis. In the second analysis, the numerical backbone of the nails is calibrated such that the conserved energy is the same as found experimentally. The last two analyses implement a fine mesh, in which the largest element size is 33 mm. The two analyses with a fine mesh also consider the two different calibration methods for the nailed connections. The parameters for the COMBIN40 elements, which represent the nails, for each calibration method are given in table 6-9 and table 6-10. A summary of the analyses can be seen in figure 6-31.

Table 6-9: Parameters for the COMBIN40 elements calibrated on the experimental hysteresis

	Loading perpendicular to joist					
	K1 (N/mm)	K2 (N/mm)	Fslide (N)	Initial gap (mm)	C (N*s/mm)	M (kg)
COMBIN40 - 1	10.000	4.22	192	0	0	0
COMBIN40 - 2	250	50	450	0.001	0	0
COMBIN40 - 3	250	50	450	0.001	0	0
	Loading parallel to joist					
	K1 (N/mm)	K2 (N/mm)	Fslide (N)	Initial gap (mm)	C (N*s/mm)	M (kg)
COMBIN40 - 1	10.000	2.5	145	0	0	0
COMBIN40 - 2	210	45	700	0.001	0	0
COMBIN40 - 3	210	45	700	0.001	0	0

Table 6-10: Parameters for the COMBIN40 elements calibrated on the experimental backbone

	Loading perpendicular to joist					
	K1 (N/mm)	K2 (N/mm)	Fslide (N)	Initial gap (mm)	C (N*s/mm)	M (kg)
COMBIN40 - 1	10.000	4.22	192	0	0	0
COMBIN40 - 2	150	0.0001	700	0.001	0	0
COMBIN40 - 3	150	0.0001	700	0.001	0	0
	Loading parallel to joist					
	K1 (N/mm)	K2 (N/mm)	Fslide (N)	Initial gap (mm)	C (N*s/mm)	M (kg)
COMBIN40 - 1	10.000	2.5	145	0	0	0
COMBIN40 - 2	500	0.001	840	0.001	0	0
COMBIN40 - 3	500	0.001	840	0.001	0	0

Figure 6-31: Numerical analyses for the as-built diaphragm

6.3.1 COARSE MESH

For the two analyses with a coarse mesh, the mesh is irregular and element sizes differ depending on the location. For the beam elements, one element is placed between each nail. This means that the element length for the beam elements is either 32.5, 63.5, 67 or 100 mm. For the shell elements (timber planks), the element size in y-direction (along the length of the beams) is either 32.5 or 100 mm. The element size in x-direction (along the length of the plank) is either 30 mm, 50 mm or 130 mm. The mesh can be seen in figure 6-32 and figure 6-33. A total of 2810 elements are used for the model of the as-built diaphragm with a coarse mesh, of which 188 BEAM188 elements, 1518 SHELL181 elements and 1104 COMBIN40 elements. The ANSYS APDL script for the models with a coarse mesh can be found in appendix F.
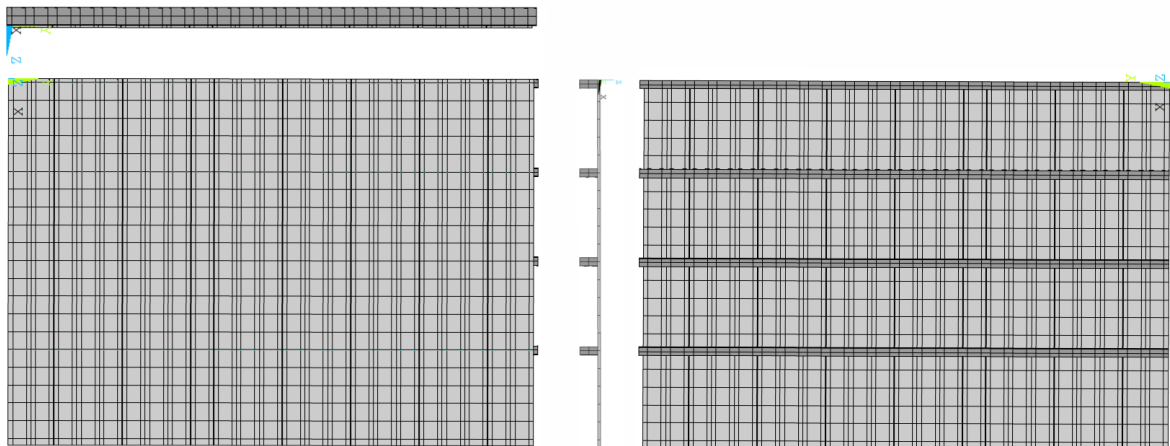
Figure 6-32: Front and back view of as-built diaphragm with coarse mesh, along with top and side views
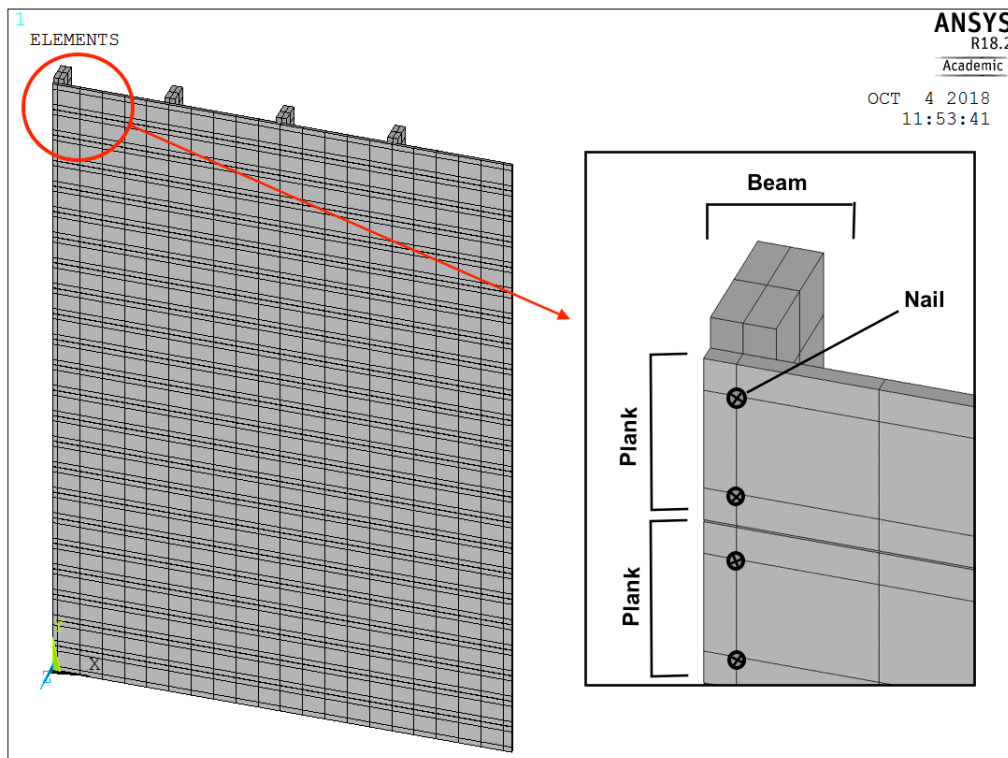
Figure 6-33: 3D view of as-built diaphragm with coarse mesh, along with positioning of nails

FIRST CALIBRATION APPROACH

For the first analysis, in which the numerical hysteresis of the nailed connections is calibrated on the experimental hysteresis, the result of the numerical analysis (along with its loading scheme) can be seen in figure 6-34. A comparison with the experimental result can be seen in figure 6-35. One can see that the numerical reloading branches are represented through a bilinear curve. Additionally, the backbone of the hysteresis seems to be fairly linear. Comparing the result to the experimental result, it can be said that the behaviour of the numerical model can capture the experimental hysteresis quite accurately. However, the numerically calculated reaction forces are not very accurate as the maximum predicted force per cycle is underestimated. This underestimation becomes larger for higher displacements, with the largest error being 27.3% at the largest displacement.

To validate whether the connection still exhibits the correct behaviour when implemented in a diaphragm, the upper left nailed connection in the as-built diaphragm is regarded in y-direction. The response of the connection as extracted from the diaphragm and as modelled in subsection 6.1.2 can be seen in figure 6-36. As the connection is implemented in a floor that is cyclically loaded, the local displacements of the connection are not the same as the cyclic loading scheme imposed on the diaphragm. The connection in the diaphragm remains in the elastic phase. Considering the behaviour of both the connection in the diaphragm and the connection on its own, it can be concluded that they still exhibit similar results. Therefore, it can be said that the connection within the diaphragm accurately represents the behaviour of the connection on its own. As a similar result is expected for the other connections as well as for the second calibration method, the validation of these connections will be omitted.
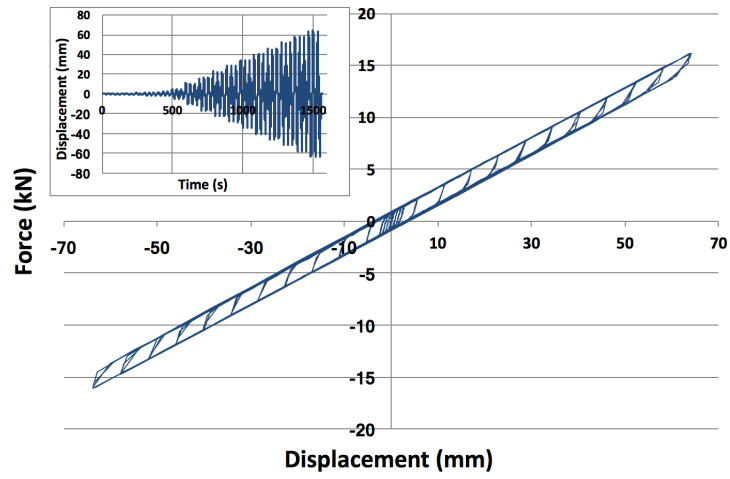
Figure 6-34: Numerical result for as-built diaphragm
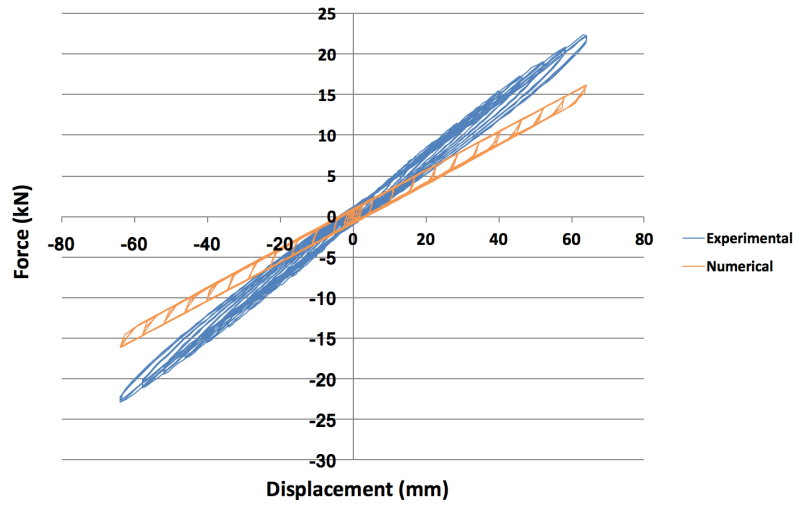
Figure 6-35: Comparison between numerical and experimental result for as-built diaphragm
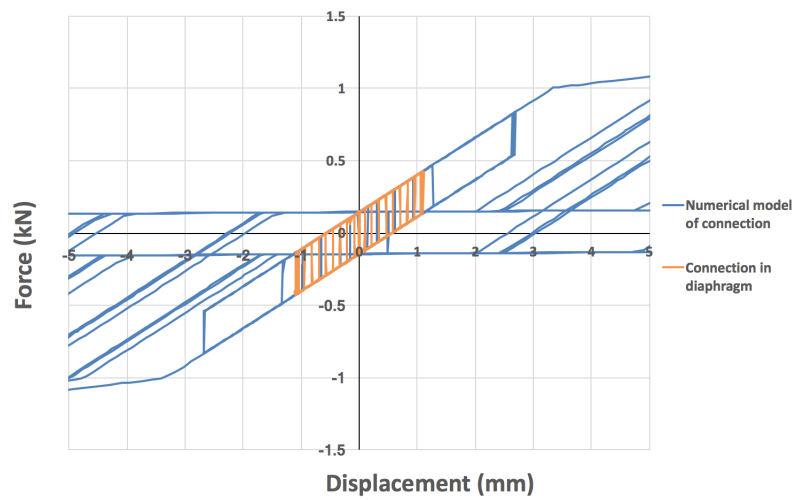
Figure 6-36: Comparison between numerical model of connection and connection within diaphragm

SECOND CALIBRATION APPROACH

For the second analysis, in which the numerical backbone of the nailed connections is calibrated such that the preserved energy matches the energy of the experimental backbone, the result of the numerical analysis (along with its loading scheme) can be seen in figure 6-37. A comparison with the experimental result can be seen in figure 6-38. The response of the as-built diaphragm with this calibration approach is similar to the response with the first calibration approach. The hysteresis curve exhibits the same behaviour, but the maximum forces per cycle are lower. For the second calibration approach, the largest error is 30.7% at the largest displacement. The error for the second calibration approach is larger than for the first calibration approach. The difference in error will only become larger for increasing displacement.
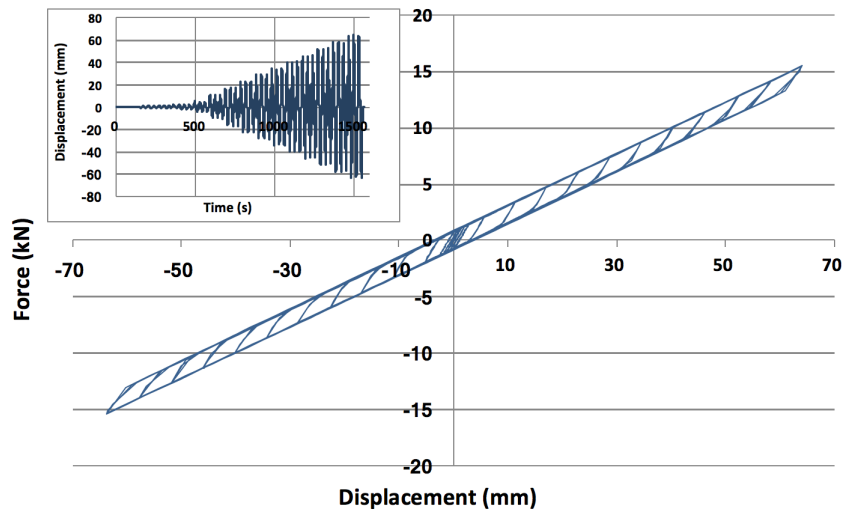
Figure 6-37: Numerical result for as-built diaphragm
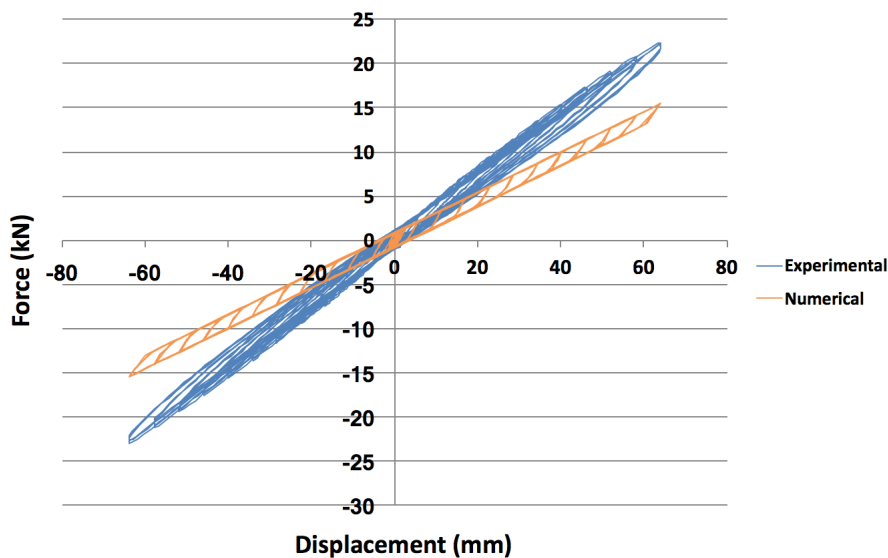
Figure 6-38: Comparison between numerical and experimental result for as-built diaphragm

6.3.2 Fine mesh

For the two analyses with a fine mesh, the mesh is regular the element sizes are consistent for each timber member (see figure 6-39 and figure 6-40). For both beam and shell elements, the element size is 33 mm. A total of 12006 elements are used for the model of the as-built diaphragm with a fine mesh, of which 552 BEAM188 elements, 10350 SHELL181 elements and 1104 COMBIN40 elements. The ANSYS APDL script for the models with a fine mesh can be found in appendix G.
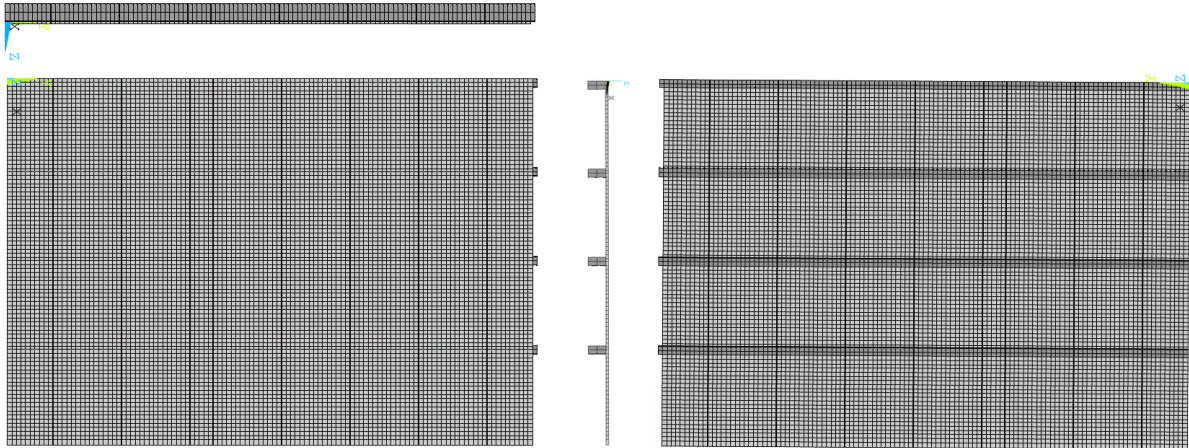
Figure 6-39: Front and back view of as-built diaphragm with fine mesh, along with top and side views
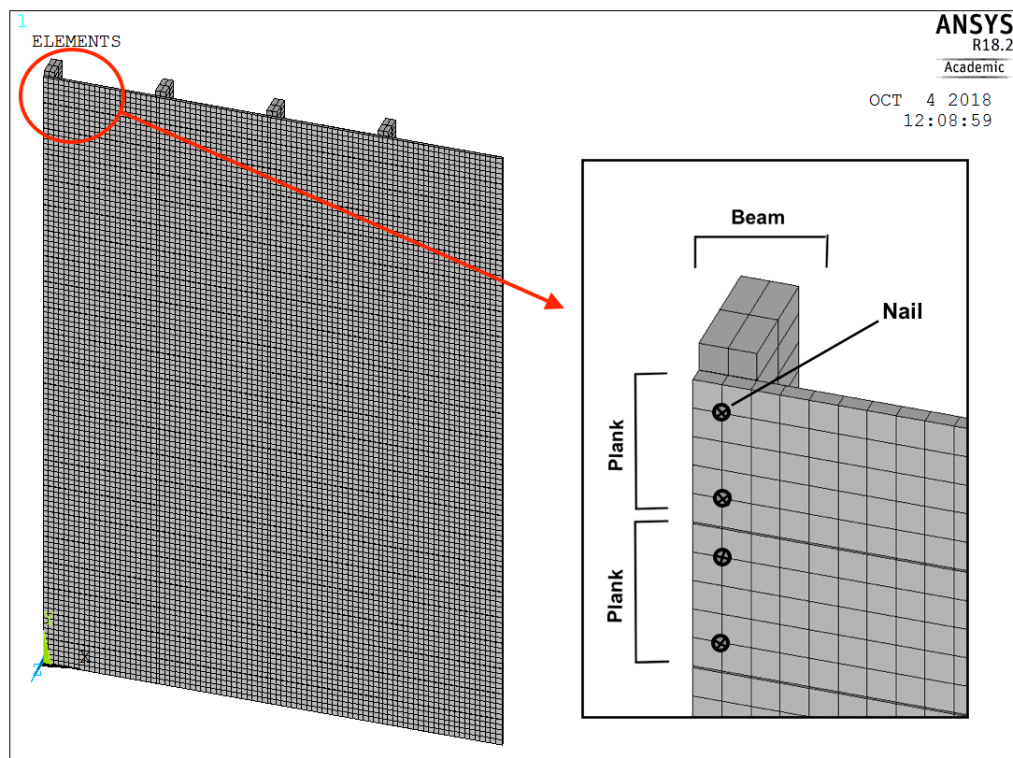
Figure 6-40: 3D view of as-built diaphragm with fine mesh, along with positioning of nails

For the first analysis, in which the numerical hysteresis of the nailed connections is calibrated on the experimental hysteresis, the result of the numerical analysis (along with its loading scheme) can be seen in figure 6-41. A comparison with the experimental result can be seen in figure 6-42. Considering this result, the backbone remains fairly linear and the numerical reloading branches are represented through a bilinear curve. Comparing the result to the experimental result, it can be said that the behaviour of the numerical model can capture the experimental hysteresis quite accurately. The numerically calculated reaction forces are quite close to the ones found experimentally. It can be seen that the error increases with increasing displacement. The maximum error is valued at 12.6% occurring at the largest displacement.
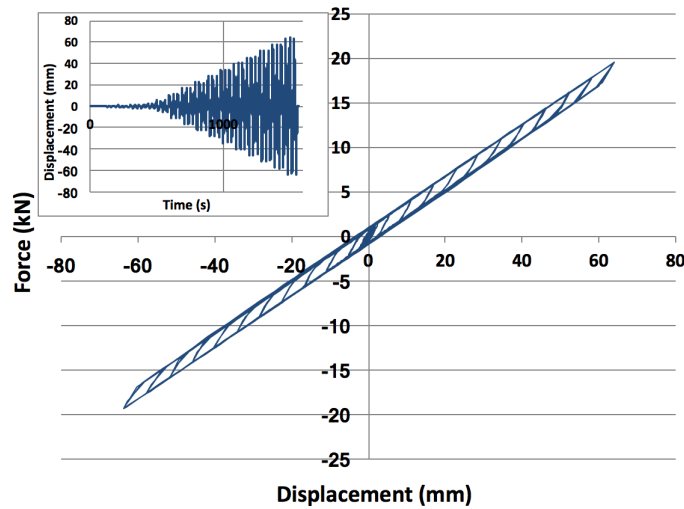
Figure 6-41: Numerical result for as-built diaphragm
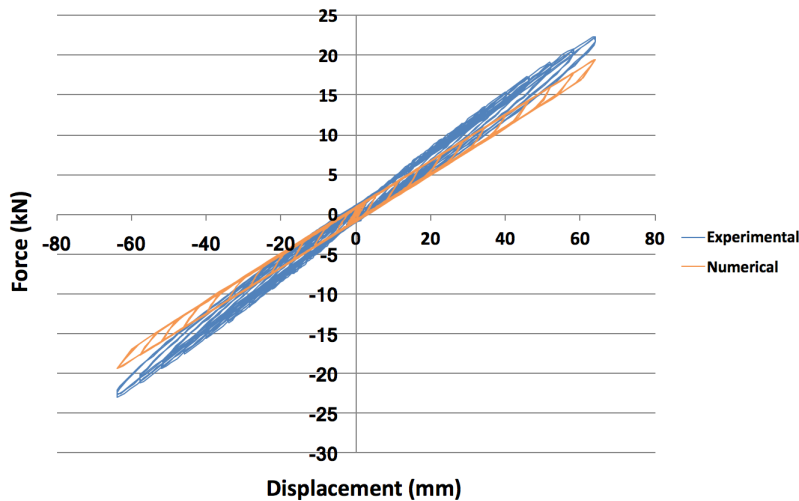
Figure 6-42: Comparison between numerical and experimental result for as-built diaphragm

Second calibration approach

For the second analysis, in which the numerical backbone of the nailed connections is calibrated such that the preserved energy matches the energy of the experimental backbone, the result of the numerical analysis (along with its loading scheme) can be seen in figure 6-43. A comparison with the experimental result can be seen in figure 6-44. The response of the as-built diaphragm with this calibration approach is similar to the response with the first calibration approach. The hysteresis curve exhibits the same behaviour, but the maximum forces per cycle are lower. For the second calibration approach, the largest error is 15.6% at the largest displacement. The error for the second calibration approach is larger than for the first calibration approach. The difference in error will only become larger for increasing displacement.
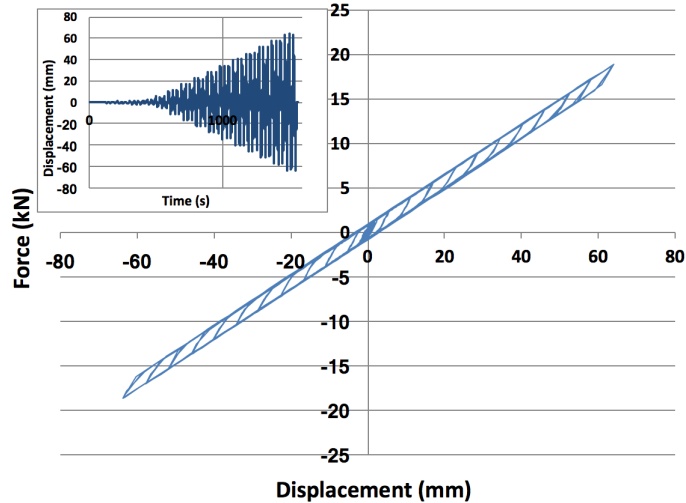
Figure 6-43: Numerical result for as-built diaphragm
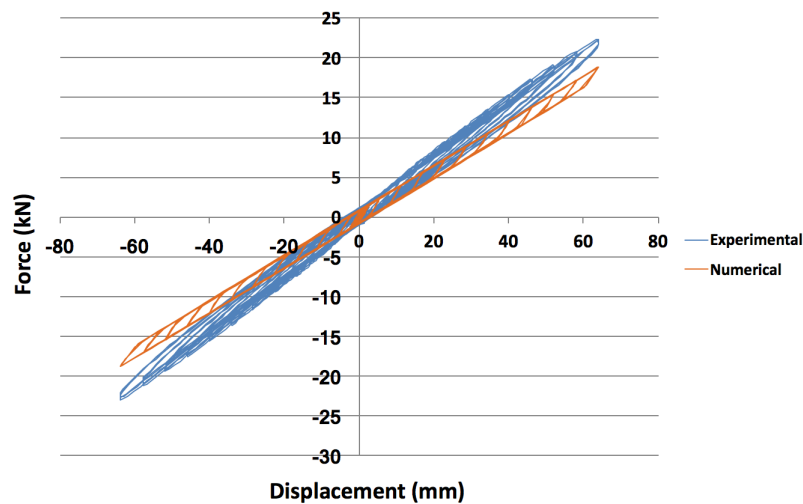
Figure 6-44: Comparison between numerical and experimental result for as-built diaphragm

6.3.3 Comparison

With the four analyses that have been carried out for the as-built diaphragm, the results can be compared to each other. In this section, a comparison between the two calibration methods, a comparison between the two meshes and an overall comparison will be given.

Comparison between calibration methods

For both meshes, two analyses have been carried out in which the calibration of the COMBIN40 elements for the nailed connections was different. The first calibration method, which is referred to as 'Numerical 1' in graphs hereafter, calibrates the numerical hysteresis on the experimental hysteresis such that the reloading and unloading branches match as much as possible. The second calibration method, which is referred to as 'Numerical 2' in graphs hereafter, calibrates the numerical backbone on the experimental backbone such that it conserves the same energy. A comparison between both calibrations methods for the coarse mesh can be seen in figure 6-45 and for the fine mesh in figure 6-46. For both meshes, it can be seen that the first calibration method yields results which are more close to the result found experimentally. This is in line with expectations, as the first calibration method conserves more energy and is better able to simulate local behaviour of the nails in the diaphragm. Therefore, this calibration method is more suitable to model a diaphragm similar to the one tested at the TU Delft, subjected under gradual loading. Under more random loading, the first calibration method may yield results that are not in line with reality. Random loading may cause an overestimation of the strength of the numerical model of the diaphragm, as the conserved energy is not controlled and may increase infinitely.

The second calibration method for the nailed connections yields similar results to the first calibration method. The second method underestimates the strength of the diaphragm more than the first method, as the preserved energy in the COMBIN40 elements is lower. However, the difference between the second and first calibration is very small. For the coarse mesh, the largest difference in reaction force is 0.76 kN. For the fine mesh, the largest difference in reaction force is 0.66 kN. One can conclude that the difference between both calibration methods is smaller for the analyses with a fine mesh. The second calibration method may prove to be more suitable for analyses with a more random loading scheme, such as a nonlinear time history analysis. This is due to the fact that the preserved energy in the nailed connections is limited in the numerical model. Overestimations of reaction forces are therefore less likely to occur. In terms of energy, the second calibration method yields a more realistic model for a timber diaphragm.
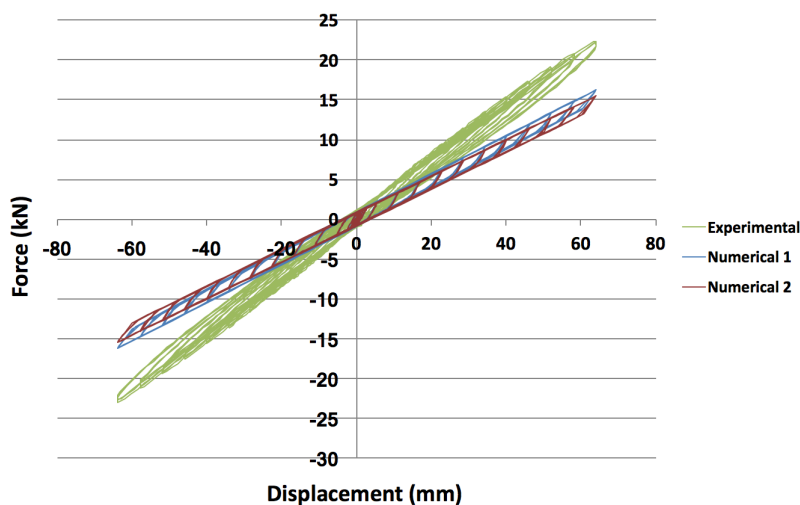
Figure 6-45: Comparison between numerical results with coarse mesh and experimental results
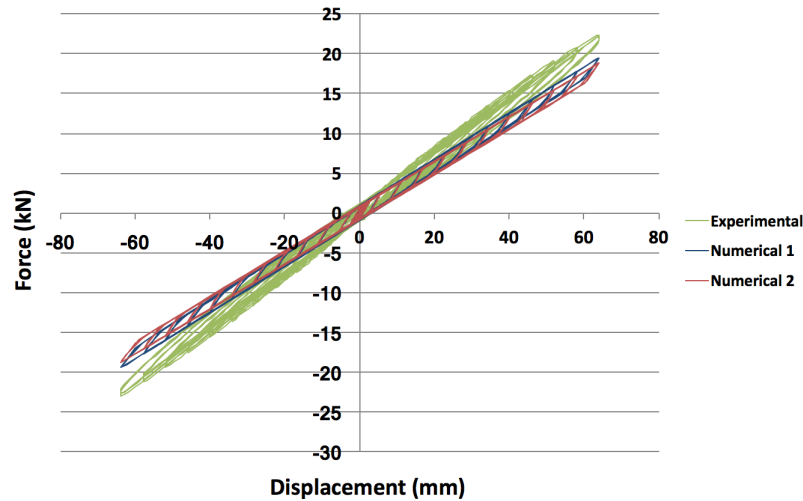
Figure 6-46: Comparison between numerical results with fine mesh and experimental results

COMPARISON BETWEEN MESHES

For both calibration methods of the nails, two analyses have been carried out in which the meshes differed. The first mesh is a rather coarse mesh with element dimensions up to 130 mm. The second mesh is a fine mesh in which the largest element dimension is 33 mm. A comparison between results for both meshes for the first calibration method can be seen in figure 6-47 and for the second calibration method in figure 6-48. For both calibration methods, it can be seen that the fine mesh yields more accurate results. However, the difference between coarse and fine mesh is not the same for both calibration methods. The difference is slightly bigger for the second calibration approach, in which the numerical backbone of the nails was calibrated on the experimental backbone.
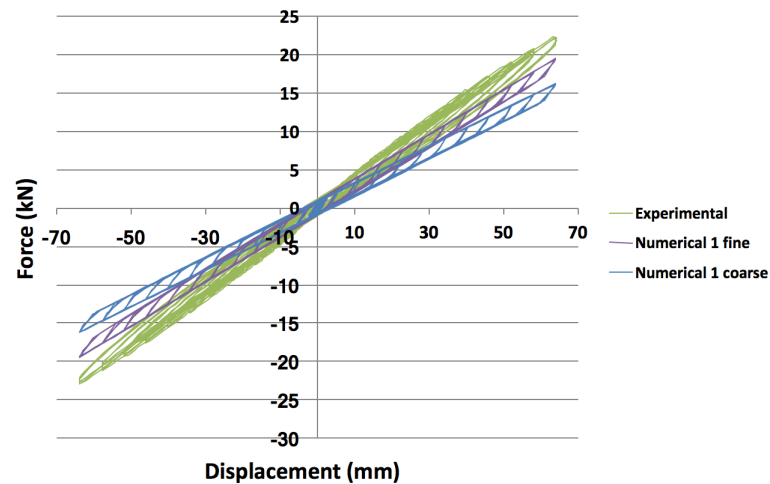
Figure 6-47: Comparison between numerical results for first calibration method and experimental result
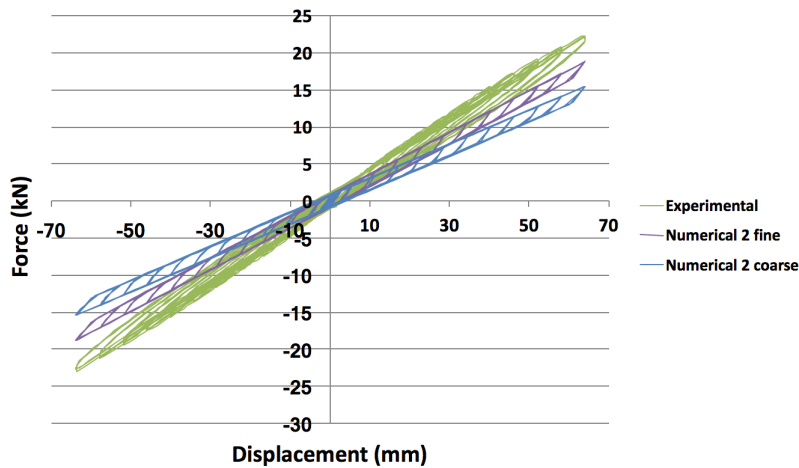
Figure 6-48: Comparison between numerical result for second calibration method and experimental result

The difference between the results for a coarse and fine mesh can be explained by looking at the nodal displacements at the position of the nails. Taking the first calibration method and looking at the upper left nailed connection at the top beam (intersection between first plank and top beam), one can compare the displacements for both meshes. It is chosen to consider a nail at the top, as the highest displacements take place at the top. For the coarse mesh, only one element is placed between the two nails at the plank-beam intersection. This means that there are no additional nodes between the nodes to which the nails are attached. For the fine mesh, three elements are placed between the two nails. This results in an additional two nodes being placed between the nodes to which the nails are attached. At a time of 1467 seconds (at which the largest displacement takes place), the displacements of the beam and planks for both the coarse and fine mesh can be seen in figure 6-49. The displacement of the top beam is the same for both meshes, as the displacement-controlled loading is applied at this beam. Thus, the deformation of the nails connected to the top beam depend on the calculated displacements in the planks. From the graph, it can be seen that the displacement of the plank is lower for the finer mesh. This results in a higher relative displacement between beam and plank for the finer mesh. The relative displacement for both meshes can be seen in figure 6-50. A higher relative displacement results in bigger forces in the nails, explaining why the finer mesh yields larger reaction forces for the as-built diaphragm. The relative nodal displacement of the coarse mesh at the position of the nails is approximately 73% of that of the fine mesh.
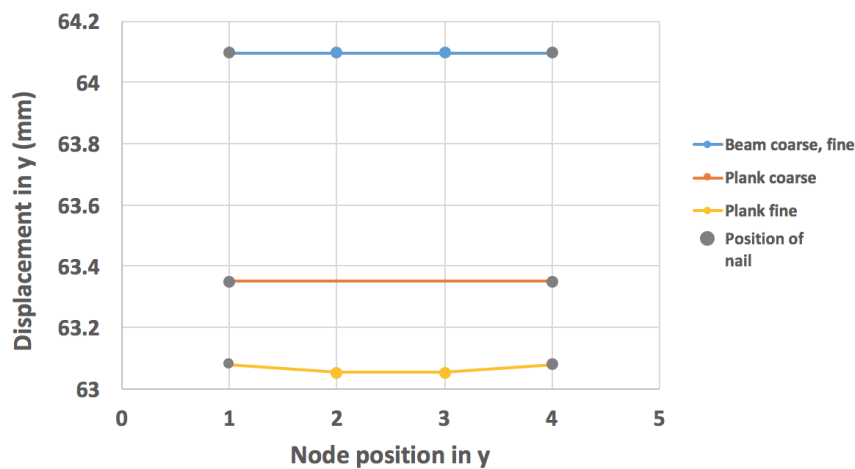
Figure 6-49: Displacements of plank and beam at top left connection for both meshes
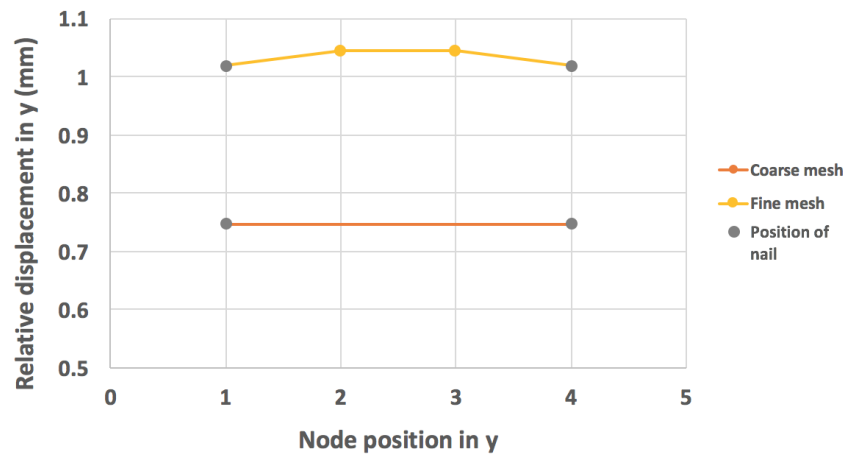
Figure 6-50: Relative displacement between beam and plank at top left connection for both meshes

The higher forces for the fine mesh result in a higher stiffness in diaphragm response for a finer mesh. This seems contradictory, as a finer mesh should yield an increase in a system's flexibility (higher amount of elements), thus reducing its stiffness. The seemingly stiffer response for a finer mesh for the as-built diaphragm can be explained by regarding the interaction between planks and beams. The movement of the planks cause a rotation at the connection between each plank and beam. As the beams are connected to each plank with two nails, the rotation causes a bending moment (see figure 6-51) resulting from the forces in x-direction (along the length of the planks) from both nails. These forces cause the beams to deform like a sinusoidal wave in x-direction on micro level, as there is an upward and a downward force from each plank. At a time of 1467 seconds (at which the highest displacement in y-direction occurs), the deformation of the beams in x-direction for both the coarse and fine mesh with the first calibration method for the connections can be seen in figure 6-52 and figure 6-53. The beams are numbered from bottom to top, with beam 1 referring to the bottom beam and beam 4 referring to the top (loaded) beam. In these figures, a wavelike deformation can be seen on macro and micro level. On micro level, the wavelike deformation is more evident for the fine mesh, which can be explained by the increased flexibility of the beams. With a higher flexibility, the beams are better able to follow the movements of the planks. The wavelike deformation of the beams on micro level is confirmed by the moment distribution in the beams (see figure 6-54 and figure 6-55). For the coarse mesh, the moment distribution is less sinusoidal due to the averaging of the bending moment over an element. This mesh yields lower bending moments and thus lower (local) curvatures. This is in support of the finding that the beams deform less like a wave for the coarse mesh. For the fine mesh, the bending moments in the beams are higher and more wavelike (due to the smaller elements), resulting in higher (local) curvatures. The higher curvatures cause the beams to deform in a more flexible manner and thus the beams are better able to follow the movements of the planks for the fine mesh.

On macro level, the overall deformation of the beams looks like a third order polynomial. The ends of the beams are able to move freely, as the ends are not constrained and are not connected to an adjacent plank. Therefore, the displacement in x-direction is highest at the ends of the beams. Both ends of the beams move in opposite directions due to the deformation of the planks. Thus, in order to connect the ends of the beams, the overall deformation of the beam is similar to a third order polynomial. On micro level, it is more difficult for stiffer beams to assume a wavelike deformation. This may result in a higher deformation of the planks, as stiffer beams tend to pull the planks more (see figure 6-56). A similar mechanism may occur on macro level, causing the displacement in y-direction to be higher for the planks in the coarse mesh. Due to the pulling of the planks due to the

stiff beams in the coarse mesh, the nail deformations become smaller and thus the overall response is less stiff. For the fine mesh, the beams are better able to follow the movements of the planks, causing a lower displacement of the planks (as the beams do not pull the planks). This results in higher nail deformations and thus a stiffer response of the diaphragm.
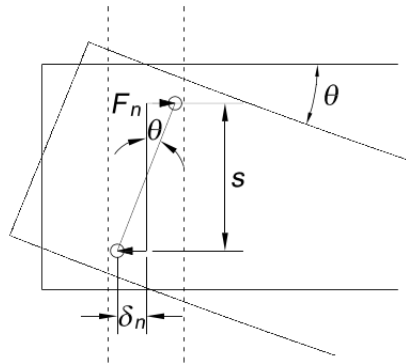
Figure 6-51: Bending moment due to rotation
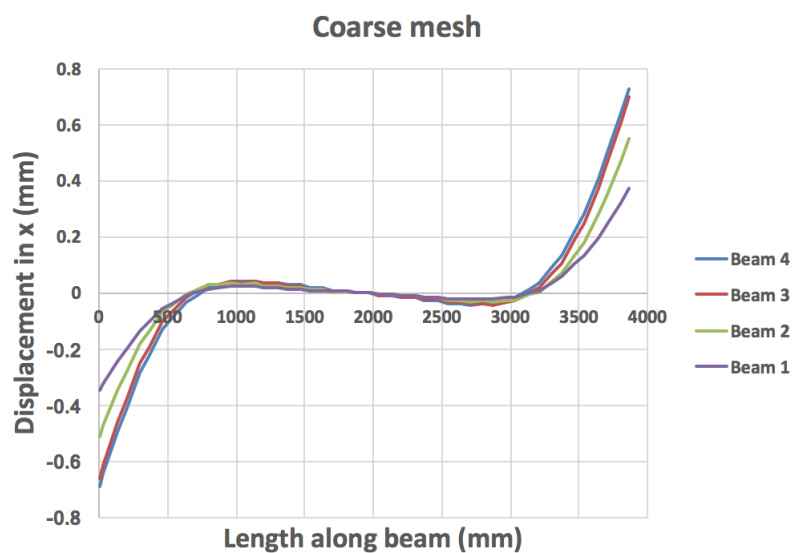
Figure 6-52: Displacement in x-direction for beams for coarse mesh at t=1467 s
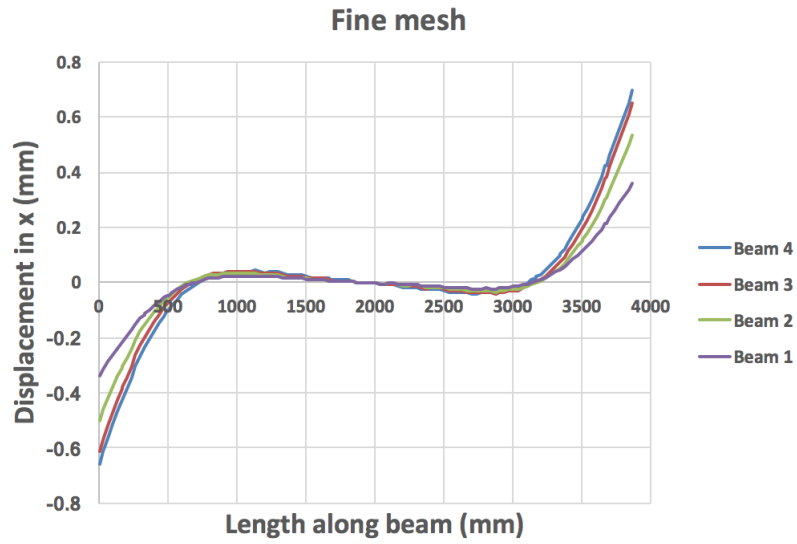
Figure 6-53: Displacement in x-direction for beams for fine mesh at t=1467 s
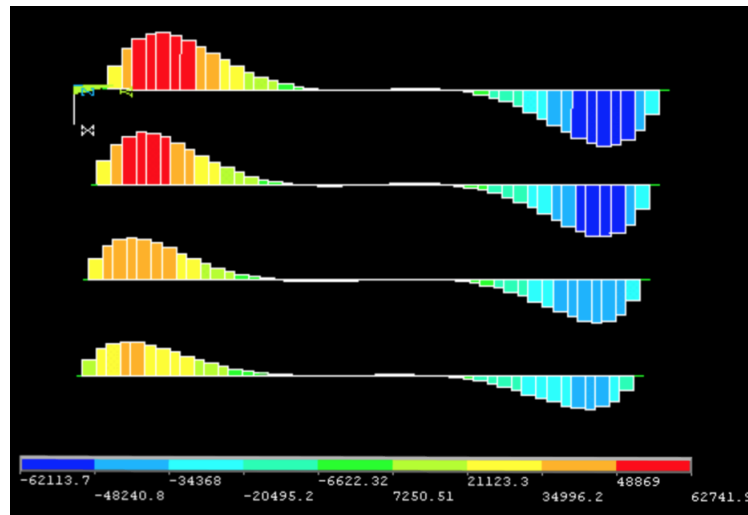
Figure 6-54: Moment distribution in the beams for coarse mesh for first calibration method
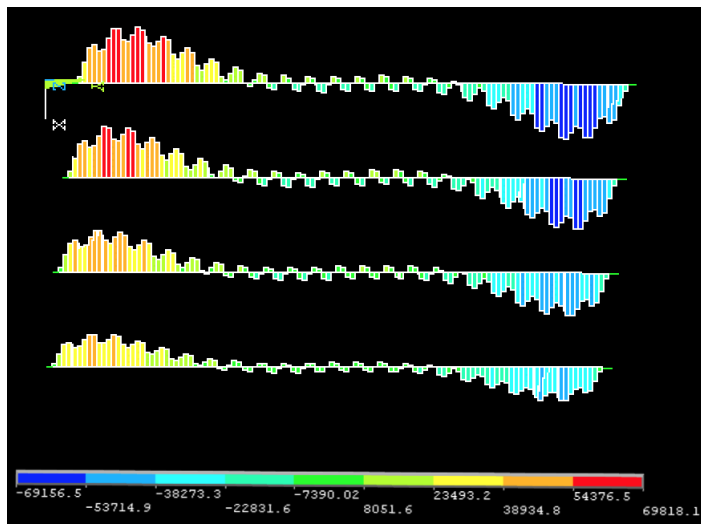
Figure 6-55: Moment distribution in the beams for fine mesh for first calibration method
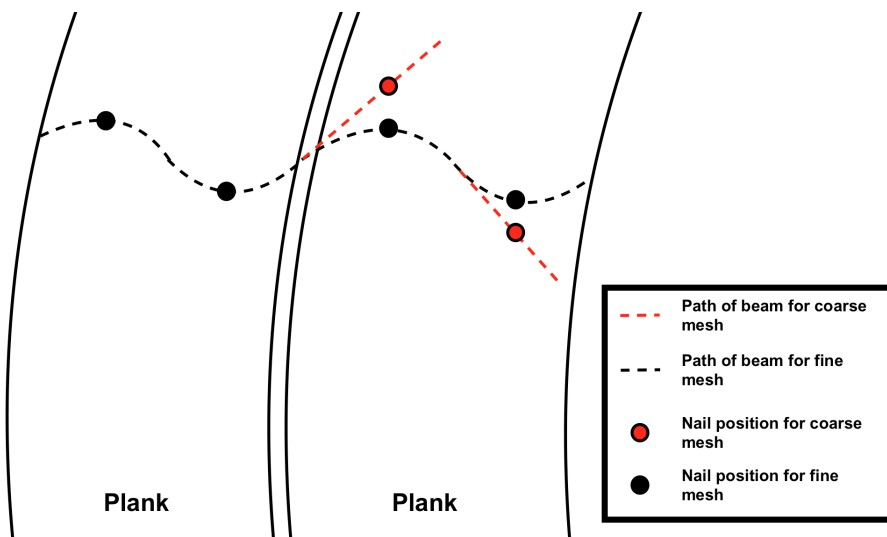
Figure 6-56: Theoretical deformation of beams

As the displacement of the beams in x-direction is higher for the coarse mesh (due to the inability of the stiffer beams assuming the deformation of the planks), forces in the nails are higher as opposed to the fine mesh. This generates a higher bending moment at a beam-plank intersection with two nails. It is expected that each nail at an intersection generates the same magnitude of forces, as the centre of rotation is in the middle of the nails. This is the case for the inner planks, however for the two outer planks this is not applicable. The outer planks do not have symmetry as one edge is not placed adjacent to an other plank. The nail closest to the free edge of an outer plank generates a lower force as the beam is not connected to an other plank and is able to move freely at the free edge. Inner planks have symmetry as these planks are adjacent to other planks at both sides. This results in lower bending moments at a beam-plank intersection for the outer planks as opposed to the inner planks. The bending moments (resulting from forces in x-direction) at the beam-plank intersections for the left plank ("plank 1") and the middle plank ("plank 12") are shown in figure 6-57 and figure 6-58 and listed in table 6-11 and table 6-12, with a moment arm of 100 mm. The bending moments at the intersections resist the bending deformation of the planks and lower the displacement at the top of the plank (thus increasing nail deformation). From figure 6-57 and figure 6-58, it can

be confirmed that the bending moments are lower for the outer plank. Furthermore, the bending moments are slightly lower for the fine mesh (due to the lower forces in the nails resulting from the higher flexibility of the beams). However, for both coarse and fine mesh the bending moments are very similar. The similar bending moments yield a lower displacement of the planks for the fine mesh, as the planks are more flexible for the fine mesh.
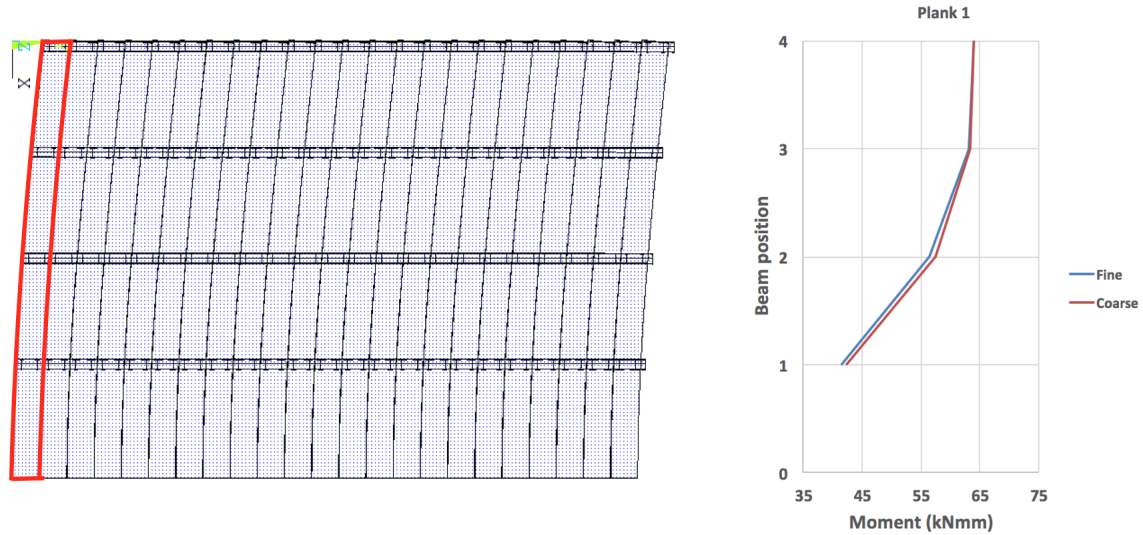
Figure 6-57: Moment at position of beams for first plank, for coarse and fine mesh

Table 6-11: Forces and moments in plank 1 for coarse and fine mesh

| | Coarse mesh | | | Fine mesh | | |
	Force in left nail (kN)	Force in right nail (kN)	Moment (kNmm)	Force in left nail (kN)	Force in right nail (kN)	Moment (kNmm)
Beam 4	0.52868	-0.7538	64.124	0.52925	-0.75295	64.110
Beam 3	0.51688	-0.7521	63.449	0.51439	-0.74874	63.157
Beam 2	0.45988	-0.6905	57.517	0.45239	-0.67616	56.428
Beam 1	0.34435	-0.5054	42.488	0.33851	-0.49477	41.664
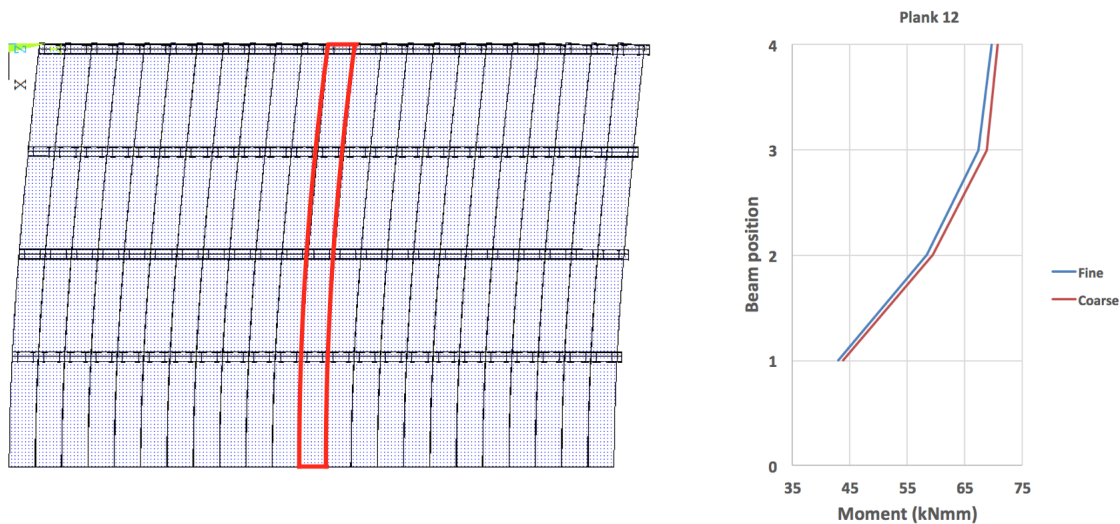
Figure 6-58: Moment at position of beams for twelfth plank, for coarse and fine mesh

Table 6-12: Forces and moments in plank 12 for coarse and fine mesh

	Coarse mesh			Fine mesh		
	Force in left nail (kN)	Force in right nail (kN)	Moment (kNmm)	Force in left nail (kN)	Force in right nail (kN)	Moment (kNmm)
Beam 4	0.70764	-0.70761	70.763	0.69793	-0.6979	69.792
Beam 3	0.68871	-0.68862	68.867	0.6735	-0.67351	67.351
Beam 2	0.59552	-0.59561	59.557	0.58439	-0.58455	58.447
Beam 1	0.43808	-0.43815	43.812	0.42979	-0.42989	42.984

Regarding the nailed connections, a maximum deformation for each nail can be obtained for both meshes with the first calibration method for the nails. The maximum deformation in x-direction for all the nails per beam can be seen in figure 6-59. From this figure, it can be seen that the maximum deformation of the nails increases per beam which is closer to the top. This results in the highest resisting moments at the top beam. The coarse mesh yields higher deformations (and higher resisting moments) than the fine mesh, which is caused by the stiffer beams. The maximum deformation of the nails is 2.2 mm for the coarse mesh and 2.1 mm for the fine mesh, both occurring at the top beam. In x-direction, the numerical model of the nailed connection enter plasticity at a deformation of approximately 1.8 mm (see figure 6-8). Thus, it can be said that plasticity in x-direction occurs in the nails for both meshes. Considering the relative displacement in y-direction between plank and beam at the position of the nails, a maximum absolute deformation for all the nails in each beam can be obtained. The maximum deformation in y-direction for all the nails per beam can be seen in figure 6-60. One can see that for the lower three beams, the deformation of the nails is very close to zero. The highest nail deformations occur at the top beam where loading was applied. It can be said that the nail deformations are lumped at the top beam, thus generating the highest reaction forces (originating from the connections) at this beam. For the coarse mesh, the maximum deformation in y-direction of the nails in the top beam is 1.1 mm, as opposed to 1.4 mm for the fine mesh. Additionally, figure 6-60 shows that the deformation of the diaphragm is characterised by the bending of the planks, rather than the shear deformation. The diaphragm is analogous to a standard bending problem, with the highest rate of deformation being at the edges (top of diaphragm) and the lowest rate of deformation, being near zero, in the middle (bottom of diaphragm). In y-direction, the numerical model of the nailed connection enter plasticity at a deformation of about 3.3 mm (see

figure 6-18). Thus, it can be concluded that none of the nailed connections enter plasticity in this direction for both meshes. Regarding the behaviour of the connections in both x- and y-direction, it can be said that the deformation in x-direction is higher for the coarse mesh, whereas the deformation in y-direction is higher for the fine mesh. Furthermore, most of the nails remain largely in the elastic regime for both meshes. This may explain the fairly linear behaviour of the as-built diaphragm. As no nails come near failure, the lack of implementation of failure in the nailed connections is not disastrous and may not even be needed for the as-built diaphragm (under the given loading scheme). A summary of the maximum nail deformation for both coarse and fine mesh with the first calibration method is given in table 6-13. A visualisation of the maximum deformation of the nails within the backbone curves in both x- and y-direction can be seen in figure 6-61. In this figure, the green vertical lines represents the onset of plasticity. From this figure, it is more evident that the maximum deformation of the nails is either still in the elastic phase or very near the elastic phase.
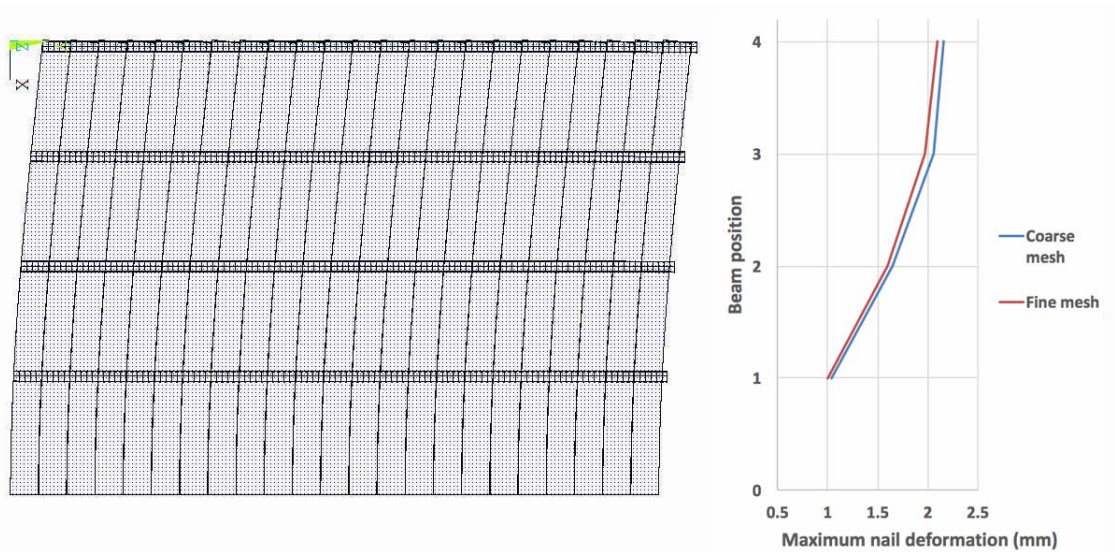
Figure 6-59: Maximum relative displacement in x-direction between plank and beam at the position of the nails
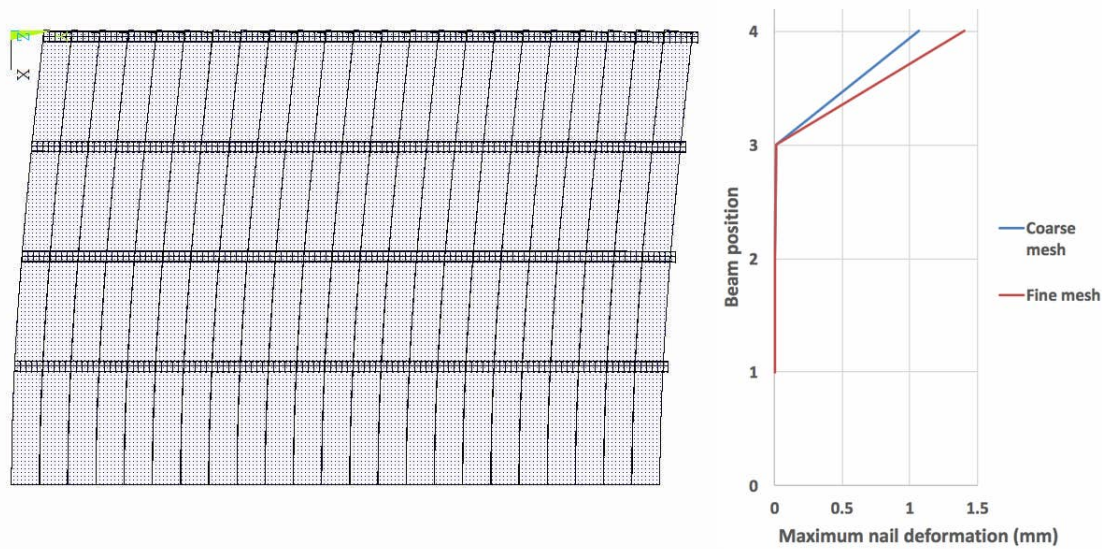
Figure 6-60: Maximum relative displacement in y-direction between plank and beam at the position of the nails

Table 6-13: Maximum deformation of the nails for coarse and fine mesh with first calibration method

	x-direction		y-direction	
	Maximum deformation (mm)	Onset of plasticity (mm)	Maximum deformation (mm)	Onset of plasticity (mm)
Coarse mesh	2.2	1.8	1.1	3.3
Fine mesh	2.1	1.8	1.4	3.3
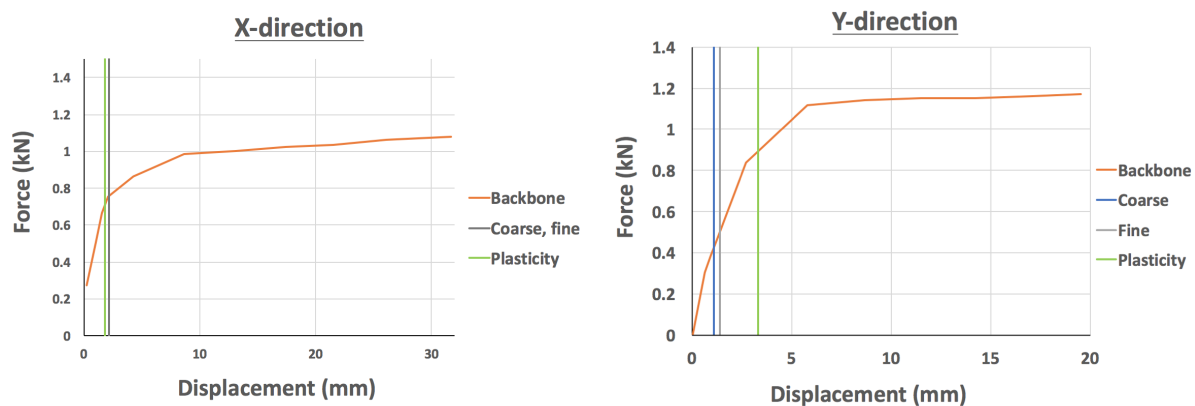
Figure 6-61: Maximum deformation of nails within the backbone curve for first calibration method for both meshes

OVERALL COMPARISON

A comparison between the four numerical analyses and the experimental result can be seen in figure 6-62. A comparison between the backbones can be seen in figure 6-63. The slopes of the linear regression of each backbone and the maximum force is listed in table 6-14, along with its errors. One can see that the results for both calibration methods are similar for each mesh. The numerical results match the experimental results better for a finer mesh. However, none of the numerical results completely match the experimental results. This may be caused by the (small) errors in the modelling of the nailed connections. Furthermore, friction and contact (opening and closing of gaps)

between planks have been neglected. Disregarding the conserved energy in these interactions may also contribute to the fact that the numerical result does not match the experimental result entirely. Neglecting these interactions results in a lower amount of conserved energy, which is in line with the numerical results. Looking at the results from this section, it can be seen that the experimental result is best predicted by the numerical model with the first calibration method for the nails and a fine mesh. Thus, this numerical model is proposed to model a diaphragm as tested at the TU Delft. The errors are deemed small enough and the experimental hysteresis is captured in an accurate manner.
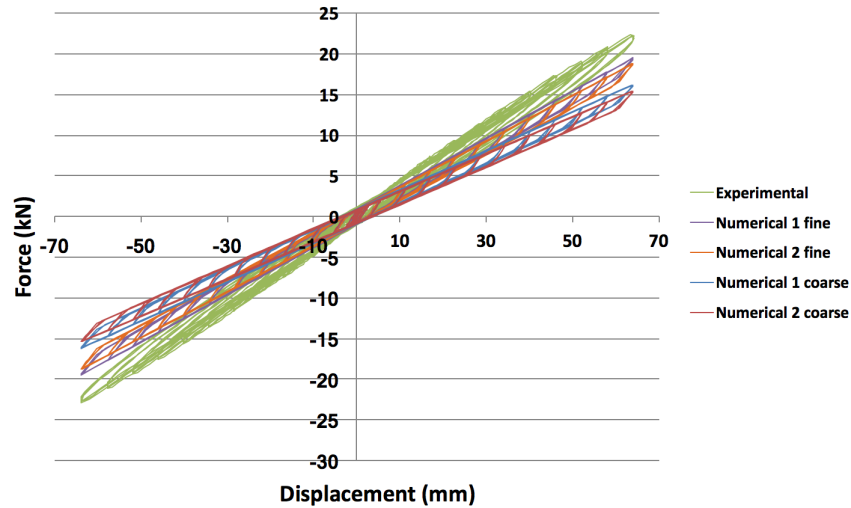
Figure 6-62: Comparison between numerical and experimental result for as-built diaphragm
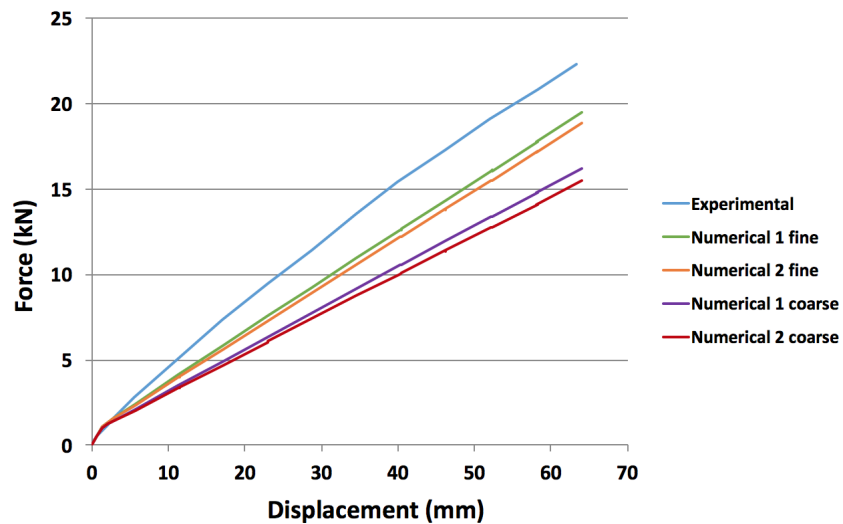
Figure 6-63: Comparison between numerical and experimental backbones for as-built diaphragm

Table 6-14: Comparison of backbone between four analyses and experimental result

	Experimental	Numerical 1 fine	Numerical 2 fine	Numerical 1 coarse	Numerical 2 coarse
Slope of linear regression	0.372 kN/mm	0.311 kN/mm	0.3 kN/mm	0.26 kN/mm	0.247 kN/mm
Error in slope	-	16%	19%	30%	34%
Maximum force	22.33 kN	19.51 kN	18.85 kN	16.24 kN	15.48 kN
Error in maximum force	-	12.6%	15.6%	27.3%	30.7%

ADDITIONAL ANALYSIS

In order to stress the importance of the nonlinear modelling of the connections within a diaphragm, an additional analysis is carried out. In this analysis, the nonlinear nailed connections are replaced with linear springs with a stiffness of 20.000 N/mm (very stiff) for the as-built diaphragm with a fine mesh. The result of this analysis can be seen in figure 6-64, along with the experimental result and the numerical result for the first calibration method as discussed previously. One can see that with stiff linear connections, the result differs very much from the experimental result. The stiffness of the diaphragm is gravely overestimated due to the very high stiffness of the connections. As the diaphragm is entirely linear, no energy can be dissipated and the system is completely conservative. This results in an overlap for the un- and reloading branches for a diaphragm with stiff linear connections. However, the overall behaviour is still similar to the experimental result and to the numerical result with nonlinear connections. This is due to the fact that the as-built diaphragm still remains largely in elasticity, thus a simplification with only linear elements does not produce too large discrepancies. Should the diaphragm enter plasticity, errors would become larger for the linear approximation as no energy dissipation is implemented. For the retrofitted diaphragm, a linear simplification would yield highly inaccurate results as the behaviour of the diaphragm is highly nonlinear. A linear simplification would omit energy dissipation, pinching behaviour and nonlinear loading paths. These elements of the hysteresis curve are crucial for the retrofitted diaphragm and a linear approximation would not be suitable.
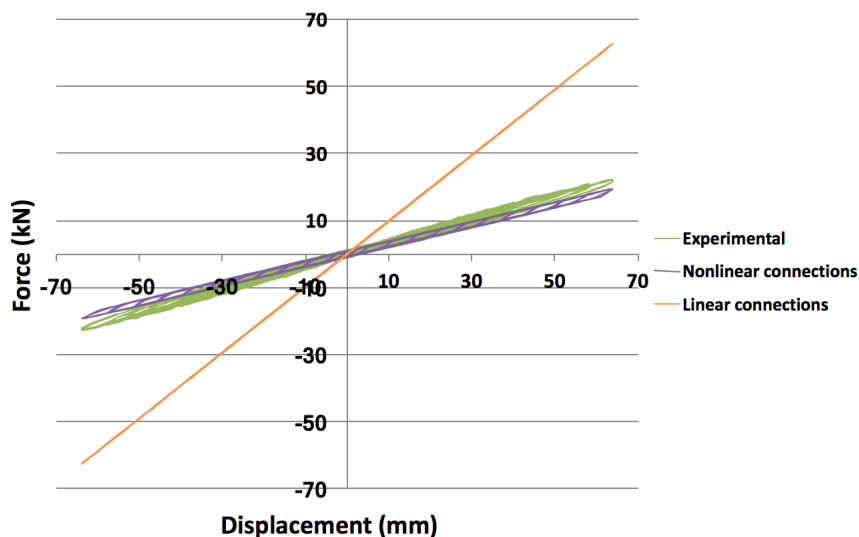
Figure 6-64: Comparison between linear and nonlinear connections for as-built diaphragm with fine mesh

7

EXTENSIVE MODEL OF RETROFITTED DIAPHRAGM

This chapter will present an extensive finite element model for the retrofitted diaphragm. Similar to the as-built diaphragm, this model is scripted in ANSYS Mechanical APDL 18.2. The model for the as-built diaphragm can be extended to create a model for the retrofitted diaphragm. Only the screws and the panels are added for the retrofitted diaphragm. First, the screwed connection between panel and plank needs to be modelled uniaxially in both in-plane directions (section 7.1). Thereafter, the screwed connection between panel, plank and beam needs to be modelled uniaxially in both in-plane directions (section 7.2). With the models of the screws, the retrofitted diaphragm can be modelled cyclically in its entirety (section 7.3). The diaphragm as regarded for numerical interpretation is a simple retrofitted diaphragm as tested in June 2017 at the TU Delft as discussed in chapter 5.
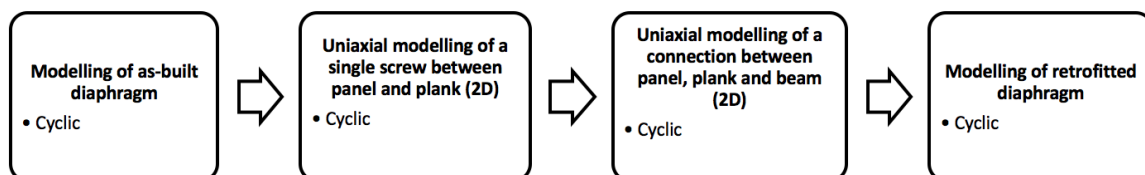
Figure 7-1: Workflow for modelling the retrofitted diaphragm

7.1 UNIAXIAL MODELLING OF A CONNECTION BETWEEN PANEL AND PLANK WITH A SINGLE SCREW

For the modelling of a connection with a single screw between panel and plank, the results of the laboratory tests as presented in chapter 5 are used to calibrate the numerical model. As the laboratory tests were conducted on specimens containing two screws, it is assumed that one screw absorbs half the force in the connection. Half of the average hysteresis and backbone curve of a connection with two screws is deemed to be representative for a single screw. For the modelling of the screws, the same numerical model is used as for the connections within the as-built diaphragm (see section 6.1). This model contains three COMBIN40 elements placed in parallel to model a single screw. The same approach is taken as for the modelling of the nails for the as-built diaphragm. The models of the screws will first be constructed by calibrating the numerical hysteresis curve to match the experimental hysteresis curve. Hereafter, a second model will be constructed for which the numerical

backbone curve conserves the same energy as the experimental backbone curve. This accumulates into two models for each model of a connection, based on two calibration methods.

7.1.1 LOADING PERPENDICULAR TO THE PLANK

For the first calibration approach, the numerical result can be seen in figure 7-2. The corresponding parameters of the COMBIN40 elements are listed in table 7-1. The numerical model is subjected to the same cyclic loading scheme as in the laboratory tests (three load cycles for each amplitude). When looking at the numerical results, one can see that the second and third cycle of the same displacement amplitude conserves far less energy than the first cycle. This is evident when comparing the area under the graph for all three cycles. Furthermore, the peaks of the second and third cycles occur at a lower force than for the first cycle. Thus, it can be concluded that there is a lot of strength and energy loss after the first cycle. When comparing the numerical result to experimental results (see figure 7-3), one can see that the numerical hysteresis roughly matches the experimental hysteresis. The pinching region shows a similar width and slope for both numerical and experimental result. Also, the slopes of the reloading branch for the first loading cycle at each displacement amplitude are comparable. However, for the second and third cycle, the slopes do not show a striking match. This is due to the increasing nonlinearity in experimental results for these successive cycles. For the second and third loading cycles, the numerical reloading stiffnesses are higher than the experimental reloading stiffnesses. But if the numerical reloading stiffnesses were to be reduced, the pinching part and the peaks of the hysteresis would not be captured accurate enough. Thus it is chosen not to do so. The dissimilarities between numerical and experimental hysteresis increase for cycles of higher displacements, as the experimental results exhibit a higher degree of nonlinearity for larger displacements. Such a high form of nonlinearity cannot be modelled properly with the current numerical model. Additionally, the numerical model tends to overestimate the connection strength for the first loading cycles. However, for later loading cycles, the model underestimates the connection strength. Despite the dissimilarities, the numerical model still exhibits accurate behaviour to model a single-screw connection which is loaded perpendicular to the plank. Thus, it is chosen to move forward with this model. The chosen parameters give quite a good estimation of the maximum loads per cycle and capture the pinching behaviour sufficiently accurate. The comparison between numerical and experimental backbone can be seen in figure 7-4. In this graph, the experimental backbone is taken as the mean backbone of all tested specimens. The numerical backbone keeps increasing as it does not implement failure, thus the numerical backbone differs quite a bit from the experimental backbone. The experimental backbone curve conserves less energy and is far more nonlinear as compared to the numerical backbone.

Table 7-1: Parameters for the COMBIN40 elements calibrated on the experimental hysteresis

	K1 (N/mm)	K2 (N/mm)	Fslide (N)	Initial gap (mm)	C (N*s/mm)	M (kg)
COMBIN40 - 1	100.000	2	50	0	0	0
COMBIN40 - 2	300	90	800	0.001	0	0
COMBIN40 - 3	300	90	800	0.001	0	0
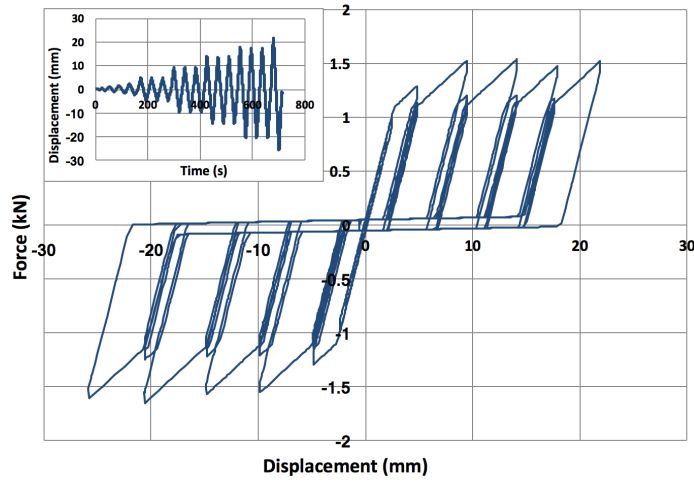
Figure 7-2: Numerical result for loading perpendicular to the plank
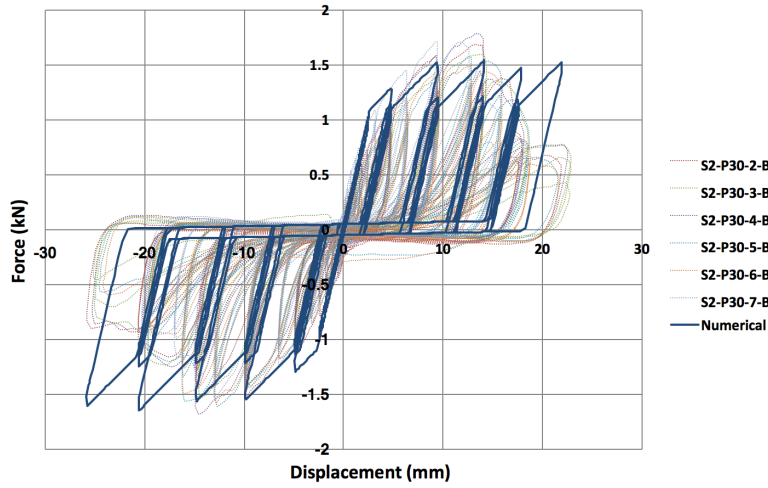
Figure 7-3: Comparison between numerical and experimental result
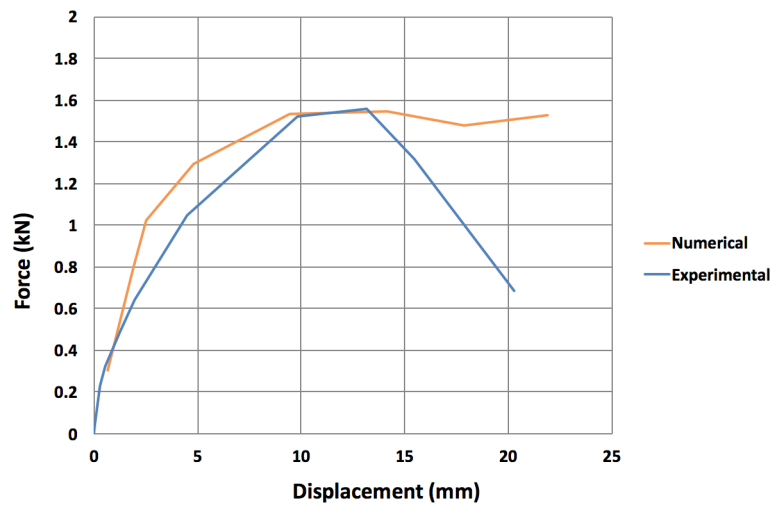
Figure 7-4: Comparison between numerical and experimental backbone

For the second calibration approach, in which the numerical backbone curve is calibrated on the experimental backbone, the parameters for each of the COMBIN40 elements are given in table 7-2. Only the parameters for the second and third COMBIN40 elements are changed. The area under the numerical backbone matches the area under the experimental backbone up to a displacement of 20 mm. The numerical model is subjected to the same cyclic loading scheme as applied in the experimental tests. The numerical result can be seen in figure 7-5. Comparing this approach to the previous approach in which the numerical hysteresis was matched to the experimental hysteresis, one can see that the second stiffness of the reloading branches is very much lower. This results in a lower peak force for each cycle. Furthermore, the maximum force for each successive cycle of the same amplitude is similar. This leads to the conclusion that there is less strength loss after the first loading cycle as compared to the previous calibration approach. The pinching part is the same as for the previous approach. Comparing the numerical result to the experimental result (figure 7-6), one can see that the hysteresis is not captured accurately. The maximum loads per cycle show greater errors and the reloading stiffnesses are far more higher for the numerical results. The comparison between numerical and experimental backbone can be seen in figure 7-7. Both curves conserve the same energy, but the curves do not look alike. The maximum force is lower and the initial stiffness is higher for the numerical backbone.

Table 7-2: Parameters for the COMBIN40 elements calibrated on the preserved energy

	K1 (N/mm)	K2 (N/mm)	Fslide (N)	Initial gap (mm)	C (N*s/mm)	M (kg)
COMBIN40 - 1	100.000	2	50	0	0	0
COMBIN40 - 2	500	0.001	1150	0.001	0	0
COMBIN40 - 3	500	0.001	1150	0.001	0	0
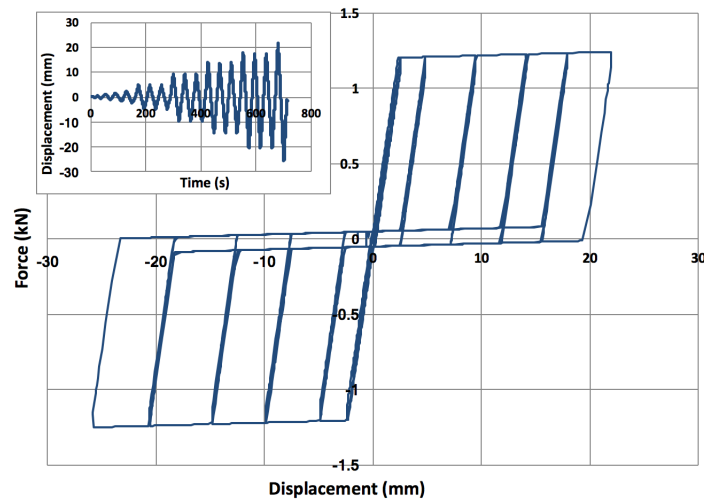
Figure 7-5: Numerical result for loading perpendicular to the plank
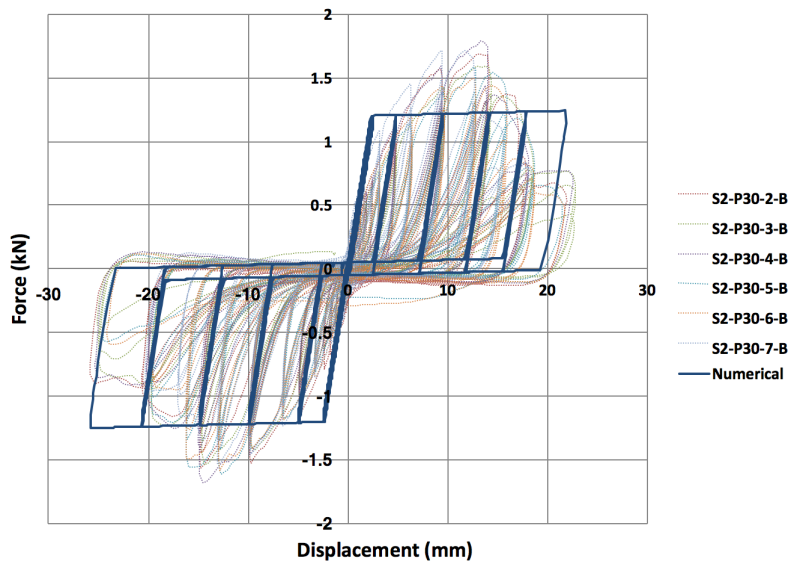
Figure 7-6: Comparison between numerical and experimental result
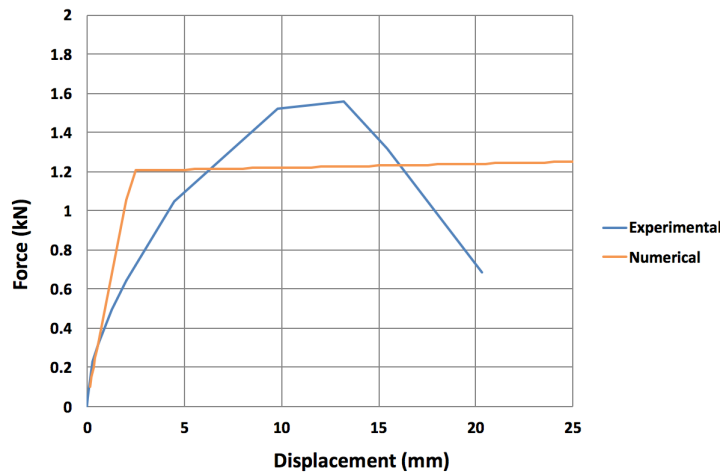
Figure 7-7: Comparison between numerical and experimental backbone

7.1.2 LOADING PARALLEL TO THE PLANK

For a single-screw connection which is loaded parallel to the plank, the numerical result for the first calibration approach can be seen in figure 7-8. The corresponding parameters of the COMBIN40 elements are listed in table 7-3. The numerical model is subjected to the same cyclic loading as in the laboratory tests (three load cycles for each amplitude). When looking at the numerical results, one can see that the second and third cycle of the same displacement amplitude conserves far less energy than the first cycle. This is evident when comparing the area under the graph for all three cycles. Furthermore, the peaks of the second and third cycles occur at a lower force than for the first cycle. Thus, it can be concluded that there is a lot of strength and energy loss after the first cycle. When comparing the numerical result to experimental results (see figure 7-9), one can see that the numerical hysteresis roughly matches the experimental hysteresis. The pinching region shows a similar width and slope for both numerical and experimental result. Also, the slopes of the reloading branch for the first loading cycle at each displacement amplitude are comparable. However, for the second and third cycle, the slopes do not show a striking match. This is due to the increasing nonlinearity in experimental results for these successive cycles. For the second and third loading

cycles, the numerical reloading stiffnesses are higher than the experimental reloading stiffnesses. But if the numerical reloading stiffnesses were to be reduced, the pinching part and the peaks of the hysteresis would not be captured accurate enough. Thus it is chosen not to do so. The dissimilarities between numerical and experimental hysteresis increase for cycles of higher displacements, as the experimental results show greater nonlinearities. Such a high form of nonlinearity cannot be modelled properly with the current numerical model. Additionally, the numerical model tends to overestimate the connection strength for the first loading cycles. However, for later loading cycles, the model underestimates the connection strength. Despite the dissimilarities, the numerical model still exhibits accurate behaviour to model a single-screw connection which is loaded parallel to the plank. Thus, it is chosen to move forward with this model. The chosen parameters give quite a good estimation of the maximum loads per cycle and capture the pinching behaviour sufficiently accurate. The comparison between numerical and experimental backbone can be seen in figure 7-10. In this graph, the experimental backbone is taken as the mean backbone of all tested specimens. The numerical backbone keeps increasing as it does not implement failure, thus the numerical backbone differs quite a bit from the experimental backbone. The experimental backbone curve conserves less energy and is far more nonlinear as compared to the numerical backbone.

Table 7-3: Parameters for the COMBIN40 elements calibrated on the experimental hysteresis

	K1 (N/mm)	K2 (N/mm)	Fslide (N)	Initial gap (mm)	C (N*s/mm)	M (kg)
COMBIN40 - 1	100.000	0.5	70	0	0	0
COMBIN40 - 2	500	80	1000	0.001	0	0
COMBIN40 - 3	500	80	1000	0.001	0	0
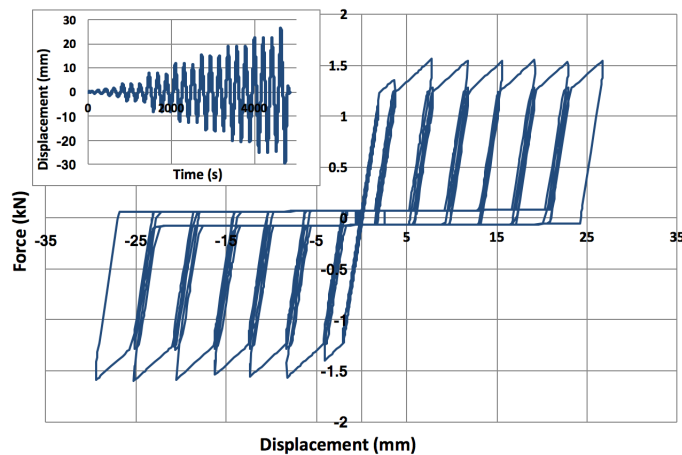
Figure 7-8: Numerical result for loading parallel to the plank
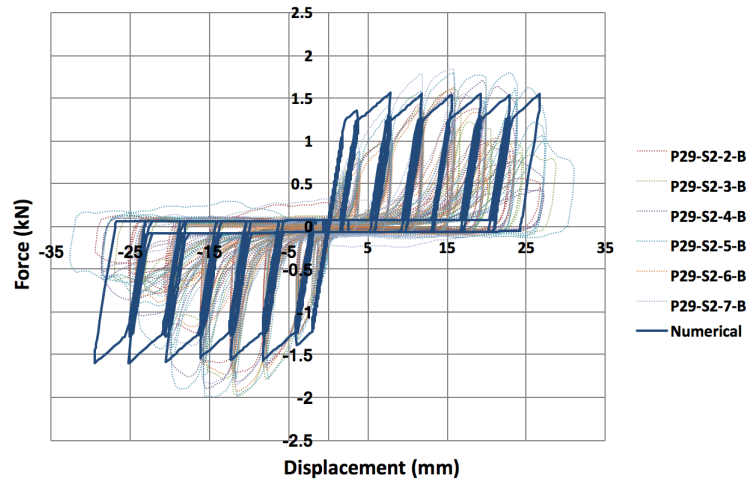
Figure 7-9: Comparison between numerical and experimental result
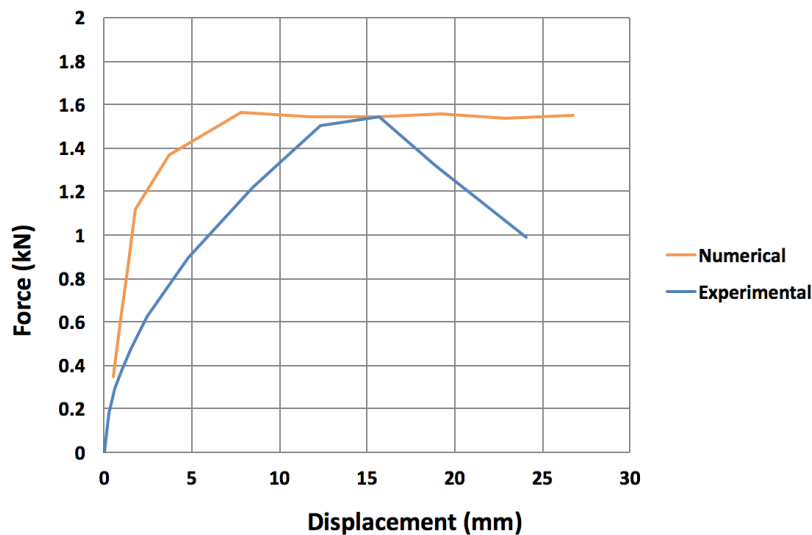
Figure 7-10: Comparison between numerical and experimental backbone

For the second calibration approach, the parameters for each of the COMBIN40 elements are given in table 7-4. Only the parameters for the second and third COMBIN40 elements are changed. The area under the numerical backbone matches the area under the experimental backbone up to a displacement of 24 mm. The numerical model is subjected to the same cyclic loading scheme as applied in the experimental tests. The numerical result can be seen in figure 7-11. Comparing this approach to the previous approach in which the numerical hysteresis was matched to the experimental hysteresis, one can see that the second stiffness of the reloading branches is very much lower. This results in a lower peak force for each cycle. Furthermore, the maximum force for each successive cycle of the same amplitude is similar. This leads to the conclusion that there is less strength loss after the first loading cycle as compared to the previous calibration approach. The pinching part is the same as for the previous approach. Comparing the numerical result to the experimental result (figure 7-12), one can see that the hysteresis is not captured accurately. The maximum loads per cycle show greater errors and the reloading stiffnesses are far more higher for the numerical results. The comparison between numerical and experimental backbone can be seen in figure 7-13. Both curves conserve the same energy, but the curves do not look alike. The maximum force is lower and the initial stiffness is higher for the numerical backbone.

Table 7-4: Parameters for the COMBIN40 elements calibrated on the preserved energy

	K1 (N/mm)	K2 (N/mm)	Fslide (N)	Initial gap (mm)	C (N*s/mm)	M (kg)
COMBIN40 - 1	100.000	0.5	70	0	0	0
COMBIN40 - 2	500	0.001	1100	0.001	0	0
COMBIN40 - 3	500	0.001	1100	0.001	0	0
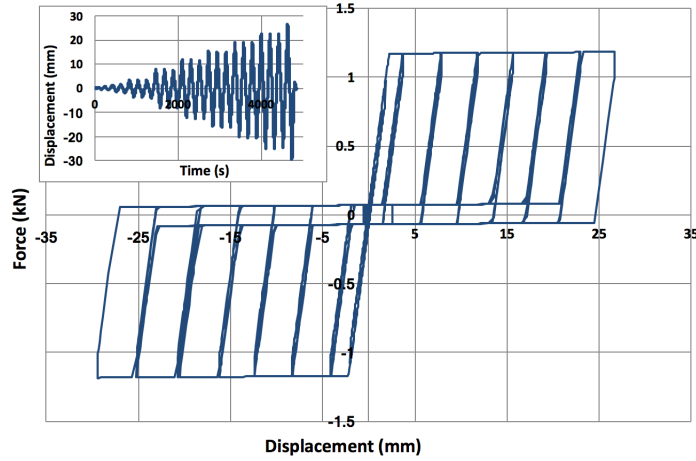
Figure 7-11: Numerical result for loading parallel to the plank
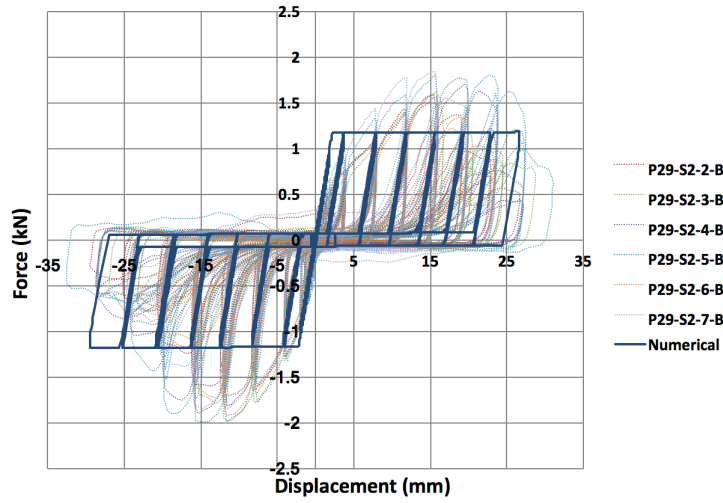
Figure 7-12: Comparison between numerical and experimental result
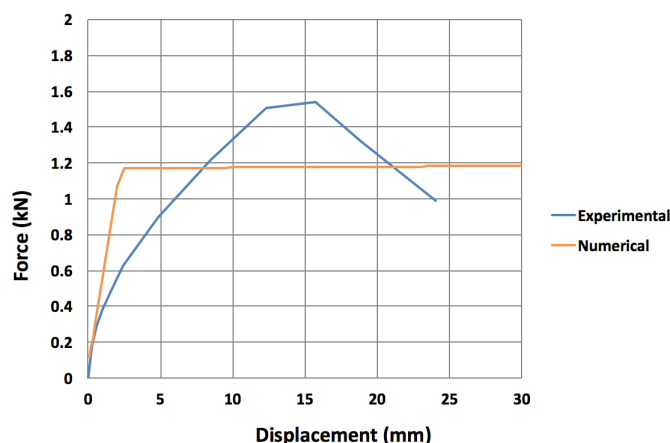
Figure 7-13: Comparison between numerical and experimental backbone

7.2 Uniaxial modelling of a connection between panel, plank and joist

At the top beam of the retrofitted diaphragm, the screws are placed such that it goes through the panel, plank and beam. At each plank, one screw is placed between both nails. These nails are attached only to the plank and beam. Thus, only the screws are attached to all three timber members. This connection at the top beam is tested in the laboratory with specimens containing a segment of a panel, plank and beam connected by one screw and two nails. As this connection is more complex and it is not clear what the contribution of each nail or screw is to the entirety of the connection, it is chosen to model this connection in its entirety. This means that in both in-plane directions, three COMBIN40 elements will be used to model the two nails and screw in its whole. For the modelling of this connection, the results of the laboratory tests as presented in chapter 5 are used to calibrate the numerical model. The same approach is taken as for the modelling of the nails for the as-built diaphragm. The models of the connections will first be constructed by calibrating the numerical hysteresis curve to match the experimental hysteresis curve. Hereafter, a second model will be constructed for which the numerical backbone curve conserves the same energy as the experimental backbone curve. This accumulates into two models for each model of a connection, based on two calibration methods.

7.2.1 Loading parallel to the joist

For loading parallel to the joist, the numerical result for the first calibration approach can be seen in figure 7-14. The corresponding parameters of the COMBIN40 elements are listed in table 7-5. The numerical model is subjected to the same cyclic loading scheme as in the laboratory tests (three load cycles for each amplitude). From the numerical results, it can be seen that there is a significant strength loss for the second and third cycle of the same amplitude. These cycles conserve less energy than the first cycle. Comparing the numerical result to experimental results (see figure 7-15), one can see that the numerical hysteresis roughly matches the experimental hysteresis. The pinching region shows a similar width and slope for both numerical and experimental result. The maximum force for the first loading cycle of each amplitude is also similar for both results. The numerical results show greater discrepancies for larger displacements, as the experimental results showcase more nonlinearities. These nonlinearities cannot be fully accounted for in the numerical model. Nevertheless, the numerical model still provides an accurate representation and is deemed sufficient to model the connection. The chosen parameters give quite a good estimation of the maximum loads per cycle and capture the pinching behaviour sufficiently accurate. The comparison

between numerical and experimental backbone can be seen in figure 7-16. In this graph, the experimental backbone is taken as the mean backbone of all tested specimens. The numerical backbone keeps increasing as it does not implement failure, thus the numerical backbone differs very much from the experimental backbone. The experimental backbone curve conserves less energy and is far more nonlinear as compared to the numerical backbone.

Table 7-5: Parameters for the COMBIN40 elements calibrated on the experimental hysteresis

	K1 (N/mm)	K2 (N/mm)	Fslide (N)	Initial gap (mm)	C (N*s/mm)	M (kg)
COMBIN40 - 1	100.000	3	250	0	0	0
COMBIN40 - 2	400	250	800	0.001	0	0
COMBIN40 - 3	400	250	800	0.001	0	0
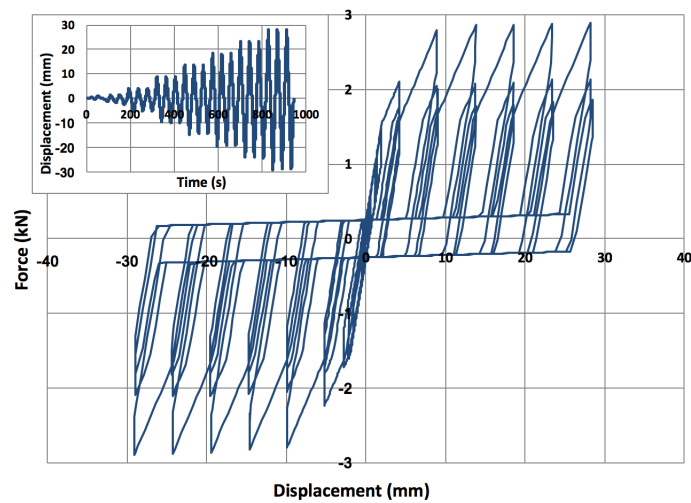
Figure 7-14: Numerical result for loading parallel to the joist
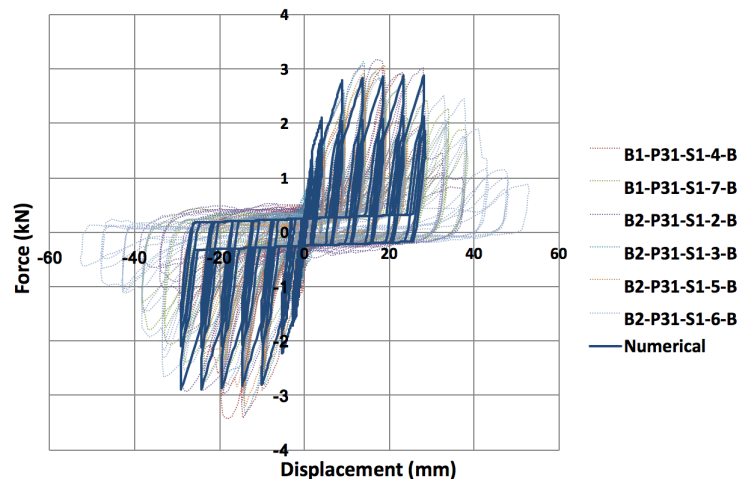
Figure 7-15: Comparison between numerical and experimental result
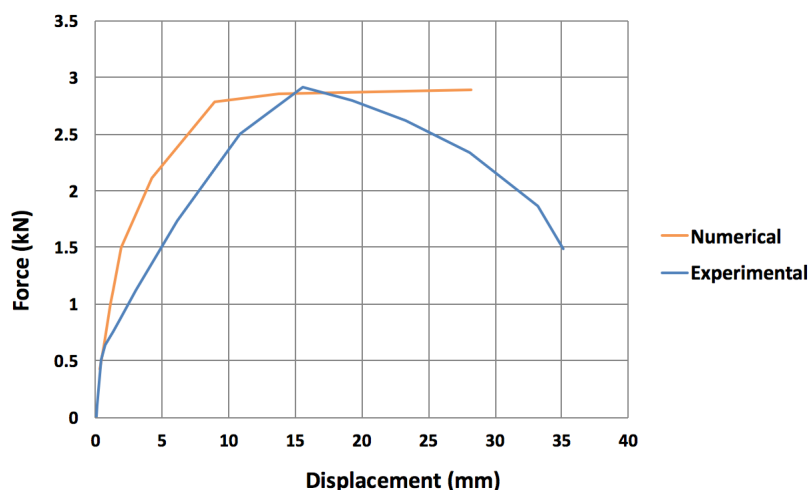
Figure 7-16: Comparison between numerical and experimental backbone

For the second calibration approach, in which the numerical backbone curve is calibrated on the experimental backbone, the parameters for each of the COMBIN40 elements are given in table 7-6. Only the parameters for the second and third COMBIN40 elements are modified. The area under the numerical backbone matches the area under the experimental backbone up to a displacement of 35 mm. The numerical model is subjected to the same cyclic loading scheme as applied in the experimental tests. The numerical result can be seen in figure 7-17. Comparing this approach to the previous approach in which the numerical hysteresis was matched to the experimental hysteresis, one can see that the second stiffness of the reloading branches is very much lower. This results in a lower peak force for each cycle. Furthermore, the maximum force for each successive cycle of the same amplitude is similar. This leads to the conclusion that there is less strength loss after the first loading cycle as compared to the previous calibration approach. The pinching part is the same as for the previous approach. Comparing the numerical result to the experimental result (figure 7-18), one can see that the hysteresis is not captured accurately. The maximum loads per cycle show greater errors and the reloading stiffnesses are far more higher for the numerical results. For the first cycles, the numerical model greatly overestimates the maximum strength. For later cycles, the strength is underestimated. The comparison between numerical and experimental backbone can be seen in figure 7-19. Both curves conserve the same energy, but the curves do not look alike. The initial stiffness for very small displacements is similar, but the maximum force is lower for the numerical backbone.

Table 7-6: Parameters for the COMBIN40 elements calibrated on the preserved energy

	K1 (N/mm)	K2 (N/mm)	Fslide (N)	Initial gap (mm)	C (N*s/mm)	M (kg)
COMBIN40 - 1	100.000	3	250	0	0	0
COMBIN40 - 2	800	0.01	1950	0.001	0	0
COMBIN40 - 3	800	0.01	1950	0.001	0	0
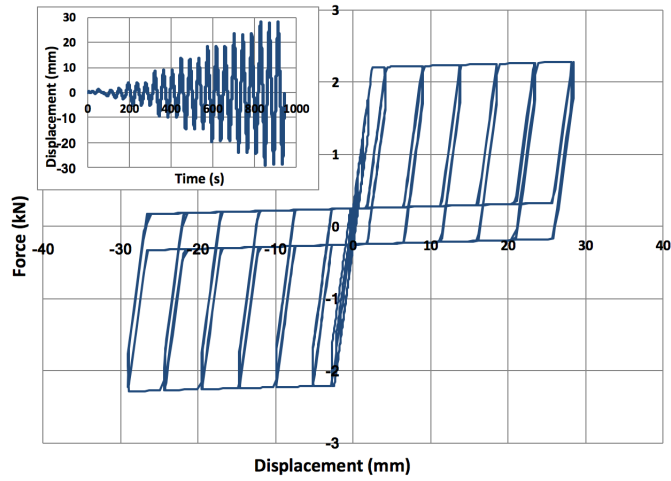
Figure 7-17: Numerical result for loading parallel to the joist
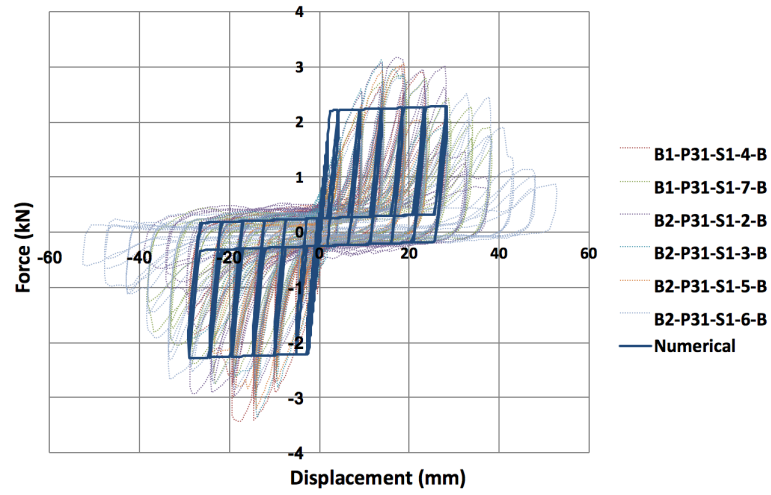
Figure 7-18: Comparison between numerical and experimental result
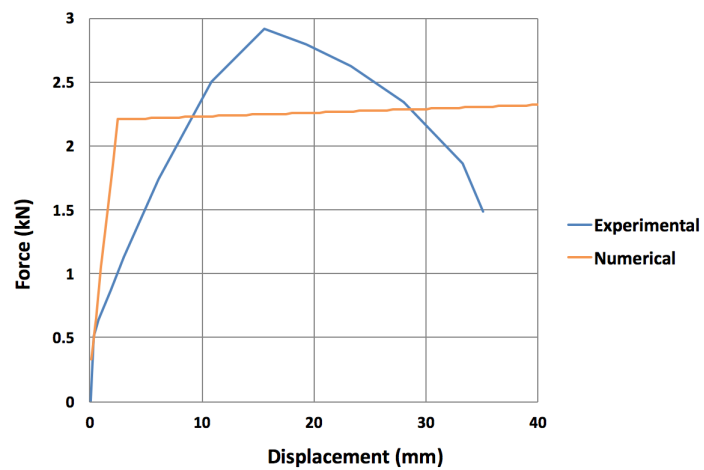
Figure 7-19: Comparison between numerical and experimental backbone

7.2.2 Loading perpendicular to the joist

For loading perpendicular to the joist, the numerical result for the first calibration approach can be seen in figure 7-20. The corresponding parameters of the COMBIN40 elements are listed in table 7-7. The numerical model is subjected to the same cyclic loading as in the laboratory tests (three load cycles for each amplitude). From the numerical results, it can be seen that there is a strength loss for the second and third cycle of the same amplitude. These cycles conserve less energy than the first cycle. Comparing the numerical result to experimental results (see figure 7-21), it can be seen that the pinching region shows a similar width and slope for both numerical and experimental result. However, the peaks are not modelled with the same degree of accuracy. From the graphs, one can see that the strength is underestimated for cycles with a displacement from approximately 5 mm. The numerical results show greater discrepancies for larger displacements, as the experimental results showcase more nonlinearities for greater displacements. These nonlinearities cannot be fully accounted for in the numerical model. Nevertheless, the numerical model still provides a sufficient representation. The comparison between numerical and experimental backbone can be seen in figure 7-22. In this graph, the experimental backbone is taken as the mean backbone of all tested specimens. The numerical backbone keeps increasing as it does not implement failure, thus the numerical backbone differs very much from the experimental backbone. The experimental backbone curve conserves less energy and is far more nonlinear as compared to the numerical backbone.

Table 7-7: Parameters for the COMBIN40 elements calibrated on the experimental hysteresis

	K1 (N/mm)	K2 (N/mm)	Fslide (N)	Initial gap (mm)	C (N*s/mm)	M (kg)
COMBIN40 - 1	100.000	3	250	0	0	0
COMBIN40 - 2	600	250	1300	0.001	0	0
COMBIN40 - 3	600	250	1300	0.001	0	0
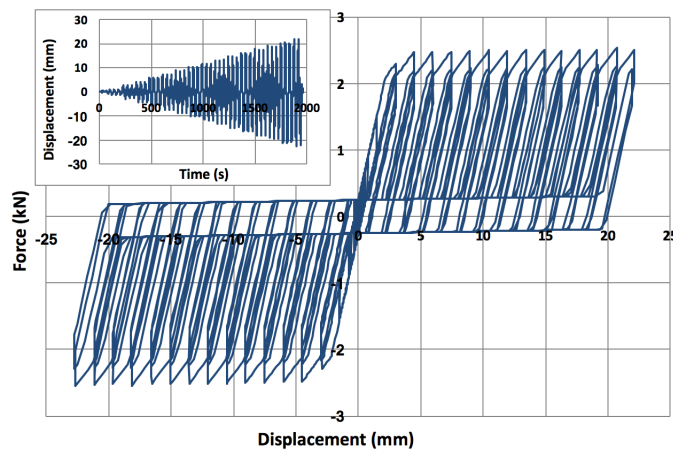
Figure 7-20: Numerical result for loading perpendicular to the joist
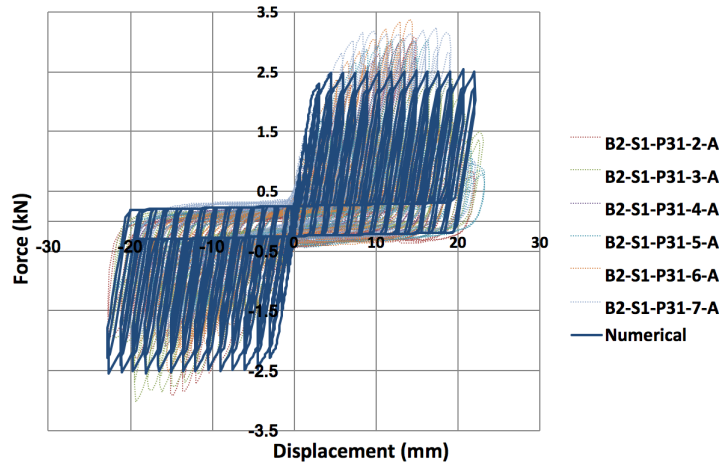
Figure 7-21: Comparison between numerical and experimental result
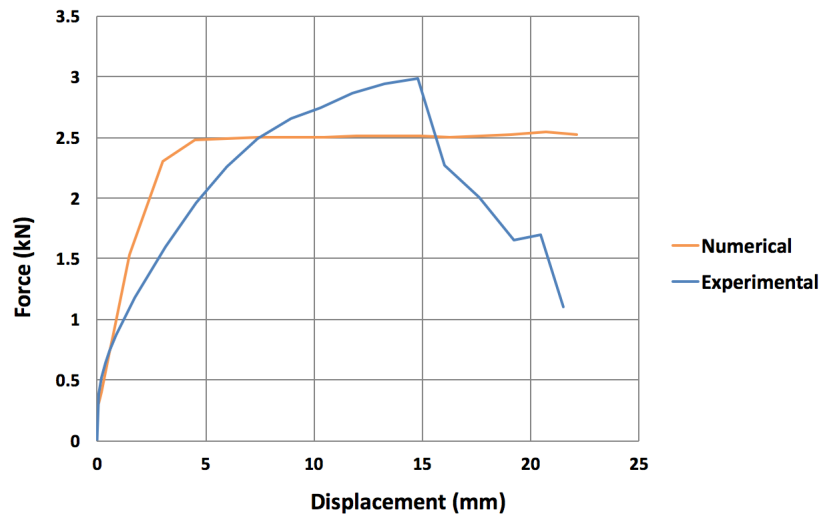
Figure 7-22: Comparison between numerical and experimental backbone

For the second approach, in which the numerical backbone curve is calibrated on the experimental backbone, the parameters for each of the COMBIN40 elements are given in table 7-8. The area under the numerical backbone matches the area under the experimental backbone up to a displacement of 21 mm. The numerical model is subjected to the same cyclic loading scheme as applied in the experimental tests. The numerical result can be seen in figure 7-23. Comparing this approach to the previous approach in which the numerical hysteresis was matched to the experimental hysteresis, one can see that the second stiffness of the reloading branches is very much lower. This results in a lower peak force for each cycle. Furthermore, the maximum force for each successive cycle of the same amplitude is similar. This leads to the conclusion that there is less strength loss after the first loading cycle as compared to the previous calibration approach. The pinching part is the same as for the previous approach. Comparing the numerical result to the experimental result (figure 7-24), one can see that the hysteresis is not captured accurately. The maximum loads per cycle show greater errors and the reloading stiffnesses are far more higher for the numerical results. For the first cycles, the numerical model greatly overestimates the maximum strength. For later cycles, the strength is underestimated. The comparison between numerical and experimental backbone can be seen in figure 7-25. Both curves conserve the same energy, but the curves do not look alike. The maximum force is lower for the numerical backbone as opposed to the experimental backbone.

Table 7-8: Parameters for the COMBIN40 elements calibrated on the preserved energy

	K1 (N/mm)	K2 (N/mm)	Fslide (N)	Initial gap (mm)	C (N*s/mm)	M (kg)
COMBIN40 - 1	100.000	3	250	0	0	0
COMBIN40 - 2	1000	0.01	2000	0.001	0	0
COMBIN40 - 3	1000	0.01	2000	0.001	0	0
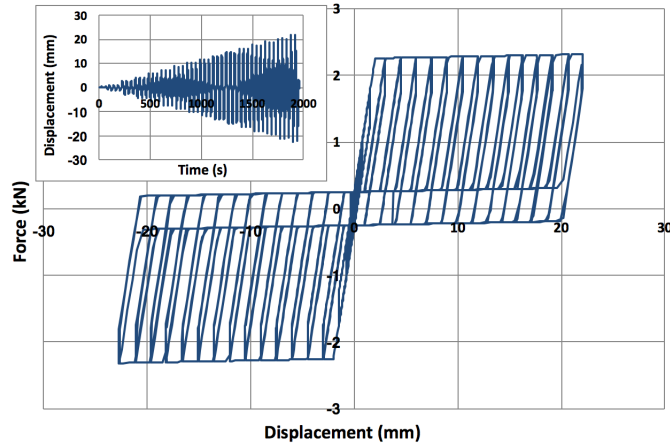
Figure 7-23: Numerical result for loading perpendicular to the joist
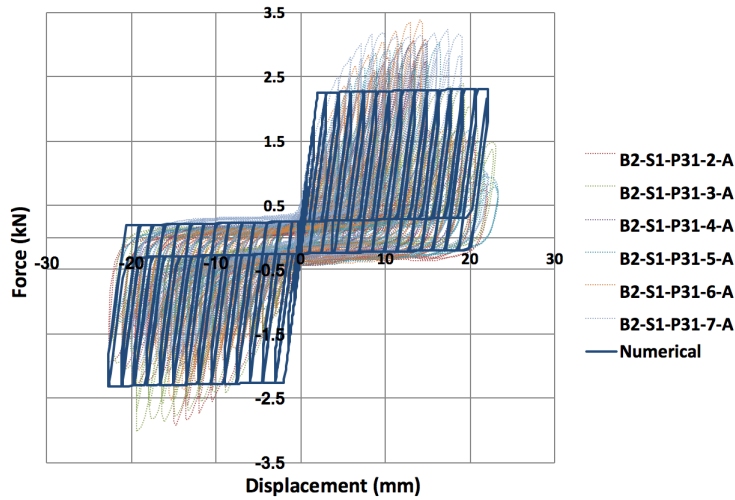
Figure 7-24: Comparison between numerical and experimental result
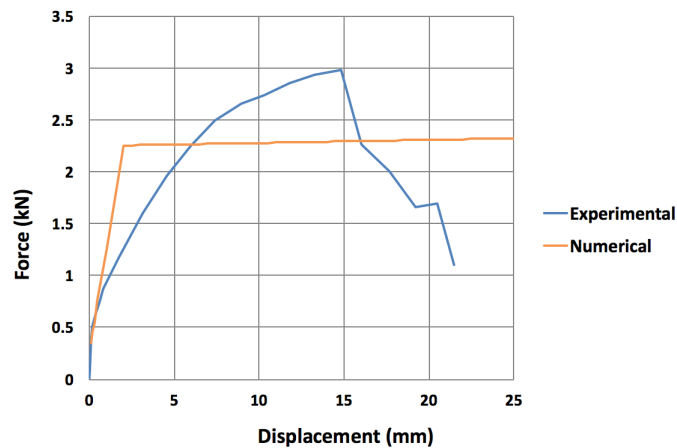
Figure 7-25: Comparison between numerical and experimental backbone

7.3 CYCLIC MODELLING OF THE RETROFITTED DIAPHRAGM

For the modelling of the retrofitted diaphragm, the model of the as-built diaphragm is extended. With the previously discussed models for the screws, the model of the retrofitted diaphragm can be constructed. This model is scripted in ANSYS Mechanical APDL 18.2, similar to the model for the as-built diaphragm. The as-built model is kept the same as much as possible, meaning that boundary conditions and material parameters are left unaltered and are only changed or added where needed. This is done in order to closely represent the laboratory tests. The script for the retrofitted diaphragm is annexed in appendix H.

GEOMETRY

The numerical model of the retrofitted diaphragm is modelled such that it closely represents the experimentally tested diaphragm. The model can be divided into five components: the panels, the planks, the beams, the nails and the screws. Two types of screws can be distinguished: screws between panel and plank, and screws between panel, plank and beam. The diaphragm consists of 15 plywood panels, 23 timber planks and 4 timber beams. At each beam-plank intersection, a pair of nails is placed with a spacing of 100 mm. These nails have a length of 64.2 mm and a diameter of 3.0 mm. Along the perimeter of each panel, screws are placed with a spacing of approximately 100 mm. The screws have a diameter of 4.5 mm and a length of 40 mm. At the top joist, where the screws were connected to panel, plank and joist, the screws have a diameter of 5.0 mm and a length of 70 mm. The 15 panels are placed irregularly on the planks, such that they can transmit forces onto each other. When looking at the front view of the diaphragm (figure 5-31), a total of six columns of panels can be seen. The odd-numbered columns contain two panels, whereas the even-numbered columns contain three panels. Thus, the length of the panels depend on their position in the diaphragm. These lengths can be either 1200, 1100, 600 or 500 mm. The width of the panels in the first and last column is 590 mm. For the other columns, the width of the panels is 670 mm. Each panel has a thickness of 18 mm. The 23 timber planks have a thickness of 18 mm, a width of 165 mm and a length of 2680 mm. The spacing between each plank is 2 mm, meaning that the centre-to-centre distance of each plank is 167 mm. Perpendicular to the direction of the planks, 4 timber beams are placed with a width of 60 mm, a height of 130 mm and a length of 1870 mm. The centre-to-centre distance of each beam is 650 mm. For a summary of the dimensions of the retrofitted diaphragm, refer to table 7-9. The coordinate system for the diaphragm is defined as follows: the x-axis runs along the length of the planks, the y-axis is placed along the length of the beams and the z-axis is the out-of-plane axis perpendicular to the beams and planks.

MATERIAL PROPERTIES

For the modelling of the retrofitted diaphragm, it is assumed that the nails and screws are the only source of nonlinearity. Furthermore, the effects of friction between planks, between panels and between panel and plank are neglected. The timber members are given orthotropic linear elastic material properties ($E_x, E_y, E_z, G_{xy}, G_{yz}, G_{xz}, \nu_{xy}, \nu_{yz}, \nu_{xz}$). For the beams and planks, the Young's modulus along the grain of the timber members was measured in the laboratory of the TU Delft and is adopted for the numerical model. The Young's moduli in other directions and the shear moduli can be determined from the measured Young's modulus using empirical relations from the Wood Handbook [38]. The Poisson's ratios are also taken from the Wood Handbook. The material properties for the beams and planks as used for the numerical model are annexed in appendix E. For the panels, a Young's modulus of 7500 N/mm^2, a shear modulus of 430 N/mm^2 and a Poisson's ratio of 0.3 is adopted in all directions.

ELEMENTS

As the retrofitted diaphragm is a more complex problem as opposed to the as-built diaphragm, ANSYS requires the user to address contact problems which can occur. Therefore, it is necessary to add an extra element to prevent the panels from moving into each other. This element can also prevent the planks from moving into each other. Thus, a total of four elements are used to model the retrofitted diaphragm. For the beams, linear beam element BEAM188 is used. For the panels and planks, linear shell element SHELL181 is used. The nailed and screwed connections are modelled with nonlinear COMBIN40 elements. As the connections in the top beam have been modelled as a connection with two nails and a screw (see section 7.2), the nails are not modelled separately at this location. This means that the COMBIN40 elements are placed in the middle of each plank at the top beam, modelling both the two nails which connects the plank and beam, as well as the screw which connects the panel, plank and beam. The contact problem between panels (and planks) is modelled using CONTA178 elements. This is a two-noded contact element with a damper and a gap element, which controls the contact and sliding between the two nodes. As it is chosen not to implement friction, the sliding is neglected in this element (no friction resistance). Thus, only the contact (opening and closing of gap between members) is modelled using this element in the model for the retrofitted diaphragm. There are three translational degrees of freedom at both nodes of the contact element. The contact algorithm is set to Augmented Lagrange Method, which means that the user can define a contact normal stiffness, a maximum allowable penetration, a sliding stiffness and a maximum allowable slip. The contact behaviour is set to standard, meaning that the normal pressure is zero when the gap is open. For the CONTA178 elements, the normal stiffness K_n is set to 10.000 N/mm^2 and the sliding stiffness K_s is set to 0.001 N/mm^2. The maximum allowable penetration is 0.01 mm and the maximum amount of sliding is defined as 200 mm. The initial gap size is 2 mm and is initially set to 'open', meaning that there is no contact initially. A summary of the used elements can be seen in table 7-10, along with a schematisation of the elements in figure 7-26.

Table 7-9: Dimensions of retrofitted diaphragm

	Width (mm)	Height (mm)	Length (mm)	Thickness (mm)	Centre-to-centre distance (mm)
Panels	590 or 670	18	1200, 1100, 600 or 500	-	-
Joists	60	130	3870	-	650
Planks	165	18	2680	-	167
Nails	-	-	64.2	3.0	100
Screws	-	-	40 or 70	4.5 or 5.0	100
Specimen	-	2680	3870	-	-

Table 7-10: Elements for the members

Member	Element	Number of nodes	Element behaviour	Degrees of freedom per node	Material input parameters
Joists	BEAM188 (Line element)	2	Linear	6	E_x, E_y, E_z G_{xy}, G_{yz}, G_{xz} ν_{xy}, ν_{yz}, ν_{xz}
Planks	SHELL181 (Shell element)	4	Linear	6	E_x, E_y, E_z G_{xy}, G_{yz}, G_{xz} ν_{xy}, ν_{yz}, ν_{xz}
Panels	SHELL181 (Shell element)	4	Linear	6	E_x, E_y, E_z G_{xy}, G_{yz}, G_{xz} ν_{xy}, ν_{yz}, ν_{xz}
Nails	COMBIN40 (Line element)	2	Nonlinear	1	K_1, K_2, F_{slide}, initial gap, C, M
Screws	COMBIN40 (Line element)	2	Nonlinear	1	K_1, K_2, F_{slide}, initial gap, C, M
Contact regions	CONTA178 (Line element)	2	Nonlinear	3	K_n, K_s, initial gap, initial gap status, max penetration max slip

a) Element BEAM188

b) Element SHELL181

c) Element COMBIN40

d) Element CONTA178
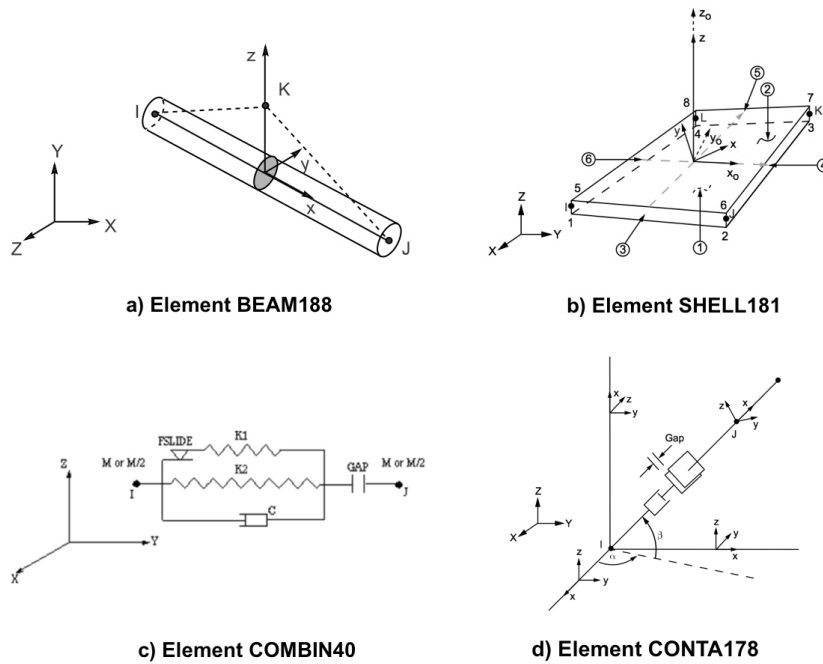
Figure 7-26: Schematisations of used elements [26]

Meshing

It is of importance to properly mesh the model for the retrofitted diaphragm. As there are many two-noded connections with specific locations, the nodes must be placed such that they coincide and their locations must be sufficiently accurate. For the beams, the nodes are placed such that there is a node at each location for the nails, a node positioned in the middle of the planks and a node between each plank. Node positions on the beam are irregular, thus the beam element size can be either 32.5 or 50 mm. For the x-direction of the planks, nodes must be placed at the height of the beams. Between the beams, the plank element size in x-direction is 20, 30 or 50 mm. In y-direction, the nodes on the plank must be positioned at the edges of the plank and at the positions of the nails and screws. This makes for an element size of 32.5 or 25 mm in y-direction for the planks. The panels are meshed in a similar manner as the planks. In x-direction, the panel element size is either 20, 30 or 50 mm. In y-direction, the panel element size can be either 32.5 or 25 mm. Regarding all elements, the maximum element size in the mesh is 50 mm. A total of 372 BEAM188 elements are used for the beams, 33603 SHELL181 elements for the planks and panels, 3294 COMBIN40 elements for the nails and screws and 3660 CONTA178 for the contact regions. The model contains a total of 40929 elements. The mesh can be seen in figure 7-27 and figure 7-28. The positioning of the nails and screws can be seen in figure 7-29. The mesh is a rather fine mesh, this was necessary in order to position the nodes at the correct locations for the nailed and screwed connections.

Boundary conditions

The boundary conditions are chosen such that the numerical model represents the laboratory test. The upper edge of the diaphragm is constraint against rotations about the x-axis and against translations in z-direction. These constraints are applied at the top nodes of the planks and panels (near the loaded beam). The lower edge of the diaphragm is clamped, meaning that the bottom nodes of the planks are constrained against all degrees of freedom. All nodes of the beams are constraint against translations in z-direction and rotations about the y-axis. This is to prevent rigid body motions of the beams. The panels are constraint against translations in z-direction to simplify the problem. The boundary conditions can be seen in figure 7-30. In this figure, the constraints in z-direction on the panels have been left out to maintain clarity.

Loading

The same cyclic loading scheme as used in the laboratory test is applied to the numerical model. This loading scheme imposes three cycles for each displacement amplitude. The loading is displacement controlled and is applied at the nodes along the length of the top beam. Gravitational loads are neglected as these are assumed to have little effects on the response of the diaphragm.

Analysis settings

As the laboratory test was quasi-static, it is chosen to use a static structural analysis in ANSYS 18.2. This analysis type is deemed suitable, as inertial effects can be neglected for a quasi-static test. Due to the nailed and screwed connections, the static analysis is nonlinear. For this analysis type, the default analysis method in ANSYS 18.2 is full Newton-Raphson. To properly solve the implemented nonlinearities, an iterative solver is used. For a better convergence of a nonlinear analysis, it is of importance that the loading is applied gradually. This can be done by ramping the loads and by increasing the number of substeps. The analysis settings are summarised in table 7-11.

Analyses

A total of two analyses are carried out for the retrofitted diaphragm. The first analysis considers the first calibration method for the nails and screws, whereas the second analysis considers the second calibration method for the nails and screws. For the first calibration method, the numerical hysteresis of the nails and screws is calibrated to match the experimental hysteresis. In the second calibration method, the numerical backbone of the nails and screws is calibrated such that the

conserved energy is the same as found experimentally. A summary of the analyses can be seen in figure 7-31.
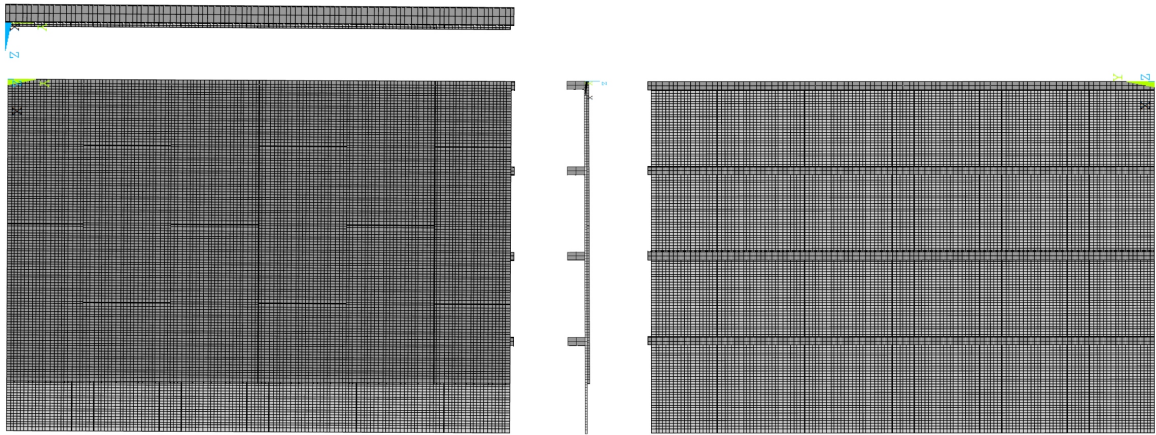
Figure 7-27: Front and back view of retrofitted diaphragm, along with top and side views
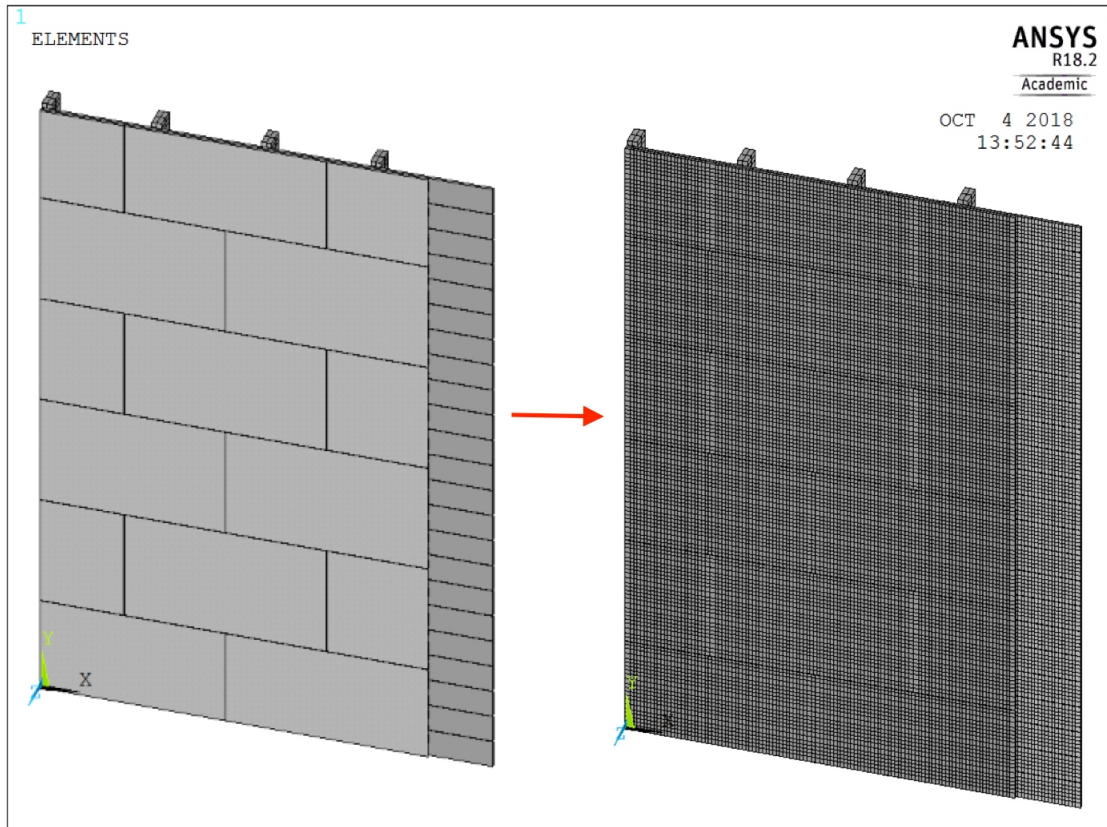
Figure 7-28: 3D view of retrofitted diaphragm

(a) Positioning of nails

(b) Positioning of screws
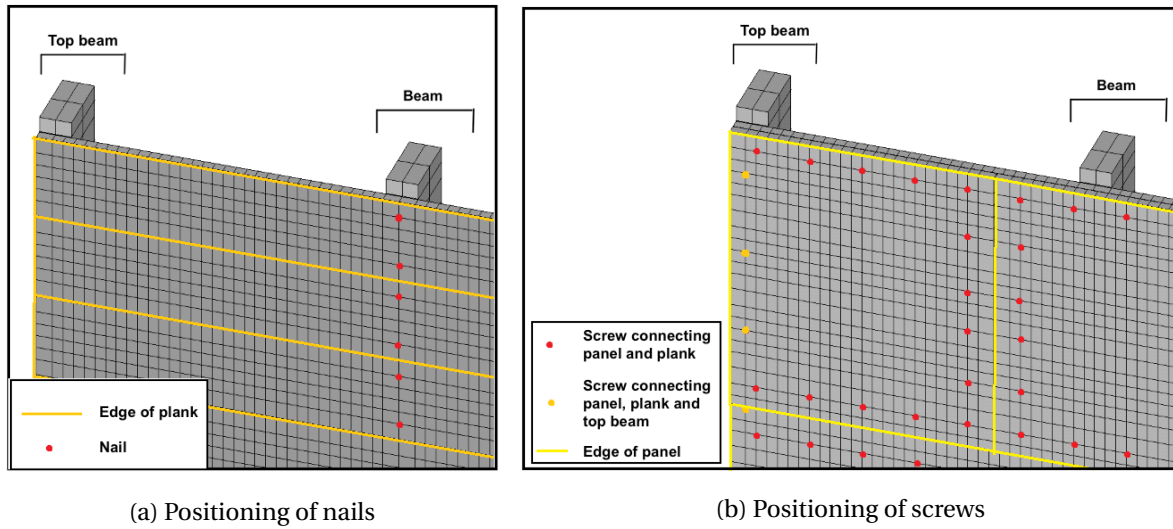
Figure 7-29: Positioning of nails and screws in retrofitted diaphragm
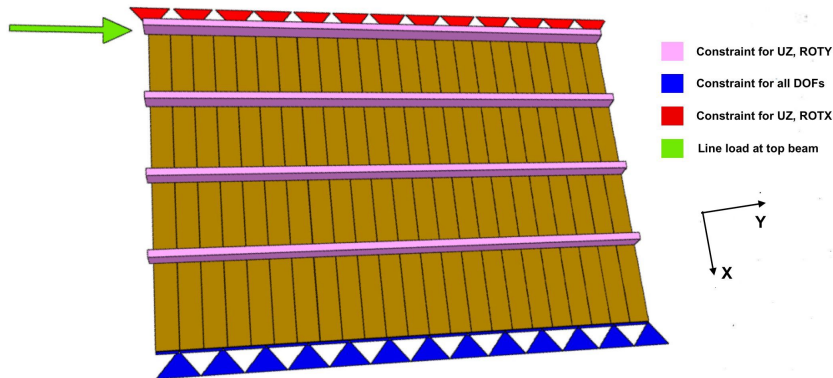
Figure 7-30: Boundary conditions

Table 7-11: Analysis settings

Analysis type	Static nonlinear
Analysis method	Full Newton-Raphson
Solver type	Iterative
Loading	Displacement controlled
Load step size	0.5 s
Load stepping method	Ramped loads
Maximum number of substeps	30 000
Maximum number of iterations	2 000
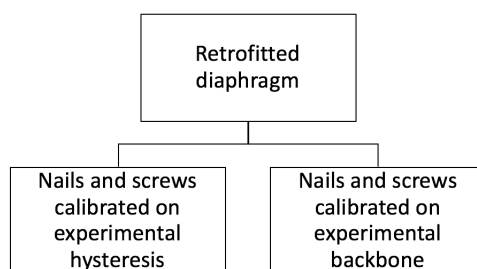
Figure 7-31: Numerical analyses for the retrofitted diaphragm

7.3.1 FIRST CALIBRATION METHOD

For the first analysis, in which the numerical hysteresis of the nailed and screwed connections is calibrated on the experimental hysteresis, the parameters for the nailed and screwed connections are listed in table 7-12, table 7-13 and table 7-14. The result of the numerical analysis (along with its loading scheme) can be seen in figure 7-32. A comparison with the experimental result can be seen in figure 7-33 and figure 7-34. The numerical result of the retrofitted diaphragm exhibits far more nonlinear behaviour as opposed to the as-built diaphragm. This is due to the accumulation of the nonlinear responses of all nailed and screwed connections in the retrofitted diaphragm. Comparing the result to the experimental result, one can see similarities as well as differences. The maximum peak load per cycle is best approximated in the first few cycles. After a displacement of about 30 mm, the peak loads start to differ increasingly, with a maximum error of approximately 30% at a displacement of 55 mm. The error decreases again when the failure mechanism is initiated for the experimental result. The numerical result does not implement failure, thus the experimental and numerical result move closer again near the end of the loading. When looking at the pinching region, it can be said that the numerical slope is too low as opposed to the experimental result. Furthermore, the width of the pinching region is bigger for the numerical result. Regarding the peaks, one can see that the slopes of the un- and reloading branches are lower for the numerically calculated results. The path of the peaks do not match the experimental path. Overall, the numerical model provides a fairly sufficient approximation to predict the peak loads. However, the local behaviour such as the slopes and conserved energy are a less sufficient approximation.

Table 7-12: Parameters for the COMBIN40 elements of the nailed connections, calibrated on the experimental hysteresis

Loading perpendicular to joist						
	K1 (N/mm)	K2 (N/mm)	Fslide (N)	Initial gap (mm)	C (N*s/mm)	M (kg)
COMBIN40 - 1	10.000	4.22	192	0	0	0
COMBIN40 - 2	250	50	450	0.001	0	0
COMBIN40 - 3	250	50	450	0.001	0	0
Loading parallel to joist						
	K1 (N/mm)	K2 (N/mm)	Fslide (N)	Initial gap (mm)	C (N*s/mm)	M (kg)
COMBIN40 - 1	10.000	2.5	145	0	0	0
COMBIN40 - 2	210	45	700	0.001	0	0
COMBIN40 - 3	210	45	700	0.001	0	0

Table 7-13: Parameters for the COMBIN40 elements of the screwed connections between panel and plank, calibrated on the experimental hysteresis

	Loading perpendicular to plank					
	K1 (N/mm)	K2 (N/mm)	Fslide (N)	Initial gap (mm)	C (N*s/mm)	M (kg)
COMBIN40 - 1	10.000	2	50	0	0	0
COMBIN40 - 2	300	90	800	0.001	0	0
COMBIN40 - 3	300	90	800	0.001	0	0
	Loading parallel to plank					
	K1 (N/mm)	K2 (N/mm)	Fslide (N)	Initial gap (mm)	C (N*s/mm)	M (kg)
COMBIN40 - 1	10.000	0.5	70	0	0	0
COMBIN40 - 2	500	80	1000	0.001	0	0
COMBIN40 - 3	500	80	1000	0.001	0	0

Table 7-14: Parameters for the COMBIN40 elements of the screwed connections between panel, plank and beam, calibrated on the experimental hysteresis

	Loading parallel to joist					
	K1 (N/mm)	K2 (N/mm)	Fslide (N)	Initial gap (mm)	C (N*s/mm)	M (kg)
COMBIN40 - 1	10.000	3	250	0	0	0
COMBIN40 - 2	400	250	800	0.001	0	0
COMBIN40 - 3	400	250	800	0.001	0	0
	Loading perpendicular to joist					
	K1 (N/mm)	K2 (N/mm)	Fslide (N)	Initial gap (mm)	C (N*s/mm)	M (kg)
COMBIN40 - 1	10.000	3	250	0	0	0
COMBIN40 - 2	600	250	1300	0.001	0	0
COMBIN40 - 3	600	250	1300	0.001	0	0

Figure 7-32: Numerical result for retrofitted diaphragm
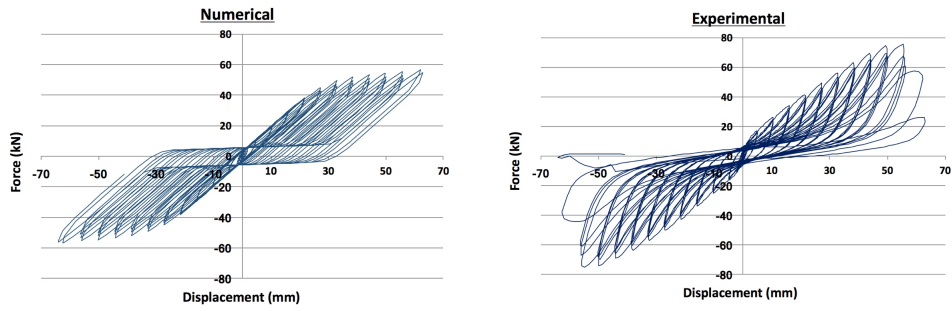
Figure 7-33: Comparison between numerical and experimental result for retrofitted diaphragm
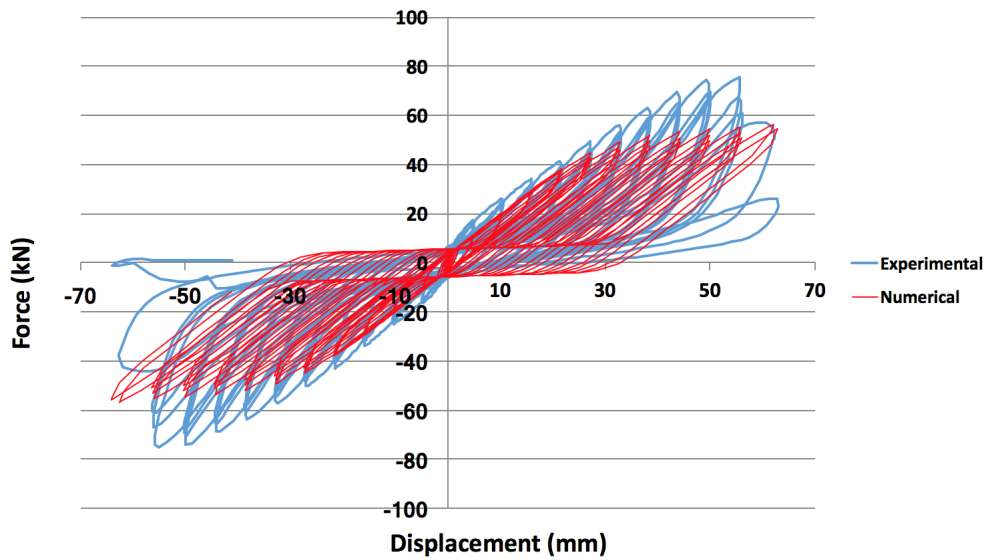
Figure 7-34: Comparison between numerical and experimental result for retrofitted diaphragm

As the numerical result differs from the experimental result (bigger errors as compared to the as-built model), it is chosen to look at the behaviour of a connection within the retrofitted diaphragm. This is done to check whether the connections still exhibit correct behaviour when implemented in a diaphragm. For this purpose, the connection between panel, plank and beam at the upper left corner (at the top loaded beam) is considered. The response of the connection as extracted from the retrofitted diaphragm and as modelled in subsection 7.2.1 can be seen in figure 7-35 for y-direction. As the connection is implemented in a floor that is cyclically loaded, the local displacements of the connection are not the same as for the whole diaphragm. The connection within the diaphragm is no longer loaded such that each displacement is loaded in three cycles. For the result which is extracted from the diaphragm, loading cycles increase more gradually in displacement as opposed to the loading scheme from the model of the connection only. This results in peaks that are closer to each other in displacement. The maximum peaks are lower for the connection in the diaphragm, which may be caused by the higher proximity of the peaks. As the peaks are nearer to each other, it is more likely that a consecutive peak is still affected by the damage caused by the previous peak. Hence, the peaks give lower maximum forces. Some cycles of both graphs are coinciding, these cycles show similar paths. Considering the behaviour of both the connection in a diaphragm and the connection on its own, it can be concluded that they still exhibit similar results and that the connection within the diaphragm accurately represents the modelled behaviour of the connection on its own. As a similar result is expected for the second calibration method, the zoom-in on a connection to verify numerical results is neglected for the second calibration method (section hereafter).
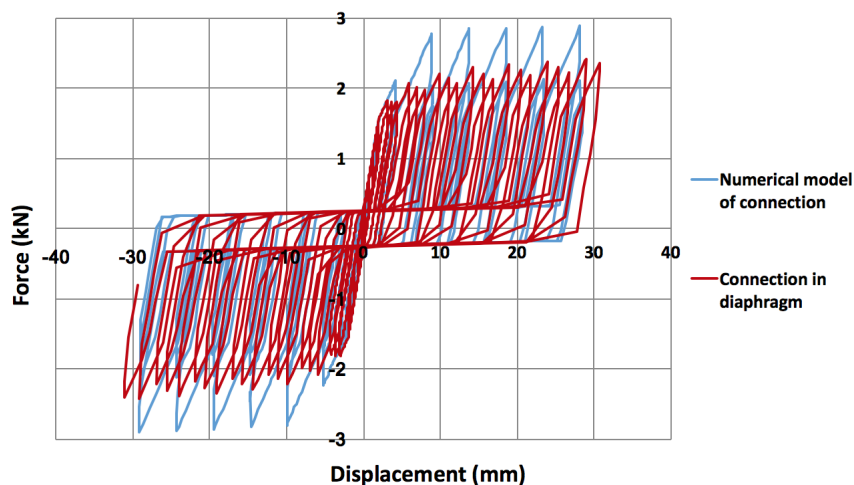
Figure 7-35: Comparison between numerical model of connection and connection within diaphragm

7.3.2 SECOND CALIBRATION METHOD

For the second analysis, in which the numerical backbone of the nailed and screwed connections is calibrated on the experimental backbone, the parameters for the nailed and screwed connections are listed in table 7-15, table 7-16 and table 7-17. The result of the numerical analysis (along with its loading scheme) can be seen in figure 7-36. A comparison with the experimental result can be seen in figure 7-37 and figure 7-38. The maximum peak load per cycle is best approximated in the first few cycles. After a displacement of about 30 mm, the peak loads start to differ increasingly, with a maximum error of approximately 30% at a displacement of 55 mm. The error decreases again when the failure mechanism is initiated for the experimental result. The numerical result does not implement failure, thus the experimental and numerical result move closer again near the end of the loading. When looking at the pinching region, it can be said that the numerical slope is too low as opposed to the experimental result. Furthermore, the width of the pinching region is bigger for the numerical result. Regarding the peaks, one can see that the slopes of the un- and reloading branches

are lower for the numerically calculated results. The path of the peaks do not match the experimental path. Overall, the numerical model provides a fairly sufficient approximation to predict the peak loads. However, the local behaviour such as the slopes and conserved energy are a less sufficient approximation.

Table 7-15: Parameters for the COMBIN40 elements of the nailed connections, calibrated on the experimental backbone

	Loading perpendicular to joist					
	K1 (N/mm)	K2 (N/mm)	Fslide (N)	Initial gap (mm)	C (N*s/mm)	M (kg)
COMBIN40 - 1	10.000	4.22	192	0	0	0
COMBIN40 - 2	150	0.0001	700	0.001	0	0
COMBIN40 - 3	150	0.0001	700	0.001	0	0
	Loading parallel to joist					
	K1 (N/mm)	K2 (N/mm)	Fslide (N)	Initial gap (mm)	C (N*s/mm)	M (kg)
COMBIN40 - 1	10.000	2.5	145	0	0	0
COMBIN40 - 2	500	0.001	840	0.001	0	0
COMBIN40 - 3	500	0.001	840	0.001	0	0

Table 7-16: Parameters for the COMBIN40 elements of the screwed connections between panel and plank, calibrated on the experimental backbone

	Loading perpendicular to plank					
	K1 (N/mm)	K2 (N/mm)	Fslide (N)	Initial gap (mm)	C (N*s/mm)	M (kg)
COMBIN40 - 1	10.000	2	50	0	0	0
COMBIN40 - 2	500	0.001	1150	0.001	0	0
COMBIN40 - 3	500	0.001	1150	0.001	0	0
	Loading parallel to plank					
	K1 (N/mm)	K2 (N/mm)	Fslide (N)	Initial gap (mm)	C (N*s/mm)	M (kg)
COMBIN40 - 1	10.000	0.5	70	0	0	0
COMBIN40 - 2	500	0.001	1100	0.001	0	0
COMBIN40 - 3	500	0.001	1100	0.001	0	0

Table 7-17: Parameters for the COMBIN40 elements of the screwed connections between panel, plank and beam, calibrated on the experimental backbone

Loading parallel to joist						
	K1 (N/mm)	K2 (N/mm)	Fslide (N)	Initial gap (mm)	C (N*s/mm)	M (kg)
COMBIN40 - 1	10.000	3	250	0	0	0
COMBIN40 - 2	800	0.01	1950	0.001	0	0
COMBIN40 - 3	800	0.01	1950	0.001	0	0
Loading perpendicular to joist						
	K1 (N/mm)	K2 (N/mm)	Fslide (N)	Initial gap (mm)	C (N*s/mm)	M (kg)
COMBIN40 - 1	10.000	3	250	0	0	0
COMBIN40 - 2	1000	0.01	2000	0.001	0	0
COMBIN40 - 3	1000	0.01	2000	0.001	0	0

Figure 7-36: Numerical result for retrofitted diaphragm
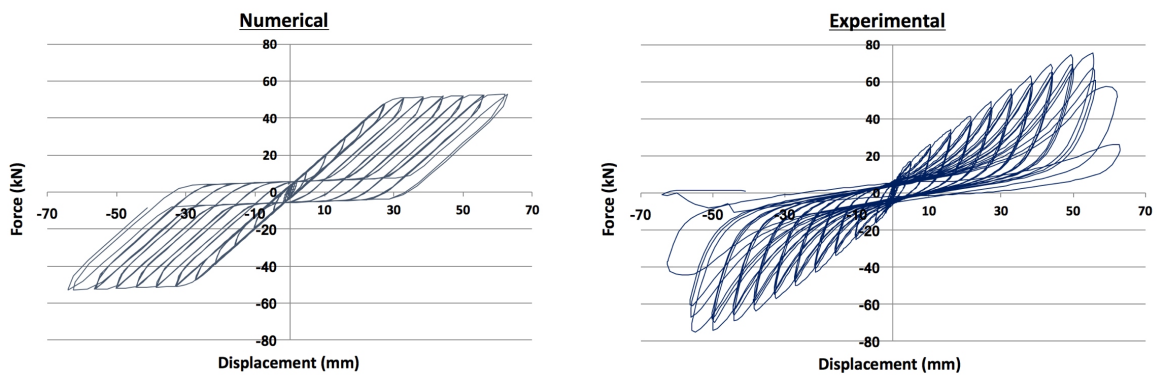
Figure 7-37: Comparison between numerical and experimental result for retrofitted diaphragm
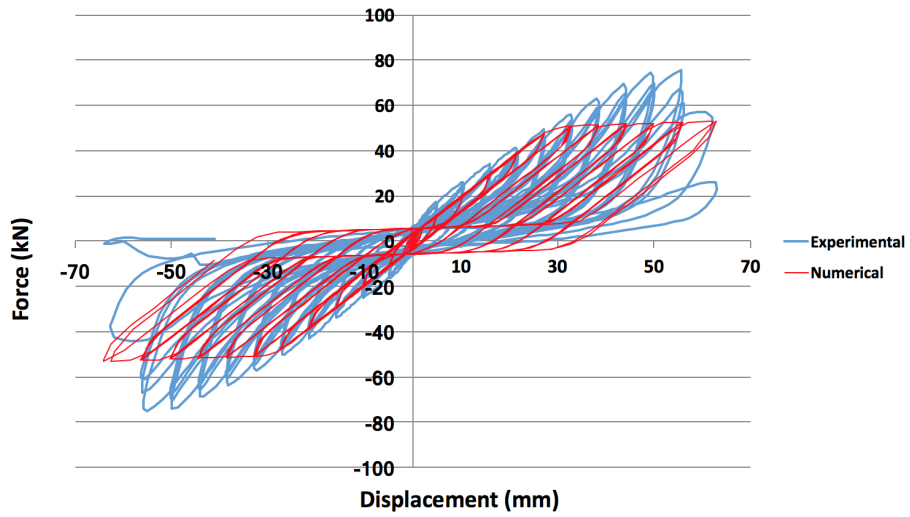
Figure 7-38: Comparison between numerical and experimental result for retrofitted diaphragm

7.3.3 COMPARISON BETWEEN CALIBRATION METHODS
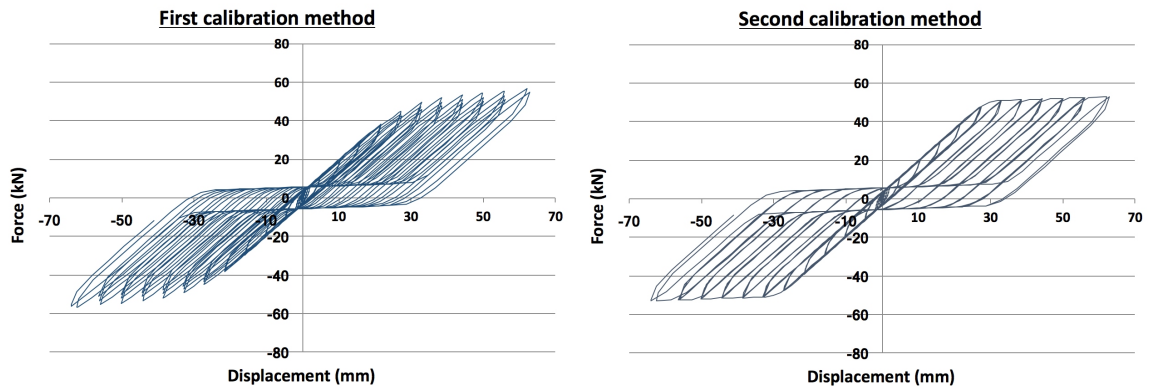
Figure 7-39: Comparison between the two calibration methods
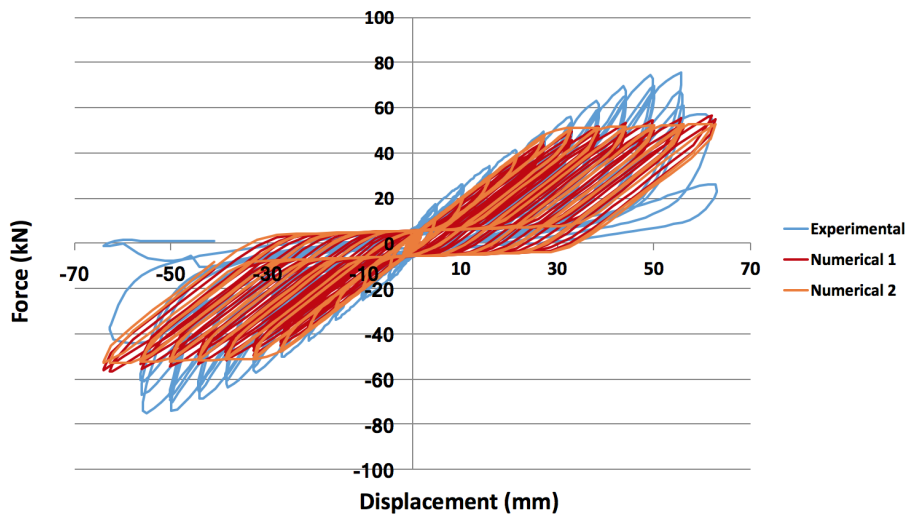
Figure 7-40: Comparison between numerical results and experimental results

A comparison between the numerical results as discussed in this section can be seen in figure 7-39 and figure 7-40. The first calibration method is referred to as 'Numerical 1', and the second calibration method is referred to as 'Numerical 2'. One can see that the two calibration methods yield similar results in terms of maximum peaks and slopes. The second calibration method produces slightly higher peaks for smaller displacements, but lower peaks for bigger displacements as opposed to the first calibration method. The peaks of the second calibration method seem to have a plateau, whereas the first method exhibits sharper peaks. This is due to a lower second reloading stiffness for the second method. The numerical results match the experimental results best for cycles up to a displacement of about 30 mm. At bigger displacements, the results show greater discrepancies with the experimental results. This may be caused by the deviant behaviour of the panels in the numerical model. In the numerical model, the contact region between panels is given a finite stiffness (finite to prevent divergence), which prevents the panels from moving into each other. However, the finite stiffness does not entirely prevent the panels from moving into each other at higher displacements. In reality, the stiffness of the region between panels is much larger and thus gives more stiffness to the system. The deformation of the panels in the experimental test can be seen in figure 7-41. In the experimental test, the relative vertical displacement (UX) between the two lower right panels and the relative horizontal displacement (UY) between the two lower most right panels were measured. These relative displacements can be compared to the numerical displacements. In figure 7-42, the relative displacements (UX and UY) can be seen for both the experimental and the numerical result. In x-direction, the relative displacement is larger for the experimental result as opposed to the numerical result. In y-direction (the direction of loading), the relative displacement is larger for the numerical result. The larger numerical displacement in y-direction may be caused by the lack of friction between the panels, enabling the panels to translate more. As the y-direction is the direction of loading, a lack of friction tends to cause larger translations in this direction. The larger translation reduces the need for rotation of the panels, thus reducing the relative displacement in x-direction. Although the numerical behaviour of the panels differ from the experiments on some aspects, it can be said that the overall behaviour of the panels in the numerical model is still similar to the experiment. The panels have the same workings both numerically and experimentally, meaning that the panels deform such that there is a continuous opening and closing of the gaps between the panels, rather than bending of the panels. Therefore, it can be said that the numerical model accurately captures the behaviour of the panels, however there are still flaws (such as the lower stiffness of the contact regions and the lack of friction). Due to the behaviour of the panels, the deformation of the diaphragm is more shear-based as opposed to the as-built diaphragm (which was more bending-oriented). Overall, the numerical results tend to underestimate the real strength for both calibration methods. This may be caused by the lack of friction between panels and planks in the numerical model. Friction adds more energy to the system, which may increase the maximum strength. Furthermore, the numerical error for the connections increase for higher displacements, which may contribute to the larger error for the diaphragm for larger displacements.
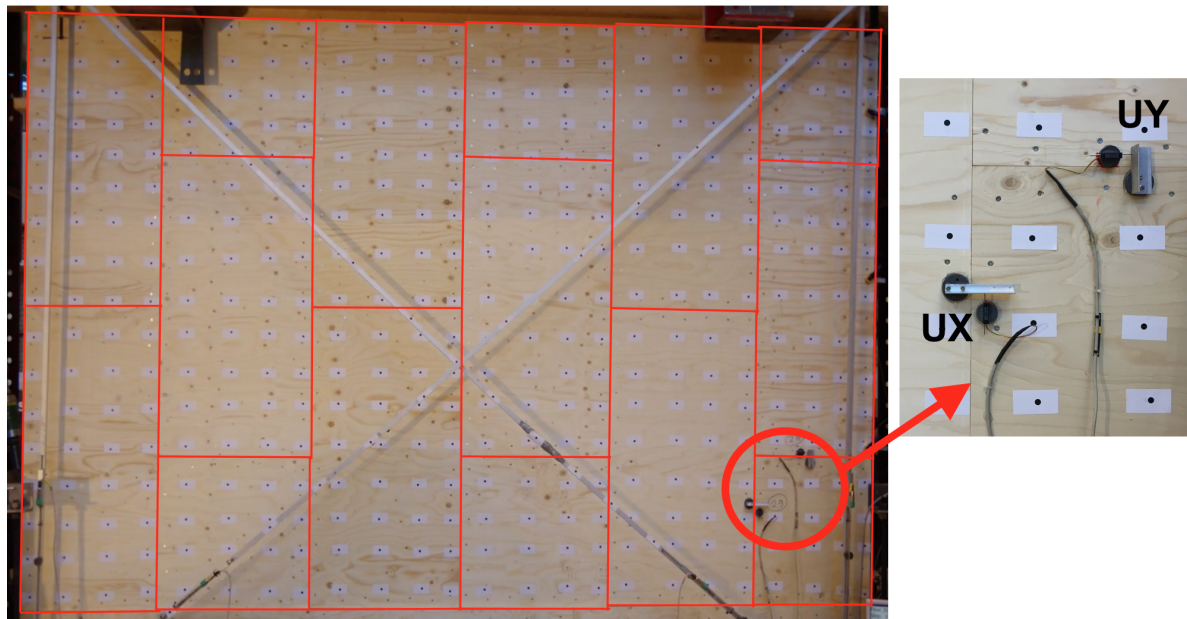
Figure 7-41: Experimental deformation of panels
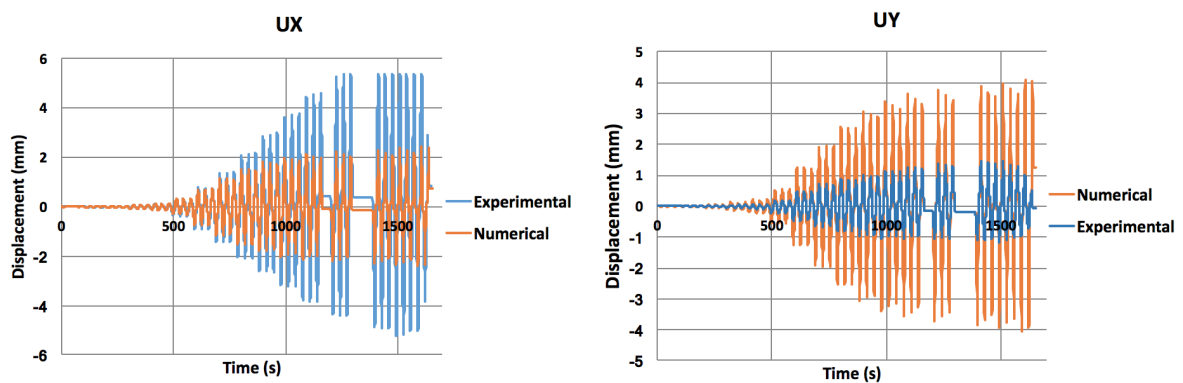
Figure 7-42: Relative displacement of lower right panels

Comparing the backbones of the three graphs (see figure 7-43), one can see that both numerical methods conserve less energy than the experimental result. This is due to the fact that friction is not implemented in the numerical model. Furthermore, the numerical models for the connections showed some discrepancies when compared to the numerical results, which may contribute to the error of the overall response of the diaphragm. For both numerical models, the backbones exhibit similar behaviour up to a displacement of about 20 mm. After a displacement of 20 mm, the second numerical model shows a larger stiffness. However, this stiffness quickly reduces and the stiffness of the first numerical model becomes greater. The second numerical model eventually stabilises (slope of backbone becomes nearly zero), whereas the first numerical model does not (slope of backbone never becomes zero or negative). Considering the local behaviour of the diaphragm, the first calibration method is a better approximation for the retrofitted diaphragm. The first calibration method produces more accurate curve paths than the first calibration method. However, in terms of maximum peaks, both methods yield similar results. In terms of preserved energy, both calibration methods yield similar results up to a displacement of approximately 60 mm. The numerical backbones both seem trilinear, with a high initial stiffness for very low displacements (less than 2 mm). Between a displacement of 2 mm and about 30 mm, the stiffness is lower (secondary

stiffness). After a displacement of 30 mm, the stiffness is even lower. The trilinear backbone curve may be caused by the behaviour of the nonlinear connections. For small displacements, the deformation of the connections in y-direction is very small and thus the connections have a very high stiffness. When the deformations become larger, the stiffness of the connections lowers. At even larger displacements, the connections start to enter plasticity and the stiffness becomes even lower. An illustration of the correlation between the hysteresis of the connections and the backbone of the retrofitted diaphragm can be seen in figure 7-44. The backbone exhibits a transition between the secondary stiffness (green line) and tertiary stiffness (red line). This is caused by the fact that some connections have already reached plasticity, whereas others do not.
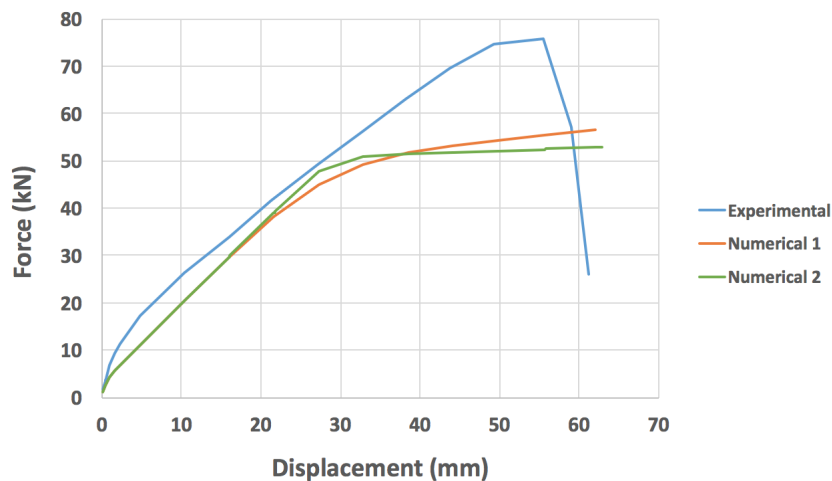
Figure 7-43: Comparison between backbones
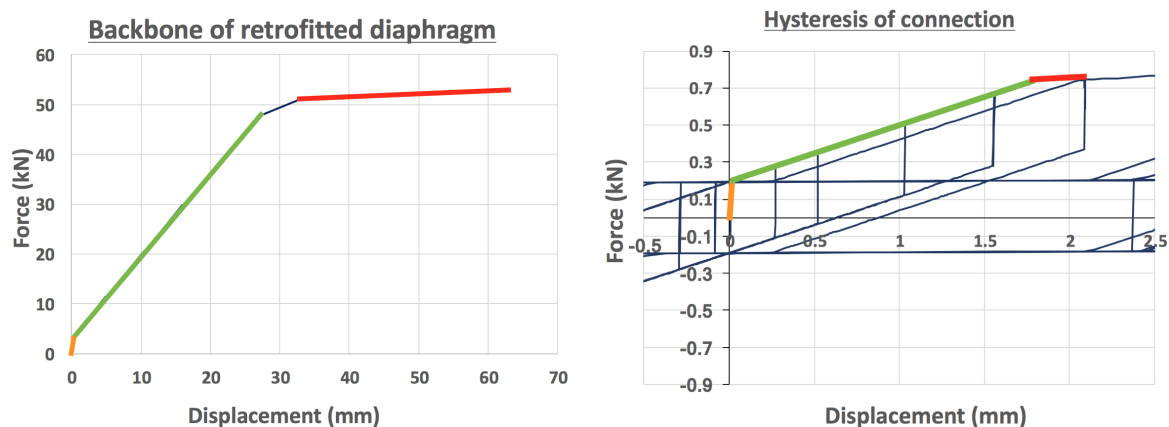
Figure 7-44: Correlation between backbone of diaphragm and hysteresis of connection

In the retrofitted diaphragm, three types of connections can be regarded: the nails (between plank and beam), the screws (between panel and plank) and the top screws (between panel, plank and beam). A maximum deformation of all the connections can be obtained to verify whether they enter plasticity and if they come near failure. This is done so for the model with the first calibration method for the connections. Regarding the x-direction (parallel to the planks), the maximum deformation of the top screws (which occur at the top beam) is 2.1 mm. The top screws enter plasticity at a displacement of 2.1 mm for the x-direction (see figure 7-20). In this direction, the top screws are just leaving elasticity and are about to enter plasticity. The maximum deformation of the screwed connections between panel and plank is 3.4 mm. The screwed connections enter plasticity at a dis-

placement of 2.0 mm in x-direction (see figure 7-8), thus it can be said that they enter plasticity. For the nails, the maximum deformation is 1.1 mm. As the nails enter plasticity at a displacement of 1.8 mm in x-direction (see figure 6-8), they remain in the elastic regime. Considering the y-direction (parallel to the beams), the maximum deformation of the top screws is 33.7 mm. The model for the top screw in y-direction enters plasticity at a displacement of approximately 1.9 mm (see figure 7-14). In the experimental test of the retrofitted diaphragm, the diaphragm failed due to breakage of the top screws. Thus it can be said that a deformation of 33.7 mm is sufficient to cause failure. As the experiment showed that the top screws fail, it may be needed for the numerical model to implement failure for these screws. The implementation of failure will increase the accuracy of the numerical model. Regarding the screws, the maximum deformation in y-direction is 3.0 mm. The screws enter plasticity at a displacement of approximately 2.6 mm in the numerical model (see figure 7-2). The screwed connections enter plasticity, albeit it is still close to the elastic regime. For the nails, the maximum deformation in y-direction is 0.9 mm. The model of the nailed connection enters plasticity at a displacement of about 3.3 mm (see figure 6-18). A summary of the maximum deformation of the connections within the retrofitted diaphragm with the first calibration method for the connections is given in table 7-18. The maximum deformations of the connections within the backbones can be seen in figure 7-45, figure 7-46 and figure 7-47.

Table 7-18: Summary of maximum deformation of connections for retrofitted diaphragm with first calibration method for connections

	x-direction		y-direction	
	Maximum deformation (mm)	Onset of plasticity (mm)	Maximum deformation (mm)	Onset of plasticity (mm)
Nails	1.1	1.8	0.9	3.3
Screws	3.4	2.0	3.0	2.6
Top screws	2.1	2.1	33.7	1.9
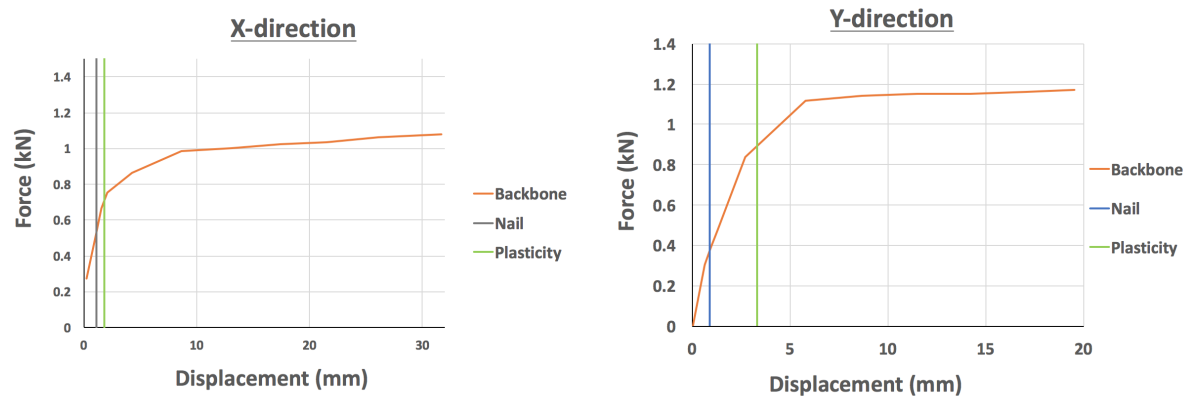
Figure 7-45: Maximum nail deformation within backbone curve for first calibration method
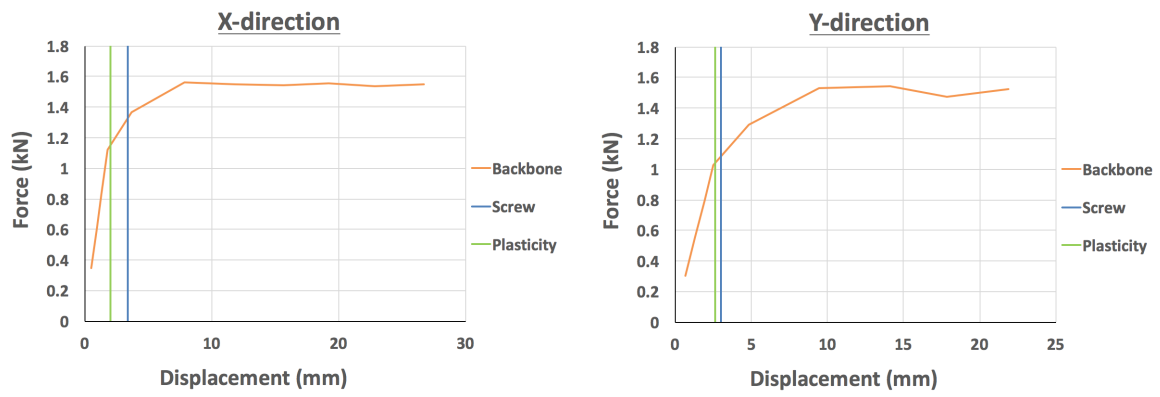
Figure 7-46: Maximum screw deformation within backbone curve for first calibration method
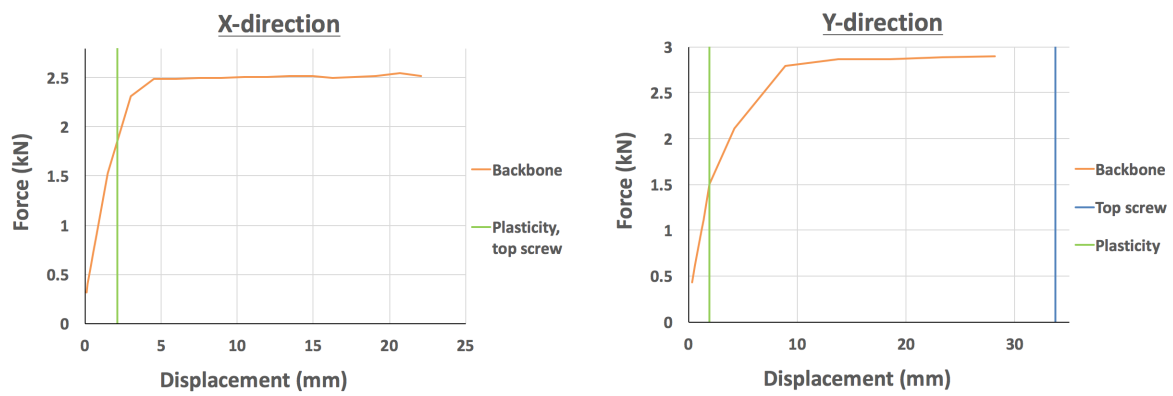
Figure 7-47: Maximum deformation of top screw within backbone curve for first calibration method

8

CONCLUSIONS AND RECOMMENDATIONS

8.1 CONCLUSIONS

The goal of this thesis is to construct numerical models that can properly describe diaphragm behaviour. These numerical models support the objective of this report. The objective is to explore whether extensive modelling of a diaphragm is suitable modelling approach. The main research question is formulated as:

> *'Is it possible to create accurate numerical models of flexible timber diaphragms by modelling the separate components?'.*

Additionally, subquestions are formulated in support of the main research question:

1. *Which FEM-software is most suitable for the modelling of a flexible timber diaphragm?*
2. *Which numerical models are suitable to simulate nonlinear components within a diaphragm?*
3. *Can certain diaphragm members be modelled linearly?*

Furthermore, this report seeks to create a tool for further development. The models created in this report serve as a starting point for future improvements, simplifications and modifications.

In this report, models for both a replicated as-built flexible timber diaphragm and a replicated retrofitted flexible timber diaphragm were constructed to represent the diaphragms as tested at the TU Delft. These models were subjected to a nonlinear quasi-static analysis under a displacement controlled cyclic loading scheme. Material properties were kept as linear elastic, except for the nonlinear connections. The numerical models exhibited nonlinear hystereses, which is in line with the experimental results. Regarding the research question and research objectives, the following conclusions can be drawn with the numerical results:

1. The experimental behaviour of both as-built and retrofitted diaphragms can be accurately captured numerically by modelling the diaphragms through its individual members. The numerical models of both diaphragms considered each individual member: planks, beams, nails, panels and screws. This modelling approach yielded accurate numerical results.

2. To capture the necessary nonlinear characteristics within the diaphragms, software ANSYS Mechanical 18.2 is most suitable. This FEM-software offers satisfactory nonlinear models for the modelling of the connections within the diaphragms.

171

3. The nonlinear connections within the diaphragms can be modelled through three COMBIN40 elements, which are placed in parallel. This model accurately captures the pinching behaviour and the hysteresis peaks of a cyclically loaded nonlinear connection. However, the model yields larger errors for higher nonlinearities at larger displacements. Furthermore, the model for the connections does not implement failure.

4. The first calibration method for the nonlinear connections, in which the numerical hysteresis curve was matched to the experimental hysteresis curve, is most suitable to describe experimental behaviour as obtained at the TU Delft. This method yields better results than the second calibration method, as the local hysteretic behaviour is better described. The second calibration method of the nails may prove to be better suitable for problems in which the diaphragm is subjected to loading of a more random nature.

5. The assumption of linear elastic timber members and nonlinear connecting elements yields accurate results and is deemed a suitable assumption for the modelling of diaphragms.

6. Lack of implementation of friction and improper contact modelling may contribute to numerical errors and a lower energy conservation. Friction and contact regions may add another nonlinearity to consider for diaphragm modelling.

7. The errors for both diaphragms become greater for larger displacements, which is partly caused by the increased errors in the connections for larger displacements.

The above stated conclusions concern the research questions and the research objective. With the obtained numerical results, several additional conclusions can be drawn. Regarding the as-built diaphragm, the following conclusions can be made:

8. The deformation of the as-built diaphragm is characterised by the bending of the planks, rather than the shear deformation.

9. No contact formulations are needed for the numerical model of the as-built diaphragm, as it is a fairly simple model in which the elements do not move into each other under the given loading. However, contact formulations may be needed for the as-built diaphragm if subjected to an other loading scheme.

10. The numerical result of the as-built diaphragm is mesh-dependent, with a finer mesh yielding greater accuracy. The finer mesh yields a stiffer overall response of the diaphragm, which seems contradicting. However, the beams seem to have a larger stiffening effect with a finer mesh due to the higher flexibility of the beams.

11. The numerical model of the as-built diaphragm does not implement friction and contact (opening and closing of gap) between planks. This results in a lower conserved energy for the numerical result as opposed to the experimental result.

12. The as-built diaphragm is best represented through the model with a fine mesh in which the nails are calibrated on the experimental hysteresis. This model yields smaller errors as compared to experimental results and as compared to the models with a coarse mesh and a different calibration method for the nailed connections.

Regarding the retrofitted diaphragm, the following additional conclusions can be stated:

13. The numerical result of the retrofitted diaphragm showcases a higher level of nonlinearity than the as-built diaphragm, which is caused by the increased number of nonlinear connections.

14. The model of the retrofitted diaphragm does require contact formulations to prevent elements from moving into each other.

15. The contact regions between panels have a lower stiffness than in reality. This results in a lower stiffness (lower slope of un- and reloading branches in the hysteresis) and a lower strength (lower peak forces in the hysteresis) for the numerical results.

16. The numerical model of the retrofitted diaphragm did not implement friction between panels and planks, resulting in a lower conserved energy as opposed to the experimental result.

17. The lack of friction and the improper modelling of the contact regions result in a deviant numerical behaviour of the retrofitted diaphragm as opposed to the experimental test. However, the overall behaviour of the retrofitted diaphragm is still captured sufficiently in the numerical model.

18. Regarding the overall behaviour of the retrofitted diaphragm, both calibration methods for nails and screws yield similar results.

8.2 RECOMMENDATIONS

The models for the as-built and retrofitted diaphragm as constructed in this report can serve as a starting point for further research. Considering the numerical models are very detailed, they serve as an excellent starting point for improvements, simplifications or for modifications. Various recommendations can be made to complete the numerical models and to create a better understanding of diaphragm behaviour. These recommendations will be discussed in this section.

8.2.1 RECOMMENDATIONS FOR IMPROVEMENTS

IMPLEMENTATION OF FAILURE IN THE CONNECTIONS

In the numerical models of the diaphragms, no failure is implemented in the nonlinear connections. This is not realistic and prevents the model from entering a failure mechanism. The lack of failure also causes the numerical error to be greater for higher displacements. To improve the models, failure should be implemented in the models for the nonlinear connections. Failure can be implemented in two ways: by letting the force go to zero when the connection reaches a certain displacement or by implementing softening and failure (see figure 8-1). The latter is the most suitable implementation of failure, as it resembles reality better. Implementing softening and failure will yield better numerical results, but its implementation may be more difficult.

(a) Force to zero at certain displacement   (b) Softening and failure
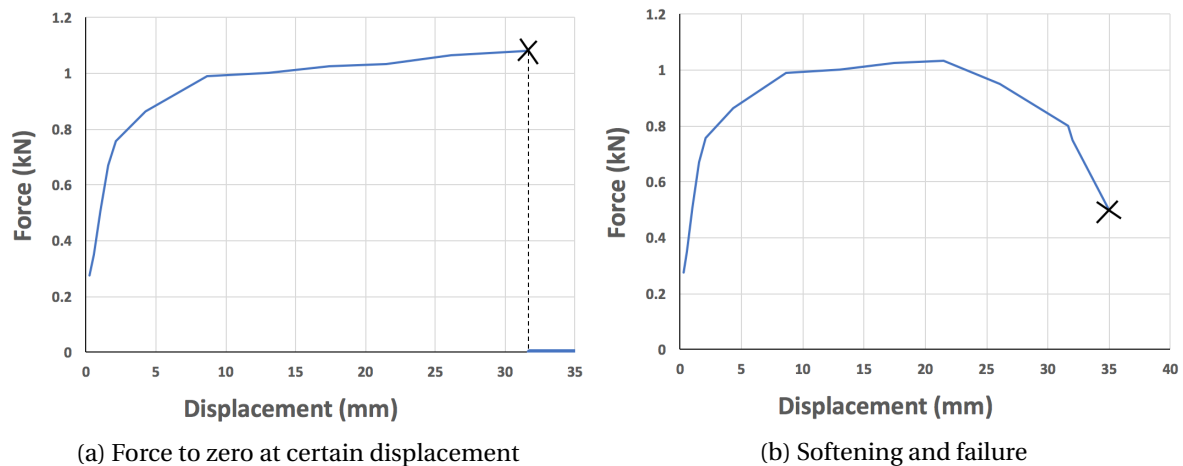
Figure 8-1: Two ways to implement failure in the backbone of the connections

BETTER MODELLING OF CONTACT REGIONS

The contact between timber members (planks and panels) should be modelled in a more proper way, as it adds stiffness to the diaphragm (especially for higher displacements). The contact regions are of particular importance for the retrofitted diaphragm, as the panels tend to move into each other if the contact region is not modelled properly. The improper modelling of the contact regions can yield unrealistic diaphragm behaviour and can cause greater numerical discrepancies. The closing and opening of the gaps between timber members is an important interaction which should not be disregarded.

IMPLEMENTATION OF FRICTION BETWEEN TIMBER MEMBERS

Friction may add another layer of nonlinearity between timber members. However, for small relative displacements between timber members, frictional behaviour may still be linear (see section 4.6). Nevertheless, it is still of importance to implement friction between timber members as it increases the system's energy and thus increases the accuracy of the model. In particular, the friction between timber planks, between timber panels and between panels and plank are important to consider.

SENSITIVITY TO MESH DENSITY

In this report, the as-built diaphragm was analysed using two meshes. The two meshes produced different results and yielded additional questions regarding the numerical behaviour of the diaphragm. For further understanding, it may be useful to analyse the diaphragm using multiple meshes. Multiple meshes may also give insight into the convergence of the diaphragm and it can be used for optimisation purposes (least computational effort for minimum accuracy). It may also be useful to analyse the retrofitted diaphragm using multiple meshes, to verify its numerical behaviour.

SENSITIVITY TO MATERIAL PROPERTIES

The timber members are each given individual linear orthotropic material properties (E_x, E_y, E_z, G_{xy}, $G_{yz}, G_{xz}, \nu_{xy}, \nu_{yz}, \nu_{xz}$). These material properties are specific for the diaphragm as regarded in this report and may vary for other floors. For this reason, it may be interesting to investigate the effect of the various material properties on diaphragm behaviour. A study of the sensitivity to material properties gives insight into which properties have a bigger effect on the diaphragm behaviour and which direction is most important to consider. A material property study may also give useful recommendations for preferred timber classes to use for the construction of the diaphragm.

8.2.2 RECOMMENDATIONS FOR SIMPLIFICATIONS

MATERIAL PROPERTIES

In this report, each beam and each plank are given individual orthotropic material properties. This is cumbersome and may not be needed to achieve the desired numerical accuracy. Instead, it may be more practical to give each beam and each plank the same material properties (for example, the average of all planks and beams) as the beams and planks are constructed from the same timber.

MODELLING OF A PLATE

Instead of modelling all the planks separately, as is done in this report, one can choose to model the diaphragms such that the planks are simulated through an orthotropic plate (see figure 8-2). This removes the need for individual modelling of all planks and may simplify the problem. However, it should be investigated whether this simplification still yields accurate results and can describe diaphragm behaviour in a proper manner. By modelling the planks through a plate, one also eliminates the need for friction and contact modelling.

(a) Modelling the planks individually

(b) Modelling of the planks through a plate
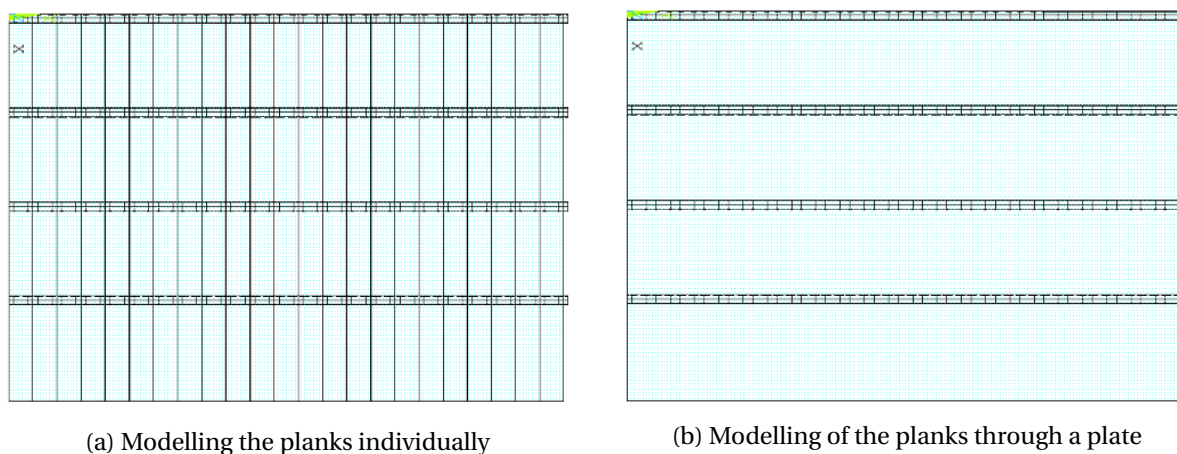
Figure 8-2: Different modelling approaches for the timber planks

8.2.3 RECOMMENDATIONS FOR MODIFICATIONS

LOADING PERPENDICULAR TO JOISTS

The numerical analyses in this report only consider loading parallel to the joists. As a diaphragm acts in two dimensions, it is also of importance to study the behaviour in the direction perpendicular to the joists. With analyses regarding both in-plane directions, one can determine which direction is weaker. This knowledge can be taken into account when designing a house with flexible diaphragms. The deformation mechanics may be different for the two directions. For loading parallel to the joists, diaphragm deformation is mostly governed by the bending of the planks. For loading perpendicular to the joists, diaphragm deformation is mostly governed by the bending of the joists. For the latter loading case, friction between the planks may play a bigger role in diaphragm mechanics.

DIFFERENT PLANK CONFIGURATIONS

The diaphragm configuration in this report is specific to the tested floor and may vary for other floors. Therefore, it may be interesting to consider different plank configurations and its effect on diaphragm behaviour. In this report, the planks spanned the whole diaphragm length. In reality, the planks may be discontinuous and configured differently (see figure 8-3). Discontinuous planks may cause the deformation of the diaphragm to be less bending-dominated.

(a) Configuration 1

(b) Configuration 2
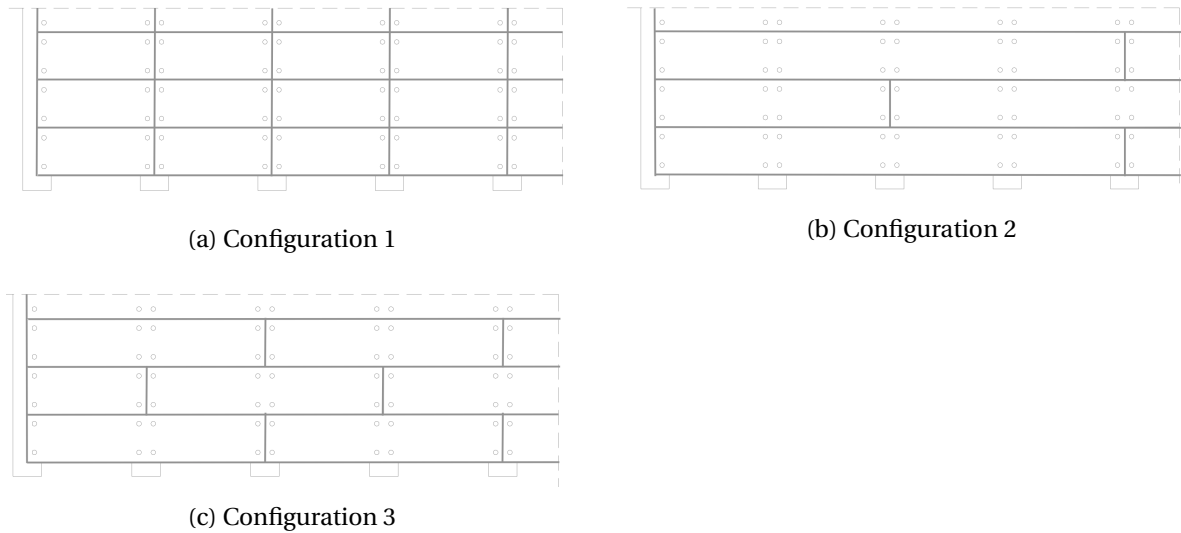
(c) Configuration 3

Figure 8-3: Different configurations of planks [3]

DIFFERENT DIMENSIONS OF TIMBER MEMBERS

Flexible timber diaphragms can have different dimensions for both the beams, planks and panels. These features affect the behaviour of the diaphragm and may be interesting to study. By varying the dimensions of the timber members, one could investigate which timber members have a greater effect on diaphragm behaviour and which directions are dominant. Additionally, the centre-to-centre distance between the beams can be varied. The centre-to-centre distance between beams determines the amount of beams per unit length. The amount of beams determines the stiffening effect of the beams on the diaphragm response and is of interest when designing the floor.

DIFFERENT FLOOR PLANS

For buildings with multiple storeys, the diaphragm floor plan may not be rectangular on higher storeys. The floor plan may have an opening for a staircase. The staircase may be positioned at the edges of the diaphragm or somewhere within the diaphragm (see figure 8-4). It could be interesting to study what the effect is on the response of the diaphragm if an opening for a staircase is present in the floor plan. The presence of an opening may be disadvantageous for the strength of the diaphragm.

(a) Staircase opening within the diaphragm

(b) Staircase opening at the edge of the diaphragm
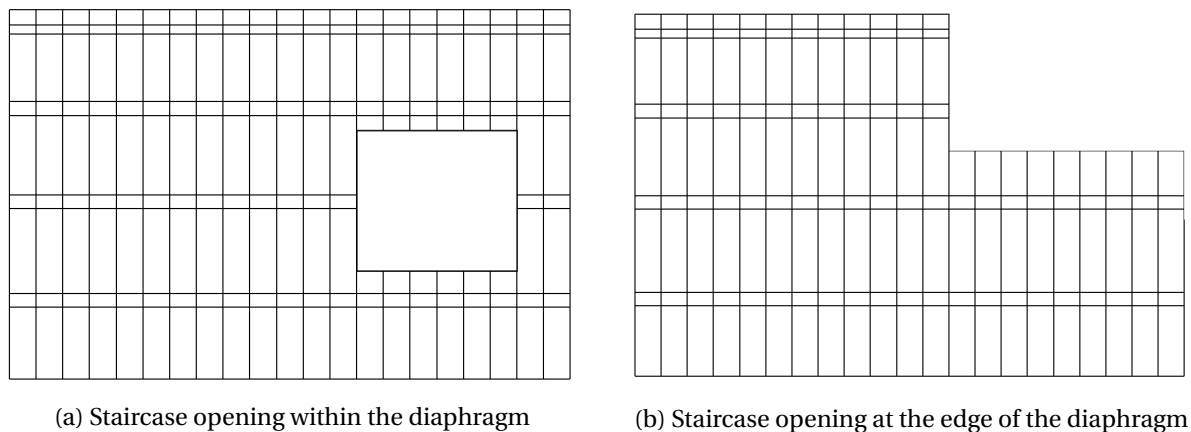
Figure 8-4: Non-rectangular floor plans

DIFFERENT RETROFIT MEASURES

To strengthen a flexible timber diaphragm, different retrofit measures can be carried out. In this report, only one retrofit measure was considered in which panels were screwed on top of the floor. In reality, retrofitting can be done in may ways and these measures may be interesting to study as well. A study of the different retrofit measures gives insight into which measure has the most favourable strengthening properties. This is helpful for the retrofitting of existing buildings. The different retrofit measures each impose various new numerical issues and may be interesting for a broader understanding of the behaviour of retrofitted diaphragms. Apart from retrofitting with panels, the following retrofit measures are available (see figure 8-5) [3]:

- Application of diagonal bracing
- Adding a concrete layer on top of the floor

(a) Diagonal bracing

(b) Concrete layer
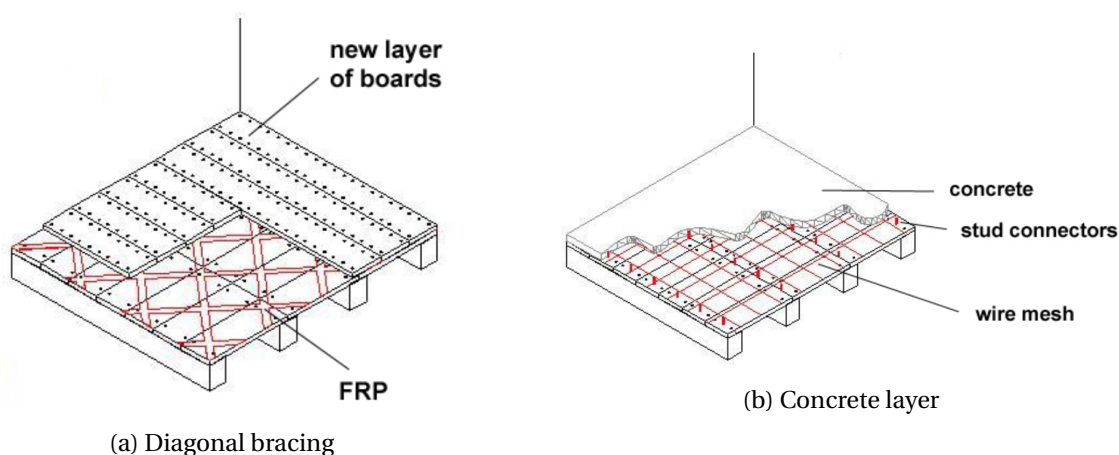
Figure 8-5: Retrofitting measures [3]

NONLINEAR TIME HISTORY ANALYSIS

In this report, the numerical analyses were limited to static nonlinear cyclic pushover analyses. This was done so in order to verify the numerical results with the experimental results. Although a cyclic pushover analysis is sufficient for the scope of this report, it is of course very interesting to consider nonlinear time history (NLTH) analyses as well. By performing NLTH analyses, one can verify whether the constructed numerical models are suitable for cases with random loadings as well. An NLTH analysis has a broader purpose and adds value to the model. By doing both a pushover and an NLTH analysis, the performance of the numerical models can be validated.

IMPLEMENTATION IN A BUILDING

For the bigger picture, it is of interest to implement the diaphragms in a building. Implementation in a building helps to verify whether the diaphragms behave correctly and gives insight into the effect of the diaphragm on the structure. It also provides valuable knowledge on whether diaphragm behaviour is decisive in structural failure. For the implementation of the diaphragm in a building, one should also consider the wall-floor connections. The behaviour of these connections must be studied and modelled correctly. The effect of wall-floor connections on diaphragm behaviour can be verified separately, by changing the boundary conditions of the diaphragm. These boundary conditions must reflect the behaviour of the wall-floor connections. Furthermore, it may be interesting to study the difference in the structural response of terraced and detached buildings, in which the numerical models of the diaphragms are implemented.

BIBLIOGRAPHY

[1] NAM, *Nam - aantal aardbevingen in het groningen-gasveld,* .

[2] Kees Van De Veen, *Reportage photography with a human touch,* .

[3] A. Brignola, S. Podestà, and S. Pampanin, *In-plane stiffness of wooden floor,* (2008).

[4] J. W. Bott, *Horizontal stiffness of wood diaphragms,* (2005).

[5] M. Piazza, C. Baldessari, and R. Tomasi, *The role of in-plane floor stiffness in the seismic behaviour of traditional buildings,* in *14th World Conference on Earthquake Engineering, Beijing, China* (2008) pp. 12–17.

[6] D. F. D'Ayala, *An integrated procedure for the assessment of seismic vulnerability of historic buildings. in 12th european conf earthq eng,* (2002).

[7] S. Rajasekaran, *Structural dynamics of earthquake engineering: theory and application using MATHEMATICA and MATLAB* (Elsevier, 2009) p. 595.

[8] J. Spijkers, A. Vrouwenvelder, and E. Klaver, *Structural Dynamics: CT4140: Part 1-Structural Vibrations* (TU Delft, 2006) p. 156.

[9] A. Brignola, S. Pampanin, and S. Podestà, *Experimental evaluation of the in-plane stiffness of timber diaphragms,* Earthquake Spectra **28**, 1687 (2012).

[10] A. Wilson, P. J. Quenneville, and J. M. Ingham, *In-plane orthotropic behavior of timber floor diaphragms in unreinforced masonry buildings,* Journal of Structural Engineering **140**, 04013038 (2013).

[11] D. F. Peralta, J. M. Bracci, and M. B. Hueste, *Seismic performance of rehabilitated wood diaphragms,* Mid-America Earthquake Center CD Release 03-01 (2003).

[12] A. W. Wilson, *Seismic assessment of timber floor diaphragms in unreinforced masonry buildings,* Ph.D. thesis, ResearchSpace@ Auckland (2012).

[13] B. Folz and A. Filiatrault, *Cyclic analysis of wood shear walls,* Journal of Structural Engineering **127**, 433 (2001).

[14] ANSYS, *Elements reference, chapter 4.40,* ().

[15] A. Blasetti, R. Hoffman, and D. Dinehart, *Simplified hysteretic finite-element model for wood and viscoelastic polymer connections for the dynamic analysis of shear walls,* Journal of structural engineering **134**, 77 (2008).

[16] J. P. Judd and F. S. Fonseca, *Analytical model for sheathing-to-framing connections in wood shear walls and diaphragms,* Journal of Structural Engineering **131**, 345 (2005).

[17] H. J. Blaß and P. Schädle, *Verhalten einer Massivholzbauweise unter Erdbebenlasten,* Vol. 18 (KIT Scientific Publishing, 2011).

[18] L. F. Ibarra, R. A. Medina, and H. Krawinkler, *Hysteretic models that incorporate strength and stiffness deterioration,* Earthquake engineering & structural dynamics **34**, 1489 (2005).

[19] H. P. Gavin, *Bilinear hysteresis,* (2014).

[20] F. Al-Bender, *Fundamentals of friction modeling,* in *Proceedings, ASPE Spring Topical Meeting on Control of Precision Systems, MIT, April 11-13, 2010* (ASPE-The American Society of precision Engineering, 2010) pp. 117–122.

[21] T. Lin and J. M. LaFave, *Experimental behavior and modeling of wall-diaphragm connections for older masonry buildings,* in *15th World Conference on Earthquake Engineering* (2012).

[22] E. Sionti, *Non-linear seismic assessment and retrofitting of unreinforced masonry buildings,* (2016).

[23] B. Dost and D. Kraaijpoel, *The august 16, 2012 earthquake near huizinge (groningen),* KNMI Scientific report (2013).

[24] G. J. P. Ravenshorst and D. P. Kroon, *Plank-joist connection testing of as-built specimens, report number C31B67WP4-4, version 2, 27-03-2017,* Delft University of Technology .

[25] International Organization for Standardization, *Iso 16670:2003, timber structures - joints made with mechanical fasteners - quasi-static reversed-cyclic test method,* .

[26] ANSYS, *Elements reference,* ().

[27] ARUP, *Seismic risk study - earthquake scenario-based risk assessment,* .

[28] NU.nl, *Versnelde inspectie 22.000 huizen in aardbevingsgebied groningen,* .

[29] ASCE, *Seismic rehabilitation of existing buildings,* (2007).

[30] N. Z. S. for Earthquake Engineering (1998-), *Assessment and Improvement of the Structural Performance of Buildings in Earthquakes: Prioritisation, Initial Evaluation, Detailed Assessment, Improvement Measures: Recommendations of a NZSEE Study Group on Earthquake Risk Buildings* (New Zealand Society for Earthquake Engineering, 2014) pp. 11–3.

[31] K. Cobeen, J. Dolan, D. Thompson, and J. Van de Lindt, *Seismic design of wood light-framed structural diaphragm systems,* A Guide for Practicing Engineers. NEHRP Seismic Design Technical Brief , 5.

[32] CSI, SAP2000, *Sap2000 integrated finite element analysis and design of structures: Basic analysis reference, version 7.0,* Computers and Structures, Inc., Berkeley, California, USA (1998).

[33] J. Aleman, G. Mosqueda, and A. Whittaker, *Seismic Analysis of Multi-story Unreinforced Masonry Buildings with Flexible Diaphragms,* Tech. Rep. (MCEER, 2015).

[34] CSI, SAP2000, *Sap2000 integrated software for structural analysis and design: Analysis reference manual, version 8.0,* Computers and Structures, Inc., Berkeley, California, USA (2002).

[35] W. B. Cross and N. P. Jones, *Seismic performance of joist-pocket connections. i: modeling,* Journal of Structural Engineering **119**, 2986 (1993).

[36] L. Liping, X. Kui, and C. Xuan, *The research of applied pushover method in the earthquake resistance analysis of soil-structure interaction system,* in *14th World Conference On Earthquake Engineering Beijing, China October* (2008) pp. 12–17.

[37] A. Kappos, T. Paraskeva, and A. Sextos, *Seismic assessment of a major bridge using modal pushover analysis and dynamic time-history analysis,* in *Proceedings of the International Conference on Computational and Experimental Engineering and Sciences* (2004).

[38] R. J. Ross *et al., Wood handbook: Wood as an engineering material,* (2010).

APPENDICES

A

SPECIFICATIONS OF THE AS-BUILT TIMBER FLOOR SPECIMEN, TESTED AT THE TU DELFT

		Weight (kg)	Length (mm)	Width (mm)	Thickness (mm)	Density (kg/m^3)	Frequency (1/s)	E_dynamic (N/mm^2)
Beams	b1	17,390	4900	130	60	454,9974	595	15470,17
	b2	16,770	4900	130	60	438,7755	566	13499,80
	b3	16,730	4900	130	60	437,7289	520	11367,48
	b4	16,830	4900	130	60	440,3454	508	10913,73
	b5	18,790	4900	130	60	491,6274	551	14334,79
Boards	p01	3,570	2680	164	18	451,2498	903	10571,15
	p02	3,755	2680	164	18	474,6339	844	9713,44
	p03	4,390	2680	160	18	568,7707	976	15565,62
	p04	4,590	2680	164	18	580,1784	878	12849,32
	p05	4,270	2680	163	18	543,0414	971	14709,61
	p06	4,150	2680	162	18	531,0382	1020	15872,88
	p07	3,035	2680	164	18	383,6256	810	7231,15
	p08	3,180	2680	164	18	401,9536	1044	12586,55
	p09	3,175	2680	164	18	401,3216	752	6520,15
	p10	3,480	2680	164	18	439,8738	864	9433,77
	p11	3,660	2680	164	19	438,2772	893	10041,10
	p12	4,010	2681	164	18	506,6770	961	13453,39
	p13	3,625	2680	165	18	455,4249	903	10668,95
	p14	4,155	2680	164	18	525,1942	771	8969,29
	p15	3,660	2680	164	18	462,6259	908	10958,00
	p16	3,955	2680	164	18	499,9140	971	13541,39
	p17	3,615	2681	165	18	453,9991	903	10643,49
	p18	3,830	2680	164	17	512,5913	854	10740,30
	p19	3,450	2680	164	18	436,0818	932	10882,52
	p20	3,635	2680	164	18	459,4659	956	12064,20
	p21	3,265	2680	163	18	415,2296	898	9619,90
	p22	3,985	2680	164	18	503,7061	1030	15352,57
	p23	3,825	2680	164	18	483,4820	908	11452,01
	p24	3,830	2681	164	18	483,9334	810	9128,71
	p25	4,485	2680	164	18	566,9063	961	15041,38
	p26	3,450	2681	164	18	435,9191	952	11358,83
	p27	4,040	2680	164	18	510,6581	1035	15715,94
	p28	3,605	2680	165	18	452,9122	800	8327,67
	p29	3,855	2681	164	18	487,0922	903	11419,32
	p30	3,630	2680	164	18	458,8339	1025	13849,46

*   Beams b1 and b2 were glued together and positioned at the edge of the diaphragm where loading was applied.

**   Boards p01 to p23 were used in the tested timber diaphragm.

***   The dynamic modulus of elasticity is calculated using $E_{dyn} = (2 * l * f)^2 * \rho * 10^{-12}$, in which l is the length of the member, f is the measured frequency and ρ is the density of the member.

B

INSTRUMENTATION OF EXPERIMENTAL TESTS
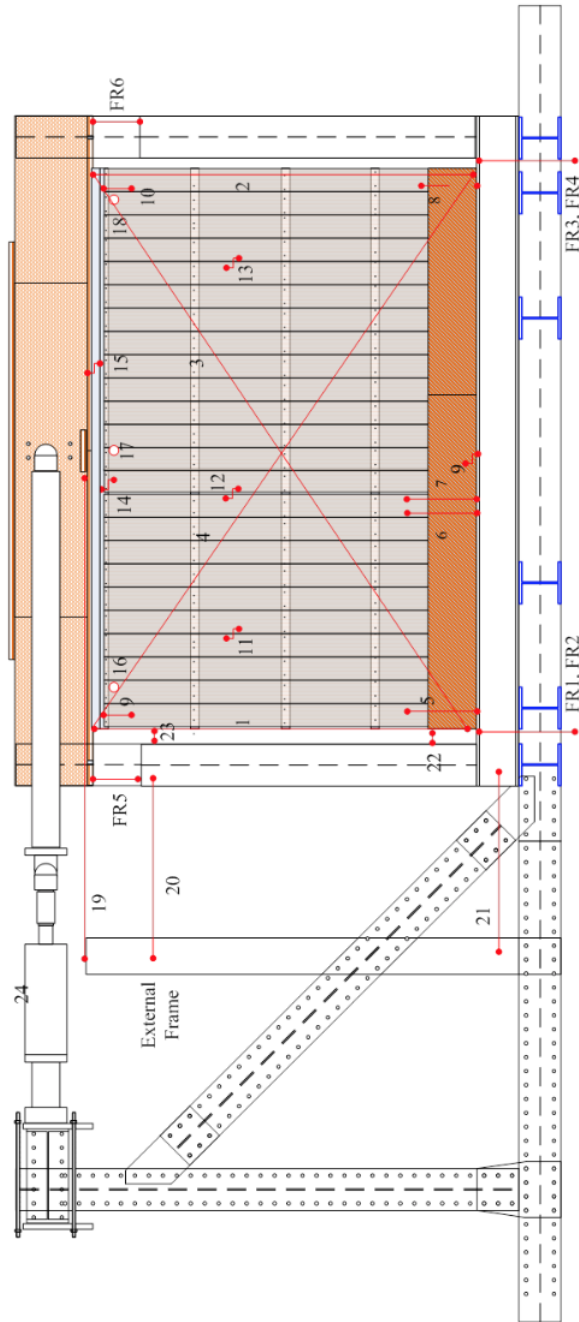
No.	Description	Sensor Type	Stroke (mm)
1	Vertical displacement between top and bottom steel beam (front-right side)	Linear potentiometer	+/-100
2	Vertical displacement between top and bottom steel beam (front-right side)	Linear potentiometer	+/-100
3	Diagonal displacement between steel beams (front side)	Linear potentiometer	+/-100
4	Diagonal displacement between steel beams (front side)	Linear potentiometer	+/-100
5	Vertical displacement between bottom steel beam and plank (back side)	Linear potentiometer	+/-50
6	Vertical displacement between bottom steel beam and plank (back side)	Linear potentiometer	+/-50
7	Vertical displacement between bottom steel beam and plank (back side)	Linear potentiometer	+/-50
8	Vertical displacement between bottom steel beam and plank (back side)	Linear potentiometer	+/-50
9	Vertical displacement between top joist and plank (back side)	Linear potentiometer	+/-50
10	Vertical displacement between top joist and plank (back side)	Linear potentiometer	+/-50
11	Vertical displacement between two planks (back side)	Linear potentiometer	+/-50
12	Vertical displacement between two planks (back side)	Linear potentiometer	+/-50
13	Vertical displacement between two planks (back side)	Linear potentiometer	+/-50
14	Horizontal displacement between plank and top joist (back side)	Linear potentiometer	+/-50
15	Horizontal displacement between top joist and bottom flange of LVL-I-beam	Linear potentiometer	+/-50
16	Out-of-plane displacement at the top of the wall (back side)	Laser	+/-100
17	Out-of-plane displacement at the top of the wall (back side)	Laser	+/-100
18	Out-of-plane displacement at the top of the wall (back side)	Laser	+/-100
19	Horizontal displacement top steel beam	Linear potentiometer	+/-100
20	Horizontal displacement steel column on bottom beam in test frame to external frame	Linear potentiometer	+/-100
21	Horizontal displacement bottom steel beam to external frame.	Linear potentiometer	+/-10
22	Horizontal displacement top plywood panel to steel column at bottom beam.	Linear potentiometer	+/-50
23	Horizontal displacement top diaphragm to steel column at bottom beam.	Linear potentiometer	+/-175
24	Horizontal actuator 400 kN – load and displacement	Load cell and HBM LVDT	+/-100
FR1-FR4	Vertical displacement of the bottom steel beam with respect to the floor	Linear potentiometer	+/-10
FR5-FR6	Vertical displacement between top beam and columns	Linear potentiometer	+/-100
25	Horizontal displacement top plywood panel to steel column bottom beam	Linear potentiometer	+/-50
26	Horizontal displacement top plywood panel to steel column bottom beam	Linear potentiometer	+/-50

*   Note that sensors 25 and 26 were only used during the testing of the retrofitted diaphragm.

C

SPECIFICATIONS OF NAILED CONNECTION SPECIMENS

C.1 LOADING PERPENDICULAR TO JOISTS

(a) 3D-view   (b) top-view
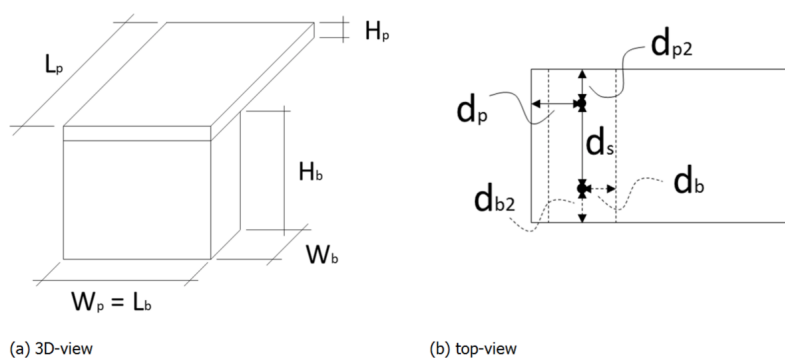
Specimen	Test	Component	Height (mm)	Width (mm)	Length (mm)	Density (kg/m^3)	Moisture content (%)
F1-b2-26-A	Monotonic	Plank	18	163	203	424,8	11,21
		Joist	129	59	162	437,4	11,90
F1-b2-24-A	Cyclic	Plank	18	162	202	452,4	11,27
		Joist	128	60	168	445,0	11,61
F1-b2-25-A	Cyclic	Plank	18	161	203	499,6	11,17
		Joist	129	59	163	439,0	11,84
F1-b2-27-A	Cyclic	Plank	18	162	202	492,6	11,20
		Joist	128	60	165	442,3	11,86
F1-b2-28-A	Cyclic	Plank	18	163	203	418,3	11,12
		Joist	129	60	173	436,5	11,79
F1-b5-26-A	Cyclic	Plank	18	163	224	418,6	11,40
		Joist	128	59	166	490,6	12,02

Specimen	Test	Component	Length (mm)	Thickness (mm)	d_b (mm)	d_p (mm)	d_s (mm)	d_{b2} (mm)	d_{p2} (mm)
F1-b2-26-A	Monotonic	Nail 1	64,2	3,0	28	31	94,0	33	34
		Nail 2	64,2	3,0	29	37		34	34
F1-b2-24-A	Cyclic	Nail 1	64,2	3,0	30	30	95,0	36	36
		Nail 2	64,2	3,0	30	31		35	31
F1-b2-25-A	Cyclic	Nail 1	64,2	3,0	29	33	88,0	38	39
		Nail 2	64,2	3,0	27	31		40	33
F1-b2-27-A	Cyclic	Nail 1	64,2	3,0	28	32	89,0	36	35
		Nail 2	64,2	3,0	30	29		39	38
F1-b2-28-A	Cyclic	Nail 1	64,2	3,0	25	32	101,0	32	32
		Nail 2	64,2	3,0	28	32		40	3
F1-b5-26-A	Cyclic	Nail 1	64,2	3,0	25	66	88,0	26	28
		Nail 2	64,2	3,0	26	65		41	36

Specimen	Test	Maximum load (kN)	Corresponding displacement (mm)	Failure mode
F1-b2-26-A	Monotonic	2,07	33,30	Pulling out of both nails
F1-b2-24-A	Cyclic	2,14	25,44	Bending failure of both nails
F1-b2-25-A	Cyclic	2,05	20,53	Bending failure of both nails
F1-b2-27-A	Cyclic	1,96	30,15	Bending failure of both nails
F1-b2-28-A	Cyclic	2,16	21,79	Bending failure of both nails
F1-b5-26-A	Cyclic	2,34	17,23	Bending failure of both nails

*   Cyclic loading scheme was based on a yield displacement of 22 mm.

**   Minimum displacement rate for cyclic tests was 0.1 mm/s.

***   Time between zero and maximum displacement was 10 s for each cycle of the cyclic loading scheme.

****   Parameters denoted in red are likely measured incorrectly.

C.2 LOADING PARALLEL TO JOISTS
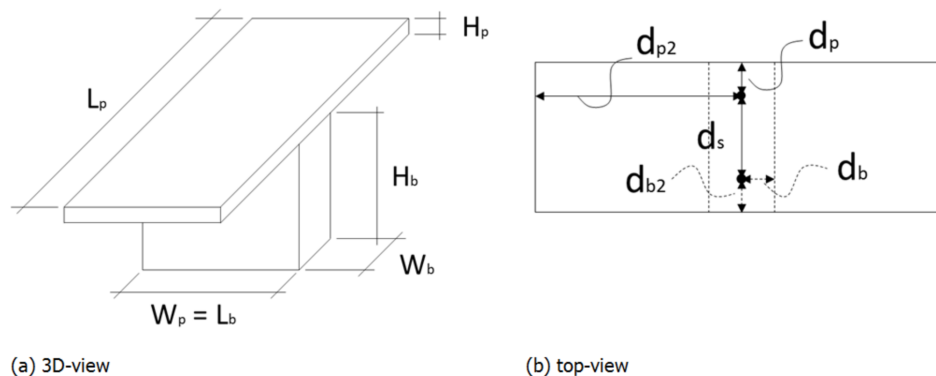
(a) 3D-view   (b) top-view

Specimen	Test	Component	Height (mm)	Width (mm)	Length (mm)	Density (kg/m³)	Moisture content (%)
F1-b3-25-B	Cyclic	Plank	18	162	411	572,1	-
		Joist	129	59	164	415,8	-
F1-b3-27-B	Cyclic	Plank	18	162	412	485,8	-
		Joist	129	59	166	406,5	-
F1-b5-25-B	Cyclic	Plank	18	162	415	513,9	-
		Joist	128	59	164	489,1	-

Specimen	Test	Component	Length (mm)	Thickness (mm)	d_b (mm)	d_p (mm)	d_s (mm)	d_{b2} (mm)	d_{p2} (mm)
F1-b3-25-B	Cyclic	Nail 1	64,2	3,0	32	33	100,0	26	202
		Nail 2	64,2	3,0	29	29		27	205
F1-b3-27-B	Cyclic	Nail 1	64,2	3,0	32	34	94,0	29	205
		Nail 2	64,2	3,0	34	34		28	205
F1-b5-25-B	Cyclic	Nail 1	64,2	3,0	33	34	98,0	28	205
		Nail 2	64,2	3,0	31	30		25	202

Specimen	Test	Maximum load (kN)	Corresponding displacement (mm)	Failure mode
F1-b3-25-B	Cyclic	2,32	14,11	Pulling out of one nail, bending failure of one nail
F1-b3-27-B	Cyclic	2,39	21,78	Bending failure of both nails
F1-b5-25-B	Cyclic	2,42	13,33	Pulling out of one nail, bending failure of one nail

* Cyclic loading scheme was based on a yield displacement of 14 mm.
** Minimum displacement rate for cyclic tests was 0.1 mm/s.
*** Time between zero and maximum displacement was 10 s for each cycle of the cyclic loading scheme.
**** Missing geometry data is denoted by "-".

C.3 ROTATIONAL LOADING

(a) 3D-view   (b) top-view
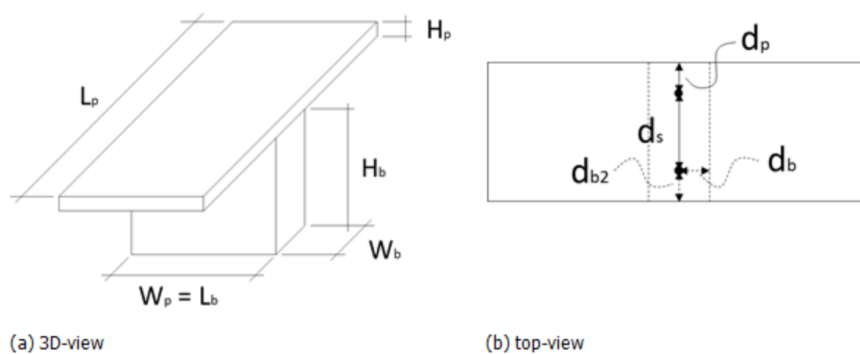
Specimen	Test	Component	Height (mm)	Width (mm)	Length (mm)	Density (kg/m³)	Moisture content (%)
F1-b3-26-C	Monotonic	Plank	18	162	412	407,90	11,40
		Joist	128	60	164	405,80	11,77
F1-b5-28-C	Monotonic	Plank	18	163	410	428,70	11,23
		Joist	128	60	170	480,60	11,72
F1-b3-24-C	Cyclic	Plank	18	162	410	431,10	11,13
		Joist	128	60	168	420,70	11,11
F1-b3-28-C	Cyclic	Plank	18	163	411	412,60	11,12
		Joist	128	60	174	404,00	11,64
F1-b4-27-C	Cyclic	Plank	18	162	414	483,60	11,06
		Joist	128	59	165	404,90	11,78

Specimen	Test	Component	Length (mm)	Thickness (mm)	d_b (mm)	d_p (mm)	d_s (mm)	d_{b2} (mm)
F1-b3-26-C	Monotonic	Nail 1	64,2	3,0	-	10	80,0	-
		Nail 2	64,2	3,0	-	79		-
F1-b5-28-C	Monotonic	Nail 1	64,2	3,0	29	30	96,0	37
		Nail 2	64,2	3,0	26	36		37
F1-b3-24-C	Cyclic	Nail 1	64,2	3,0	27	39	96,0	43
		Nail 2	64,2	3,0	28	28		28
F1-b3-28-C	Cyclic	Nail 1	64,2	3,0	27	32	99,0	34
		Nail 2	64,2	3,0	29	33		40
F1-b4-27-C	Cyclic	Nail 1	64,2	3,0	24	33	95,0	33
		Nail 2	64,2	3,0	29	34		34

Specimen	Test	Maximum moment (kNmm)	Corresponding rotation (rad)	Failure mode
F1-b3-26-C	Monotonic	119.77	0.52	-
F1-b5-28-C	Monotonic	134.58	0.46	-
F1-b3-24-C	Cyclic	92.72	0.37	Bending failure of both nails
F1-b3-28-C	Cyclic	81.64	0.19	Bending failure of both nails
F1-b4-27-C	Cyclic	106.17	0.34	Bending failure of both nails

   *   Cyclic loading scheme was based on a yield displacement of 15 mm.

   **   Minimum displacement rate for cyclic tests was 0.1 mm/s.

   ***   Time between zero and maximum displacement was 10 s for each cycle of the cyclic loading scheme.

   ****   Missing geometry data is denoted by "-".

D

SPECIFICATIONS OF SCREWED CONNECTION SPECIMENS

D.1 SCREWED CONNECTION BETWEEN PANEL AND PLANK

D.1.1 LOADING PERPENDICULAR TO PLANK

(a) 3D-view   (b) top-view
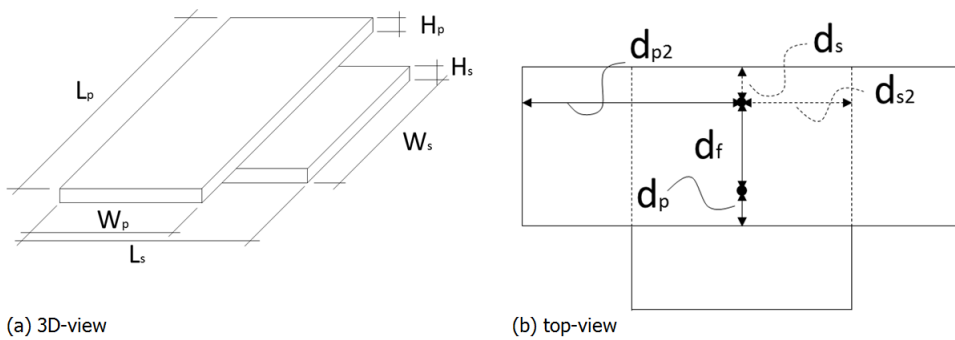
Specimen	Test	Component	Height (mm)	Width (mm)	Length (mm)	Density (kg/m³)	Moisture content (%)
S2-P29-1-B	Monotonic	Panel	17	166	251	458.1	-
		Plank	18	163	401	471.1	-
S2-P30-2-B	Cyclic	Panel	17	166	251	480.8	-
		Plank	18	162	401	426.3	-
S2-P30-3-B	Cyclic	Panel	17	166	251	460.5	-
		Plank	18	162	401	423.4	-
S2-P30-4-B	Cyclic	Panel	17	166	250	186.5	-
		Plank	18	162	401	430.4	-
S2-P30-5-B	Cyclic	Panel	17	166	250	461.3	-
		Plank	18	162	401	416.6	-
S2-P30-6-B	Cyclic	Panel	17	166	250	470.6	-
		Plank	18	162	401	437.7	-
S2-P30-7-B	Cyclic	Panel	17	166	252	484.9	-
		Plank	18	162	401	428.7	-

Specimen	Test	Component	Length (mm)	Thickness (mm)	d_s (mm)	d_p (mm)	d_{s2} (mm)	d_{p2} (mm)	d_f (mm)
S2-P29-1-B	Monotonic	Screw 1	40.0	4.5	43	44	80	179	99
		Screw 2	40.0	4.5	109	22	74	174	
S2-P30-2-B	Cyclic	Screw 1	40.0	4.5	44	43	83	192	98
		Screw 2	40.0	4.5	111	21	79	190	
S2-P30-3-B	Cyclic	Screw 1	40.0	4.5	42	42	80	199	99
		Screw 2	40.0	4.5	111	22	73	193	
S2-P30-4-B	Cyclic	Screw 1	40.0	4.5	44	42	81	199	97
		Screw 2	40.0	4.5	108	22	83	193	
S2-P30-5-B	Cyclic	Screw 1	40.0	4.5	44	42	81	199	97
		Screw 2	40.0	4.5	108	22	83	193	
S2-P30-6-B	Cyclic	Screw 1	40.0	4.5	43	42	81	192	98
		Screw 2	40.0	4.5	110	22	77	188	
S2-P30-7-B	Cyclic	Screw 1	40.0	4.5	42	41	82	190	98
		Screw 2	40.0	4.5	111	23	78	186	

Specimen	Test	Maximum load (kN)	Corresponding displacement (mm)	Failure mode
S2-P29-1-B	Monotonic	3.73	15.37	Pulling out of both screws
S2-P30-2-B	Cyclic	3.38	13.31	Pulling out of both screws
S2-P30-3-B	Cyclic	3.19	13.80	Pulling out of both screws
S2-P30-4-B	Cyclic	3.58	13.33	Pulling out of both screws
S2-P30-5-B	Cyclic	3.22	12.66	Pulling out of both screws
S2-P30-6-B	Cyclic	3.10	12.86	Pulling out of one screw, bending failure of one screw
S2-P30-7-B	Cyclic	3.43	9.43	Pulling out of both screws

*   Cyclic loading scheme was based on a yield displacement of 24 mm for the first three specimens, 16 mm for the other specimens.

**   Minimum displacement rate for cyclic tests was 0.1 mm/s.

***   Time between zero and maximum displacement was 10 s for each cycle of the cyclic loading scheme.

****   Parameters denoted in red are likely measured incorrectly.

D.1.2 LOADING PARALLEL TO PLANK

(a) 3D-view   (b) top-view
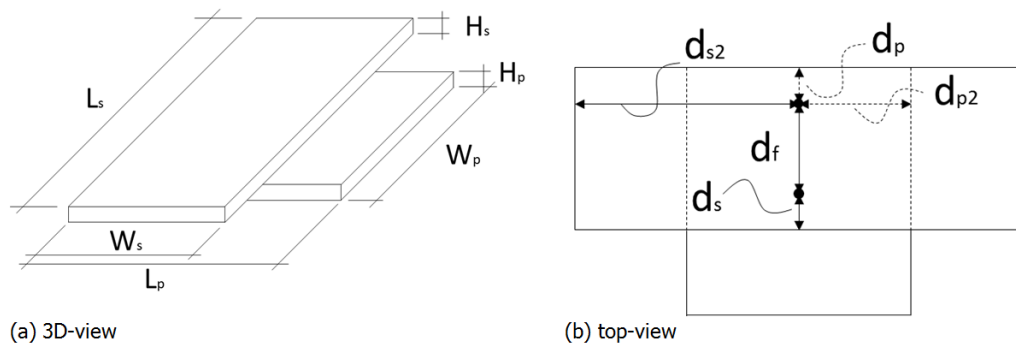
Specimen	Test	Component	Height (mm)	Width (mm)	Length (mm)	Density (kg/m³)	Moisture content (%)
P29-S2-1-B	Monotonic	Plank	18	163	250	451.9	-
		Panel	18	166	400	462.1	-
P29-S2-2-B	Cyclic	Plank	18	163	250	454.3	-
		Panel	18	166	400	460.8	-
P29-S2-3-B	Cyclic	Plank	18	164	250	455.9	-
		Panel	17	166	400	462.3	-
P29-S2-4-B	Cyclic	Plank	18	163	250	452.7	-
		Panel	17	166	400	465.0	-
P29-S2-5-B	Cyclic	Plank	18	163	250	458.9	-
		Panel	17	166	400	467.8	-
P29-S2-6-B	Cyclic	Plank	18	163	250	448.3	-
		Panel	17	166	400	472.7	-
P29-S2-7-B	Cyclic	Plank	18	162	250	453.4	-
		Panel	18	166	400	488.8	-

Specimen	Test	Component	Length (mm)	Thickness (mm)	d_p (mm)	d_s (mm)	d_{p2} (mm)	d_{s2} (mm)	d_f (mm)
P29-S2-1-B	Monotonic	Screw 1	40.0	4.5	35	37	75	190	90
		Screw 2	40.0	4.5	123	37	75	189	
P29-S2-2-B	Cyclic	Screw 1	40.0	4.5	38	39	82	187	92
		Screw 2	40.0	4.5	124	35	81	191	
P29-S2-3-B	Cyclic	Screw 1	40.0	4.5	35	39	69	189	90
		Screw 2	40.0	4.5	124	38	72	192	
P29-S2-4-B	Cyclic	Screw 1	40.0	4.5	35	38	80	190	91
		Screw 2	40.0	4.5	125	37	81	192	
P29-S2-5-B	Cyclic	Screw 1	40.0	4.5	37	40	81	188	91
		Screw 2	40.0	4.5	95	35	81	191	
P29-S2-6-B	Cyclic	Screw 1	40.0	4.5	34	37	78	189	90
		Screw 2	40.0	4.5	124	38	80	191	
P29-S2-7-B	Cyclic	Screw 1	40.0	4.5	37	37	77	188	91
		Screw 2	40.0	4.5	122	36	74	191	

Specimen	Test	Maximum load (kN)	Corresponding displacement (mm)	Failure mode
P29-S2-1-B	Monotonic	3.93	18.30	Crack in plank, pulling out of one screw
P29-S2-2-B	Cyclic	3.43	11.73	Pulling out of one screw, bending failure of one screw
P29-S2-3-B	Cyclic	3.96	11.31	Crack in plank
P29-S2-4-B	Cyclic	3.79	15.42	Pulling out of both screws
P29-S2-5-B	Cyclic	3.99	14.47	Pulling out of both screws
P29-S2-6-B	Cyclic	3.85	11.44	Pulling out of both screws
P29-S2-7-B	Cyclic	3.73	11.75	Pulling out of both screws

*   Cyclic loading scheme was based on a yield displacement of 20 mm.

**   Minimum displacement rate for cyclic tests was 0.1 mm/s.

***   Time between zero and maximum displacement was 10 s for each cycle of the cyclic loading scheme.

**** Parameters denoted in red are likely measured incorrectly.

D.2 SCREWED CONNECTION BETWEEN PANEL, PLANK AND BEAM

D.2.1 LOADING PARALLEL TO JOIST

(a) 3D-view   (b) top-view
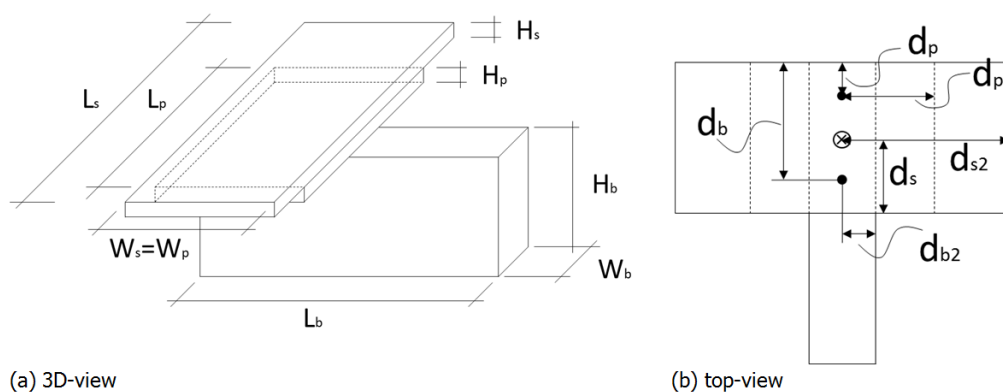
Specimen	Test	Component	Height (mm)	Width (mm)	Length (mm)	Density (kg/m³)	Moisture content (%)
B1-P31-S1-1-B	Monotonic	Joist	128	59	300	373.9	
		Plank	18	163	150	407.2	
		Panel	17	166	400	504.4	-
B1-P31-S1-4-B	Cyclic	Joist	128	59	300	378.1	-
		Plank	18	163	149	393.1	
		Panel	17	166	401	492.6	-
B1-P31-S1-7-B	Cyclic	Joist	128	59	300	378.5	-
		Plank	18	163	134	373.6	
		Panel	17	166	401	484.7	-
B2-P31-S1-2-B	Cyclic	Joist	128	59	300	369.6	-
		Plank	18	163	50	373.4	
		Panel	17	166	401	477.4	-
B2-P31-S1-3-B	Cyclic	Joist	128	59	300	377.2	-
		Plank	18	163	149	377.5	
		Panel	17	166	401	499.9	-
B2-P31-S1-5-B	Cyclic	Joist	128	59	300	368.2	-
		Plank	18	163	150	384.7	
		Panel	17	166	400	477.2	-
B2-P31-S1-6-B	Cyclic	Joist	128	59	300	376.4	-
		Plank	18	163	128	372.9	
		Panel	17	166	401	480.1	-

Specimen	Test	Component	Length (mm)	Thickness (mm)	d_b (mm)	d_p (mm)	d_s (mm)	d_{b2} (mm)	d_{p2} (mm)	d_{s2} (mm)
B1-P31-S1-1-B	Monotonic	Nail 1	64.2	3.0	35	36		27	74	
		Nail 2	64.2	3.0	124	38		27	73	
		Screw	70.0	5.0	77	77	76	22	68	189
B1-P31-S1-4-B	Cyclic	Nail 1	64.2	3.0	35	33		27	73	
		Nail 2	64.2	3.0	127	35		28	73	
		Screw	75.0	5.0	84	79	82	27	74	192
B1-P31-S1-7-B	Cyclic	Nail 1	64.2	3.0	37	35		26	57	
		Nail 2	64.2	3.0	127	34		22	62	
		Screw	75.0	5.0	81	81	81	22	59	191
B2-P31-S1-2-B	Cyclic	Nail 1	64.2	3.0	40	35		26	72	
		Nail 2	64.2	3.0	135	29		28	71	
		Screw	75.0	5.0	79	78	78	26	71	200
B2-P31-S1-3-B	Cyclic	Nail 1	64.2	3.0	34	35		28	74	
		Nail 2	64.2	3.0	130	34		29	73	
		Screw	75.0	5.0	82	80	83	26	71	192
B2-P31-S1-5-B	Cyclic	Nail 1	64.2	3.0	24	24		28	74	
		Nail 2	64.2	3.0	137	27		27	72	
		Screw	75.0	5.0	83	81	81	28	75	198
B2-P31-S1-6-B	Cyclic	Nail 1	64.2	3.0	39	33		23	57	
		Nail 2	64.2	3.0	122	41		25	57	
		Screw	75.0	5.0	76	75	74	29	63	199

Specimen	Test	Maximum load (kN)	Corresponding displacement (mm)	Failure mode
B1-P31-S1-1-B	Monotonic	3.35	26.70	Pulling out of nails and screw
B1-P31-S1-4-B	Cyclic	3.43	18.06	Pulling out/bending failure of screw
B1-P31-S1-7-B	Cyclic	2.80	23.78	Pulling out of screw
B2-P31-S1-2-B	Cyclic	3.18	17.06	Pulling out of screw
B2-P31-S1-3-B	Cyclic	3.36	13.93	Pulling out of screw
B2-P31-S1-5-B	Cyclic	3.20	14.05	Pulling out of screw
B2-P31-S1-6-B	Cyclic	2.87	18.88	Pulling out of screw

*   Cyclic loading scheme was based on a yield displacement of 24 mm.

**   Minimum displacement rate for cyclic tests was 0.1 mm/s.

***   Time between zero and maximum displacement was 10 s for each cycle of the cyclic loading scheme.

****   Parameters denoted in red are likely measured incorrectly.

D.2.2 Loading perpendicular to joist
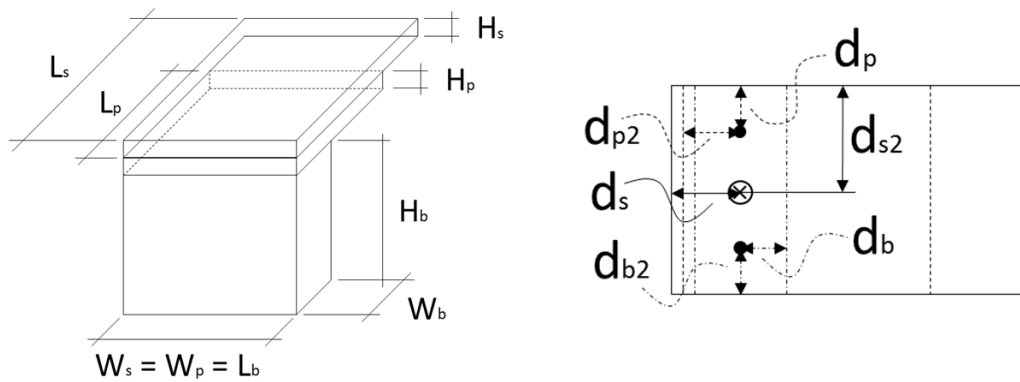
(a) 3D-view   (b) top-view

Specimen	Test	Component	Height (mm)	Width (mm)	Length (mm)	Density (kg/m^3)	Moisture content (%)
B2-S1-P31-1-A	Monotonic	Joist	128	59	166	342.1	-
		Plank	18	164	152	375.4	
		Panel	17	166	217	482.0	-
B2-S1-P31-2-A	Cyclic	Joist	128	59	165	382.2	-
		Plank	18	164	153	386.7	
		Panel	17	166	218	472.9	-
B2-S1-P31-3-A	Cyclic	Joist	128	59	166	379.4	-
		Plank	18	163	152	368.6	
		Panel	17	166	216	505.7	-
B2-S1-P31-4-A	Cyclic	Joist	128	59	165	372.9	-
		Plank	18	163	153	386.1	
		Panel	17	166	216	492.6	-
B2-S1-P31-5-A	Cyclic	Joist	128	59	165	371.3	-
		Plank	18	163	153	385.3	
		Panel	17	166	218	498.3	-
B2-S1-P31-6-A	Cyclic	Joist	127	58	165	380.2	-
		Plank	18	163	153	379.9	
		Panel	17	166	218	488.1	-
B2-S1-P31-7-A	Cyclic	Joist	128	59	165	367.0	-
		Plank	18	163	152	401.2	
		Panel	17	166	217	485.1	-

Specimen	Test	Component	Length (mm)	Thickness (mm)	d_b (mm)	d_p (mm)	d_s (mm)	d_{b2} (mm)	d_{p2} (mm)	d_{s2} (mm)
B2-S1-P31-1-A	Monotonic	Nail 1	64.2	3.0	28	28		50	52	
		Nail 2	64.2	3.0	28	28		36	32	
		Screw	70.0	5.0	26	29	30	76	78	78
B2-S1-P31-2-A	Cyclic	Nail 1	64.2	3.0	29	29		46	49	
		Nail 2	64.2	3.0	25	27		41	33	
		Screw	75.0	5.0	25	34	35	79	72	77
B2-S1-P31-3-A	Cyclic	Nail 1	64.2	3.0	26	27		36	37	
		Nail 2	64.2	3.0	25	27		47	42	
		Screw	75.0	5.0	28	36	28	76	73	81
B2-S1-P31-4-A	Cyclic	Nail 1	64.2	3.0	27	28		55	50	
		Nail 2	64.2	3.0	29	29		45	45	
		Screw	75.0	5.0	27	27	28	78	75	79
B2-S1-P31-5-A	Cyclic	Nail 1	64.2	3.0	26	25		39	38	
		Nail 2	64.2	3.0	29	27		37	36	
		Screw	75.0	5.0	28	29	31	76	78	77
B2-S1-P31-6-A	Cyclic	Nail 1	64.2	3.0	23	26		38	39	
		Nail 2	64.2	3.0	29	27		37	35	
		Screw	75.0	5.0	28	29	29	76	78	80
B2-S1-P31-7-A	Cyclic	Nail 1	64.2	3.0	28	30		37	37	
		Nail 2	64.2	3.0	27	28		46	37	
		Screw	75.0	5.0	25	27	29	79	80	78

Specimen	Test	Maximum load (kN)	Corresponding displacement (mm)	Failure mode
B2-S1-P31-1-A	Monotonic	2.86	33.30	Pulling out of nails and screw
B2-S1-P31-2-A	Cyclic	3.08	14.62	Failure of nail and screw
B2-S1-P31-3-A	Cyclic	3.02	19.37	Failure of screw
B2-S1-P31-4-A	Cyclic	3.02	14.60	Failure of screw
B2-S1-P31-5-A	Cyclic	3.04	11.92	Pulling out of nails and screw
B2-S1-P31-6-A	Cyclic	3.39	14.15	Bending failure of screw
B2-S1-P31-7-A	Cyclic	3.23	17.41	Bending failure of screw

*   Cyclic loading scheme was based on a yield displacement of 7.2 mm.

** Minimum displacement rate for cyclic tests was 0.1 mm/s.

*** Time between zero and maximum displacement was 10 s for each cycle of the cyclic loading scheme.

**** Parameters denoted in red are likely measured incorrectly.

INPUT PARAMETERS FOR BOARDS AND JOISTS

		Ex (N/mm^2)	Ey/Ex	Ey (N/mm^2)	Ez/Ex	Ez (N/mm^2)	Gxz/Ex	Gxz (N/mm^2)	Gxy/Ex	Gxy (N/mm^2)	Gzy/Ex	Gzy (N/mm^2)	υxz	υxy	υyz
Beams	b1	15470.17	0.06	926.4911	0.0979	1514.357	0.07967	1232.457	0.07133	1103.539	0.01122	173.6096	0.33522	0.35778	0.35011
	b2	13499.80	0.06	808.4881	0.0979	1321.481	0.07967	1075.484	0.07133	962.9859	0.01122	151.4978	0.33522	0.35778	0.35011
	b3	11367.48	0.06	680.7856	0.0979	1112.75	0.07967	905.609	0.07133	810.88	0.01122	127.5684	0.33522	0.35778	0.35011
	b4	10913.73	0.06	653.6109	0.0979	1068.332	0.07967	869.4601	0.07133	778.5124	0.01122	122.4762	0.33522	0.35778	0.35011
	b5	14334.79	0.06	858.4949	0.0979	1403.217	0.07967	1142.005	0.07133	1022.549	0.01122	160.8682	0.33522	0.35778	0.35011
	p01	10571.15	0.06	633.0943	0.0979	1034.798	0.07967	842.1681	0.07133	754.0752	0.01122	118.6318	0.33522	0.35778	0.35011
	p02	9713.44	0.06	581.7274	0.0979	950.8383	0.07967	773.8378	0.07133	692.8924	0.01122	109.0064	0.33522	0.35778	0.35011
	p03	15565.62	0.06	932.2077	0.0979	1523.701	0.07967	1240.061	0.07133	1110.348	0.01122	174.6809	0.33522	0.35778	0.35011
	p04	12849.32	0.06	769.5315	0.0979	1257.806	0.07967	1023.663	0.07133	916.5848	0.01122	144.1979	0.33522	0.35778	0.35011
	p05	14709.61	0.06	880.9419	0.0979	1439.907	0.07967	1171.865	0.07133	1049.285	0.01122	165.0745	0.33522	0.35778	0.35011
	p06	15872.88	0.06	950.6091	0.0979	1553.778	0.07967	1264.539	0.07133	1132.265	0.01122	178.129	0.33522	0.35778	0.35011
	p07	7231.15	0.06	433.0653	0.0979	707.8489	0.07967	576.0813	0.07133	515.8218	0.01122	81.14953	0.33522	0.35778	0.35011
	p08	12586.55	0.06	753.7942	0.0979	1232.083	0.07967	1002.728	0.07133	897.8402	0.01122	141.249	0.33522	0.35778	0.35011
	p09	6520.15	0.06	390.4848	0.0979	638.2506	0.07967	519.4389	0.07133	465.1043	0.01122	73.17062	0.33522	0.35778	0.35011
	p10	9433.77	0.06	564.9778	0.0979	923.461	0.07967	751.5568	0.07133	672.9421	0.01122	105.8678	0.33522	0.35778	0.35011
	p11	10041.10	0.06	601.3504	0.0979	982.9122	0.07967	799.9411	0.07133	716.2652	0.01122	112.6835	0.33522	0.35778	0.35011
	p12	13453.39	0.06	805.7083	0.0979	1316.937	0.07967	1071.786	0.07133	959.6749	0.01122	150.9769	0.33522	0.35778	0.35011
	p13	10668.95	0.06	638.9518	0.0979	1044.372	0.07967	849.96	0.07133	761.0521	0.01122	119.7294	0.33522	0.35778	0.35011
	p14	8969.29	0.06	537.161	0.0979	877.9941	0.07967	714.5537	0.07133	639.8096	0.01122	100.6554	0.33522	0.35778	0.35011
Boards	p15	10958.00	0.06	656.2623	0.0979	1072.666	0.07967	872.9872	0.07133	781.6705	0.01122	122.9731	0.33522	0.35778	0.35011
	p16	13541.39	0.06	810.9791	0.0979	1325.552	0.07967	1078.798	0.07133	965.9528	0.01122	151.9645	0.33522	0.35778	0.35011
	p17	10643.49	0.06	637.4269	0.0979	1041.88	0.07967	847.9316	0.07133	759.2358	0.01122	119.4436	0.33522	0.35778	0.35011
	p18	10740.30	0.06	643.2248	0.0979	1051.356	0.07967	855.6441	0.07133	766.1416	0.01122	120.5301	0.33522	0.35778	0.35011
	p19	10882.52	0.06	651.7418	0.0979	1065.277	0.07967	866.9738	0.07133	776.2862	0.01122	122.126	0.33522	0.35778	0.35011
	p20	12064.20	0.06	722.5117	0.0979	1180.951	0.07967	961.1148	0.07133	860.5798	0.01122	135.3872	0.33522	0.35778	0.35011
	p21	9619.90	0.06	576.1251	0.0979	941.6813	0.07967	766.3853	0.07133	686.2195	0.01122	107.9566	0.33522	0.35778	0.35011
	p22	15352.57	0.06	919.4486	0.0979	1502.846	0.07967	1223.088	0.07133	1095.15	0.01122	172.29	0.33522	0.35778	0.35011
	p23	11452.01	0.06	685.8479	0.0979	1121.024	0.07967	912.3431	0.07133	816.9098	0.01122	128.517	0.33522	0.35778	0.35011
	p24	9128.71	0.06	546.7081	0.0979	893.599	0.07967	727.2537	0.07133	651.1811	0.01122	102.4444	0.33522	0.35778	0.35011
	p25	15041.38	0.06	900.8115	0.0979	1472.384	0.07967	1198.297	0.07133	1072.952	0.01122	168.7977	0.33522	0.35778	0.35011
	p26	11358.83	0.06	680.2675	0.0979	1111.903	0.07967	904.9198	0.07133	810.2629	0.01122	127.4713	0.33522	0.35778	0.35011
	p27	15715.94	0.06	941.2105	0.0979	1538.416	0.07967	1252.037	0.07133	1121.071	0.01122	176.3678	0.33522	0.35778	0.35011
	p28	8327.67	0.06	498.735	0.0979	815.1865	0.07967	663.4378	0.07133	594.0406	0.01122	93.45498	0.33522	0.35778	0.35011
	p29	11419.32	0.06	683.8905	0.0979	1117.825	0.07967	909.7394	0.07133	814.5783	0.01122	128.1502	0.33522	0.35778	0.35011
	p30	13849.46	0.06	829.4287	0.0979	1355.708	0.07967	1103.34	0.07133	987.928	0.01122	155.4217	0.33522	0.35778	0.35011

Measured data in laboratory
Data from Wood Handbook
Input parameters calculated from measured data and data from Wood Handbook

*   Young's modulus E_x is taken as the measured dynamic Young's modulus.

**   The (Poisson's) ratios taken from the Wood Handbook are taken as the average values for pinewood.

F

ANSYS MECHANICAL APDL SCRIPT FOR COARSE MESH FOR AS-BUILT DIAPHRAGM

- **ANSYS APDL scripting language**
- **Script read from top to bottom**
- **ANSYS specific commands**
- **Commands from online database**
- **Starting a line with '!' indicates a comment and will not be read**

!——**START OF SCRIPT**——
FINISH
/CLEAR,NOSTART   !Restarts database

!——**PREPROCESSING**——

/PREP7   !Enter preprocessor
/NERR,-5,99999999,,,   !Limits number of displayed warn-
                                                  ing and error messages
/UNITS,USER,0.001,,,,,,   !User defined units (mm, kg, s, N)

!——DEFINE ELEMENT TYPES——

ET,1,COMBIN40,0,,1,0,,1
!Spring 1 perpendicular to joist - UX

R,1,100000,0,0,0,192,4.22
!Real constants for spring 1: K1,C,M,GAP,FSLIDE, K2

ET,2,COMBIN40,0,,1,0,,1
!Spring 2,3 perpendicular to joist - UX

R,2,250,0,0,0.001,450,50
!Real constants for spring 2,3: K1,C,M,GAP,FSLIDE, K2. **This is changed to: R,2,150,0,0,0.001,700,0.0001 for the second calibration method.**

ET,4,COMBIN40,0,,2,0,,1
!Spring 1 parallel to joist - UY

R,4,100000,0,0,0,145,2.5
!Real constants for spring 1: K1,C,M,GAP,FSLIDE, K2

ET,5,COMBIN40,0,,2,0,,1
!Spring 2,3 parallel to joist - UY

R,5,210,0,0,0.001,700,45
!Real constants for spring 2,3: K1,C,M,GAP,FSLIDE, K2. **This is changed to: R,5,500,0,0,0.001,840,0.001 for the second calibration approach.**

ET,7,SHELL181,
!Shell element for the planks

R,7,tplanks,tplanks,tplanks,tplanks,
!Real constants for shell elements

ET,8,BEAM188,
!Beam element for the beams

SECTYPE,8,BEAM,RECT,
!Section type for beam elements

SECDATA,60,130
!Section data for beam elements

!——DEFINE MATERIAL PROPERTIES——

*DIM,tablemat,TABLE,27,8
!Create table with size 27x8 named 'tablemat'

*TREAD,tablemat,matpropp,csv,,
!Read data from matpropp.csv into table 'tablemat'

*DIM,materprop,ARRAY,28,9
!Create array with size 28x9 named 'materprop'

*MFUN,materprop(1,1),copy,tablemat(0,0)
!Copy 'tablemat' into 'materprop'

*DEL,tablemat(1)
!Delete table 'tablemat'

```
*DO,j,1,23                              !Do-loop to define material prop-
                                         erties for 23 planks from array
                                         'materprop'

   MP,EX,j,materprop(j,1)               !E_x
   MP,EY,j,materprop(j,2)               !E_y
   MP,EZ,j,materprop(j,3)               !E_z
   MP,GXY,j,materprop(j,4)              !G_{xy}
   MP,GYZ,j,materprop(j,5)              !G_{yz}
   MP,GXZ,j,materprop(j,6)              !G_{xz}
   MP,PRXY,j,materprop(j,7)             !v_{xy}
   MP,PRYZ,j,materprop(j,8)             !v_{yz}
   MP,PRXZ,j,materprop(j,9)             !v_{xz}
*ENDDO                                  !End do-loop


*DO,j,1,4                               !Do-loop to define material prop-
                                         erties for 4 beams from array
                                         'materprop'

   MP,EX,j+23,materprop(j+24,1)         !E_x
   MP,EY,j+23,materprop(j+24,2)         !E_y
   MP,EZ,j+23,materprop(j+24,3)         !E_z
   MP,GXY,j+23,materprop(j+24,4)        !G_{xy}
   MP,GYZ,j+23,materprop(j+24,5)        !G_{yz}
   MP,GXZ,j+23,materprop(j+24,6)        !G_{xz}
   MP,PRXY,j+23,materprop(j+24,7)       !v_{xy}
   MP,PRYZ,j+23,materprop(j+24,8)       !v_{yz}
   MP,PRXZ,j+23,materprop(j+24,9)       !v_{xz}
*ENDDO                                  !End do-loop



!——CREATE NODES——

!BEAMS
N,1,30,0,-74.5                          !First node for top beam, 48 nodes
                                         per beam

N,2,30,32.5,-74.5
N,3,30,132.5,-74.5
NGEN,23,2,2,3,1,0,167,,                 !Generate other nodes on top
                                         beam

N,48,30,3870,-74.5                      !Last node on top beam
NGEN,4,48,1,48,1,650,0,0,              !Replicate top beam for other
                                         beams


!PLANKS
N,193,0,0,0                             !First node for first plank (edge
                                         y=0), 22 nodes per edge

N,194,30,0,0
```

```
N,199,680,0,0
FILL
NGEN,4,5,195,199,1,650,0,0
N,215,2680,0,0                          !Last node on first edge
NGEN,2,23,193,215,1,0,32.5,0            !Place nodes at y=32.5 mm
NGEN,2,46,193,215,1,0,132.5,0           !Place nodes at y=132.5 mm
NGEN,2,69,193,215,1,0,165,0             !Place nodes at y=165 mm
NGEN,23,92,193,284,1,0,167,0            !Replicate first plank for other
                                         planks


!——CREATE ELEMENTS——

!BEAMS
TYPE,8                                  !Activates element type 8
REAL,8                                  !Activates real constant number 8
SECNUM,8                                !Activates section number 8

N,15000,30,0,50                         !Keypoint (orientation node) for
                                         beam 2
N,15001,680,0,50                        !Keypoint (orientation node) for
                                         beam 3
N,15002,1330,0,50                       !Keypoint (orientation node) for
                                         beam 4
N,15003,1980,0,50                       !Keypoint (orientation node) for
                                         beam 5

*DO,n,1,4                               !Do-loop to create beam elements
   MAT,n+23                             !Set material properties
   *DO,j,1+48*(n-1),47+48*(n-1)
     E,j,j+1,15000+(n-1)
   *ENDDO
*ENDDO                                  !End do-loop

!PLANKS
TYPE,7                                  !Activates element type 7
REAL,7                                  !Activates real constant number 7
```

```
*DO,n,1,23                              !Do-loop to create shell elements
  MAT,n                                 !Set material properties
  *DO,i,1,3
    *DO,j,193+23*(i-1)+92*(n-1),214+23*(i-
1)+92*(n-1)
      E,j, j+1, j+24, j+23
    *ENDDO
  *ENDDO
*ENDDO                                  !End do-loop

!NAILS
!UX                                     !Nails in u_x, 2 springs from node i-j
                                        !i= node on beam, j =node on plank
                                        !2 nails per intersection, 4 rows per
                                        plank, 23 planks

*DO,n,1,2                               !Do-loop to create 2 spring ele-
                                        ments
  TYPE,n                                !Activates element type n
  REAL,n                                !Activates real constant set n
  *DO,i,1,23                            !23 planks
    *DO,j,1,4                           !4 rows per plank
      E,2+48*(j-1)+2*(i-1),217+5*(j-1)+92*(i-1)
      E,3+48*(j-1)+2*(i-1),240+5*(j-1)+92*(i-1)
    *ENDDO
  *ENDDO
*ENDDO                                  !End do-loop

!UX                                     !Nails in u_x, 1 spring from node j-i

TYPE,2                                  !Activates element type 2
REAL,2                                  !Activates real constant number 2

*DO,i,1,23                             !Do-loop to create 1 spring ele-
                                        ment
  *DO,j,1,4
    E,217+5*(j-1)+92*(i-1),2+48*(j-1)+2*(i-1)
    E,240+5*(j-1)+92*(i-1),3+48*(j-1)+2*(i-1)
  *ENDDO
*ENDDO                                  !End do-loop
```

```
!UY                                                !Nails in u_y, 2 springs from node i-j
                                                   !i= node on beam, j =node on plank
                                                   !2 nails per intersection, 4 rows per
                                                   plank, 23 planks


*DO,n,1,2                                          !Do-loop to create 2 spring ele-
                                                   ments
  TYPE,n+3                                         !Activates element type n+3
  REAL,n+3                                         !Activates real constant set n+3
   *DO,i,1,23                                      !23 planks
     *DO,j,1,4                                     !4 rows per plank
        E,2+48*(j-1)+2*(i-1),217+5*(j-1)+92*(i-1)
        E,3+48*(j-1)+2*(i-1),240+5*(j-1)+92*(i-1)
     *ENDDO
   *ENDDO
*ENDDO                                             !End do-loop


!UY                                                !Nails in u_y, 1 spring from node j-i


TYPE,5                                             !Activates element type 5
REAL,5                                             !Activates real constant number 5


*DO,i,1,23                                         !Do-loop to create 1 spring ele-
                                                   ment

  *DO,j,1,4
     E,217+5*(j-1)+92*(i-1),2+48*(j-1)+2*(i-1)
     E,240+5*(j-1)+92*(i-1),3+48*(j-1)+2*(i-1)
  *ENDDO
*ENDDO                                             !End do-loop




!——DEFINE BOUNDARY CONDITIONS——

!LOWER EDGE (x=2680 mm)
*DO,n,1,92                                         !Do-loop
  i=215+23*(n-1)                                   !Nodes at lower edge
  D,i,UX,0,,i,1,UY,UZ,ROTX,ROTY,ROTZ              !Constrain nodes for all DOFs
*ENDDO                                             !End do-loop

!UPPER EDGE (x=0 mm)
*DO,n,1,92                                         !Do-loop
  i=193+23*(n-1)                                   !Nodes at upper edge
  D,i,UZ,0,,i,1,ROTX,,,                            !Constrain for UZ and ROTX
*ENDDO                                             !End do-loop
```

```
!BEAMS
*DO,n,1,192                              !Do-loop
  D,n,UZ,0,,n,1,,ROTY                    !Constrain for UZ and ROTY
*ENDDO                                   !End do-loop



!——DEFINE LOADS——

*DIM,loading,TABLE,7850,1,1,TIME,DISPL   !Create table for loading
*TREAD,loading,lsasb,csv,,              !Read data from csv into table



/ESHAPE,1                                !Display elements with shapes
ALLSEL,ALL                               !Select all entities

FINISH                                   !Exit preprocessor
```

!——**SOLUTION**——

```
/SOLU                                    !Enter solution processor
ANTYPE,STATIC                            !Specify analysis type
NROPT,,,                                 !Specify Newton-Raphson controls
NSUBST,30000,30000,1                     !Number of substeps at load step
AUTOTS,ON                                !Automatic time stepping on
KBC,0                                    !Ramped load steps
NEQIT,2000,                              !Maximum number of iterations

NLDIAG,NRRE,ON                           !Nonlinear diagnostics
OUTRES,BASIC                             !Write basic output in result file

tm_start=0.000001                        !Start time
tm_end=1570                              !End time
tm_incr=0.5                              !Load step size

*DO,tm,tm_start,tm_end,tm_incr           !Do-loop to solve for each time
                                          step
  TIME,tm                                !Set time
  D,1,UY,loading(tm),,48,,               !Set loading on top beam
  SOLVE                                  !Solve
*ENDDO                                   !End do-loop
```

```
FINISH                                          !Exit solution processor



!——POSTPROCESSING——


/POST26                                         !Enter time-history postprocessor

/RGB,INDEX,100,100,100, 0                       !Set background to white
/RGB,INDEX, 80, 80, 80,13
/RGB,INDEX, 60, 60, 60,14
/RGB,INDEX, 0, 0, 0,15


/PBC,U,,1,                                       !Show boundary conditions


NUMVAR,200                                       !Set maximum number of variables
                                                  to 200


!——STORE DISPLACEMENT——
NSOL,2,1,U,Y,uynode1                             !Store u_y of node 1 into variable 2
*dim,uynode1,ARRAY,8000,1                        !Create array parameter for uyn-
                                                  ode1

VGET,uynode1(1),2                                !Store time-history data of variable
                                                  2 into uynode1

*CFOPEN,uynode1,csv                              !Open csv-file
*VWRITE,uynode1(1)                               !Write array in given format to file
                                                  'uynode1.csv'

(F11.5)                                          !Format
*CFCLOSE                                         !Close csv-file


!——STORE REACTION FORCES——
*dim,recforces,ARRAY,8000,93                     !Create array
*DO,n,1,92                                       !Do-loop to store reaction forces in
                                                  array

  j=n+3
  i=215+23*(n-1)
  RFORCE,j,i,F,Y,
  VGET,recforces(1,n),j
*ENDDO                                           !End do-loop


*MWRITE,recforces(1,1),reactionss,txt,,JIK,93,8000,1   !Write reaction forces to file
(92F11.5)                                        !Format


FINISH                                           !Exit postprocessor
```

G

ANSYS MECHANICAL APDL SCRIPT FOR FINE MESH FOR AS-BUILT DIAPHRAGM

```
FINISH
/CLEAR,NOSTART                          !Restarts database


!——PREPROCESSING——


/PREP7                                  !Enter preprocessor
/NERR,-5,99999999,,,                    !Limits number of displayed warn-
                                         ing and error messages

/UNITS,USER,0.001,,,,,,                 !User defined units (mm, kg, s, N)



!——DEFINE ELEMENT TYPES——

ET,1,COMBIN40,0,,1,0,,1                 !Spring 1 perpendicular to joist -
                                         UX
R,1,100000,0,0,0,192,4.22              !Real constants for spring 1:
                                         K1,C,M,GAP,FSLIDE, K2
ET,2,COMBIN40,0,,1,0,,1                 !Spring 2,3 perpendicular to joist -
                                         UX
R,2,250,0,0,0.001,450,50               !Real constants for spring
                                         2,3:       K1,C,M,GAP,FSLIDE,
                                         K2. This is changed to:
                                         R,2,150,0,0,0.001,700,0.0001 for
                                         the second calibration method.
ET,4,COMBIN40,0,,2,0,,1                 !Spring 1 parallel to joist - UY
R,4,100000,0,0,0,145,2.5               !Real constants for spring 1:
                                         K1,C,M,GAP,FSLIDE, K2
ET,5,COMBIN40,0,,2,0,,1                 !Spring 2,3 parallel to joist - UY
R,5,210,0,0,0.001,700,45               !Real constants for spring
                                         2,3:       K1,C,M,GAP,FSLIDE,
                                         K2. This is changed to:
                                         R,5,500,0,0,0.001,840,0.001 for
                                         the second calibration approach.
ET,7,SHELL181,                          !Shell element for the planks
```

```
R,7,tplanks,tplanks,tplanks,tplanks,          !Real constants for shell elements
ET,8,BEAM188,                                  !Beam element for the beams
SECTYPE,8,BEAM,RECT,                           !Section type for beam elements
SECDATA,60,130                                 !Section data for beam elements


!——DEFINE MATERIAL PROPERTIES——


*DIM,tablemat,TABLE,27,8                        !Create table with size 27x8 named
                                               'tablemat'

*TREAD,tablemat,matpropp,csv,,                  !Read data from matpropp.csv into
                                               table 'tablemat'

*DIM,materprop,ARRAY,28,9                       !Create array with size 28x9 named
                                               'materprop'

*MFUN,materprop(1,1),copy,tablemat(0,0)         !Copy 'tablemat' into 'materprop'
*DEL,tablemat(1)                                !Delete table 'tablemat'


*DO,j,1,23                                      !Do-loop to define material prop-
                                               erties for 23 planks from array
                                               'materprop'

   MP,EX,j,materprop(j,1)                       !E_x
   MP,EY,j,materprop(j,2)                       !E_y
   MP,EZ,j,materprop(j,3)                       !E_z
   MP,GXY,j,materprop(j,4)                      !G_{xy}
   MP,GYZ,j,materprop(j,5)                      !G_{yz}
   MP,GXZ,j,materprop(j,6)                      !G_{xz}
   MP,PRXY,j,materprop(j,7)                     !ν_{xy}
   MP,PRYZ,j,materprop(j,8)                     !ν_{yz}
   MP,PRXZ,j,materprop(j,9)                     !ν_{xz}
*ENDDO                                          !End do-loop


*DO,j,1,4                                       !Do-loop to define material prop-
                                               erties for 4 beams from array
                                               'materprop'

   MP,EX,j+23,materprop(j+24,1)                 !E_x
   MP,EY,j+23,materprop(j+24,2)                 !E_y
   MP,EZ,j+23,materprop(j+24,3)                 !E_z
   MP,GXY,j+23,materprop(j+24,4)                !G_{xy}
   MP,GYZ,j+23,materprop(j+24,5)                !G_{yz}
   MP,GXZ,j+23,materprop(j+24,6)                !G_{xz}
   MP,PRXY,j+23,materprop(j+24,7)               !ν_{xy}
   MP,PRYZ,j+23,materprop(j+24,8)               !ν_{yz}
   MP,PRXZ,j+23,materprop(j+24,9)               !ν_{xz}
*ENDDO                                          !End do-loop
```

!——CREATE NODES——

!BEAMS
N,1,30,0,-74.5   !First node for top beam, 139 nodes per beam

N,6,30,165,-74.5
FILL
NGEN,23,6,1,6,1,0,167,,   !Generate other nodes on top beam

N,139,30,3870,-74.5   !Last node on beam
NGEN,4,139,1,139,1,650,0,0,   !Replicate top beam for other beams

!PLANKS
N,557,0,0,0   !First node for first plank (edge y=0)

N,579,660,0,0
FILL
N,580,680,0,0
N,601,1310,0,0
FILL
NGEN,3,22,580,601,1,650,0,,
N,646,2640,0,0   !Second to last node on edge
N,647,2680,0,0   !Last node on edge
NGEN,6,91,557,647,1,0,33,,   !Generate nodes on first plank
NGEN,23,546,557,1102,1,0,167,,   !Copy first plank for rest of the planks

!——CREATE ELEMENTS——

!BEAMS
TYPE,8   !Activates element type 8
REAL,8   !Activates real constant number 8
SECNUM,8   !Activates section number 8

N,15000,30,0,50   !Keypoint (orientation node) for beam 2
N,15001,680,0,50   !Keypoint (orientation node) for beam 3
N,15002,1330,0,50   !Keypoint (orientation node) for beam 4
N,15003,1980,0,50   !Keypoint (orientation node) for beam 5

```
*DO,n,1,4                              !Do-loop to create beam elements
   MAT,n+23                            !Set material properties
   *DO,j,1+139*(n-1),138+139*(n-1)
     E,j,j+1,15000+(n-1)
   *ENDDO
*ENDDO                                 !End do-loop


!PLANKS
TYPE,7                                 !Activates element type 7
REAL,7                                 !Activates real constant number 7


*DO,n,1,23                             !Do-loop to create shell elements
   MAT,n                               !Set material properties
   *DO,i,1,5
        *DO,j,557+91*(i-1)+546*(n-1),646+91*(i-
1)+546*(n-1)
       E,j, j+1, j+92, j+91
     *ENDDO
   *ENDDO
*ENDDO                                 !End do-loop


!NAILS
!UX                                    !Nails in $u_x$, 2 springs from node i-j
                                       !i= node on beam, j =node on plank
                                       !2 nails per intersection, 4 rows per
                                       plank, 23 planks


*DO,n,1,2                              !Do-loop  to create 2 spring ele-
                                       ments
   TYPE,n                              !Activates element type n
   REAL,n                              !Activates real constant set n
   *DO,i,1,23                          !23 planks
     *DO,j,1,4                         !4rows per plank
       E,2+139*(j-1)+6*(i-1),649+22*(j-1)+546*(i-
1)
       E,5+139*(j-1)+6*(i-1),922+22*(j-1)+546*(i-
1)
     *ENDDO
   *ENDDO
*ENDDO                                 !End do-loop
```

```
!UX                                          !Nails in u_x, 1 spring from node j-i

TYPE,2                                       !Activates element type 2
REAL,2                                       !Activates real constant number 2

*DO,i,1,23                                   !Do-loop to create 1 spring ele-
                                             ment

  *DO,j,1,4
    E,649+22*(j-1)+546*(i-1),2+139*(j-1)+6*(i-1)
    E,922+22*(j-1)+546*(i-1),5+139*(j-1)+6*(i-1)
  *ENDDO
*ENDDO                                       !End do-loop

!UY                                          !Nails in u_y, 2 springs from node i-j
                                             !i= node on beam, j =node on plank
                                             !2 nails per intersection, 4 rows per
                                             plank, 23 planks

*DO,n,1,2                                    !Do-loop to create 2 spring ele-
                                             ments
  TYPE,n+3                                   !Activates element type n+3
  REAL,n+3                                   !Activates real constant set n+3
  *DO,i,1,23                                 !23 planks
    *DO,j,1,4                                !4 rows per plank
      E,2+139*(j-1)+6*(i-1),649+22*(j-1)+546*(i-
1)
      E,5+139*(j-1)+6*(i-1),922+22*(j-1)+546*(i-
1)
    *ENDDO
  *ENDDO
*ENDDO                                       !End do-loop

!UY                                          !Nails in u_y, 1 spring from node j-i

TYPE,5                                       !Activates element type 5
REAL,5                                       !Activates real constant number 5

*DO,i,1,23                                   !Do-loop to create 1 spring ele-
                                             ment

  *DO,j,1,4
    E,649+22*(j-1)+546*(i-1),2+139*(j-1)+6*(i-1)
    E,922+22*(j-1)+546*(i-1),5+139*(j-1)+6*(i-1)
  *ENDDO
*ENDDO                                       !End do-loop
```

```
!——DEFINE BOUNDARY CONDITIONS——

!LOWER EDGE (x=2680 mm)
*DO,n,1,138                                    !Do-loop
  i=647+91*(n-1)                               !Nodes at lower edge
  D,i,UX,0,,i,1,UY,UZ,ROTX,ROTY,ROTZ           !Constrain nodes for all DOFs
*ENDDO                                         !End do-loop

!UPPER EDGE (x=0 mm)
*DO,n,1,138                                    !Do-loop
  i=557+91*(n-1)                               !Nodes at upper edge
  D,i,UZ,0,,i,1,ROTX,,,                        !Constrain for UZ and ROTX
*ENDDO                                         !End do-loop

!BEAMS
*DO,n,1,556                                    !Do-loop
  D,n,UZ,0,,n,1,,ROTY                          !Constrain for UZ and ROTY
*ENDDO                                         !End do-loop


!——DEFINE LOADS——

*DIM,loading,TABLE,7850,1,1,TIME,DISPL         !Create table for loading
*TREAD,loading,lsasb,csv,,                     !Read data from csv into table



/ESHAPE,1                                      !Display elements with shapes
ALLSEL,ALL                                     !Select all entities

FINISH                                         !Exit preprocessor
```

!——**SOLUTION**——


```
/SOLU                                          !Enter solution processor
ANTYPE,STATIC                                  !Specify analysis type
NROPT,,,                                       !Specify Newton-Raphson controls
NSUBST,30000,30000,1                           !Number of substeps at load step
AUTOTS,ON                                      !Automatic time stepping on
KBC,0                                          !Ramped load steps
NEQIT,2000,                                    !Maximum number of iterations
```

```
NLDIAG,NRRE,ON                          !Nonlinear diagnostics
OUTRES,BASIC                            !Write basic output in result file

tm_start=0.000001                       !Start time
tm_end=1570                             !End time
tm_incr=0.5                             !Load step size

*DO,tm,tm_start,tm_end,tm_incr          !Do-loop to solve for each time
                                         step
  TIME,tm                               !Set time
  D,1,UY,loading(tm),,139,,             !Set loading on top beam
  SOLVE                                 !Solve
*ENDDO                                  !End do-loop

FINISH                                  !Exit solution processor
```

!——**POSTPROCESSING**——

```
/POST26                                 !Enter time-history postprocessor

/RGB,INDEX,100,100,100, 0               !Set background to white
/RGB,INDEX, 80, 80, 80,13
/RGB,INDEX, 60, 60, 60,14
/RGB,INDEX, 0, 0, 0,15

/PBC,U,,1,                              !Show boundary conditions

NUMVAR,200                              !Set maximum number of variables
                                         to 200

!——STORE DISPLACEMENT——
NSOL,2,1,U,Y,uynode1                    !Store $u_y$ of node 1 into variable 2
*dim,uynode1,ARRAY,8000,1               !Create array parameter for uyn-
                                         ode1

VGET,uynode1(1),2                       !Store time-history data of variable
                                         2 into uynode1

*CFOPEN,uynode1,csv                     !Open csv-file
*VWRITE,uynode1(1)                      !Write array in given format to file
                                         'uynode1.csv'

(F11.5)                                 !Format
*CFCLOSE                                !Close csv-file
```

```
!——STORE REACTION FORCES——
*dim,recforces,ARRAY,8000,139                          !Create array
*DO,n,1,138                                            !Do-loop to store reaction forces in
                                                       array

  j=n+3
  i=647+91*(n-1)
  RFORCE,j,i,F,Y,
  VGET,recforces(1,n),j
*ENDDO                                                 !End do-loop

*MWRITE,recforces(1,1),reactionss,txt,,JIK,139,8000,1  !Write reaction forces to file
(139F11.5)                                             !Format

FINISH                                                 !Exit postprocessor
```

H

ANSYS MECHANICAL APDL SCRIPT FOR RETROFITTED DIAPHRAGM

```
FINISH
/CLEAR,NOSTART                          !Restarts database
```

!——PREPROCESSING——

```
/PREP7                                  !Enter preprocessor
/NERR,-5,99999999,,,                    !Limits number of displayed warn-
                                        ing and error messages
/UNITS,USER,0.001,,,,,,                 !User defined units (mm, kg, s, N)
```

```
!——DEFINE ELEMENT TYPES——
```

```
ET,1,COMBIN40,0,,1,0,,1                 !Spring 1 perpendicular to joist -
                                        UX
R,1,100000,0,0,0,192,4.22              !Real constants for spring 1:
                                        K1,C,M,GAP,FSLIDE, K2
ET,2,COMBIN40,0,,1,0,,1                 !Spring 2,3 perpendicular to joist -
                                        UX
R,2,250,0,0,0.001,450,50               !Real constants for spring
                                        2,3:        K1,C,M,GAP,FSLIDE,
                                        K2. **This is changed to:
                                        R,2,150,0,0,0.001,700,0.0001 for
                                        the second calibration method.**
ET,4,COMBIN40,0,,2,0,,1                 !Spring 1 parallel to joist - UY
R,4,100000,0,0,0,145,2.5               !Real constants for spring 1:
                                        K1,C,M,GAP,FSLIDE, K2
ET,5,COMBIN40,0,,2,0,,1                 !Spring 2,3 parallel to joist - UY
R,5,210,0,0,0.001,700,45               !Real constants for spring
                                        2,3:        K1,C,M,GAP,FSLIDE,
                                        K2. **This is changed to:
                                        R,5,500,0,0,0.001,840,0.001 for
                                        the second calibration method.**
ET,7,SHELL181,                          !Shell element for the planks
```

Code	Comment
R,7,tplanks,tplanks,tplanks,tplanks,	!Real constants for shell elements
ET,8,BEAM188,	!Beam element for the beams
SECTYPE,8,BEAM,RECT,	!Section type for beam elements
SECDATA,60,130	!Section data for beam elements
ET,9,SHELL181	!Shell element for the panels
R,9,tpanels,tpanels,tpanels,tpanels,	!Real constants for shell elements
R,10,10000,0,0,0,70,0.5	!Real constants spring 1 for single screw in UX (parallel to plank): K1,C,M,GAP,FSLIDE, K2
R,11,500,0,0,0.001,1000,80	!Real constants spring 2,3 for single screw in UX (parallel to plank):K1,C,M,GAP,FSLIDE, K2. **This is changed to: R,11,500,0,0,0.001,1100,0.001 for the second calibration approach.**
R,12,10000,0,0,0,50,2	!Real constants spring 1 for single screw in UY (perpendicular to plank): K1,C,M,GAP,FSLIDE, K2
R,13,300,0,0,0.001,800,90	!Real constants spring 2,3 for single screw in UY (perpendicular to plank): K1,C,M,GAP,FSLIDE, K2. **This is changed to: R,13,500,0,0,0.001,1150,0.001 for the second calibration approach.**
R,14,10000,0,0,0,250,3	!Real constants spring 1 for screw and two nails in UX (perpendicular to joist): K1,C,M,GAP,FSLIDE, K2
R,15,600,0,0,0.001,1300,250	!Real constants spring 2,3 for screw and two nails in UX (perpendicular to joist): K1,C,M,GAP,FSLIDE, K2. **This is changed to: R,15,1000,0,0,0.001,2000,0.01 for the second calibration approach.**
R,16,10000,0,0,0,250,3	!Real constants spring 1 for screw and two nails in UY (parallel to joist): K1,C,M,GAP,FSLIDE, K2
R,17,400,0,0,0.001,800,250	!Real constants spring 2,3 for screw and two nails in UY (parallel to joist): K1,C,M,GAP,FSLIDE, K2. **This is changed to: R,17,800,0,0,0.001,1950,0.01 for the second calibration approach.**
ET,10,CONTA178,0,0,0,0,0,0	!Contact element between panels
KEYOPT,10,7,0	!Set keyopts
KEYOPT,10,9,0	

```
KEYOPT,10,10,0
R,18,-10000,2,1,-0.001,,,                          !Real constants for contact ele-
                                                   ments: Kn, gap size, initial contact
                                                   status, Fks

RMORE,,,0.01,,200,                                 !Additional real constants: pene-
                                                   tration tolerance, maximum slip
```

!——DEFINE MATERIAL PROPERTIES——

```
*DIM,tablemat,TABLE,27,8                           !Create table with size 27x8 named
                                                   'tablemat'

*TREAD,tablemat,matpropp,csv,,                     !Read data from matpropp.csv into
                                                   table 'tablemat'

*DIM,materprop,ARRAY,28,9                          !Create array with size 28x9 named
                                                   'materprop'

*MFUN,materprop(1,1),copy,tablemat(0,0)            !Copy 'tablemat' into 'materprop'
*DEL,tablemat(1)                                   !Delete table 'tablemat'

*DO,j,1,23                                         !Do-loop to define material prop-
                                                   erties for 23 planks from array
                                                   'materprop'

  MP,EX,j,materprop(j,1)                           !$E_x$
  MP,EY,j,materprop(j,2)                           !$E_y$
  MP,EZ,j,materprop(j,3)                           !$E_z$
  MP,GXY,j,materprop(j,4)                          !$G_{xy}$
  MP,GYZ,j,materprop(j,5)                          !$G_{yz}$
  MP,GXZ,j,materprop(j,6)                          !$G_{xz}$
  MP,PRXY,j,materprop(j,7)                         !$\nu_{xy}$
  MP,PRYZ,j,materprop(j,8)                         !$\nu_{yz}$
  MP,PRXZ,j,materprop(j,9)                         !$\nu_{xz}$
*ENDDO                                             !End do-loop

*DO,j,1,4                                          !Do-loop to define material prop-
                                                   erties for 4 beams from array
                                                   'materprop'

  MP,EX,j+23,materprop(j+24,1)                     !$E_x$
  MP,EY,j+23,materprop(j+24,2)                     !$E_y$
  MP,EZ,j+23,materprop(j+24,3)                     !$E_z$
  MP,GXY,j+23,materprop(j+24,4)                    !$G_{xy}$
  MP,GYZ,j+23,materprop(j+24,5)                    !$G_{yz}$
  MP,GXZ,j+23,materprop(j+24,6)                    !$G_{xz}$
  MP,PRXY,j+23,materprop(j+24,7)                   !$\nu_{xy}$
  MP,PRYZ,j+23,materprop(j+24,8)                   !$\nu_{yz}$
  MP,PRXZ,j+23,materprop(j+24,9)                   !$\nu_{xz}$
*ENDDO                                             !End do-loop
```

```
MP,EX,30,7500                              !Define Ex for panels
MP,EY,30,7500                              !Define Ey for panels
MP,EZ,30,7500                              !Define Ez for panels
MP,GXY,30,430                              !Define Gxy for panels
MP,GYZ,30,430                              !Define Gyz for panels
MP,GXZ,30,430                              !Define Gxz for panels
MP,PRXY,30,0.3                             !Define νxy for panels
MP,PRYZ,30,0.3                             !Define νyz for panels
MP,PRXZ,30,0.3                             !Define νxz for panels



!——CREATE NODES——

!BEAMS
N,1,30,0,-74.5                             !First node for top beam, 94 nodes
                                            per beam

N,2,30,32.5,-74.5
N,3,30,82.5,-74.5
N,4,30,132.5,-74.5
N,5,30,166,-74.5
NGEN,23,4,2,5,1,0,167,                     !Generate other nodes on top
                                            beam

N,94,30,3870,-74.5                         !Last node on top beam
NGEN,4,94,1,94,1,650,0,0                    !Replicate top beam for other
                                            beams


!PLANKS
N,377,0,0,0                                !First node for first plank (edge
                                            y=0)

N,378,30,0,0
N,379,50,0,0
N,409,650,0,0
FILL
N,410,680,0,0
N,411,710,0,0
N,412,730,0,0
N,413,750,0,0
N,473,1950,0,0
FILL
N,474,1980,0,0
N,475,2010,0,0
N,476,2030,0,0
N,477,2050,0,0
N,507,2650,0,0
FILL
```

```
N,508,2680,0,0                              !Last node on edge y=0
NGEN,2,132,377,508,1,0,32.5,0               !Generate nodes on first plank
NGEN,5,132,509,640,1,0,25,0
NGEN,2,792,377,508,1,0,165,0
NGEN,23,924,377,1300,1,0,167,0              !Replicate first plank for other
                                            planks


!PANELS
!First column
N,21629,0,0,18.5                            !First node at top left corner
N,21630,30,0,18.5
N,21631,50,0,18.5
N,21681,1050,0,18.5
FILL
N,21682,1070,0,18.5
N,21683,1099,0,18.5                         !Last node of first panel on left
                                            edge
N,21684,1101,0,18.5                         !First node of second panel
N,21685,1120,0,18.5
N,21686,1150,0,18.5
N,21741,2250,0,18.5
FILL
N,21742,2270,0,18.5
N,21743,2300,0,18.5                         !Last node of left edge
NGEN,2,115,21629,21743,1,0,32.5,0           !Generate other nodes in first col-
                                            umn of panels
NGEN,5,115,21744,21858,1,0,25,0
NGEN,3,690,21629,22318,1,0,167,0

NGEN,2,2070,21629,21973,1,0,501,0
NGEN,2,2415,21629,21743,1,0,579,0


!Second column
N,24159,0,581,18.5                          !First node on left edge
N,24160,30,581,18.5
N,24161,50,581,18.5
N,24181,450,581,18.5
FILL
N,24182,470,581,18.5
N,24183,499,581,18.5                         !Last node of first panel on left
                                            edge
N,24184,501,581,18.5                         !First node of second panel
N,24185,530,581,18.5
N,24186,550,581,18.5
N,24241,1650,581,18.5
```

```
FILL
N,24242,1670,581,18.5
N,24243,1699,581,18.5                                    !Last node of second panel
N,24244,1701,581,18.5                                    !First node of third panel
N,24245,1730,581,18.5
N,24246,1750,581,18.5
N,24271,2250,581,18.5
FILL
N,24272,2270,581,18.5
N,24273,2300,581,18.5                                    !Last node of left edge
NGEN,2,115,24159,24273,1,0,27.5,0                        !Generate other nodes in second
                                                          column of panels

NGEN,2,115,24274,24388,1,0,25,0
NGEN,2,230,24274,24388,1,0,59.5,0


NGEN,2,115,24504,24618,1,0,32.5,0
NGEN,5,115,24619,24733,1,0,25,0
NGEN,3,690,24504,25193,1,0,167,0


NGEN,2,115,26459,26573,1,0,34.5,0
NGEN,2,115,26574,26688,1,0,32.5,0
NGEN,2,115,26689,26803,1,0,25,0
NGEN,2,115,26804,26918,1,0,22.5,0


!Third column
NGEN,2,5405,21629,21743,1,0,1251,0                       !Replicate first column of panels
NGEN,2,115,27034,27148,1,0,25.5,0
NGEN,2,115,27149,27263,1,0,25,0
NGEN,2,5750,21629,24043,1,0,1336,0
NGEN,2,115,29679,29793,1,0,24.5,0


!Fourth column
NGEN,2,5750,24159,24273,1,0,1340,0                       !Replicate second column of pan-
                                                          els

NGEN,2,5750,24274,26918,1,0,1336,0
NGEN,2,115,32554,32668,1,0,26.5,0


!Fifth column
NGEN,2,5750,27034,27148,1,0,1340,0                       !Replicate third column of panels
NGEN,2,5750,27149,29793,1,0,1336,0
NGEN,2,115,35429,35543,1,0,28.5,0


!Sixth column
NGEN,2,5750,29909,30023,1,0,1340,0                       !Replicate fourth column of panels
NGEN,2,5750,30024,32323,1,0,1336,0
```

NGEN,2,115, 37959,38073,1,0,32.5,0

!——CREATE ELEMENTS——

!BEAMS
TYPE,8	!Activates element type 8
REAL,8	!Activates real constant number 8
SECNUM,8	!Activates section number 8

N,15000,30,0,50	!Keypoint (orientation node) for beam 2
N,15001,680,0,50	!Keypoint (orientation node) for beam 3
N,15002,1330,0,50	!Keypoint (orientation node) for beam 4
N,15003,1980,0,50	!Keypoint (orientation node) for beam 5

*DO,n,1,4	!Do-loop to create beam elements
MAT,n+23	!Set material properties
DO,j,1+94(n-1),93+94*(n-1)	
E,j,j+1,50000+(n-1)	
*ENDDO	
*ENDDO	!End do-loop

!PLANKS
TYPE,7	!Activates element type 7
REAL,7	!Activates real constant number 7

*DO,n,1,23	!Do-loop to create shell elements
MAT,n	!Set material properties
*DO,i,1,6	
DO,j,377+132(i-1)+924*(n-1),507+132*(i-1)+924*(n-1)	
E,j,j+1,j+133,j+132	
*ENDDO	
*ENDDO	
*ENDDO	!End do-loop

!PANELS
TYPE,7	!Activates element type 7
REAL,7	!Activates real constant number 7
MAT,30	!Activates material properties 30

```
!First column
*DO,n,1,21                                                  !Do-loop to create shell elements
                                                            on first panel

  *DO,j,21629+115*(n-1),21682+115*(n-1)
    E,j,j+1,j+116,j+115
  *ENDDO
*ENDDO                                                      !End do-loop


*DO,n,1,21                                                  !Do-loop to create shell elements
                                                            on second panel

  *DO,j,21684+115*(n-1),21742+115*(n-1)
    E,j,j+1,j+116,j+115
  *ENDDO
*ENDDO                                                      !End do-loop


!Second and fourth column
*DO,i,1,2                                                   !Do-loop to create shell elements
                                                            on first panel

  *DO,n,1,24
            *DO,j,24159+115*(n-1)+5750*(i-
1),24182+115*(n-1)+5750*(i-1)
      E,j,j+1,j+116,j+115
    *ENDDO
  *ENDDO
*ENDDO                                                      !End do-loop


*DO,i,1,2                                                   !Do-loop to create shell elements
                                                            on second panel

  *DO,n,1,24
            *DO,j,24184+115*(n-1)+5750*(i-
1),24242+115*(n-1)+5750*(i-1)
      E,j,j+1,j+116,j+115
    *ENDDO
  *ENDDO
*ENDDO                                                      !End do-loop


*DO,i,1,2                                                   !Do-loop to create shell elements
                                                            on third panel

  *DO,n,1,24
            *DO,j,24244+115*(n-1)+5750*(i-
1),24272+115*(n-1)+5750*(i-1)
      E,j,j+1,j+116,j+115
    *ENDDO
  *ENDDO
*ENDDO                                                      !End do-loop
```

```
!Third and fifth column
*DO,i,1,2                                    !Do-loop to create shell elements
                                             on first panel

  *DO,n,1,24
            *DO,j,27034+115*(n-1)+5750*(i-
1),27087+115*(n-1)+5750*(i-1)
     E,j,j+1,j+116,j+115
    *ENDDO
   *ENDDO
*ENDDO                                       !End do-loop
*DO,i,1,2                                    !Do-loop to create shell elements
                                             on second panel

  *DO,n,1,24
            *DO,j,27089+115*(n-1)+5750*(i-
1),27147+115*(n-1)+5750*(i-1)
     E,j,j+1,j+116,j+115
    *ENDDO
   *ENDDO
*ENDDO                                       !End do-loop


!Sixth column
*DO,n,1,21                                   !Do-loop to create shell elements
                                             on first panel

  *DO,j,35659+115*(n-1),35682+115*(n-1)
    E,j,j+1,j+116,j+115
  *ENDDO
*ENDDO                                       !End do-loop


*DO,n,1,21                                   !Do-loop to create shell elements
                                             on second panel

  *DO,j,35684+115*(n-1),35742+115*(n-1)
    E,j,j+1,j+116,j+115
  *ENDDO
*ENDDO                                       !End do-loop


*DO,n,1,21                                   !Do-loop to create shell elements
                                             on third panel

  *DO,j,35744+115*(n-1),35772+115*(n-1)
    E,j,j+1,j+116,j+115
  *ENDDO
*ENDDO                                       !End do-loop


!NAILS
!UX                                          !Nails in ux, 2 springs from node i-j
```

```
*DO,n,1,2                                          !Do-loop to create 2 spring ele-
                                                   ments
  TYPE,n                                           !Activates element type n
  REAL,n                                           !Activates real constant set n
  *DO,i,1,23                                        !23 planks
    *DO,j,1,3                                       !3 rows per plank
      E,96+94*(j-1)+4*(i-1),542+32*(j-1)+924*(i-
1)
              E,98+94*(j-1)+4*(i-1),1070+32*(j-
1)+924*(i-1)
    *ENDDO
  *ENDDO
*ENDDO                                             !End do-loop


!UX                                                !Nails in $u_x$, 1 spring from node j-i


TYPE,2                                             !Activates element type 2
REAL,2                                             !Activates real constant number 2


*DO,i,1,23                                          !Do-loop to create 1 spring ele-
                                                   ment

  *DO,j,1,3
    E,542+32*(j-1)+924*(i-1),96+94*(j-1)+4*(i-1)
      E,1070+32*(j-1)+924*(i-1),98+94*(j-1)+4*(i-
1)
  *ENDDO
*ENDDO                                             !End do-loop


!UY                                                !Nails in $u_y$, 2 springs from node i-j


*DO,n,1,2                                          !Do-loop to create 2 spring ele-
                                                   ments
  TYPE,n+3                                         !Activates element type n+3
  REAL,n+3                                         !Activates real constant set n+3
  *DO,i,1,23                                        !23 planks
    *DO,j,1,3                                       !3 rows per plank
      E,96+94*(j-1)+4*(i-1),542+32*(j-1)+924*(i-
1)
              E,98+94*(j-1)+4*(i-1),1070+32*(j-
1)+924*(i-1)
    *ENDDO
  *ENDDO
*ENDDO


!UY                                                !Nails in $u_y$, 1 spring from node j-i
```

```
TYPE,5                                    !Activates element type 5
REAL,5                                    !Activates real constant number 5

*DO,i,1,23                                !Do-loop to create 1 spring ele-
                                          ment

  *DO,j,1,3
    E,542+32*(j-1)+924*(i-1),96+94*(j-1)+4*(i-1)
      E,1070+32*(j-1)+924*(i-1),98+94*(j-1)+4*(i-
1)
  *ENDDO
*ENDDO                                    !End do-loop


!SCREWS

!SCREWS ON TOP BEAM (1 screw+2 nails)
!UX                                       !Screws in u_x, 2 springs from node
                                          i-j


*DO,n,1,2                                 !Do-loop for first column of panels
  TYPE,1
  REAL,n+13
  *DO,j,1,4
    E,3+4*(j-1),21975+690*(j-1)
  *ENDDO
*ENDDO                                    !End do-loop


*DO,n,1,2                                 !Do-loop for second column of
                                          panels

  TYPE,1
  REAL,n+13
  *DO,j,1,4
    E,19+4*(j-1),24850+690*(j-1)
  *ENDDO
*ENDDO                                    !End do-loop


*DO,n,1,2                                 !Do-loop for third column of pan-
                                          els

  TYPE,1
  REAL,n+13
  *DO,j,1,4
    E,35+4*(j-1),27725+690*(j-1)
  *ENDDO
*ENDDO                                    !End do-loop


*DO,n,1,2                                 !Do-loop for fourth column of pan-
                                          els
```

```
   TYPE,1
   REAL,n+13
   *DO,j,1,4
     E,51+4*(j-1),30600+690*(j-1)
   *ENDDO
*ENDDO                                          !End do-loop

*DO,n,1,2                                        !Do-loop for fifth column of panels
   TYPE,1
   REAL,n+13
   *DO,j,1,4
     E,67+4*(j-1),33475+690*(j-1)
   *ENDDO
*ENDDO                                          !End do-loop

*DO,n,1,2                                        !Do-loop for sixth column of pan-
                                                 els

   TYPE,1
   REAL,n+13
   *DO,j,1,3
     E,83+4*(j-1),36350+690*(j-1)
   *ENDDO
*ENDDO                                          !End do-loop

!UX                                              !Screws in $u_x$, 1 spring from node
                                                 j-i

TYPE,1
REAL,15

*DO,j,1,4                                        !Do-loop for first column of panels
   E,21975+690*(j-1),3+4*(j-1)
*ENDDO                                          !End do-loop

*DO,j,1,4                                        !Do-loop for second column of
                                                 panels
   E,24850+690*(j-1),19+4*(j-1)
*ENDDO                                          !End do-loop

*DO,j,1,4                                        !Do-loop for third column of pan-
                                                 els
   E,27725+690*(j-1),35+4*(j-1)
*ENDDO                                          !End do-loop
```

```
*DO,j,1,4                                   !Do-loop for fourth column of pan-
                                            els

   E,30600+690*(j-1),51+4*(j-1)
*ENDDO                                      !End do-loop


*DO,j,1,4                                   !Do-loop for fifth column of panels
   E,33475+690*(j-1),67+4*(j-1)
*ENDDO                                      !End do-loop


*DO,j,1,3                                   !Do-loop for sixth column of pan-
                                            els

   E,36350+690*(j-1),83+4*(j-1)
*ENDDO                                      !End do-loop


!UY                                         !Screws in u_y, 2 springs from node
                                            i-j


*DO,n,1,2                                   !Do-loop for first column of panels
   TYPE,4
   REAL,n+15
   *DO,j,1,4
     E,3+4*(j-1),21975+690*(j-1)
   *ENDDO
*ENDDO                                      !End do-loop


*DO,n,1,2                                   !Do-loop for second column of
                                            panels

   TYPE,4
   REAL,n+15
   *DO,j,1,4
     E,19+4*(j-1),24850+690*(j-1)
   *ENDDO
*ENDDO                                      !End do-loop


*DO,n,1,2                                   !Do-loop for third column of pan-
                                            els

   TYPE,4
   REAL,n+15
   *DO,j,1,4
     E,35+4*(j-1),27725+690*(j-1)
   *ENDDO
*ENDDO                                      !End do-loop


*DO,n,1,2                                   !Do-loop for fourth column of pan-
                                            els
```

```
    TYPE,4
    REAL,n+15
    *DO,j,1,4
      E,51+4*(j-1),30600+690*(j-1)
    *ENDDO
*ENDDO                                          !End do-loop

*DO,n,1,2                                        !Do-loop for fifth column of panels
    TYPE,4
    REAL,n+15
    *DO,j,1,4
      E,67+4*(j-1),33475+690*(j-1)
    *ENDDO
*ENDDO                                          !End do-loop

*DO,n,1,2                                        !Do-loop for sixth column of pan-
                                                 els

    TYPE,4
    REAL,n+15
    *DO,j,1,3
      E,83+4*(j-1),36350+690*(j-1)
    *ENDDO
*ENDDO                                          !End do-loop

!UY                                             !Screws in $u_y$, 1 spring from node
                                                 j-i

TYPE,4
REAL,17

*DO,j,1,4                                        !Do-loop for first column of panels
   E,21975+690*(j-1),3+4*(j-1)
*ENDDO                                          !End do-loop

*DO,j,1,4                                        !Do-loop for second column of
                                                 panels

   E,24850+690*(j-1),19+4*(j-1)
*ENDDO                                          !End do-loop

*DO,j,1,4                                        !Do-loop for third column of pan-
                                                 els

   E,27725+690*(j-1),35+4*(j-1)
*ENDDO                                          !End do-loop
```

```
*DO,j,1,4                                    !Do-loop for fourth column of pan-
                                             els

   E,30600+690*(j-1),51+4*(j-1)
*ENDDO                                       !End do-loop


*DO,j,1,4                                    !Do-loop for fifth column of panels
   E,33475+690*(j-1),67+4*(j-1)
*ENDDO                                       !End do-loop


*DO,j,1,3                                    !Do-loop for sixth column of pan-
                                             els

   E,36350+690*(j-1),83+4*(j-1)
*ENDDO                                       !End do-loop



!OTHER SCREWS (SINGLE SCREW)
!UX                                          !Screws in u_x, 2 springs from node
                                             i-j


!First column of panels, first vertical rows of
screws, then horizontal rows of screws
*DO,n,1,2
   TYPE,1
   REAL,n+9
   *DO,i,1,2
     *DO,j,1,7
           E,511+5*(j-1)+2772*(i-1),21746+5*(j-
1)+2070*(i-1)
     *ENDDO
   *ENDDO
*ENDDO

*DO,n,1,2
   TYPE,1
   REAL,n+9
   *DO,i,1,2
     *DO,j,1,4
           E,545+5*(j-1)+2772*(i-1),21781+5*(j-
1)+2070*(i-1)
     *ENDDO
   *ENDDO
*ENDDO

*DO,n,1,2
   TYPE,1
```

Note: in the comment line "!UX" the subscript is u_x.

```
    REAL,n+9
    *DO,i,1,2
      E,565+2772*(i-1),21801+2070*(i-1)
      E,570+2772*(i-1),21806+2070*(i-1)
    *ENDDO
*ENDDO

*DO,n,1,2
  TYPE,1
  REAL,n+9
  *DO,i,1,2
    *DO,j,1,7
          E,575+5*(j-1)+2772*(i-1),21811+5*(j-
1)+2070*(i-1)
    *ENDDO
  *ENDDO
*ENDDO

*DO,n,1,2
  TYPE,1
  REAL,n+9
  *DO,i,1,2
    *DO,j,1,3
          E,609+5*(j-1)+2772*(i-1),21846+5*(j-
1)+2070*(i-1)
    *ENDDO
  *ENDDO
*ENDDO

*DO,n,1,2
  TYPE,1
  REAL,n+9
  *DO,i,1,2
    E,1088+5*(i-1),22256+5*(i-1)
    E,1748+5*(i-1),22716+5*(i-1)
    E,2408+5*(i-1),23176+5*(i-1)
    E,2936+5*(i-1),23636+5*(i-1)
  *ENDDO
*ENDDO

*DO,n,1,2
  TYPE,1
  REAL,n+9
  E,1147,22316
  E,1807,22776
```

```
    E,2467,23236
    E,2995,23696
*ENDDO


!Second and fourth column of panels, first ver-
tical rows of screws, then horizontal rows of
screws
*DO,k,1,2


*DO,n,1,2
   TYPE,1
   REAL,n+9
   *DO,i,1,2
     *DO,j,1,5
             E,3679+5*(j-1)+3432*(i-1)+7392*(k-
1),24276+5*(j-1)+2530*(i-1)+5750*(k-1)
     *ENDDO
   *ENDDO
*ENDDO


*DO,n,1,2
   TYPE,1
   REAL,n+9
   *DO,i,1,2
                   E,3704+3432*(i-1)+7392*(k-
1),24301+2530*(i-1)+5750*(k-1)
                   E,3709+3432*(i-1)+7392*(k-
1),24306+2530*(i-1)+5750*(k-1)
   *ENDDO
*ENDDO


*DO,n,1,2
   TYPE,1
   REAL,n+9
   *DO,i,1,2
     *DO,j,1,6
             E,3713+5*(j-1)+3432*(i-1)+7392*(k-
1),24311+5*(j-1)+2530*(i-1)+5750*(k-1)
     *ENDDO
   *ENDDO
*ENDDO


*DO,n,1,2
   TYPE,1
   REAL,n+9
```

```
*DO,i,1,2
  *DO,j,1,4
            E,3743+5*(j-1)+3432*(i-1)+7392*(k-
1),24341+5*(j-1)+2530*(i-1)+5750*(k-1)
    *ENDDO
  *ENDDO
*ENDDO

*DO,n,1,2
  TYPE,1
  REAL,n+9
  *DO,i,1,2
    *DO,j,1,3
            E,3763+5*(j-1)+3432*(i-1)+7392*(k-
1),24361+5*(j-1)+2530*(i-1)+5750*(k-1)
    *ENDDO
  *ENDDO
*ENDDO

*DO,n,1,2
  TYPE,1
  REAL,n+9
  *DO,i,1,2
    *DO,j,1,3
            E,3777+5*(j-1)+3432*(i-1)+7392*(k-
1),24376+5*(j-1)+2530*(i-1)+5750*(k-1)
    *ENDDO
  *ENDDO
*ENDDO

*DO,n,1,2
  TYPE,1
  REAL,n+9
  *DO,i,1,2
        E,4359+5*(i-1)+7392*(k-1),24756+5*(i-
1)+5750*(k-1)
        E,4755+5*(i-1)+7392*(k-1),25101+5*(i-
1)+5750*(k-1)
        E,5415+5*(i-1)+7392*(k-1),25561+5*(i-
1)+5750*(k-1)
        E,5943+5*(i-1)+7392*(k-1),25906+5*(i-
1)+5750*(k-1)
        E,6471+5*(i-1)+7392*(k-1),26366+5*(i-
1)+5750*(k-1)
    *ENDDO
*ENDDO
```

```
*DO,n,1,2
  TYPE,1
  REAL,n+9
  *DO,i,1,2
        E,4418+5*(i-1)+7392*(k-1),24816+5*(i-
1)+5750*(k-1)
        E,4814+5*(i-1)+7392*(k-1),25161+5*(i-
1)+5750*(k-1)
        E,5474+5*(i-1)+7392*(k-1),25621+5*(i-
1)+5750*(k-1)
        E,6002+5*(i-1)+7392*(k-1),25966+5*(i-
1)+5750*(k-1)
        E,6530+5*(i-1)+7392*(k-1),26426+5*(i-
1)+5750*(k-1)
  *ENDDO
*ENDDO

*DO,n,1,2
  TYPE,1
  REAL,n+9
  E,4447+7392*(k-1),24846+5750*(k-1)
  E,4843+7392*(k-1),25191+5750*(k-1)
  E,5503+7392*(k-1),25651+5750*(k-1)
  E,6031+7392*(k-1),25996+5750*(k-1)
  E,6559+7392*(k-1),26456+5750*(k-1)
*ENDDO

*ENDDO

!Third and fifth column of panels, first vertical
rows of screws, then horizontal rows of screws
*DO,k,1,2

*DO,n,1,2
  TYPE,1
  REAL,n+9
  *DO,i,1,2
    *DO,j,1,7
          E,7375+5*(j-1)+3432*(i-1)+7392*(k-
1),27151+5*(j-1)+2530*(i-1)+5750*(k-1)
    *ENDDO
  *ENDDO
*ENDDO

*DO,n,1,2
```

```
TYPE,1
REAL,n+9
*DO,i,1,2
  *DO,j,1,4
          E,7409+5*(j-1)+3432*(i-1)+7392*(k-
1),27186+5*(j-1)+2530*(i-1)+5750*(k-1)
    *ENDDO
  *ENDDO
*ENDDO

*DO,n,1,2
  TYPE,1
  REAL,n+9
  *DO,i,1,2
                E,7429+3432*(i-1)+7392*(k-
1),27206+2530*(i-1)+5750*(k-1)
                E,7434+3432*(i-1)+7392*(k-
1),27211+2530*(i-1)+5750*(k-1)
  *ENDDO
*ENDDO

*DO,n,1,2
  TYPE,1
  REAL,n+9
  *DO,i,1,2
    *DO,j,1,7
          E,7439+5*(j-1)+3432*(i-1)+7392*(k-
1),27216+5*(j-1)+2530*(i-1)+5750*(k-1)
    *ENDDO
  *ENDDO
*ENDDO

*DO,n,1,2
  TYPE,1
  REAL,n+9
  *DO,i,1,2
    *DO,j,1,3
          E,7473+5*(j-1)+3432*(i-1)+7392*(k-
1),27251+5*(j-1)+2530*(i-1)+5750*(k-1)
    *ENDDO
  *ENDDO
*ENDDO

*DO,n,1,2
  TYPE,1
```

```
     REAL,n+9
  *DO,i,1,2
         E,8084+5*(i-1)+7392*(k-1),27661+5*(i-
1)+5750*(k-1)
         E,8744+5*(i-1)+7392*(k-1),28121+5*(i-
1)+5750*(k-1)
         E,9140+5*(i-1)+7392*(k-1),28466+5*(i-
1)+5750*(k-1)
         E,9668+5*(i-1)+7392*(k-1),28811+5*(i-
1)+5750*(k-1)
        E,10196+5*(i-1)+7392*(k-1),29271+5*(i-
1)+5750*(k-1)
  *ENDDO
*ENDDO

*DO,n,1,2
  TYPE,1
  REAL,n+9
  E,8143+7392*(k-1),27721+5750*(k-1)
  E,8803+7392*(k-1),28181+5750*(k-1)
  E,9199+7392*(k-1),28526+5750*(k-1)
  E,9727+7392*(k-1),28871+5750*(k-1)
  E,10255+7392*(k-1),29331+5750*(k-1)
*ENDDO

*ENDDO

!Sixth column of panels, first vertical rows of
screws, then horizontal rows of screws

*DO,n,1,2
  TYPE,1
  REAL,n+9
  *DO,i,1,2
    *DO,j,1,5
         E,18595+5*(j-1)+2772*(i-1),35891+5*(j-
1)+2070*(i-1)
     *ENDDO
  *ENDDO
*ENDDO

*DO,n,1,2
  TYPE,1
  REAL,n+9
  *DO,i,1,2
    E,18620+2772*(i-1),35916+2070*(i-1)
```

```
    E,18625+2772*(i-1),35921+2070*(i-1)
  *ENDDO
*ENDDO

*DO,n,1,2
  TYPE,1
  REAL,n+9
  *DO,i,1,2
    *DO,j,1,6
        E,18629+5*(j-1)+2772*(i-1),35926+5*(j-
1)+2070*(i-1)
    *ENDDO
  *ENDDO
*ENDDO

*DO,n,1,2
  TYPE,1
  REAL,n+9
  *DO,i,1,2
    *DO,j,1,4
        E,18659+5*(j-1)+2772*(i-1),35956+5*(j-
1)+2070*(i-1)
    *ENDDO
  *ENDDO
*ENDDO

*DO,n,1,2
  TYPE,1
  REAL,n+9
  *DO,i,1,2
    *DO,j,1,3
        E,18679+5*(j-1)+2772*(i-1),35976+5*(j-
1)+2070*(i-1)
    *ENDDO
  *ENDDO
*ENDDO

*DO,n,1,2
  TYPE,1
  REAL,n+9
  *DO,i,1,2
    *DO,j,1,3
        E,18693+5*(j-1)+2772*(i-1),35991+5*(j-
1)+2070*(i-1)
    *ENDDO
```

```
  *ENDDO
*ENDDO

*DO,n,1,2
  TYPE,1
  REAL,n+9
  *DO,i,1,2
    E,19143+5*(i-1),36256+5*(i-1)
    E,19803+5*(i-1),36716+5*(i-1)
    E,20199+5*(i-1),37061+5*(i-1)
    E,20859+5*(i-1),37521+5*(i-1)
  *ENDDO
*ENDDO

*DO,n,1,2
  TYPE,1
  REAL,n+9
  *DO,i,1,2
    E,19202+5*(i-1),36316+5*(i-1)
    E,19862+5*(i-1),36776+5*(i-1)
    E,20258+5*(i-1),37121+5*(i-1)
    E,20918+5*(i-1),37581+5*(i-1)
  *ENDDO
*ENDDO

*DO,n,1,2
  TYPE,1
  REAL,n+9
  E,19231,36346
  E,19891,36806
  E,20287,37151
  E,20947,37611
*ENDDO
```

!UX   !Screws in u_x, 1 spring from node j-i

```
TYPE,1
REAL,11
```

!First column of panels, first vertical rows of screws, then horizontal rows of screws

```
*DO,i,1,2
  *DO,j,1,7
```

```
          E,21746+5*(j-1)+2070*(i-1),511+5*(j-
1)+2772*(i-1)
    *ENDDO
*ENDDO


*DO,i,1,2
  *DO,j,1,4
          E,21781+5*(j-1)+2070*(i-1),545+5*(j-
1)+2772*(i-1)
    *ENDDO
*ENDDO


*DO,i,1,2
  E,21801+2070*(i-1),565+2772*(i-1)
  E,21806+2070*(i-1),570+2772*(i-1)
*ENDDO


*DO,i,1,2
  *DO,j,1,7
          E,21811+5*(j-1)+2070*(i-1),575+5*(j-
1)+2772*(i-1)
    *ENDDO
*ENDDO


*DO,i,1,2
  *DO,j,1,3
          E,21846+5*(j-1)+2070*(i-1),609+5*(j-
1)+2772*(i-1)
    *ENDDO
*ENDDO


*DO,i,1,2
  E,22256+5*(i-1),1088+5*(i-1)
  E,22716+5*(i-1),1748+5*(i-1)
  E,23176+5*(i-1),2408+5*(i-1)
  E,23636+5*(i-1),2936+5*(i-1)
*ENDDO


E,22316,1147
E,22776,1807
E,23236,2467
E,23696,2995


!Second and fourth column of panels, first ver-
tical rows of screws, then horizontal rows of
screws
```

```
*DO,k,1,2

*DO,i,1,2
   *DO,j,1,5
             E,24276+5*(j-1)+2530*(i-1)+5750*(k-
1),3679+5*(j-1)+3432*(i-1)+7392*(k-1)
   *ENDDO
*ENDDO

*DO,i,1,2
   E,24301+2530*(i-1)+5750*(k-1),3704+3432*(i-
1)+7392*(k-1)
   E,24306+2530*(i-1)+5750*(k-1),3709+3432*(i-
1)+7392*(k-1)
*ENDDO

*DO,i,1,2
   *DO,j,1,6
             E,24311+5*(j-1)+2530*(i-1)+5750*(k-
1),3713+5*(j-1)+3432*(i-1)+7392*(k-1)
   *ENDDO
*ENDDO

*DO,i,1,2
   *DO,j,1,4
             E,24341+5*(j-1)+2530*(i-1)+5750*(k-
1),3743+5*(j-1)+3432*(i-1)+7392*(k-1)
   *ENDDO
*ENDDO

*DO,i,1,2
   *DO,j,1,3
             E,24361+5*(j-1)+2530*(i-1)+5750*(k-
1),3763+5*(j-1)+3432*(i-1)+7392*(k-1)
   *ENDDO
*ENDDO

*DO,i,1,2
   *DO,j,1,3
             E,24376+5*(j-1)+2530*(i-1)+5750*(k-
1),3777+5*(j-1)+3432*(i-1)+7392*(k-1)
   *ENDDO
*ENDDO

*DO,i,1,2
```

```
        E,24756+5*(i-1)+5750*(k-1),4359+5*(i-
1)+7392*(k-1)
        E,25101+5*(i-1)+5750*(k-1),4755+5*(i-
1)+7392*(k-1)
        E,25561+5*(i-1)+5750*(k-1),5415+5*(i-
1)+7392*(k-1)
        E,25906+5*(i-1)+5750*(k-1),5943+5*(i-
1)+7392*(k-1)
        E,26366+5*(i-1)+5750*(k-1),6471+5*(i-
1)+7392*(k-1)
*ENDDO

*DO,i,1,2
        E,24816+5*(i-1)+5750*(k-1),4418+5*(i-
1)+7392*(k-1)
        E,25161+5*(i-1)+5750*(k-1),4814+5*(i-
1)+7392*(k-1)
        E,25621+5*(i-1)+5750*(k-1),5474+5*(i-
1)+7392*(k-1)
        E,25966+5*(i-1)+5750*(k-1),6002+5*(i-
1)+7392*(k-1)
        E,26426+5*(i-1)+5750*(k-1),6530+5*(i-
1)+7392*(k-1)
*ENDDO

E,24846+5750*(k-1),4447+7392*(k-1)
E,25191+5750*(k-1),4843+7392*(k-1)
E,25651+5750*(k-1),5503+7392*(k-1)
E,25996+5750*(k-1),6031+7392*(k-1)
E,26456+5750*(k-1),6559+7392*(k-1)

*ENDDO

!Third and fifth column of panels, first vertical
rows of screws, then horizontal rows of screws

*DO,k,1,2

*DO,i,1,2
  *DO,j,1,7
        E,27151+5*(j-1)+2530*(i-1)+5750*(k-
1),7375+5*(j-1)+3432*(i-1)+7392*(k-1)
  *ENDDO
*ENDDO

*DO,i,1,2
```

```
    *DO,j,1,4
            E,27186+5*(j-1)+2530*(i-1)+5750*(k-
1),7409+5*(j-1)+3432*(i-1)+7392*(k-1)
    *ENDDO
*ENDDO


*DO,i,1,2
    E,27206+2530*(i-1)+5750*(k-1),7429+3432*(i-
1)+7392*(k-1)
    E,27211+2530*(i-1)+5750*(k-1),7434+3432*(i-
1)+7392*(k-1)
*ENDDO


*DO,i,1,2
    *DO,j,1,7
            E,27216+5*(j-1)+2530*(i-1)+5750*(k-
1),7439+5*(j-1)+3432*(i-1)+7392*(k-1)
    *ENDDO
*ENDDO


*DO,i,1,2
    *DO,j,1,3
            E,27251+5*(j-1)+2530*(i-1)+5750*(k-
1),7473+5*(j-1)+3432*(i-1)+7392*(k-1)
    *ENDDO
*ENDDO


*DO,i,1,2
            E,27661+5*(i-1)+5750*(k-1),8084+5*(i-
1)+7392*(k-1)
            E,28121+5*(i-1)+5750*(k-1),8744+5*(i-
1)+7392*(k-1)
            E,28466+5*(i-1)+5750*(k-1),9140+5*(i-
1)+7392*(k-1)
            E,28811+5*(i-1)+5750*(k-1),9668+5*(i-
1)+7392*(k-1)
        E,29271+5*(i-1)+5750*(k-1),10196+5*(i-
1)+7392*(k-1)
*ENDDO


E,27721+5750*(k-1),8143+7392*(k-1)
E,28181+5750*(k-1),8803+7392*(k-1)
E,28526+5750*(k-1),9199+7392*(k-1)
E,28871+5750*(k-1),9727+7392*(k-1)
E,29331+5750*(k-1),10255+7392*(k-1)
```

```
*ENDDO

!Sixth column of panels, first vertical rows of
screws, then horizontal rows of screws

*DO,i,1,2
   *DO,j,1,5
        E,35891+5*(j-1)+2070*(i-1),18595+5*(j-
1)+2772*(i-1)
   *ENDDO
*ENDDO

*DO,i,1,2
   E,35916+2070*(i-1),18620+2772*(i-1)
   E,35921+2070*(i-1),18625+2772*(i-1)
*ENDDO

*DO,i,1,2
   *DO,j,1,6
        E,35926+5*(j-1)+2070*(i-1),18629+5*(j-
1)+2772*(i-1)
   *ENDDO
*ENDDO

*DO,i,1,2
   *DO,j,1,4
        E,35956+5*(j-1)+2070*(i-1),18659+5*(j-
1)+2772*(i-1)
   *ENDDO
*ENDDO

*DO,i,1,2
   *DO,j,1,3
        E,35976+5*(j-1)+2070*(i-1),18679+5*(j-
1)+2772*(i-1)
   *ENDDO
*ENDDO

*DO,i,1,2
   *DO,j,1,3
        E,35991+5*(j-1)+2070*(i-1),18693+5*(j-
1)+2772*(i-1)
   *ENDDO
*ENDDO
```

```
*DO,i,1,2
   E,36256+5*(i-1),19143+5*(i-1)
   E,36716+5*(i-1),19803+5*(i-1)
   E,37061+5*(i-1),20199+5*(i-1)
   E,37521+5*(i-1),20859+5*(i-1)
*ENDDO


*DO,i,1,2
   E,36316+5*(i-1),19202+5*(i-1)
   E,36776+5*(i-1),19862+5*(i-1)
   E,37121+5*(i-1),20258+5*(i-1)
   E,37581+5*(i-1),20918+5*(i-1)
*ENDDO


E,36346,19231
E,36806,19891
E,37151,20287
E,37611,20947
```

!UY   !Screws in u_y, 2 springs from node i-j


```
!First column of panels, first vertical rows of
screws, then horizontal rows of screws
*DO,n,1,2
   TYPE,4
   REAL,n+11
   *DO,i,1,2
     *DO,j,1,7
           E,511+5*(j-1)+2772*(i-1),21746+5*(j-
1)+2070*(i-1)
     *ENDDO
   *ENDDO
*ENDDO


*DO,n,1,2
   TYPE,4
   REAL,n+11
   *DO,i,1,2
     *DO,j,1,4
           E,545+5*(j-1)+2772*(i-1),21781+5*(j-
1)+2070*(i-1)
     *ENDDO
   *ENDDO
```

```
*ENDDO

*DO,n,1,2
  TYPE,4
  REAL,n+11
  *DO,i,1,2
    E,565+2772*(i-1),21801+2070*(i-1)
    E,570+2772*(i-1),21806+2070*(i-1)
  *ENDDO
*ENDDO

*DO,n,1,2
  TYPE,4
  REAL,n+11
  *DO,i,1,2
    *DO,j,1,7
          E,575+5*(j-1)+2772*(i-1),21811+5*(j-
1)+2070*(i-1)
    *ENDDO
  *ENDDO
*ENDDO

*DO,n,1,2
  TYPE,4
  REAL,n+11
  *DO,i,1,2
    *DO,j,1,3
          E,609+5*(j-1)+2772*(i-1),21846+5*(j-
1)+2070*(i-1)
    *ENDDO
  *ENDDO
*ENDDO

*DO,n,1,2
  TYPE,4
  REAL,n+11
  *DO,i,1,2
    E,1088+5*(i-1),22256+5*(i-1)
    E,1748+5*(i-1),22716+5*(i-1)
    E,2408+5*(i-1),23176+5*(i-1)
    E,2936+5*(i-1),23636+5*(i-1)
  *ENDDO
*ENDDO

*DO,n,1,2
```

```
   TYPE,4
   REAL,n+11
   E,1147,22316
   E,1807,22776
   E,2467,23236
   E,2995,23696
*ENDDO
```

!Second and fourth column of panels, first vertical rows of screws, then horizontal rows of screws

```
*DO,k,1,2

*DO,n,1,2
   TYPE,4
   REAL,n+11
   *DO,i,1,2
     *DO,j,1,5
             E,3679+5*(j-1)+3432*(i-1)+7392*(k-1),24276+5*(j-1)+2530*(i-1)+5750*(k-1)
     *ENDDO
   *ENDDO
*ENDDO

*DO,n,1,2
   TYPE,4
   REAL,n+11
   *DO,i,1,2
                    E,3704+3432*(i-1)+7392*(k-1),24301+2530*(i-1)+5750*(k-1)
                    E,3709+3432*(i-1)+7392*(k-1),24306+2530*(i-1)+5750*(k-1)
   *ENDDO
*ENDDO

*DO,n,1,2
   TYPE,4
   REAL,n+11
   *DO,i,1,2
     *DO,j,1,6
             E,3713+5*(j-1)+3432*(i-1)+7392*(k-1),24311+5*(j-1)+2530*(i-1)+5750*(k-1)
     *ENDDO
   *ENDDO
*ENDDO
```

```
*DO,n,1,2
  TYPE,4
  REAL,n+11
  *DO,i,1,2
    *DO,j,1,4
            E,3743+5*(j-1)+3432*(i-1)+7392*(k-
1),24341+5*(j-1)+2530*(i-1)+5750*(k-1)
    *ENDDO
  *ENDDO
*ENDDO

*DO,n,1,2
  TYPE,4
  REAL,n+11
  *DO,i,1,2
    *DO,j,1,3
            E,3763+5*(j-1)+3432*(i-1)+7392*(k-
1),24361+5*(j-1)+2530*(i-1)+5750*(k-1)
    *ENDDO
  *ENDDO
*ENDDO

*DO,n,1,2
  TYPE,4
  REAL,n+11
  *DO,i,1,2
    *DO,j,1,3
            E,3777+5*(j-1)+3432*(i-1)+7392*(k-
1),24376+5*(j-1)+2530*(i-1)+5750*(k-1)
    *ENDDO
  *ENDDO
*ENDDO

*DO,n,1,2
  TYPE,4
  REAL,n+11
  *DO,i,1,2
        E,4359+5*(i-1)+7392*(k-1),24756+5*(i-
1)+5750*(k-1)
        E,4755+5*(i-1)+7392*(k-1),25101+5*(i-
1)+5750*(k-1)
        E,5415+5*(i-1)+7392*(k-1),25561+5*(i-
1)+5750*(k-1)
        E,5943+5*(i-1)+7392*(k-1),25906+5*(i-
1)+5750*(k-1)
```

```
        E,6471+5*(i-1)+7392*(k-1),26366+5*(i-
1)+5750*(k-1)
    *ENDDO
*ENDDO

*DO,n,1,2
   TYPE,4
   REAL,n+11
   *DO,i,1,2
        E,4418+5*(i-1)+7392*(k-1),24816+5*(i-
1)+5750*(k-1)
        E,4814+5*(i-1)+7392*(k-1),25161+5*(i-
1)+5750*(k-1)
        E,5474+5*(i-1)+7392*(k-1),25621+5*(i-
1)+5750*(k-1)
        E,6002+5*(i-1)+7392*(k-1),25966+5*(i-
1)+5750*(k-1)
        E,6530+5*(i-1)+7392*(k-1),26426+5*(i-
1)+5750*(k-1)
    *ENDDO
*ENDDO

*DO,n,1,2
   TYPE,4
   REAL,n+11
   E,4447+7392*(k-1),24846+5750*(k-1)
   E,4843+7392*(k-1),25191+5750*(k-1)
   E,5503+7392*(k-1),25651+5750*(k-1)
   E,6031+7392*(k-1),25996+5750*(k-1)
   E,6559+7392*(k-1),26456+5750*(k-1)
*ENDDO

*ENDDO

!Third and fifth column of panels, first vertical
rows of screws, then horizontal rows of screws
*DO,k,1,2

*DO,n,1,2
   TYPE,4
   REAL,n+11
   *DO,i,1,2
     *DO,j,1,7
          E,7375+5*(j-1)+3432*(i-1)+7392*(k-
1),27151+5*(j-1)+2530*(i-1)+5750*(k-1)
     *ENDDO
```

```
        *ENDDO
    *ENDDO

    *DO,n,1,2
       TYPE,4
       REAL,n+11
       *DO,i,1,2
         *DO,j,1,4
                 E,7409+5*(j-1)+3432*(i-1)+7392*(k-
1),27186+5*(j-1)+2530*(i-1)+5750*(k-1)
         *ENDDO
       *ENDDO
    *ENDDO

    *DO,n,1,2
       TYPE,4
       REAL,n+11
       *DO,i,1,2
                      E,7429+3432*(i-1)+7392*(k-
1),27206+2530*(i-1)+5750*(k-1)
                      E,7434+3432*(i-1)+7392*(k-
1),27211+2530*(i-1)+5750*(k-1)
       *ENDDO
    *ENDDO

    *DO,n,1,2
       TYPE,4
       REAL,n+11
       *DO,i,1,2
         *DO,j,1,7
                 E,7439+5*(j-1)+3432*(i-1)+7392*(k-
1),27216+5*(j-1)+2530*(i-1)+5750*(k-1)
         *ENDDO
       *ENDDO
    *ENDDO

    *DO,n,1,2
       TYPE,4
       REAL,n+11
       *DO,i,1,2
         *DO,j,1,3
                 E,7473+5*(j-1)+3432*(i-1)+7392*(k-
1),27251+5*(j-1)+2530*(i-1)+5750*(k-1)
         *ENDDO
       *ENDDO
```

```
*ENDDO

*DO,n,1,2
  TYPE,4
  REAL,n+11
  *DO,i,1,2
        E,8084+5*(i-1)+7392*(k-1),27661+5*(i-
1)+5750*(k-1)
        E,8744+5*(i-1)+7392*(k-1),28121+5*(i-
1)+5750*(k-1)
        E,9140+5*(i-1)+7392*(k-1),28466+5*(i-
1)+5750*(k-1)
        E,9668+5*(i-1)+7392*(k-1),28811+5*(i-
1)+5750*(k-1)
        E,10196+5*(i-1)+7392*(k-1),29271+5*(i-
1)+5750*(k-1)
  *ENDDO
*ENDDO

*DO,n,1,2
  TYPE,4
  REAL,n+11
  E,8143+7392*(k-1),27721+5750*(k-1)
  E,8803+7392*(k-1),28181+5750*(k-1)
  E,9199+7392*(k-1),28526+5750*(k-1)
  E,9727+7392*(k-1),28871+5750*(k-1)
  E,10255+7392*(k-1),29331+5750*(k-1)
*ENDDO

*ENDDO

!Sixth column of panels, first vertical rows of
screws, then horizontal rows of screws

*DO,n,1,2
  TYPE,4
  REAL,n+11
  *DO,i,1,2
    *DO,j,1,5
        E,18595+5*(j-1)+2772*(i-1),35891+5*(j-
1)+2070*(i-1)
    *ENDDO
  *ENDDO
*ENDDO

*DO,n,1,2
```

```
   TYPE,4
   REAL,n+11
   *DO,i,1,2
     E,18620+2772*(i-1),35916+2070*(i-1)
     E,18625+2772*(i-1),35921+2070*(i-1)
   *ENDDO
*ENDDO

*DO,n,1,2
   TYPE,4
   REAL,n+11
   *DO,i,1,2
     *DO,j,1,6
         E,18629+5*(j-1)+2772*(i-1),35926+5*(j-
1)+2070*(i-1)
     *ENDDO
   *ENDDO
*ENDDO

*DO,n,1,2
   TYPE,4
   REAL,n+11
   *DO,i,1,2
     *DO,j,1,4
         E,18659+5*(j-1)+2772*(i-1),35956+5*(j-
1)+2070*(i-1)
     *ENDDO
   *ENDDO
*ENDDO

*DO,n,1,2
   TYPE,4
   REAL,n+11
   *DO,i,1,2
     *DO,j,1,3
         E,18679+5*(j-1)+2772*(i-1),35976+5*(j-
1)+2070*(i-1)
     *ENDDO
   *ENDDO
*ENDDO

*DO,n,1,2
   TYPE,4
   REAL,n+11
   *DO,i,1,2
```

```
   *DO,j,1,3
        E,18693+5*(j-1)+2772*(i-1),35991+5*(j-
1)+2070*(i-1)
    *ENDDO
   *ENDDO
*ENDDO


*DO,n,1,2
  TYPE,4
  REAL,n+11
  *DO,i,1,2
    E,19143+5*(i-1),36256+5*(i-1)
    E,19803+5*(i-1),36716+5*(i-1)
    E,20199+5*(i-1),37061+5*(i-1)
    E,20859+5*(i-1),37521+5*(i-1)
  *ENDDO
*ENDDO


*DO,n,1,2
  TYPE,4
  REAL,n+11
  *DO,i,1,2
    E,19202+5*(i-1),36316+5*(i-1)
    E,19862+5*(i-1),36776+5*(i-1)
    E,20258+5*(i-1),37121+5*(i-1)
    E,20918+5*(i-1),37581+5*(i-1)
  *ENDDO
*ENDDO


*DO,n,1,2
  TYPE,4
  REAL,n+11
  E,19231,36346
  E,19891,36806
  E,20287,37151
  E,20947,37611
*ENDDO
```

!UY   !Screws in u_y, 1 spring from node
                                             j-i

```
TYPE,4
REAL,13
```

```
!First column of panels, first vertical rows of
screws, then horizontal rows of screws

*DO,i,1,2
  *DO,j,1,7
          E,21746+5*(j-1)+2070*(i-1),511+5*(j-
1)+2772*(i-1)
  *ENDDO
*ENDDO

*DO,i,1,2
  *DO,j,1,4
          E,21781+5*(j-1)+2070*(i-1),545+5*(j-
1)+2772*(i-1)
  *ENDDO
*ENDDO

*DO,i,1,2
  E,21801+2070*(i-1),565+2772*(i-1)
  E,21806+2070*(i-1),570+2772*(i-1)
*ENDDO

*DO,i,1,2
  *DO,j,1,7
          E,21811+5*(j-1)+2070*(i-1),575+5*(j-
1)+2772*(i-1)
  *ENDDO
*ENDDO

*DO,i,1,2
  *DO,j,1,3
          E,21846+5*(j-1)+2070*(i-1),609+5*(j-
1)+2772*(i-1)
  *ENDDO
*ENDDO

*DO,i,1,2
  E,22256+5*(i-1),1088+5*(i-1)
  E,22716+5*(i-1),1748+5*(i-1)
  E,23176+5*(i-1),2408+5*(i-1)
  E,23636+5*(i-1),2936+5*(i-1)
*ENDDO

E,22316,1147
E,22776,1807
```

```
E,23236,2467
E,23696,2995
```

!Second and fourth column of panels, first vertical rows of screws, then horizontal rows of screws

```
*DO,k,1,2

*DO,i,1,2
  *DO,j,1,5
          E,24276+5*(j-1)+2530*(i-1)+5750*(k-
1),3679+5*(j-1)+3432*(i-1)+7392*(k-1)
  *ENDDO
*ENDDO

*DO,i,1,2
  E,24301+2530*(i-1)+5750*(k-1),3704+3432*(i-
1)+7392*(k-1)
  E,24306+2530*(i-1)+5750*(k-1),3709+3432*(i-
1)+7392*(k-1)
*ENDDO

*DO,i,1,2
  *DO,j,1,6
          E,24311+5*(j-1)+2530*(i-1)+5750*(k-
1),3713+5*(j-1)+3432*(i-1)+7392*(k-1)
  *ENDDO
*ENDDO

*DO,i,1,2
  *DO,j,1,4
          E,24341+5*(j-1)+2530*(i-1)+5750*(k-
1),3743+5*(j-1)+3432*(i-1)+7392*(k-1)
  *ENDDO
*ENDDO

*DO,i,1,2
  *DO,j,1,3
          E,24361+5*(j-1)+2530*(i-1)+5750*(k-
1),3763+5*(j-1)+3432*(i-1)+7392*(k-1)
  *ENDDO
*ENDDO

*DO,i,1,2
  *DO,j,1,3
```

```
            E,24376+5*(j-1)+2530*(i-1)+5750*(k-
1),3777+5*(j-1)+3432*(i-1)+7392*(k-1)
    *ENDDO
*ENDDO


*DO,i,1,2
            E,24756+5*(i-1)+5750*(k-1),4359+5*(i-
1)+7392*(k-1)
            E,25101+5*(i-1)+5750*(k-1),4755+5*(i-
1)+7392*(k-1)
            E,25561+5*(i-1)+5750*(k-1),5415+5*(i-
1)+7392*(k-1)
            E,25906+5*(i-1)+5750*(k-1),5943+5*(i-
1)+7392*(k-1)
            E,26366+5*(i-1)+5750*(k-1),6471+5*(i-
1)+7392*(k-1)
*ENDDO


*DO,i,1,2
            E,24816+5*(i-1)+5750*(k-1),4418+5*(i-
1)+7392*(k-1)
            E,25161+5*(i-1)+5750*(k-1),4814+5*(i-
1)+7392*(k-1)
            E,25621+5*(i-1)+5750*(k-1),5474+5*(i-
1)+7392*(k-1)
            E,25966+5*(i-1)+5750*(k-1),6002+5*(i-
1)+7392*(k-1)
            E,26426+5*(i-1)+5750*(k-1),6530+5*(i-
1)+7392*(k-1)
*ENDDO


E,24846+5750*(k-1),4447+7392*(k-1)
E,25191+5750*(k-1),4843+7392*(k-1)
E,25651+5750*(k-1),5503+7392*(k-1)
E,25996+5750*(k-1),6031+7392*(k-1)
E,26456+5750*(k-1),6559+7392*(k-1)


*ENDDO


!Third and fifth column of panels, first vertical
rows of screws, then horizontal rows of screws


*DO,k,1,2


*DO,i,1,2
    *DO,j,1,7
```

```
        E,27151+5*(j-1)+2530*(i-1)+5750*(k-
1),7375+5*(j-1)+3432*(i-1)+7392*(k-1)
  *ENDDO
*ENDDO


*DO,i,1,2
  *DO,j,1,4
        E,27186+5*(j-1)+2530*(i-1)+5750*(k-
1),7409+5*(j-1)+3432*(i-1)+7392*(k-1)
  *ENDDO
*ENDDO


*DO,i,1,2
  E,27206+2530*(i-1)+5750*(k-1),7429+3432*(i-
1)+7392*(k-1)
  E,27211+2530*(i-1)+5750*(k-1),7434+3432*(i-
1)+7392*(k-1)
*ENDDO


*DO,i,1,2
  *DO,j,1,7
        E,27216+5*(j-1)+2530*(i-1)+5750*(k-
1),7439+5*(j-1)+3432*(i-1)+7392*(k-1)
  *ENDDO
*ENDDO


*DO,i,1,2
  *DO,j,1,3
        E,27251+5*(j-1)+2530*(i-1)+5750*(k-
1),7473+5*(j-1)+3432*(i-1)+7392*(k-1)
  *ENDDO
*ENDDO


*DO,i,1,2
        E,27661+5*(i-1)+5750*(k-1),8084+5*(i-
1)+7392*(k-1)
        E,28121+5*(i-1)+5750*(k-1),8744+5*(i-
1)+7392*(k-1)
        E,28466+5*(i-1)+5750*(k-1),9140+5*(i-
1)+7392*(k-1)
        E,28811+5*(i-1)+5750*(k-1),9668+5*(i-
1)+7392*(k-1)
        E,29271+5*(i-1)+5750*(k-1),10196+5*(i-
1)+7392*(k-1)
*ENDDO
```

```
E,27721+5750*(k-1),8143+7392*(k-1)
E,28181+5750*(k-1),8803+7392*(k-1)
E,28526+5750*(k-1),9199+7392*(k-1)
E,28871+5750*(k-1),9727+7392*(k-1)
E,29331+5750*(k-1),10255+7392*(k-1)

*ENDDO
```

!Sixth column of panels, first vertical rows of screws, then horizontal rows of screws

```
*DO,i,1,2
   *DO,j,1,5
         E,35891+5*(j-1)+2070*(i-1),18595+5*(j-
1)+2772*(i-1)
   *ENDDO
*ENDDO

*DO,i,1,2
   E,35916+2070*(i-1),18620+2772*(i-1)
   E,35921+2070*(i-1),18625+2772*(i-1)
*ENDDO

*DO,i,1,2
   *DO,j,1,6
         E,35926+5*(j-1)+2070*(i-1),18629+5*(j-
1)+2772*(i-1)
   *ENDDO
*ENDDO

*DO,i,1,2
   *DO,j,1,4
         E,35956+5*(j-1)+2070*(i-1),18659+5*(j-
1)+2772*(i-1)
   *ENDDO
*ENDDO

*DO,i,1,2
   *DO,j,1,3
         E,35976+5*(j-1)+2070*(i-1),18679+5*(j-
1)+2772*(i-1)
   *ENDDO
*ENDDO

*DO,i,1,2
```

```
  *DO,j,1,3
          E,35991+5*(j-1)+2070*(i-1),18693+5*(j-
1)+2772*(i-1)
  *ENDDO
*ENDDO


*DO,i,1,2
  E,36256+5*(i-1),19143+5*(i-1)
  E,36716+5*(i-1),19803+5*(i-1)
  E,37061+5*(i-1),20199+5*(i-1)
  E,37521+5*(i-1),20859+5*(i-1)
*ENDDO


*DO,i,1,2
  E,36316+5*(i-1),19202+5*(i-1)
  E,36776+5*(i-1),19862+5*(i-1)
  E,37121+5*(i-1),20258+5*(i-1)
  E,37581+5*(i-1),20918+5*(i-1)
*ENDDO


E,36346,19231
E,36806,19891
E,37151,20287
E,37611,20947



!CONTACT BETWEEN PANELS
!Along x-axis

TYPE,10
REAL,18

*DO,n,1,3

*DO,i,1,24
          E,24044+(i-1)+5750*(n-1),24159+(i-
1)+5750*(n-1)
*ENDDO

*DO,i,1,28
          E,24070+(i-1)+5750*(n-1),24185+(i-
1)+5750*(n-1)
*ENDDO

*DO,i,1,27
```

```
         E,24101+(i-1)+5750*(n-1),24216+(i-
1)+5750*(n-1)
*ENDDO


*DO,i,1,29
         E,24130+(i-1)+5750*(n-1),24245+(i-
1)+5750*(n-1)
*ENDDO


*ENDDO



*DO,n,1,2


*DO,i,1,24
         E,26919+(i-1)+5750*(n-1),27034+(i-
1)+5750*(n-1)
*ENDDO


*DO,i,1,28
         E,26945+(i-1)+5750*(n-1),27060+(i-
1)+5750*(n-1)
*ENDDO


*DO,i,1,27
         E,26976+(i-1)+5750*(n-1),27091+(i-
1)+5750*(n-1)
*ENDDO


*DO,i,1,29
         E,27005+(i-1)+5750*(n-1),27120+(i-
1)+5750*(n-1)
*ENDDO


*ENDDO



!Along y-axis

*DO,n,1,22
  E,21683+115*(n-1),21684+115*(n-1)
*ENDDO



*DO,n,1,2
```

```
*DO,i,1,25
    E,24183+115*(i-1)+5750*(n-1),24184+115*(i-
1)+5750*(n-1)
*ENDDO


*DO,i,1,25
    E,24243+115*(i-1)+5750*(n-1),24244+115*(i-
1)+5750*(n-1)
*ENDDO


*ENDDO



*DO,n,1,2
  *DO,i,1,25
                  E,27088+115*(i-1)+5750*(n-
1),27089+115*(i-1)+5750*(n-1)
  *ENDDO
*ENDDO



*DO,n,1,22
  E,35683+115*(n-1),35684+115*(n-1)
*ENDDO


*DO,n,1,22
  E,35743+115*(n-1),35744+115*(n-1)
*ENDDO



!CONTACT BETWEEN PLANKS
!Along x-axis

*DO,n,1,22
  *DO,i,1,132
      E,1169+924*(n-1)+(i-1),1301+924*(n-1)+(i-
1)
  *ENDDO
*ENDDO




!——DEFINE BOUNDARY CONDITIONS——
```

```
!LOWER EDGE (x=2680 mm)
*DO,n,1,161                                  !Do-loop
  i=508+132*(n-1)                            !Nodes at lower edge
  D,i,UX,0,,i,1,UY,UZ,ROTX,ROTY,ROTZ         !Constrain nodes for all DOFs
*ENDDO                                       !End do-loop


!UPPER EDGE (x=0 mm)
*DO,n,1,161                                  !Do-loop
  i=377+132*(n-1)                            !Nodes at upper edge of planks
  D,i,UZ,0,,i,1,ROTX,,,                       !Constrain for UZ and ROTX
*ENDDO                                       !End do-loop


*DO,n,1,144                                  !Do-loop
  i=21629+115*(n-1)                          !Nodes at upper edge of panels
  D,i,UZ,0,,i,1,ROTX,,,                       !Constrain for UZ and ROTX
*ENDDO                                       !End do-loop


!BEAMS
*DO,n,1,376                                  !Do-loop
  D,n,UZ,0,,n,1,,ROTY                        !Constrain for UZ and ROTY
*ENDDO                                       !End do-loop


!PANELS
*DO,n,21629,38188                            !Do-loop
  D,n,UZ,0,,n,1,                             !Constrain for UZ
*ENDDO                                       !End do-loop



!———DEFINE LOADS———

*DIM,loading,TABLE,8269,1,1,TIME,DISPL       !Create table for loading
*TREAD,loading,lsretro,csv,,                 !Read data from csv into table



/ESHAPE,1                                    !Display elements with shapes
ALLSEL,ALL                                   !Select all entities



FINISH                                       !Exit preprocessor
```

!——**SOLUTION**——

```
/SOLU                                      !Enter solution processor
ANTYPE,STATIC                              !Specify analysis type
NROPT,,                                    !Specify Newton-Raphson controls
NSUBST,30000,30000,1                       !Number of substeps at load step
AUTOTS,ON                                  !Automatic time stepping on
KBC,0                                      !Ramped load steps
NEQIT,2000,                                !Maximum number of iterations

NLDIAG,NRRE,ON                             !Nonlinear diagnostics
OUTRES,BASIC                               !Write basic output in result file

tm_start=0.000001                          !Start time
tm_end=1653                                !End time
tm_incr=0.5                                !Load step size

*DO,tm,tm_start,tm_end,tm_incr             !Do-loop to solve for each time
                                            step
   TIME,tm                                 !Set time
   D,1,UY,loading(tm),,94,,                !Set loading on top beam
   SOLVE                                   !Solve
*ENDDO                                     !End do-loop

FINISH                                     !Exit solution processor
```

!——**POSTPROCESSING**——

```
/POST26                                    !Enter time-history postprocessor

/RGB,INDEX,100,100,100, 0                  !Set background to white
/RGB,INDEX, 80, 80, 80,13
/RGB,INDEX, 60, 60, 60,14
/RGB,INDEX, 0, 0, 0,15

/PBC,U,,1,                                 !Show boundary conditions

NUMVAR,200                                 !Set maximum number of variables
                                            to 200

!——STORE DISPLACEMENT——
NSOL,2,1,U,Y,uynode1                       !Store $u_y$ of node 1 into variable 2
```

```
*dim,uynode1,ARRAY,8000,1                        !Create array parameter for uyn-
                                                  ode1

VGET,uynode1(1),2                                 !Store time-history data of variable
                                                  2 into uynode1

*CFOPEN,uynode1,csv                               !Open csv-file
*VWRITE,uynode1(1)                                !Write array in given format to file
                                                  'uynode1.csv'

(F11.5)                                           !Format
*CFCLOSE                                          !Close csv-file


!——STORE REACTION FORCES——
*dim,recforces,ARRAY,8000,162                     !Create array
*DO,n,1,161                                       !Do-loop to store reaction forces in
                                                  array

  j=n+2
  i=508+132*(n-1)
  RFORCE,j,i,F,Y,
  VGET,recforces(1,n),j
*ENDDO                                            !End do-loop


*MWRITE,recforces(1,1),reactionss,txt,,JIK,162,8000,1   !Write reaction forces to file
(162F11.5)                                        !Format


FINISH                                            !Exit postprocessor
```